# Mapping micro-indicators to understand the potential of forage yield at the farm scale

Prepared for Beef + Lamb New Zealand

Completed by Manaaki Whenua – Landcare Research and Lincoln University

JULY 2022

# Mapping micro-indicators to understand the potential of forage yield at the farm scale

*Contract Report: LC4168*

Dr Nathan Odgers, Dr Jagath Ekanayake, Mr Jing Guo, Dr Stephen McNeill, Ms Veronica Penny, Mr James Barringer

*Manaaki Whenua – Landcare Research*

*PO Box 69040*
*Lincoln 7640*
*Ph. 03 321 9999*

Prof Derrick Moot

*Lincoln University*

*PO Box 85084*
*Lincoln 7647*
*Ph. 03 423 0705*

| *Reviewed by:* | *Approved for release by:* |
| --- | --- |
| John Drewry | Sam Carrick |
| Senior Researcher | Portfolio Leader – Characterising Land Resources |
| Manaaki Whenua – Landcare Research | Manaaki Whenua – Landcare Research |

# Contents

Summary ..... xv

1 Introduction ..... 1

1.1 Previous research in New Zealand ..... 3

1.2 Wireless sensor networks ..... 3

1.3 Digital soil mapping ..... 4

1.4 Objectives ..... 5

2 Methods ..... 5

2.1 Study area ..... 5

2.2 Sample site selection ..... 7

2.3 Wireless sensor networks ..... 15

2.4 Data management and analysis ..... 21

2.5 Modelling ..... 29

3 Results ..... 37

3.1 Wireless sensor networks ..... 37

3.2 Modelling ..... 42

4 Discussion ..... 61

4.1 Wireless sensor networks ..... 61

4.2 Soil temperature ..... 61

4.3 Soil moisture ..... 63

4.4 Yield modelling ..... 65

5 Summary and conclusions ..... 66

5.1 Recommendations ..... 66

5.2 Future work ..... 67

6 Acknowledgements ..... 68

7 Intellectual property ..... 69

8 References ..... 69

Appendix – maps and charts for Māhia, Prices Valley, Taihape, Taumarunui and Tourere ..75

# Figures

Figure 1. Comparison of the cell size of existing climate datasets. Location of cells depicted against hill country background is for comparative purpose only and does not reflect the true orientations of the respective grids. ..... 2

Figure 2. The VCSN prediction grid superimposed on Canterbury hill country. ..... 3

Figure 3. Locations of the wireless sensor network sites. ..... 6

Figure 4. Sampling domain and location of sensor network gateway at Mt Somers. ..... 7

Figure 5. Elevation at Mt Somers. ..... 8

Figure 6. Slope at Mt Somers. ..... 9

Figure 7. Aspect at Mt Somers. ..... 9

Figure 8. Topographic wetness index at Mt Somers. ..... 10

Figure 9. Combined elevation-aspect covariate (elasp) at Mt Somers. ..... 11

Figure 10. Variances of the principal components of elasp and topographic wetness index at Mt Somers. ..... 12

Figure 11. Images of (a) principle component 1 and (b) the quantile cut for Mt Somers. ... 13

Figure 12. Image of the Mt Somers site split into five strata based on quantiles. Plotted points are the four points selected in each or the strata. Two sets of spatially balanced points are shown. ..... 14

Figure 13. The circuit board that controls the WSN gateway, showing important components. Electronics at each sensor node are similar but omit the ESP8266 WiFi controller. ..... 16

Figure 14. Tourere WSN gateway with major components labelled. ..... 17

Figure 15. Schematic representation of how sensor nodes are set up in the field. ..... 18

Figure 16. Assembly of the sensor nodes in J. Ekanayake's living room during Covid-19 lockdown. ..... 19

Figure 17. A sensor node at Prices Valley. ..... 20

Figure 18. Location of sampling domain, WSN gateway, and sensor nodes at Mt Somers. 21

Figure 19. Distribution of the difference in time between sorted samples across all wireless sensor networks. ..... 22

Figure 20. Raw soil temperature for the Mt Somers WSN, with soil temperatures limited to the range −5 to 30°C. Panel labels indicate the relevant sensor node. ..... 23

Figure 21. Daily median soil temperature data for the Mt Somers WSN after trimming the start and end dates, and removal of low and high temperatures and periods of no change in soil temperature. Panel labels indicate the respective sensor node. Points that were removed as a result of the data trimming are shown in orange, while presumed valid points are in black. ..... 24

Figure 22. Daily median soil temperature data for all sites after trimming of the start and end dates, removal of small and large temperatures, and periods of no change in soil temperature. Locally estimated scatterplot smoothing (LOESS) lines are drawn through data for sensor nodes 1, 10, and 19 for each site. Points that have been excised from the data are shown in orange. ..... 25

Figure 23. Daily median soil temperature data for all sites for January 2021, to show fine temporal-scale behaviour. For a given day of January, each point corresponds to one sensor node. Prices Valley is not shown because there is no data from that site for January 2021. ..... 26

Figure 24. Raw soil moisture data for the Mt Somers site. Panel labels indicate the respective sensor node. ..... 27

Figure 25. Daily median soil moisture data for the Mt Somers site after trimming of the start and end dates, removal of low and high soil moisture values, and periods of no change in soil moisture. Panel labels indicate the respective sensor node. Points excised from the data are shown in orange. ..... 28

Figure 26. Daily median soil moisture data for all sites after trimming of the start and end dates, removal of small and large soil moisture values, and periods of no change in soil moisture. Smoothed LOESS lines are drawn through data for sensor nodes 1, 10, and 19 for each site. Points that have been excised from the data are shown in orange. ..... 29

Figure 27. Distribution of the difference in time between aggregated daily data, in days, for each site and sensor node. Points are coloured by sensor node. ..... 30

Figure 28. Broken stick model, which relates mean daily air temperature to daily thermal time for lucerne. ..... 35

Figure 29. Histograms of the number of WSN gateway transmissions per day. Dashed vertical line is the expected number of transmissions per day. ..... 39

Figure 30. Number of gateway transmissions per day over time. Dashed horizontal line is the expected number of transmissions per day. ..... 40

Figure 31. Median number of sensor nodes reporting soil temperature per day. Dashed horizontal line is the expected number of sensor nodes reporting soil temperature per day. ..... 41

Figure 32. Plot of the effect of the different explanatory variables for soil temperature, model 4. Explanatory variables are given in their natural units. For each panel, the explanatory variables that are not changing are held at a fixed value (generally the median or a sensible default). The limits of the vertical axis are the same for all panels. The solid line is the nominal estimate, while the shaded area (often not visible) is the 95% confidence interval of the mean estimate. ..... 43

Figure 33. Measured versus fitted soil temperature plot for the Mt Somers site using model 5. Panel labels indicate the respective sensor node. The dashed red line is the one-to-one line. ..... 44

Figure 34. Measured (points) and fitted (line) soil moisture for the Mt Somers site over time, using model 1. Panel labels indicate the respective sensor node. ..... 45

Figure 35. Predicted soil temperature at Mt Somers on 15 July, when soils are near their coolest. ..... 46

Figure 36. Predicted soil temperature at Mt Somers on 15 January, when soils are near their warmest. ..... 46

Figure 37. Predicted soil temperature at Mt Somers on 15 July, showing variation in predicted temperature across individual hillslopes. Resolution of the prediction grid is 30 m. ..... 47

Figure 38. Predicted difference in soil temperature between 15 December and 15 July. .... 47

Figure 39. Measured versus fitted soil moisture plot for the Mt Somers site using model 1. Panel labels indicate the respective sensor node. The dashed red line is the 1:1 line. ..... 51

Figure 40. Measured (points) versus fitted (line) soil moisture for the Mt Somers site over time, using model 1. Panel labels indicate the respective sensor node. ..... 52

Figure 41. Plot of the effect of the different explanatory variables for soil moisture model 1. Explanatory variables are given in their natural units. For each panel, the explanatory variables that are not changing are held at a fixed value (generally the median or a sensible default). The vertical axis is the same for all panels. The solid line represents the mean estimate, while the shaded area represents the 95% confidence interval of the mean estimate. ..... 53

Figure 42. Predicted soil moisture at Mt Somers on 1 March, when soils are near their driest. ..... 54

Figure 43. Predicted soil moisture at Mt Somers on 25 June, when soils are near their wettest. ..... 54

Figure 44. Predicted soil moisture at Mt Somers on 15 July, showing variation in predicted moisture across individual hillslopes. Resolution of the prediction grid is 30 m. ..... 55

Figure 45. Relationship between air temperature and 20 cm soil temperature measured at Canterbury weather stations. Dashed line is the 1:1 line and solid line is the line of best fit. ..... 56

Figure 46. Relationship between air temperature and 20 cm soil temperature measured at Hawke's Bay weather stations. Dashed line is the 1:1 line and solid line is the line of best fit..... 57

Figure 47. Relationship between air temperature and 20 cm soil temperature measured at Wanganui weather stations. Dashed line is the 1:1 line and solid line is the line of best fit. ..... 58

Figure 48. Predicted annual lucerne yield at Mt Somers for 2020. ..... 59

Figure 49. Predicted annual lucerne yield for Mt Somers for 2020, showing variation in predicted yield across individual hillslopes. Resolution of the prediction grid is 30 m. ..... 60

Figure 50. Measured (points) and predicted (line) soil moisture for sensor 8 at Mt Somers. Annotations indicate where soil moisture is assumed to be near field capacity and wilting point. ..... 64

Figure A1. Location of sampling domain, WSN gateway, and sensor nodes at Māhia..... 75

Figure A2. Elevation at Māhia. ..... 76

Figure A3. Slope at Māhia. ..... 76

Figure A4. Aspect at Māhia..... 77

Figure A5. Topographic wetness index at Māhia. ..... 77

Figure A6. Elasp at Māhia..... 78

Figure A7. Daily median soil temperature data for the Māhia WSN after trimming of the start and end dates, and removal of low and high temperatures, and periods of no change in soil temperature. Panel labels indicate the respective sensor node. Points that were removed as a result of the data trimming are shown in orange, while presumed valid points are in black. ..... 78

Figure A8. Measured versus fitted soil temperature plot for the Māhia site using model 5. Panel labels indicate the respective sensor node. ..... 79

Figure A9. Measured (points) versus fitted (line) soil temperature for the Māhia site over time, using model 5. Panel labels indicate the respective sensor node. ..... 79

Figure A10. Predicted soil temperature at Māhia on 15 January, when soils are near their warmest. ..... 80

Figure A11. Predicted soil temperature at Māhia on 15 July, when soils are near their coolest..... 80

Figure A12. Daily median soil moisture data for the Māhia site after trimming of the start and end dates, and removal of low and high soil moisture values, and periods of no change in soil moisture. Panel labels indicate the respective sensor node. Points excised from the data have been coloured orange. ..... 81

Figure A13. Measured versus fitted soil moisture plot for the Māhia site using model 1. Panel labels indicate the respective sensor node. ..... 81

Figure A14. Measured (points) versus fitted (line) soil moisture for the Māhia site over time, using model 1. Panel labels indicate the respective sensor node. ..... 82

Figure A15. Predicted soil moisture at Māhia on 1 March, when soils are near their driest. ..... 82

Figure A16. Predicted soil moisture at Māhia on 25 June, when soils are near their wettest. ..... 83

Figure A17. Predicted annual lucerne yield at Māhia for 2020. ..... 83

Figure A18. Location of sampling domain, WSN gateway, and sensor nodes at Prices Valley. ..... 84

Figure A19. Elevation at Prices Valley. ..... 84

Figure A20. Slope at Prices Valley. ..... 85

Figure A21. Aspect at Prices Valley. ..... 85

Figure A22. Topographic wetness index at Prices Valley. ..... 86

Figure A23. Elasp at Prices Valley. ..... 86

Figure A24. Daily median soil temperature data for the Prices Valley WSN after trimming of the start and end dates, and removal of low and high temperatures, and periods of no change in soil temperature. Panel labels indicate the respective sensor node. Points that were removed as a result of the data trimming are shown in orange, while presumed valid points are in black. ..... 87

Figure A25. Measured versus fitted soil temperature plot for the Prices Valley site using model 5. Panel labels indicate the respective sensor node. ..... 88

Figure A26. Measured (points) versus fitted (line) soil temperature for the Prices Valley site over time, using model 5. Panel labels indicate the respective sensor node. ..... 88

Figure A27. Predicted soil temperature at Prices Valley on 15 January, when soils are near their warmest. ..... 89

Figure A28. Predicted soil temperature at Prices Valley on 15 July, when soils are near their coolest. ..... 89

Figure A29. Daily median soil moisture data for the Prices Valley site after trimming of the start and end dates, and removal of low and high soil moisture values, and periods of no change in soil moisture. Panel labels indicate the respective sensor node. Points excised from the data have been coloured orange. 90

Figure A30. Measured versus fitted soil moisture plot for the Prices Valley site using model 1. Panel labels indicate the respective sensor node. 90

Figure A31. Measured (points) versus fitted (line) soil moisture for the Prices Valley site over time, using model 1. Panel labels indicate the respective sensor node. 91

Figure A32. Predicted soil moisture at Prices Valley on 1 March, when soils are near their driest. 91

Figure A33. Predicted soil moisture at Prices Valley on 25 June, when soils are near their wettest. 92

Figure A34. Predicted annual lucerne yield at Prices Valley for 2020. 92

Figure A35. Location of sampling domain, WSN gateway, and sensor nodes at Taihape. 93

Figure A36. Elevation at Taihape. 93

Figure A37. Slope at Taihape. 94

Figure A38. Aspect at Taihape. 94

Figure A39. Topographic wetness index at Taihape. 95

Figure A40. Elasp at Taihape. 95

Figure A41. Daily median soil temperature data for the Taihape WSN after trimming of the start and end dates, and removal of low and high temperatures, and periods of no change in soil temperature. Panel labels indicate the respective sensor node. Points that were removed as a result of the data trimming are shown in orange, while presumed valid points are in black. 96

Figure A42. Measured versus fitted soil temperature plot for the Taihape site using model 5. Panel labels indicate the respective sensor node. 97

Figure A43. Measured (points) versus fitted (line) soil temperature for the Taihape site over time, using model 5. Panel labels indicate the respective sensor node. 97

Figure A44. Predicted soil temperature at Taihape on 15 January, when soils are near their warmest. 98

Figure A45. Predicted soil temperature at Taihape on 15 July, when soils are near their coolest. 98

Figure A46. Daily median soil moisture data for the Taihape site after trimming of the start and end dates, and removal of low and high soil moisture values, and periods of no

change in soil moisture. Panel labels indicate the respective sensor node. Points excised from the data have been coloured orange. ..... 99

Figure A47. Measured versus fitted soil moisture plot for the Taihape site using model 1. Panel labels indicate the respective sensor node. ..... 99

Figure A48. Measured (points) versus fitted (line) soil moisture for the Taihape site over time, using model 1. Panel labels indicate the respective sensor node. ..... 100

Figure A49. Predicted soil moisture at Taihape on 1 March, when soils are near their driest. ..... 100

Figure A50. Predicted soil moisture at Taihape on 25 June, when soils are near their wettest. ..... 101

Figure A51. Predicted annual lucerne yield at Taihape for 2020. ..... 101

Figure A52. Location of sampling domain, WSN gateway, and sensor nodes at Taumarunui. ..... 102

Figure A53. Elevation at Taumarunui. ..... 102

Figure A54. Slope at Taumarunui. ..... 103

Figure A55. Aspect at Taumarunui. ..... 103

Figure A56. Topographic wetness index at Taumarunui. ..... 104

Figure A57. Elasp at Taumarunui. ..... 104

Figure A58. Daily median soil temperature data for the Taumarunui WSN after trimming of the start and end dates, and removal of low and high temperatures, and periods of no change in soil temperature. Panel labels indicate the respective sensor node. Points that were removed as a result of the data trimming are shown in orange, while presumed valid points are in black. ..... 105

Figure A59. Measured versus fitted soil temperature plot for the Taumarunui site using model 5. Panel labels indicate the respective sensor node. ..... 106

Figure A60. Measured (points) versus fitted (line) soil temperature for the Taumarunui site over time, using model 5. Panel labels indicate the respective sensor node. ..... 106

Figure A61. Predicted soil temperature at Taumarunui on 15 January, when soils are near ..... 107

Figure A62. Predicted soil temperature at Taumarunui on 15 July, when soils are near their coolest. ..... 107

Figure A63. Daily median soil moisture data for the Taumarunui site after trimming of the start and end dates, and removal of low and high soil moisture values, and periods of no

change in soil moisture. Panel labels indicate the respective sensor node. Points excised from the data have been coloured orange. 108

Figure A64. Measured versus fitted soil moisture plot for the Taumarunui site using model 1. Panel labels indicate the respective sensor node. 108

Figure A65. Measured (points) versus fitted (line) soil moisture for the Taumarunui site over time, using model 1. Panel labels indicate the respective sensor node. 109

Figure A66. Predicted soil moisture at Taumarunui on 1 March, when soils are near their driest. 109

Figure A67. Predicted soil moisture at Taumarunui on 25 June, when soils are near their wettest. 110

Figure A68. Predicted annual lucerne yield at Taumarunui for 2020. 110

Figure A69. Location of sampling domain, WSN gateway, and sensor nodes at Tourere. 111

Figure A70. Elevation at Tourere. 111

Figure A71. Slope at Tourere. 112

Figure A72. Aspect at Tourere. 112

Figure A73. Topographic wetness index at Tourere. 113

Figure A74. Elasp at Tourere. 113

Figure A75. Daily median soil temperature data for the Tourere WSN after trimming of the start and end dates, and removal of low and high temperatures, and periods of no change in soil temperature. Panel labels indicate the respective sensor node. Points that were removed as a result of the data trimming are shown in orange, while presumed valid points are in black. 114

Figure A76. Measured versus fitted soil temperature plot for the Tourere site using model 5. Panel labels indicate the respective sensor node. 115

Figure A77. Measured (points) versus fitted (line) soil temperature for the Tourere site over time, using model 5. Panel labels indicate the respective sensor node. 115

Figure A78. Predicted soil temperature at Tourere on 15 January, when soils are near their warmest. 116

Figure A79. Predicted soil temperature at Tourere on 15 July, when soils are near their coolest. 116

Figure A80. Daily median soil moisture data for the Tourere site after trimming of the start and end dates, and removal of low and high soil moisture values, and periods of no change in soil moisture. Panel labels indicate the respective sensor node. Points excised from the data have been coloured orange. 117

Figure A81. Measured versus fitted soil moisture plot for the Tourere site using model 1. Panel labels indicate the respective sensor node..... 117

Figure A82. Measured (points) versus fitted (line) soil moisture for the Tourere site over time, using model 1. Panel labels indicate the respective sensor node. ..... 118

Figure A83. Predicted soil moisture at Tourere on 1 March, when soils are near their driest. ..... 118

Figure A84. Predicted soil moisture at Tourere on 25 June, when soils are near their wettest. ..... 119

Figure A85. Predicted annual lucerne yield at Tourere for 2020. ..... 119

# Tables

Table 1. Wireless sensor network sites....6

Table 2. Ratio of the variance of the first to the second principal component for each site .... 14

Table 3. Installation periods for the WSNs .... 19

Table 4. Number of weather stations available with air temperature and soil temperature at specific depths.... 36

Table 5. Days since installation for each WSN and some metrics of performance .... 38

Table 6. Number of sensor node failures at each WSN, at 15 March 2022.... 40

Table 7. Residual deviance, Akaike's information criterion, and proportion of the total deviance explained for each of the GAMs fitted for the soil temperature data.... 42

Table 8. Statistics for the evaluation of the relationship between measured and predicted soil temperature for the chosen soil temperature, model 5 .... 44

Table 9. Summary of aspect-related differences in observed minimum soil temperature and days taken for soil temperature to reach 10°C and 15°C. Note: Because of gaps in the data, values are based on 2020 observations at some sites and 2021 observations at other sites.... 49

Table 10. Difference in number of days for soil on north- and south-facing slopes to reach 10°C and 15°C. Positive values indicate north-facing soils reached the temperature threshold sooner.... 50

Table 11. Residual deviance, Akaike's information criterion, and proportion of the total deviance explained for each of the GAMs fitted for the soil moisture data .... 50

Table 12. Statistics for the evaluation of the relationship between measured and predicted soil moisture for soil moisture model 1.... 51

Table 13. Differences in observed moisture at north- and south-facing sensor nodes, expressed as the average of the daily median on the dates indicated of sensor nodes on the indicated aspects. Data were not available for two dates at Prices Valley.... 65

Table 14. New intellectual property created during this study.... 69

# Summary

Farmers need help to quantify the key soil and terrain features of topographically diverse hill-country landscapes, including the dynamics of key micro-indicators such as soil temperature and moisture. Farm-scale information on these micro-indicators can drive yield models and help inform robust decision-making about pasture management.

Global, remotely-sensed data on micro-indicators like soil moisture have been available for nearly fifteen years, and for any location the remote sensors have impressive revisit times in the order of three days. However the grid resolution of these products, which ranges from 9000 m to 50 km, is far too coarse to provide evidence about the variation in soil variability over tens of metres that is needed to inform decision-making at the farm scale. Likewise, best-available national modelling on micro-indicators are also provided at a resolution (5,000 m) that is not informative at the farm scale.

The issue of grid resolution is especially important in New Zealand's hill-country landscapes, where soil conditions can vary markedly with topography. Farm-scale soil mapping is best suited to a grid resolution of 50 m or smaller. At this scale, modern sensor networks can in principle be coupled to digital soil mapping workflows to model the spatial variability in micro-indicators. In practice cost constraints limit the number of sensors that can be deployed, which influences the quality of the modelling. The primary objective of this study was to determine whether we can map micro-indicators at the farm scale in hill-country landscapes using a relatively small number of sensors per farm, and the secondary objective was to determine if this farm-scale information on micro-indicators can be used to map legume yield.

We installed wireless sensor networks at six hill-country sites across New Zealand and monitored soil temperature and moisture at 30 cm depth at hourly intervals from mid-2020 to July 2022. We fitted generalised additive models to relate micro-indicators to other environmental variables and produced daily maps of the micro-indicators at high resolution (30 m) for 1 year. Soil temperature was very predictable, but soil moisture was only moderately so. We predicted lucerne yield at high resolution using air temperature estimated from the soil temperature.

Based on the results, we concluded that we can map micro-indicators and legume yield at farm scale. However, the results highlight the need for additional information on soil properties and air temperature to improve the robustness of the soil moisture and yield modelling.

In principle the soil monitoring system can be scaled up to serve areas of arbitrary size, such as groups of adjacent farms or farms in a regional catchment. The modelling pipeline we describe ought to be robust to a larger number of sensors. Key issues that would need to be resolved include the number and placement of network gateways in order to minimise the cost of cellular service, and the number of sensor nodes per farm required to achieve modelling of adequate quality.

# 1 Introduction

Robust methods are needed to estimate pasture yields and determine the suitability of forage legumes in New Zealand's hill-country landscapes for on-farm application. In addition, models are required to answer broader questions on environmental impacts, climate change, nutrient leaching, and carbon sequestration of legume-based pastures.

Because hill-country farms typically have diverse landscapes within individual farms, leading to spatially variable pasture production, farmers need help to quantify key soil and terrain features of these landscapes (Mills et al. 2021). This includes how the dynamics of micro-indicators such as soil temperature and moisture vary across topographically diverse hill-country landscapes. Farm-scale information on micro-indicators could help inform robust decision-making of the most suitable locations for, and likely benefits of, introducing forage legumes into different areas of hill-country landscapes.

It is important to understand soil temperature and moisture dynamics, because these properties are key drivers of many soil and plant processes. Soil temperature, for instance, influences the growth of plant roots, including their morphology, function, and metabolism (McMichael & Burke 1998), especially during the early growing season (Kaspar & Bland 1992). Root growth tends to increase with increasing soil temperature up to a certain point, beyond which it decreases. Water and nutrient uptake by roots are also affected by temperature and are reduced at low temperatures (McMichael & Burke 1998). Chemical weathering reactions increase with increasing soil temperature, which increases the availability of nutrients for root uptake (Pregitzer & King 2005). The activity and abundance of soil fauna generally increase with increasing soil temperature, but may be limited by water availability when temperatures are too high (Pregitzer & King 2005).

Soil moisture is the main driver of plant growth on many hill-country farms. It influences the amount and timing of plant growth and therefore the animal production systems that can be supported (Moot 2012). Soil moisture also causes changes to the physical structure of the soil and participates in chemical reactions that release or detain soil nutrients, create acidity, and influence the weathering and decomposition of soil minerals (Brady & Weil 2017). Finally, it has a major influence on many landscape hydrological processes, including flooding, erosion, and solute transport (Western & Blöschl 1999).

To ensure hill-country farms are sustainable into the future, better information on key soil properties such as soil temperature and moisture are needed at the farm scale in order to inform decisions about pasture management. Implicit in this is a need to move away from sporadic measurement of soil properties at locations assumed to be 'representative' and towards the implementation of soil monitoring systems that measure soil properties at regular intervals and report information (either spatial or aspatial) in near real time (Drewry et al. 2019).

In the last fifteen years, the European Space Agency's Soil Moisture and Ocean Salinity[1] (SMOS) and the United States' National Aeronautics and Space Administration's Soil

[1] https://www.esa.int/Applications/Observing_the_Earth/FutureEO/SMOS

Moisture Active Passive[2] (SMAP) missions launched with the aim of consistently and frequently mapping global soil moisture. These remote sensors are able to produce global maps about every three days at grid resolutions (cell sizes) that range from 9,000 m (SMAP) to 50 km (SMOS). The repeat times are suitable for soil monitoring applications but the grid resolutions are too coarse to provide robust information on variability in climate conditions that exist at the farm scale, such as between individual hillslopes (Figure 1).

Currently the best available source of climate information in New Zealand is NIWA's Virtual Climate Station Network[3] (VCSN). The VCSN provides daily estimates of a range of climate variables, including soil temperature and soil moisture, on a 5,000 m grid across all of New Zealand. We suggest these estimates are unsatisfactory for hill-country pasture management for a number of reasons. As for the SMAP and SMOS data products, the grid resolution of the VCSN estimates (cell size of 5,000 m) is too coarse to provide robust farm-scale climate information (Figures 1 and 2). Also, the VCSN estimates are derived from models based on meteorological climate stations, which are conventionally sited on flat land so they cannot take into account topography-influenced variations in climate parameters.

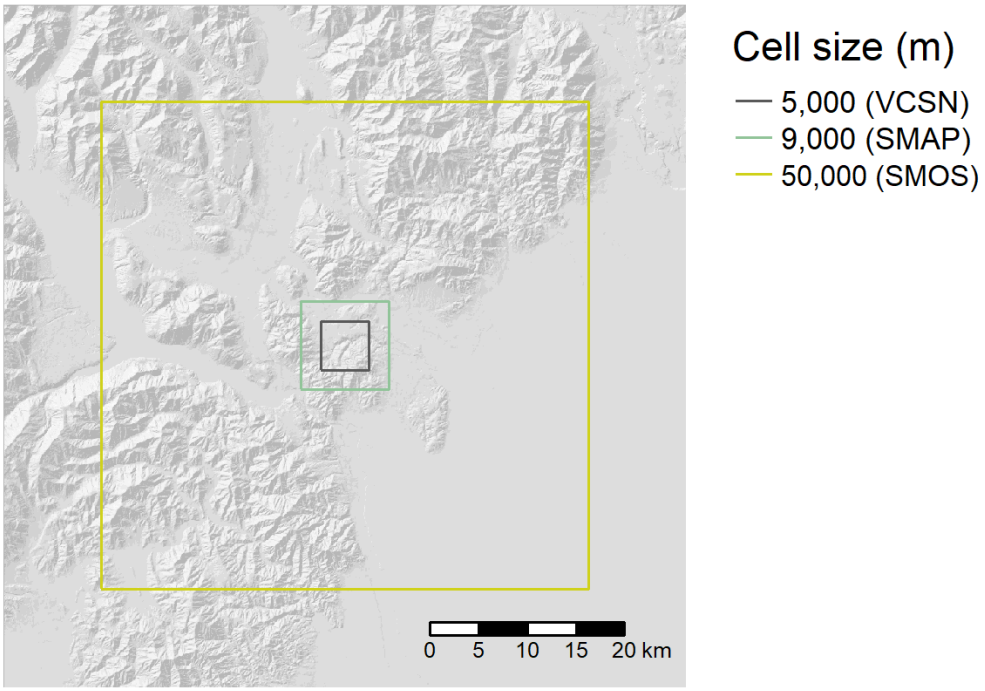


**Figure 1. Comparison of the cell size of existing climate datasets. Location of cells depicted against hill country background is for comparative purpose only and does not reflect the true orientations of the respective grids.**

[2] https://smap.jpl.nasa.gov/. Not to be confused with S-map, New Zealand's national digital soil map.

[3] https://niwa.co.nz/climate/our-services/virtual-climate-stations

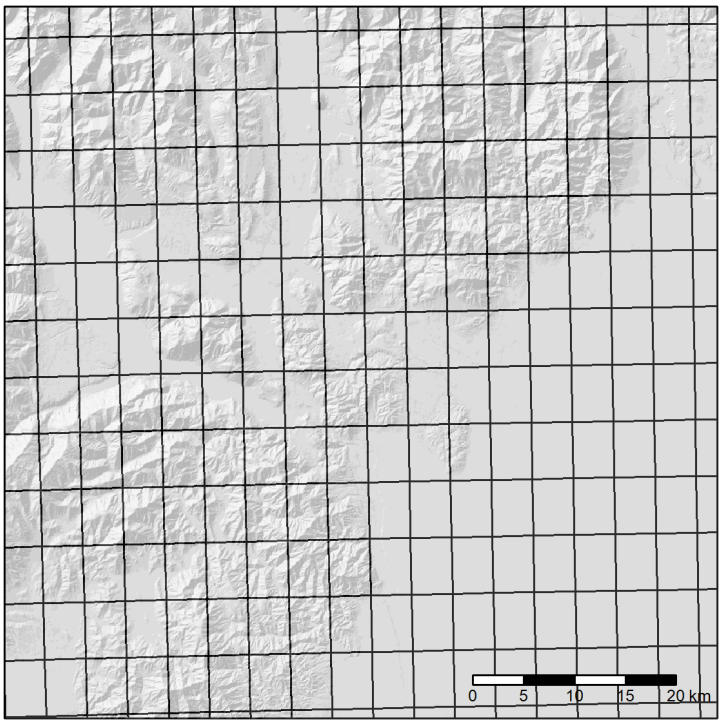


**Figure 2. The VCSN prediction grid superimposed on Canterbury hill country.**

## 1.1 Previous research in New Zealand

In hill country, soil temperature and moisture conditions can vary markedly with aspect, slope, and elevation due to differences in the amount of insolation received at the soil surface, which can contribute to spatial variability in pasture growth and composition (Sheath & Boom 1985). In New Zealand this has been studied over many decades (e.g. Will 1959; Dawson & Fisher 1964; Gillingham & Bell 1977; Radcliffe & Lefever 1981; Sheath & Boom 1985; Barringer 1997).

Measurement technology has improved over time. For example, Dawson and Fisher (1964) made weekly measurements of soil temperature using copper-constantan thermocouple chains. Gillingham and Bell (1977) took measurements at quarterly intervals across 2 years using thermistor probes mounted in open-ended stainless steel tubes. Later, Radcliffe and Lefever (1981) used thermographs to make more continuous records of soil temperature. Thermographs automated measurement and recording, but transcription of measurements from charts remained a manual process. Data loggers enabled fully automatic measurement and collation of digital soil property data in the 1990s (e.g. Barringer 1997), but they had to be retrieved from the field before the data could be analysed and interpreted.

## 1.2 Wireless sensor networks

Advances in electronics over the last couple of decades, including in the measurement, battery, and communications domains, have enabled measurement of environmental variables at higher temporal resolution (e.g. hourly) and for longer durations (e.g. 5 years or longer), with easier remote access to data for subsequent analysis and interpretation.

Internet of things (IoT) technology enables data to be transmitted from the field to a central storage medium, such as a cloud database, directly after measurement (IoT Technical Spectrum Working Group 2019).

These advances converge in the wireless sensor network (WSN). A WSN is a network of spatially dispersed sensor nodes that measure something (e.g. micro-indicators such as soil temperature and soil moisture) and transmit the measurements back to a central device called a gateway. A WSN is 'wireless' because communication between the sensors and the gateway is done over the air using radio signals. Sensor telemetry may be stored at the gateway or forwarded to a remote database.

Efficient radio communication between components of a WSN is a challenge, especially if the components are separated by hundreds or thousands of metres. In the early days there was little standardisation of technology, which meant that WSNs had to be designed from scratch. Creative solutions were often necessary, and included making use of domestic garage-door openers (Ekanayake 2021). This limited the practical size of WSNs to the order of 5 $km^2$. Nowadays communication between WSN components is standardised. WSNs fall under the umbrella of the IoT, a collection of frameworks and protocols that allow efficient wireless connection between electronic devices (IoT Technical Spectrum Working Group 2019).

One type of WSN is the so-called low-power wide-area network (LPWAN). LPWANs are designed to enable wireless communication at a low bit rate over long ranges. The low bit rate limits the type and volume of data that can be transmitted efficiently, such as a few numbers that encode a measurement and a timestamp. As a result, devices connected to the LPWAN consume little power because they may only need to be awake briefly to make a measurement and transmit associated data before returning to sleep. These characteristics make LPWANs attractive for use in environmental monitoring applications, where environmental sensors may only need to send small amounts of data a few times per hour.

## 1.3 Digital soil mapping

Since the early 1990s many authors (e.g. Odeh et al. 1994, 1995; Knotters et al. 1995; Bui et al. 1999; Lagacherie & Voltz 2000) have shown that soil properties measured at points in the landscape can be numerically related to other characteristics of the environment, such as elevation, slope, and aspect, in an approach that at one time was referred to as 'environmental correlation' (McKenzie & Ryan 1999). McBratney et al. (2003) collated the diverse efforts of previous decades and brought them under the umbrella of 'digital soil mapping'. They proposed the following framework:

$$S = f(s, c, o, r, p, a, n) + \epsilon$$

where soil classes or properties $S$ can be predicted as a mathematical function of factors, including other characteristics of the soil $(s)$, climate $(c)$, organic or biotic factors $(o)$, relief or topography $(r)$, soil parent material or lithology $(p)$, age $(a)$, and spatial position $(n)$. The function $f$ can be any mathematical model. The term $\epsilon$ is included to signify the error or residuals associated with prediction, which are often spatially autocorrelated. In models,

the scorpan factors are usually represented by proxies such as raster grids of rainfall or air temperature (representing $c$), maps of land use or remotely sensed derivatives ($o$), elevation and its derivatives ($r$), and so on. Collectively the proxies are often referred to as scorpan covariates.

Predictions are also usually made on a raster grid. The scorpan framework can be applied to spatially predict soil properties at any spatial scale, which is usually implicit in the spatial resolution of the raster grid. For example, for predicting soil at the farm scale we would usually target a spatial resolution in the order of 50 m or finer (e.g. Piikki & Söderström 2019). A much coarser resolution could see significant soil or terrain variability potentially occluded, which may be important to understand for farm or paddock scale management.

### 1.4 Objectives

In principle it should be possible to couple WSN-derived measurements of micro-indicators to the scorpan framework to make farm-scale spatial predictions. In practice cost constraints will limit the number of sensors that can be deployed, which will influence the quality of the modelling. One test of the results is the size of the numerical uncertainties (e.g. the standard errors) associated with the mapped predictions. If the uncertainties are too high, then the predictions may not be useful. They will certainly not be trustworthy.

The primary objective of this study is to determine whether we can map micro-indicators such as soil temperature and soil moisture at the farm scale. The secondary objective is to determine whether we can use predictions of the micro-indicators to model legume yield.

## 2 Methods

### 2.1 Study area

Our study area comprised 10 farms distributed across New Zealand hill country. These were grouped into six sites, as described in Table 1. Four sites were located in the North Island and two in the South Island (Figure 3). The sites ranged in area from 663 ha (Tourere) to 11,440 ha (Māhia). Some were located at sea level (Māhia, Prices Valley) and others in upland hill country (Mt Somers, Taihape). Tourere and Taihape have a high percentage of relatively low-relief terrain, whereas Prices Valley and Taumarunui were dominated by hilly and steep country. Some sites also hosted other activities in the wider Hill Country Futures project.

**Table 1. Wireless sensor network sites**

| Island | Site | Farms | Area (ha) | Min. elev. (m) | Relief (m)[a] | % easy[b] | % hilly[c] | % steep[d] |
|---|---|---|---|---|---|---|---|---|
| North Island | Māhia | Okepuha, Pongaroa Station, Taharoa Trust | 11,440 | 0 | 408 | 46.3 | 27.4 | 26.4 |
| | Taihape | Big Hill, Ohinewairua, Oruamatua | 10,094 | 436 | 767 | 60.1 | 25.6 | 14.3 |
| | Taumarunui | Paparata Farms | 3,583 | 118 | 437 | 37.1 | 33.9 | 29.0 |
| | Tourere | Watergreen | 663 | 143 | 185 | 84.2 | 14.7 | 1.1 |
| South Island | Mt Somers | Inverary | 4,328 | 444 | 925 | 42.6 | 30.9 | 26.4 |
| | Prices Valley | Willesden | 3,700 | 0 | 781 | 35.2 | 32.3 | 32.5 |

[a]Difference between maximum and minimum elevation at site; [b]percentage of site on 0–15° slopes; [c]percentage of site on 16–25° slopes; [d]percentage of site on slopes steeper than 25°. Slope classification is per Lilburne et al. 2012.

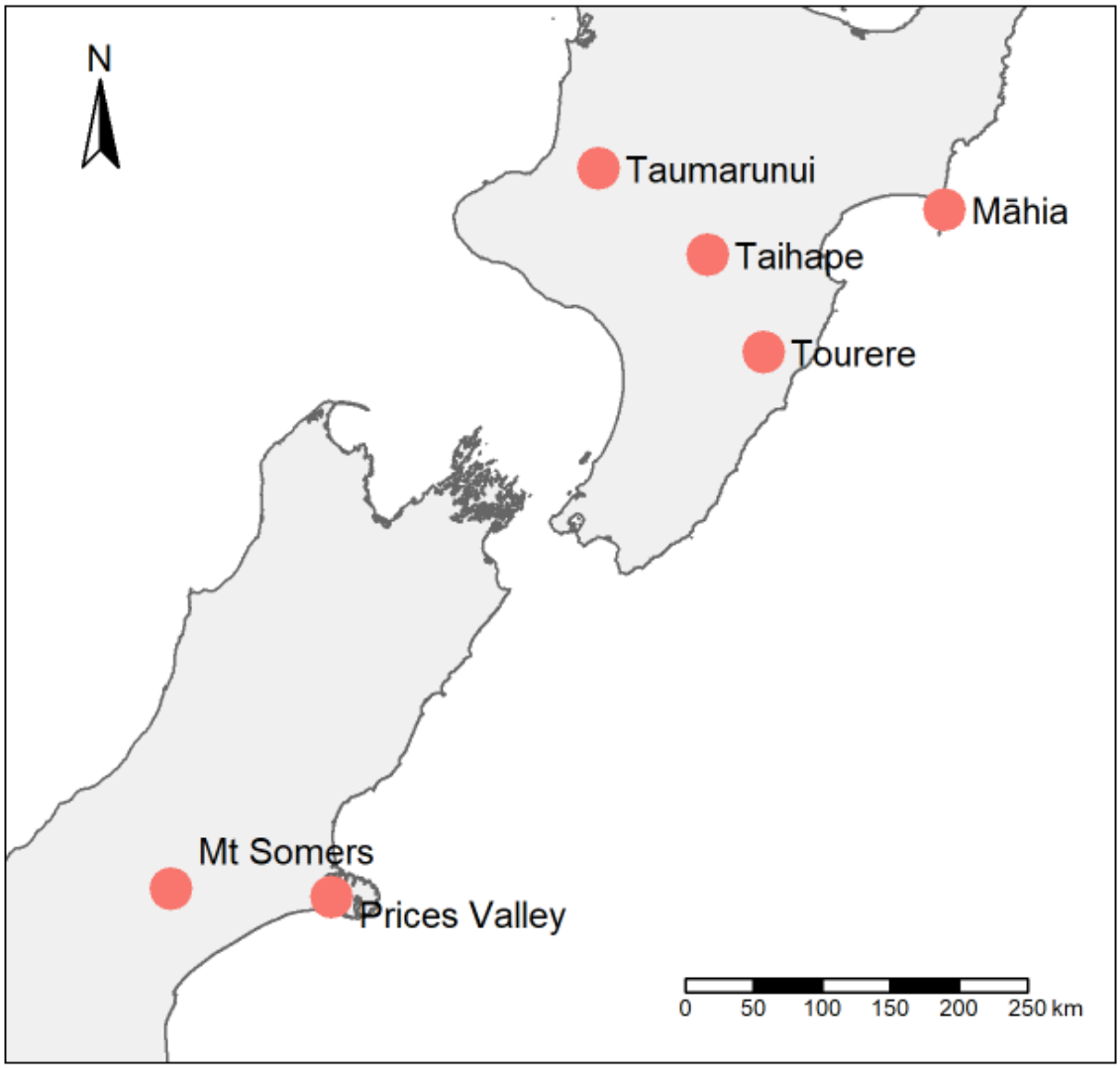


**Figure 3. Locations of the wireless sensor network sites.**

## 2.2 Sample site selection

We installed a WSN at each site. The amount of resources (cost for instrumentation, fieldwork, and monitoring) available for sampling was limited, so the choice of the number of locations within each site that could be sampled had to be fixed beforehand rather than selected through a formal statistical power analysis. The aim, then, was to determine the most effective layout of sensor nodes to sample each site, given the constraint of a fixed number of nodes, based on prior knowledge of the explanatory factors most likely to affect soil temperature and moisture.

We determined that each WSN would have a sampling allowance of 20 sensor nodes and that the locations of the nodes would be spatially distributed using a stratified random sampling approach. The stratification allows us to cover as much of the variability in perceived drivers of soil temperature and moisture at each site as possible, as represented by a small set of scorpan covariates. This should minimise the potential for extrapolation of the modelled soil temperature and moisture onto unsampled combinations of the covariates.

The scorpan covariates we used to stratify each site were elevation, aspect, and topographic wetness index (TWI; defined below). Given the small sampling budget, we combined elevation and slope aspect into a single variable so that it was only necessary to stratify across two variables. This meant we could maximise the number of replicates per stratum.

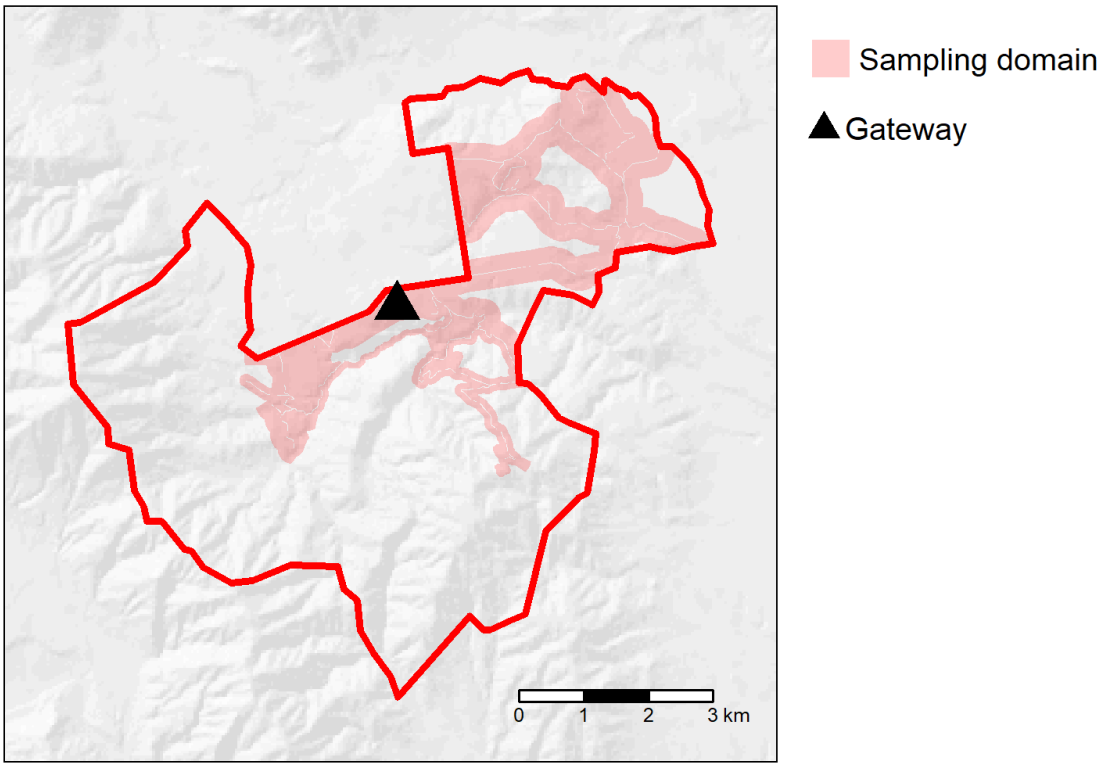


**Figure 4. Sampling domain and location of sensor network gateway at Mt Somers.**

The sampling domain was restricted to the parts of each site that were within a short distance from farm tracks (usually 250 m, but 100 m in steep landscapes) and that were within the viewshed of the WSN gateway. The sampling domain for Mt Somers is shown in Figure 4, but the sampling domains for the other sites are presented in the Appendix. The configuration of the track buffer represented a compromise between accessibility (with field equipment and WSN components) and coverage of the site. The viewshed restriction was to ensure sensor nodes had direct line-of-sight radio communication with the gateway.

Elevation (Figure 5) was chosen because there is a well-established negative correlation with soil temperature (Shreve 1924; Gloyne 1971; Schmidlin et al. 1983; Amundson et al. 1989). Soil moisture is less clearly correlated with elevation, and its distribution is more strongly driven by local or regional topographic factors.

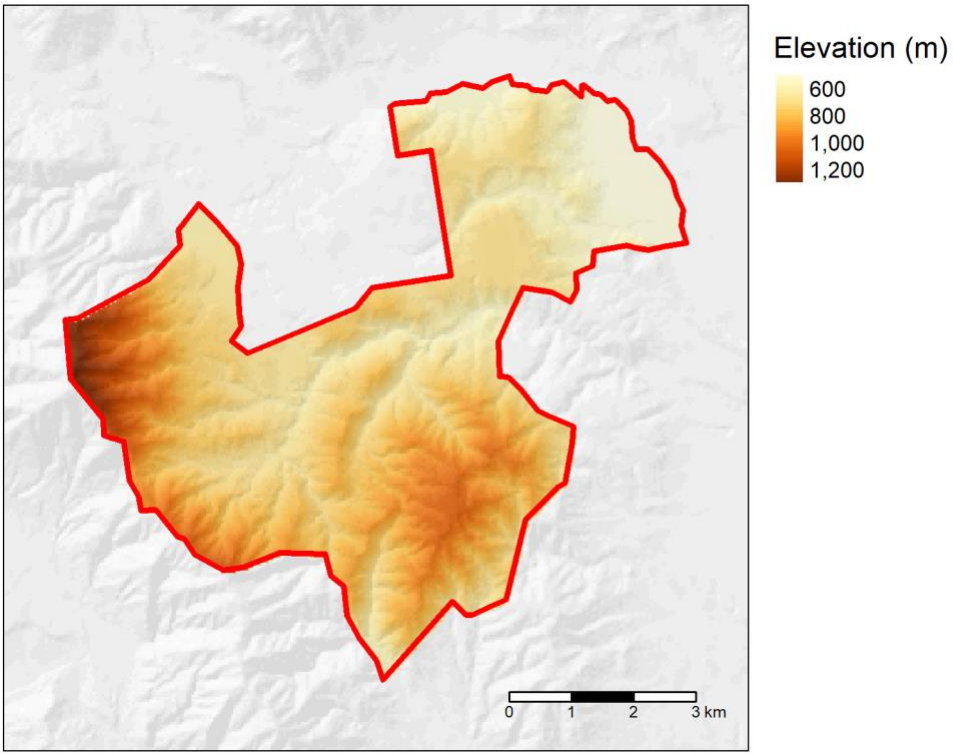


**Figure 5. Elevation at Mt Somers.**

Slope (Figure 6) and aspect (Figure 7) are key drivers of soil temperature and moisture dynamics via differences in the amount of insolation received from the sun (Pregitzer & King 2005). Slope is the steepness of a surface expressed as the angle of that surface to the horizontal. Aspect is the direction the surface faces, expressed as an angle relative to north, where 0° is north-facing, 90° is east-facing, 180° is south-facing and so on. Since aspect is measured on a circular scale, 360° is also north-facing.

In the southern hemisphere, south-facing slopes receive less direct insolation than north-facing slopes so they tend to be cooler and wetter (Sheath & Boom 1985). This has been demonstrated in New Zealand in a number of studies (e.g. Radcliffe & Lefever 1981; Radcliffe 1982; Gillingham et al. 1998).

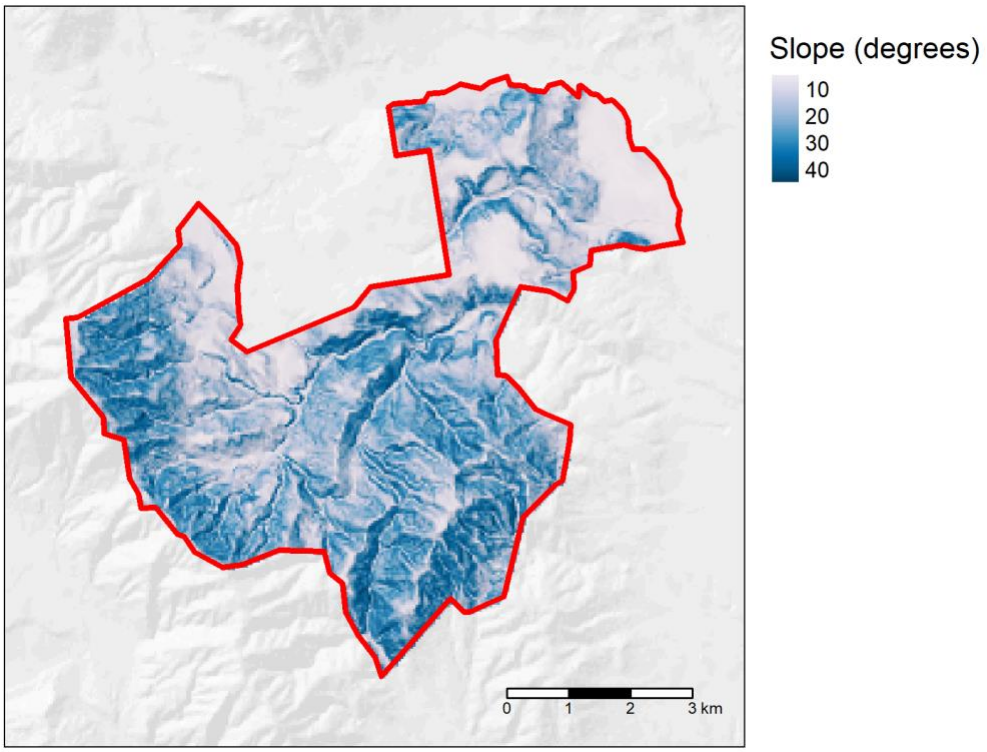


**Figure 6. Slope at Mt Somers.**

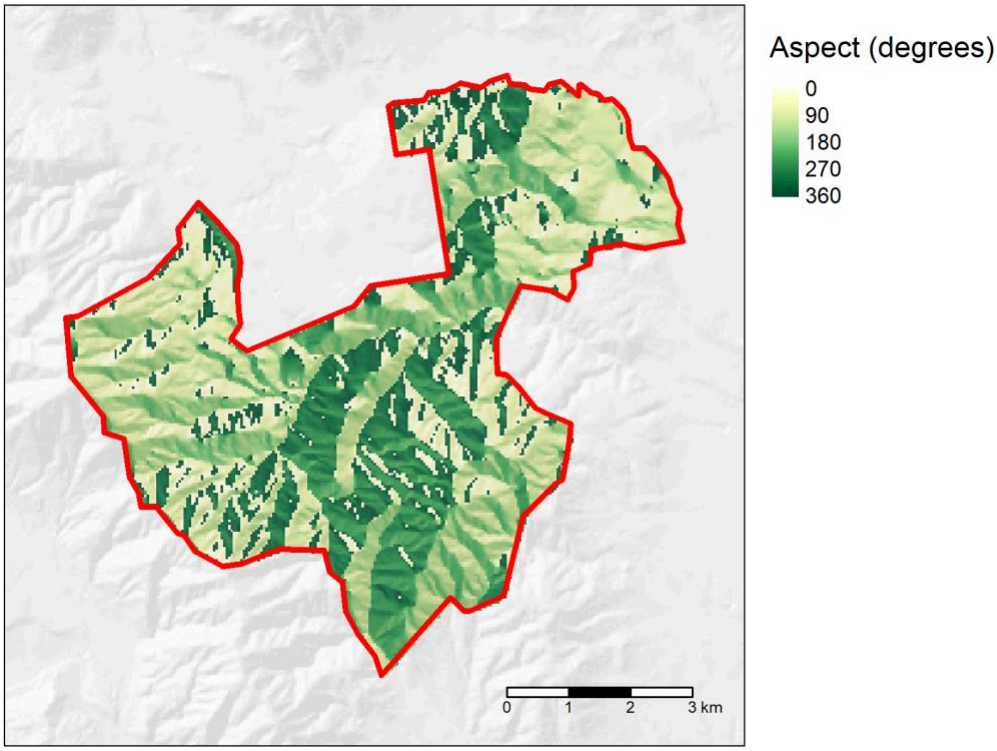


**Figure 7. Aspect at Mt Somers.**

Beven and Kirkby (1979) proposed the topographic wetness index (TWI; Figure 8) as a means of modelling the effect of variable contributing area and slope gradient on surface saturation and soil water content in a range of landscapes. The TWI is defined as:

$$\mathrm{TWI} = \ln\left(\frac{a}{\tan\beta}\right)$$

Where ln is the natural logarithm, $a$ is the specific catchment area ($m^2/m$) and $\beta$ is the slope gradient. The specific catchment area at a point in the landscape is the area of landscape drained per unit contour length. In general, larger values of TWI are supposed to indicate parts of the landscape where water is more likely to accumulate. These are typically areas of steep, concave topography where water is more likely to converge, and low-gradient landscapes, where water is likely to accumulate because of the low hydraulic gradient (Burt & Butcher 1985). We thought it might be useful for predicting soil moisture if spatial variation in TWI were captured in the sampling design. We note, however, that judging by the literature its usefulness as a predictor has been mixed (Western et al. 1999).

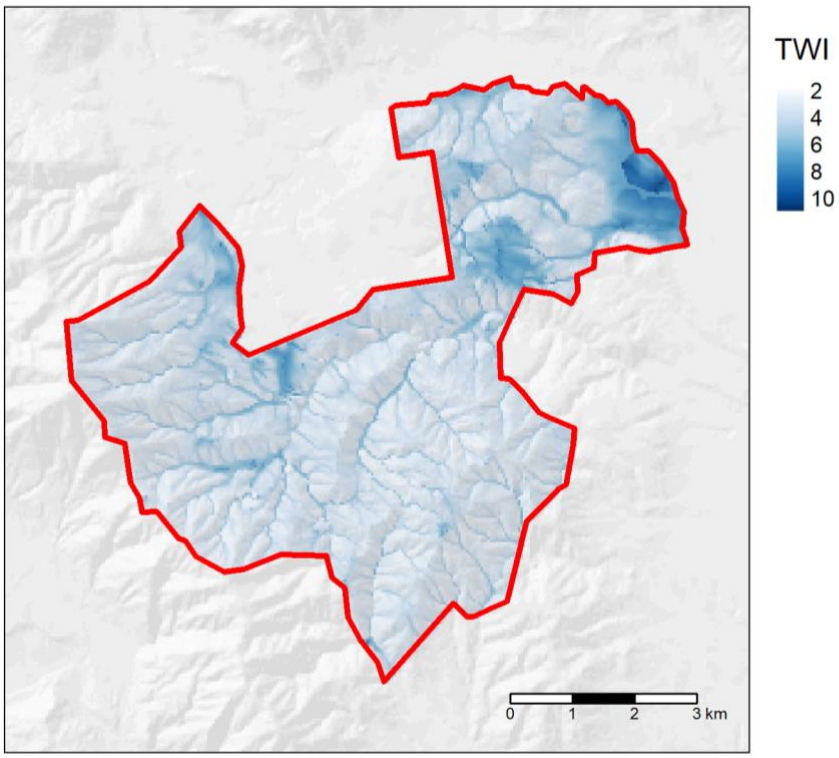


**Figure 8. Topographic wetness index at Mt Somers.**

We used our previous experience with soil temperature and moisture modelling (Barringer 1997; Barringer & Lilburne 2000) to devise a method to combine elevation and aspect into a single variable (herein called 'elasp'; Figure 9). The aim was to devise a variable that correlated with soil temperature, so that by sampling along this variable one would expect to sample the expected range of soil temperature values. We devised the following relationship.

$$\text{elasp} = \frac{\text{elevation}}{900} \cdot 2 + \frac{\text{aspect}}{180} \cdot \frac{\text{slope}}{12}$$

Elevation (in metres) is divided by 900 because it is unlikely that legumes would be sown any higher than 900 m. It is multiplied by 2 because previous work (Barringer 1997; Barringer & Lilburne 2000) had suggested the elevation effect was about twice as strong as aspect, and the slope effect was weaker again. Slope gradient was pre-treated by setting slopes less than 12° to 12°. It is divided by 12 to recognise that the effect of slope decreases as slope gradient decreases. Aspect is divided by 180 to reduce the size of the effect, and it is multiplied by slope gradient to reduce the effect of aspect on shallow slopes.

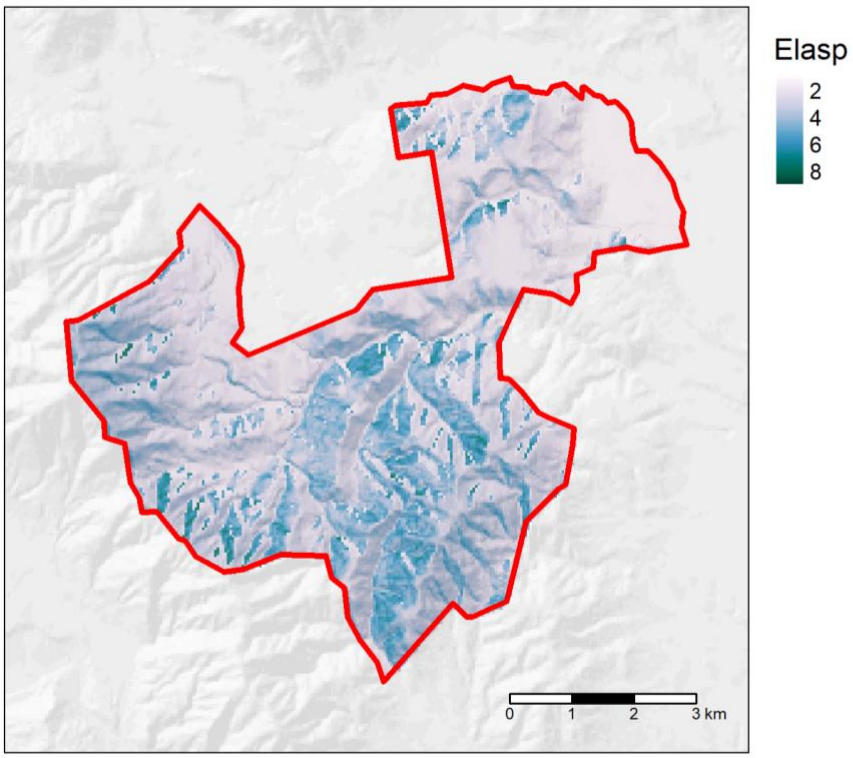


**Figure 9. Combined elevation-aspect covariate (elasp) at Mt Somers.**

The first step in the sampling analysis was to carry out a principal components analysis on the TWI and elasp rasters. Figure 10 shows a plot of the variance of the two principal components. The majority (102.7 times the variance of the second principal component) of the variance is explained by the first principal component (Figure 10). This suggests that the first principal component from the TWI and elasp could be used as the basis of the sampling.

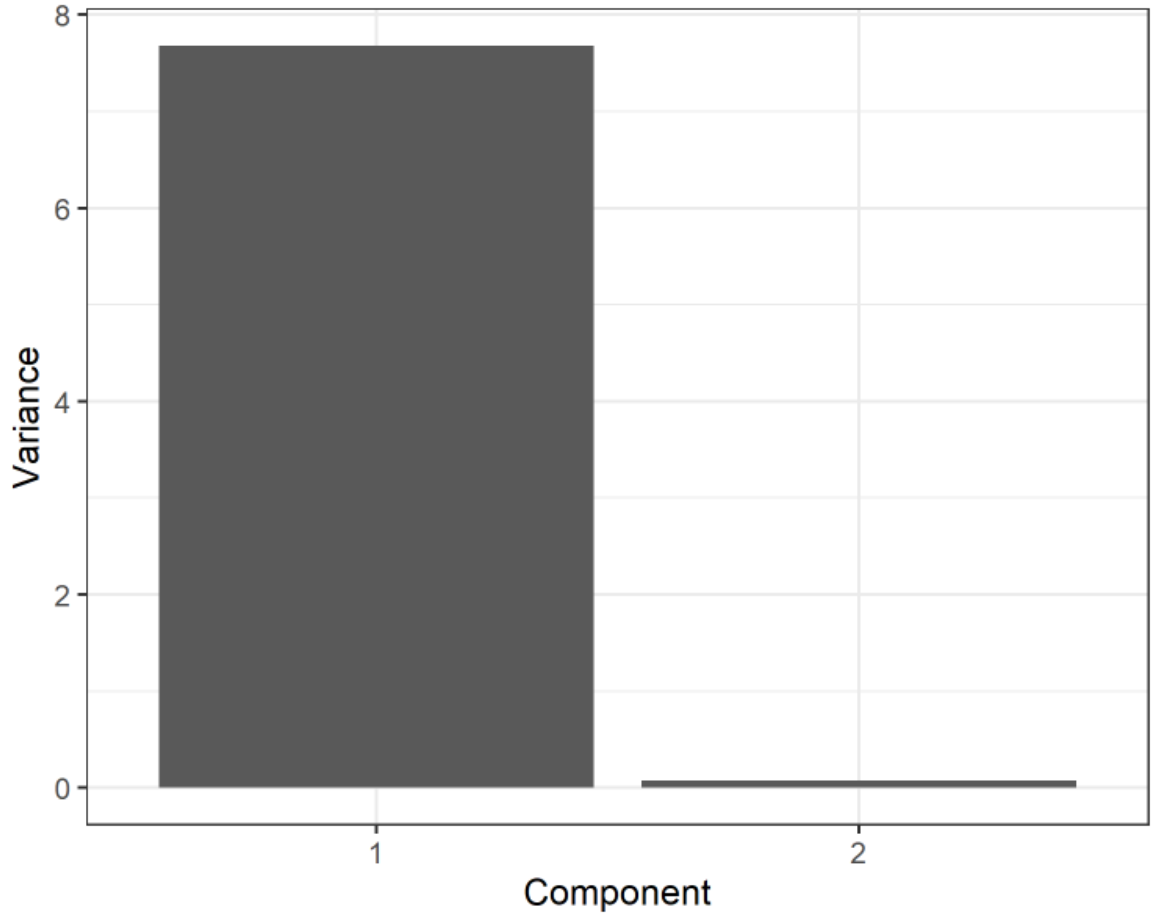


**Figure 10. Variances of the principal components of elasp and topographic wetness index at Mt Somers.**

The approach we used was to split the image of the first principal component into $N$ strata based on quantiles (Figure 11), and then each stratum is sampled based on some spatial sampling method. Using $N = 5$ strata with a total sample allowance of 20 means there were four replicate sensor nodes in each stratum. It would be desirable if these replicates were spread spatially across the stratum.

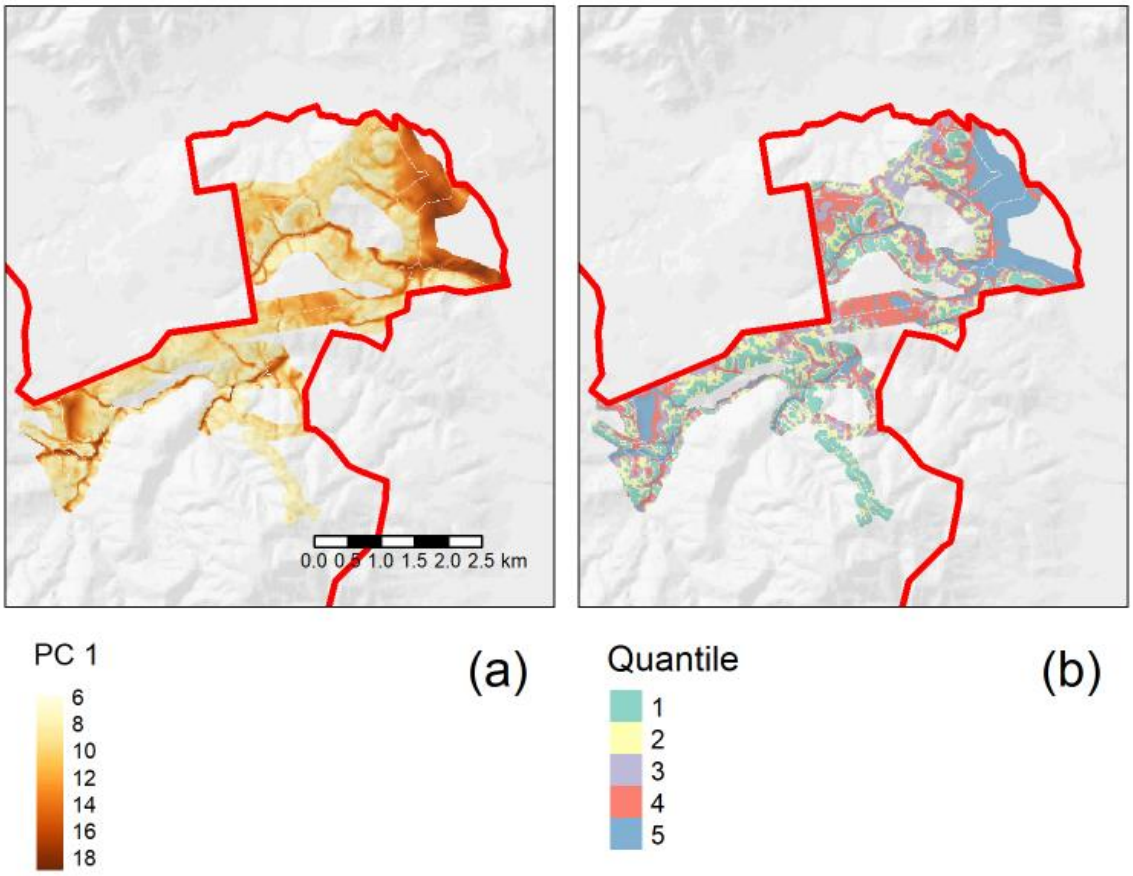


**Figure 11. Images of (a) principle component 1 and (b) the quantile cut for Mt Somers.**

One could use any one of many spatial sampling methods to distribute the sensor nodes within strata (Gruijter et al. 2006); the simplest of these would be simple random sampling. We chose to use balanced acceptance sampling (Robertson et al. 2013) for this analysis because it provides good spatial balancing within a stratum. To allow for the situation where proposed sampling points land on places where it is impossible to sample (e.g. on a building, tree, fenceline or track), we gathered five sets of 20 points so that there were plenty of alternatives if one of the sets was unsuitable.

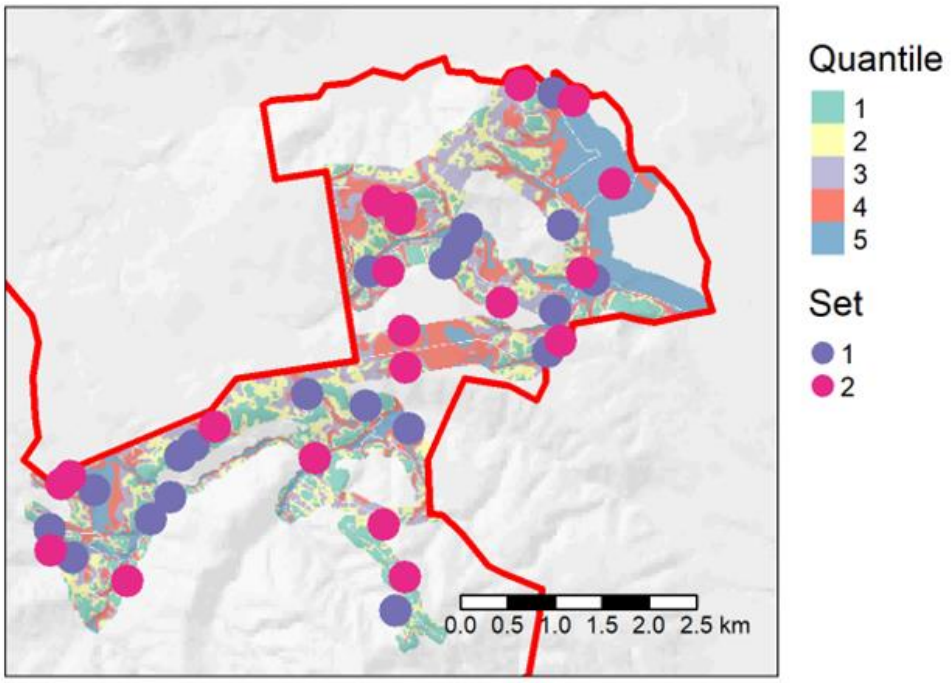


**Figure 12. Image of the Mt Somers site split into five strata based on quantiles. Plotted points are the four points selected in each or the strata. Two sets of spatially balanced points are shown.**

Figure 12 shows an image of the quantiles from the first principal component, overlaid by two sets of spatially balanced points. The points in the second (or another) set would be used if any of the points from the first set fell in inaccessible locations. Although replacing an inaccessible point disturbs the spatial balancing of the data, the result is still a random set of samples, with the same required number in each stratum. Of course, if too many of the points in a set needed replacing, it might be better to start again and use a new set. The important principle is to have the points selected by random selection, with an equal probability of every location within each stratum being selected.

A crucial assumption that underpins the success of the sampling method is that the sampling can be carried out by cutting the first principal component of the TWI and elasp rasters using quantiles, and that the first principal component is strongly dominant. If this is not the case, sampling across this principal component would not cover the range of values in the two covariate images. Table 2 gives the ratio of the variance of the first to the second principal component. In all cases, the assumption appears to be reasonable.

**Table 2. Ratio of the variance of the first to the second principal component for each site**

| Site | Variance ratio |
|---|---|
| Māhia | 105.43 |
| Mt Somers | 102.71 |
| Prices Valley | 43.07 |
| Taihape | 12.42 |
| Taumarunui | 39.11 |
| Tourere | 84.26 |

## 2.3 Wireless sensor networks

### 2.3.1 Design

The LoRa Alliance maintains standards related to one popular type of LPWAN (LoRa Alliance Technical Marketing Workgroup 2015), and we designed our WSNs to these standards. The two key components of the LoRa Alliance standard are the LoRaWAN specification, which defines the software and associated protocols that allow components to communicate with each other using a common language (the network protocol); and the LoRa specification, which defines the physical radio hardware that uses the common language to communicate between components.

Each sensor node is controlled by an Atmel SAM D21 microcontroller unit (MCU). One of the advantages of using the Atmel MCU is that it has a 32-bit ARM® Cortex® central processing unit, which is compatible with the popular Arduino integrated development environment.[4] This makes it relatively easy to write and compile the software that runs on the Atmel MCU. Each sensor node is equipped with an RFM95 LoRa transceiver module, which enables radio communication with the WSN gateway (Figure 13). The nodes are powered by two 3.6 V lithium-thionyl chloride batteries, which should be sufficient to provide a 5–10-year service life.

[4] https://www.arduino.cc

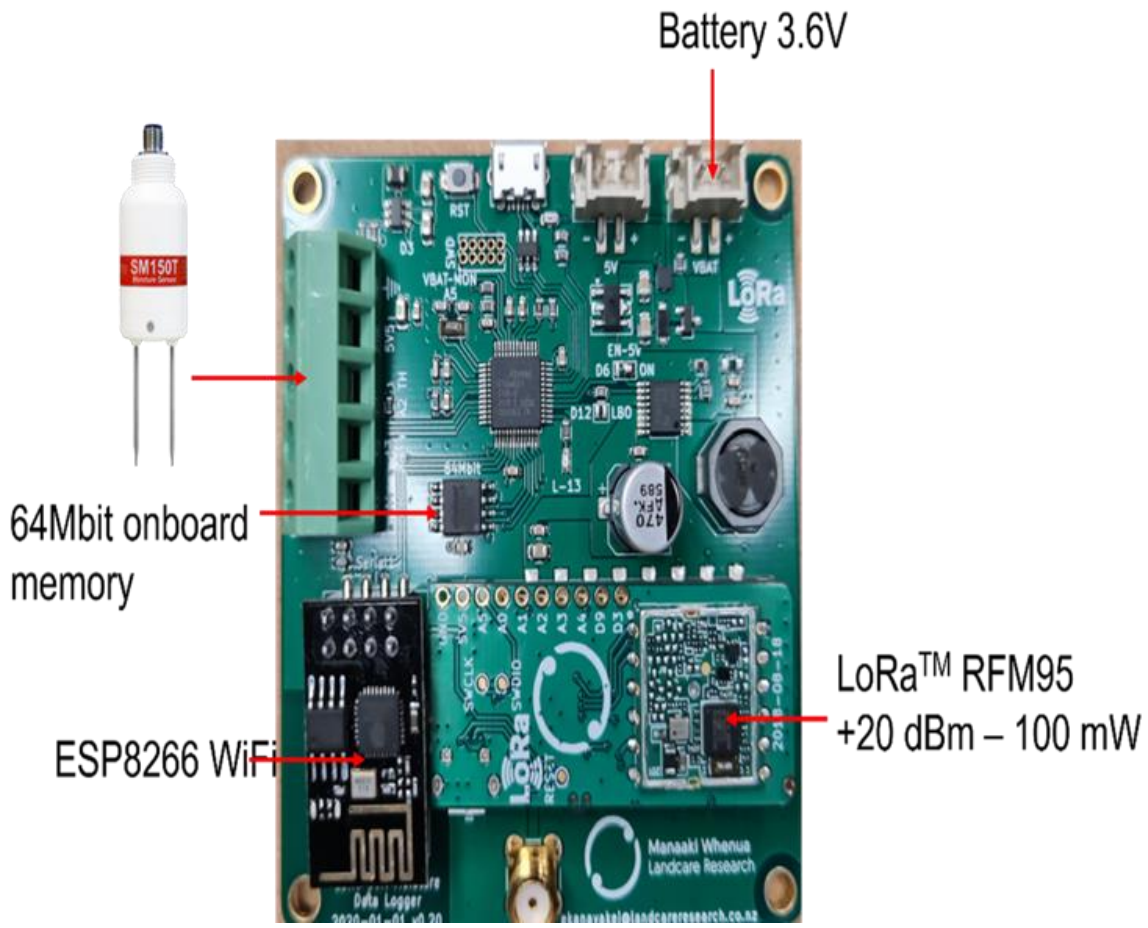


**Figure 13. The circuit board that controls the WSN gateway, showing important components. Electronics at each sensor node are similar but omit the ESP8266 WiFi controller.**

The WSN gateways are equipped with the same electronics as the sensor nodes (Figure 13). They are also equipped with an ESP8266 WiFi module to connect to a cellular modem that enables communication with the outside world, and a remote-reset device that makes it possible to reboot the gateway via the cellular network if necessary. Each gateway is powered by a 100 Ah sealed lead acid battery with 80 W photovoltaic backup (Figure 14).

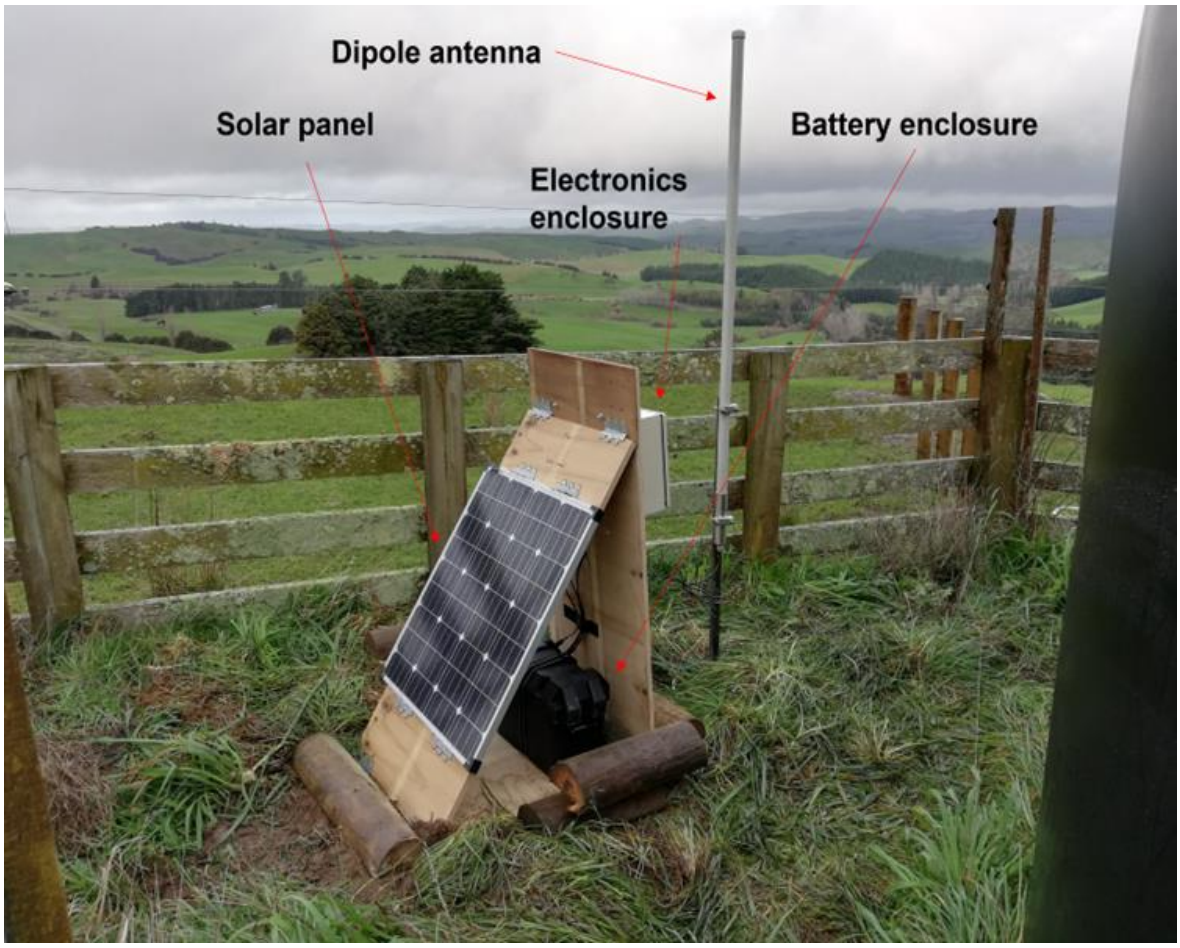


**Figure 14. Tourere WSN gateway with major components labelled.**

The sensors themselves are SM150T soil moisture sensors manufactured by Delta-T Devices in the United Kingdom.[5] We selected these sensors based on our favourable experience with an earlier model (e.g. Hedley et al. 2013; Ekanayake & Hedley 2018), and because they also measure soil temperature. This allowed us to minimise the amount of electronics we had to install in the ground.

The soil moisture values are derived from the calibration equation supplied by the sensor manufacturer to relate the raw sensor measurements to volumetric moisture content. As such, the measurements are strictly relative. It was deemed impractical to calibrate each sensor to soil conditions at each node at installation, but addressing this issue could be a focus of future work.

[5] https://delta-t.co.uk/product/sm150t/

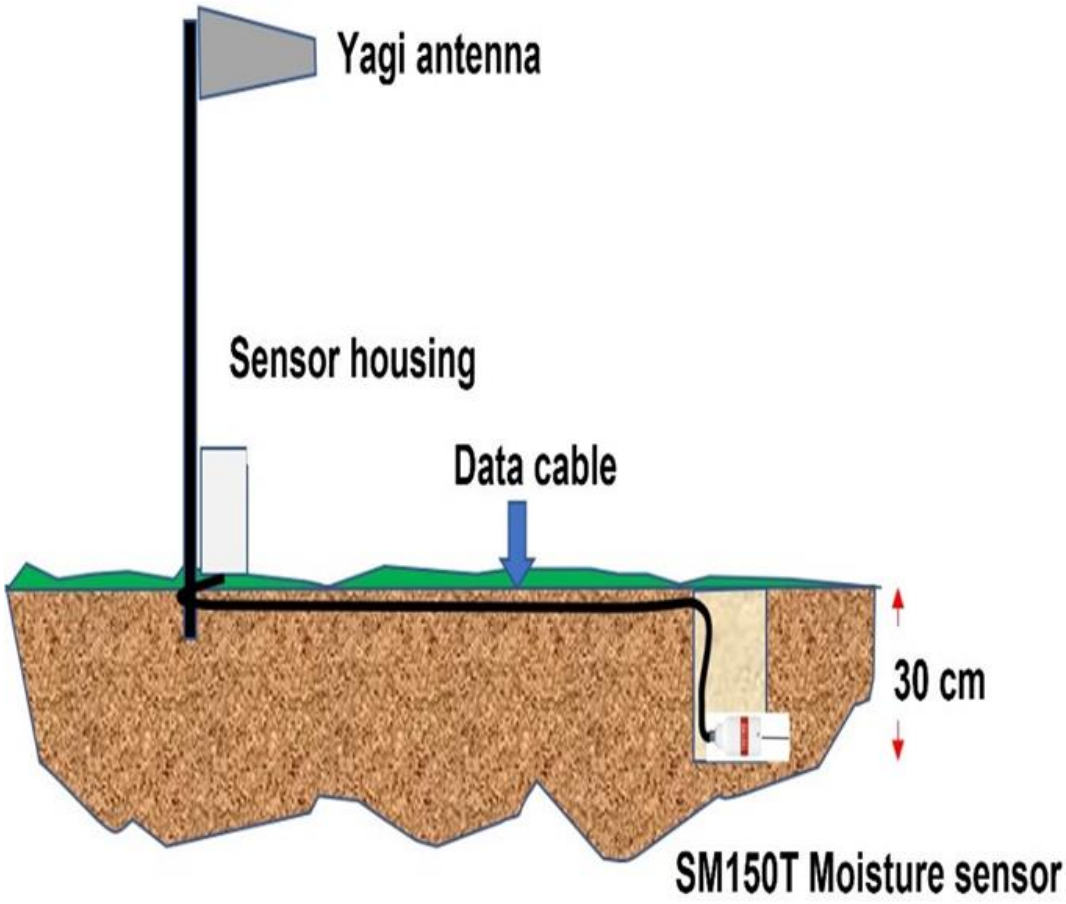


**Figure 15. Schematic representation of how sensor nodes are set up in the field.**

The sensor nodes are each equipped with a single, directional, high-gain Yagi antenna to send and receive the LoRa radio signals between the node and the gateway (Figure 15). The antenna is directional because the gateway is located at a fixed, known azimuth from true north, relative to each sensor node. On the other hand, the gateways are each equipped with a single, omnidirectional, low-power dipole antenna (Figure 14). The gateways require an omnidirectional antenna because they must communicate with 20 sensor nodes that are located at different azimuths relative to the gateway. Due to the nature of the different types of antennae, communication from the sensor node to the gateway is often more reliable than communication from the gateway to the sensor nodes.

The software running on the Atmel MCUs is written in Arduino's C-like language. The nodes are programmed to measure the soil temperature, soil moisture, and battery voltage once per hour, and to transmit the measurements to the gateway. Each hour the gateway is programmed to receive the hour's data from all sensor nodes and send it to the cloud storage in one transmission.

### 2.3.2 Assembly and installation

Assembly of the sensor nodes coincided with New Zealand's first nationwide lockdown of the Covid-19 pandemic in March and April 2020, and notably took place in J. Ekanayake's home living room (see Figure 16, MWLR 2020 and Young 2020). The WSNs were installed in the field over several months in the middle of 2020 (Table 3).

**Table 3. Installation periods for the WSNs**

| Site | Installation period |
|---|---|
| Māhia | September 2020 |
| Mt Somers | July 2020 |
| Prices Valley | June and August 2020 |
| Taihape | June 2020 |
| Taumarunui | August 2020 |
| Tourere | July 2020 |

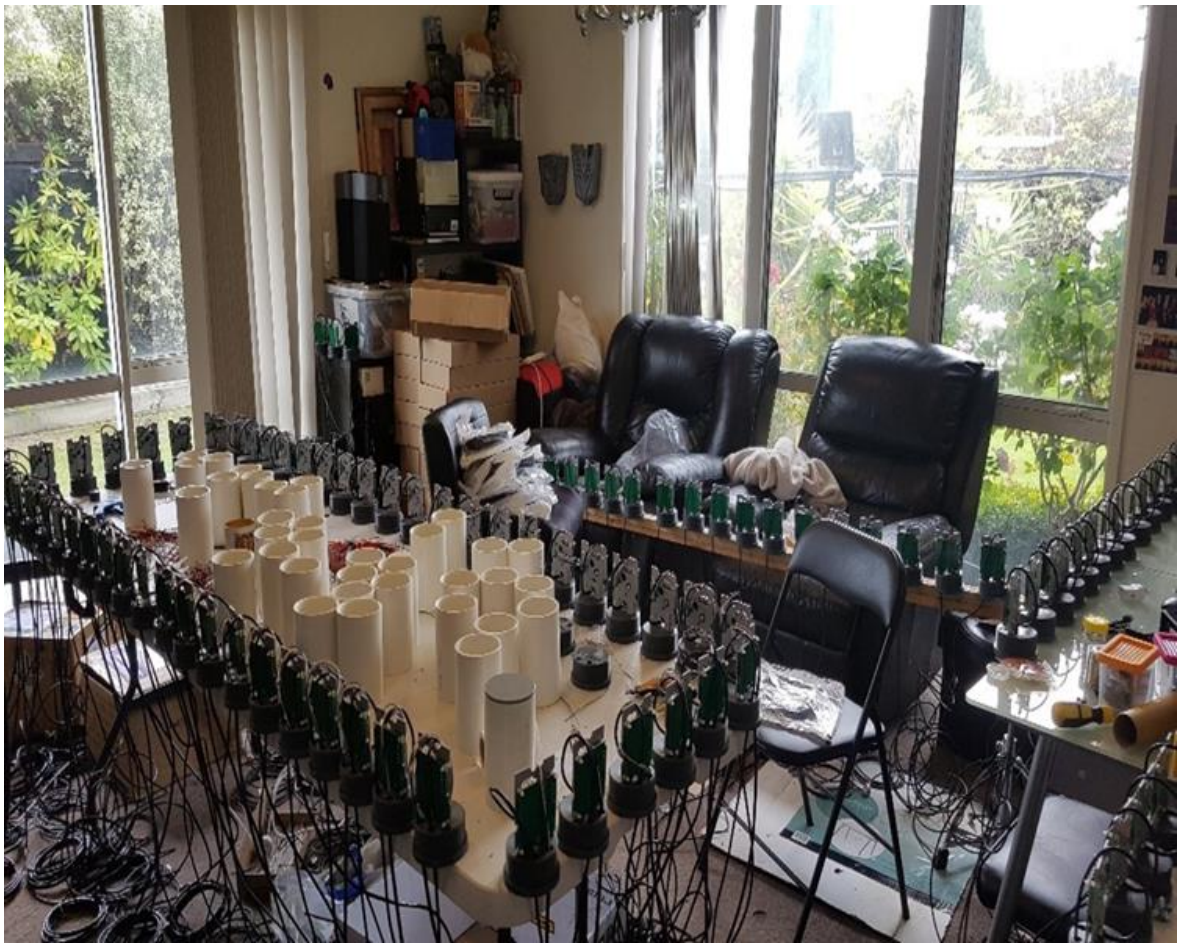

**Figure 16. Assembly of the sensor nodes in J. Ekanayake's living room during Covid-19 lockdown.**

At each sensor node, the electronics enclosure and Yagi antenna were mounted on a steel fencepost that was driven vertically into the ground. The sensors were installed about 3 m upslope at a depth of 30 cm, with the two electrodes oriented horizontally with respect to each other and at 90° from vertical (Figure 15). The installation hole was backfilled to the surface with the original soil material. On steep slopes, the steel post holding the electronics was enclosed by four steel posts and barbed wire (Figure 17), and we took advantage of the farms' electric fencing where possible. On flatter areas we used timber post-and-rail fencing.

**Figure 17. A sensor node at Prices Valley.**

At each site the gateway was sited on the hilltop that afforded the maximum visibility of the site to ensure radio communication with the sensor nodes was as good as possible, and to ensure good cellular network coverage.

Sampling locations at Mt Somers are presented in Figure 18. Maps of sampling locations at the other sites are presented in the Appendix.

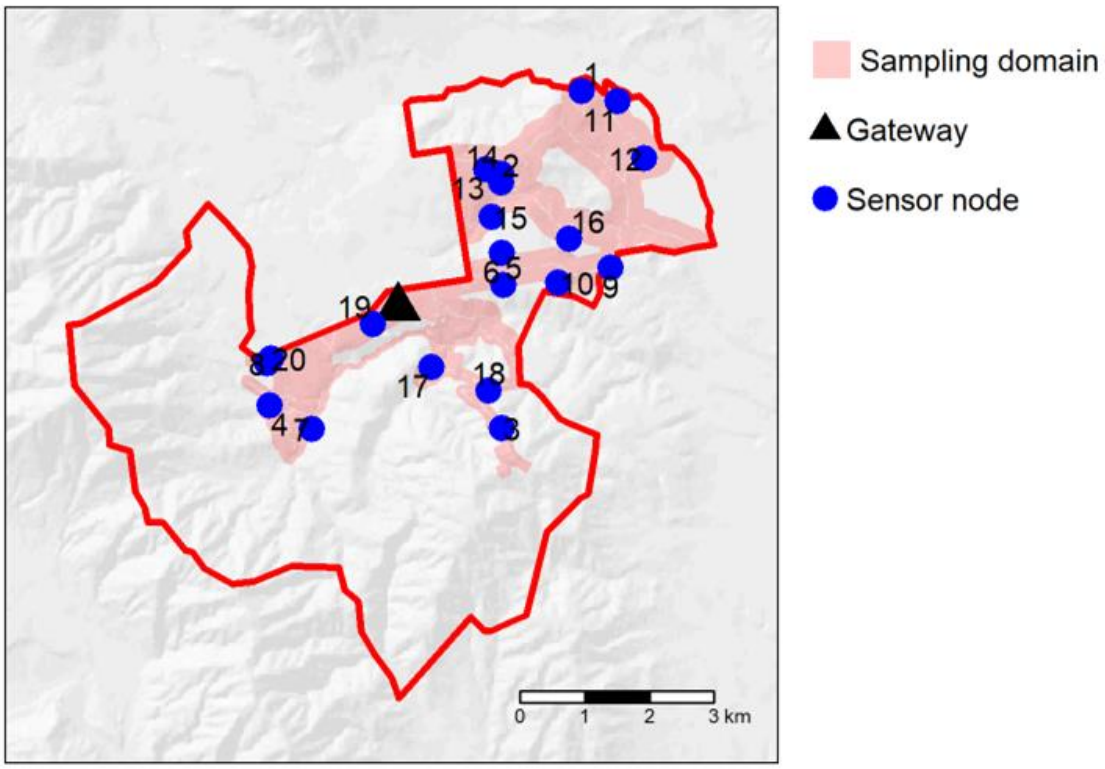


**Figure 18. Location of sampling domain, WSN gateway, and sensor nodes at Mt Somers.**

## 2.4 Data management and analysis

### 2.4.1 Soil temperature

Here we take a brief look at some characteristics of the WSN telemetry that informed the approach we took to model it. Results and interpretation of the telemetry itself are described in later sections.

Figure 19 shows plots of the difference in time between successive measurements, grouped by site and sensor node (note that the y-scale is log-transformed). The plot essentially shows the temporal sampling interval for the data. Sampling rates as high as one measurement per second can be seen, but the majority of sampling is approximately at hourly intervals.

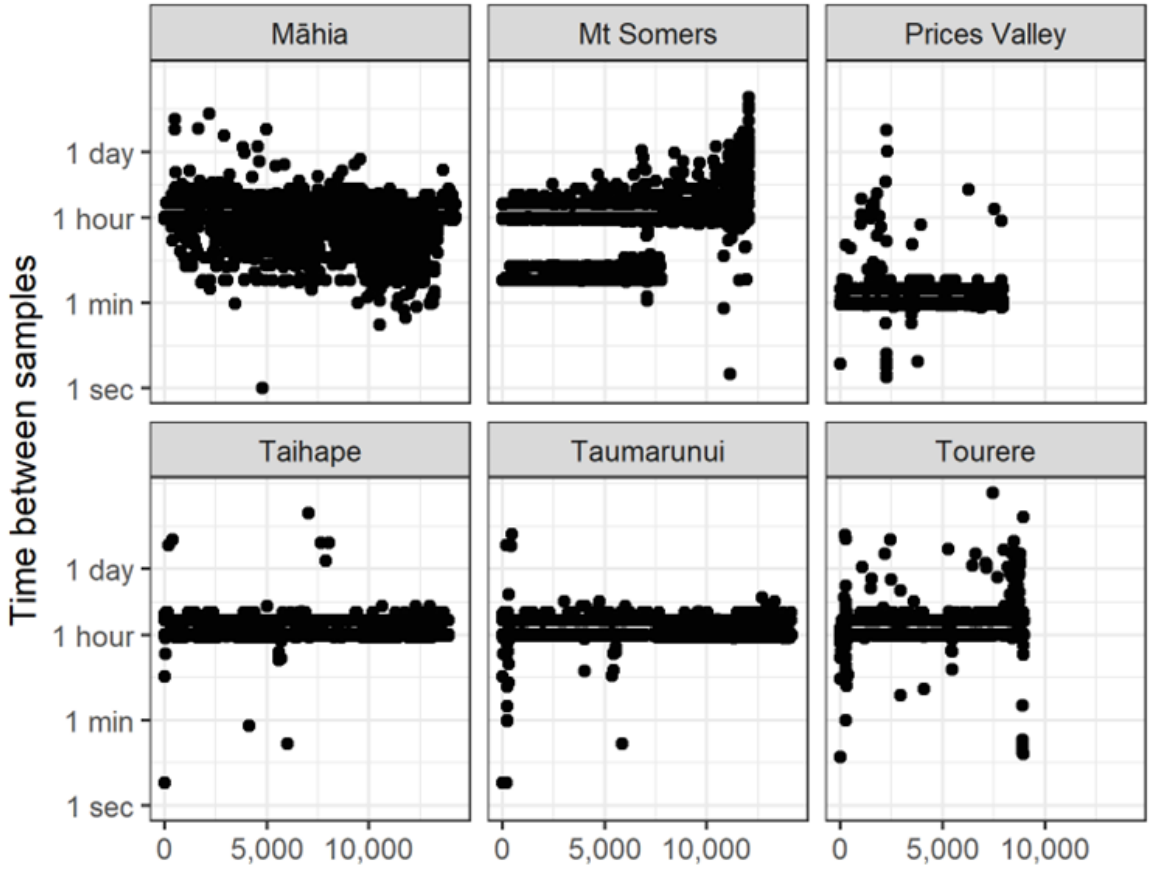


**Figure 19. Distribution of the difference in time between sorted samples across all wireless sensor networks.**

It is difficult to treat the data as a strict time series because the sampling interval varies widely, so some level of temporal aggregation is an obvious step. Figure 19 suggests aggregation to at least hourly data, and daily data are probably more convenient.

Figure 20 shows a plot of soil temperatures from Mt Somers after restricting the data to temperatures in the range –5 to 30°C to exclude implausible values. A seasonal pattern is evident, but there are several artefacts, including:

1 some periods where the temperature does not change over time, due to malfunctioning electronics

2 temperature values outside the expected range.

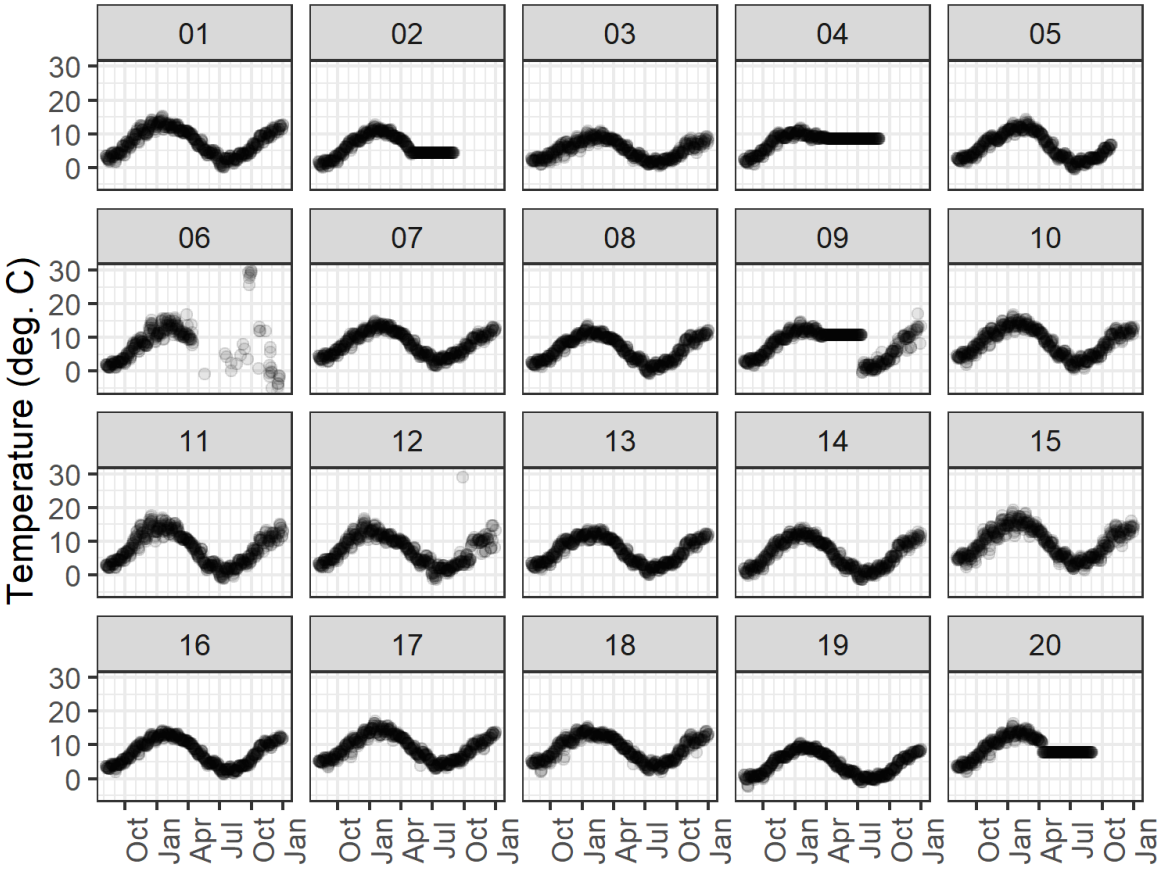


**Figure 20. Raw soil temperature for the Mt Somers WSN, with soil temperatures limited to the range –5 to 30°C. Panel labels indicate the relevant sensor node.**

The above artefacts most likely represent periods when the sensors failed, and in these cases it makes sense to remove these data. The data are also sampled hourly, which for this analysis is arguably too much data. To make the analysis simpler, the following transformations were carried out (in order).

1 Data were removed if they were outside the range –5 to 30°C.

2 Data were restricted to a window date and time to avoid spurious temperatures associated with transport and installation.

3 Data were removed if the temperature difference between samplings was precisely zero.

4 Data were removed if the number of samples within a day was less than 15.

5 The maximum, minimum, median, and standard deviation temperature were calculated for each date.

Transformation 1 retains soil temperature data that are inside the plausible range given the sampling depth. Transformation 2 removes data that were recorded after the gateway was commissioned but before sensor nodes were installed in the field. Transformation 3 accounts for malfunctioning sensor nodes. Transformation 4 allows for stable daily summary statistics of the soil temperature data.

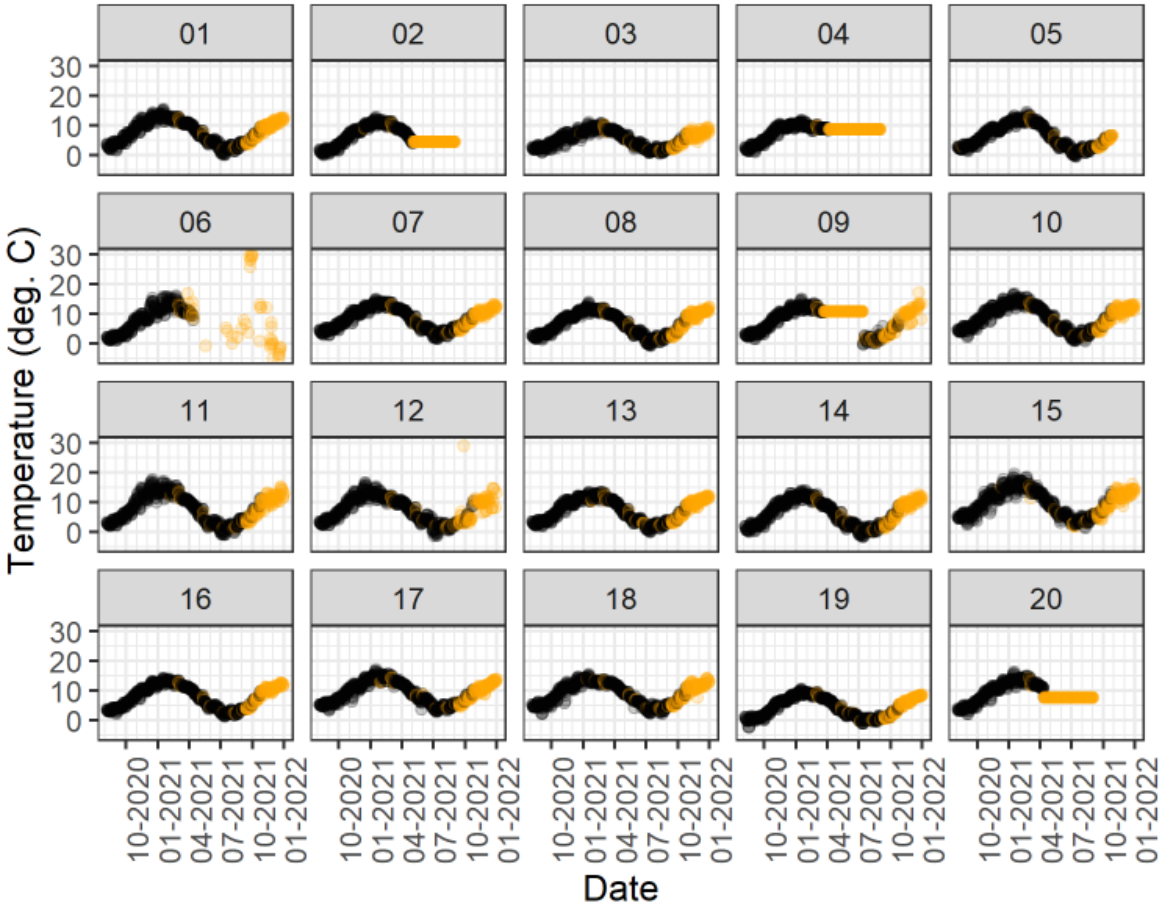


**Figure 21. Daily median soil temperature data for the Mt Somers WSN after trimming the start and end dates, and removal of low and high temperatures and periods of no change in soil temperature. Panel labels indicate the respective sensor node. Points that were removed as a result of the data trimming are shown in orange, while presumed valid points are in black.**

Figure 21 shows a plot of median soil temperatures for each date from Mt Somers after processing the data in the above manner. Plots for the other sites are presented in the Appendix. The problematic regions of data are now missing, and the trends are clearer. Extending the above analysis to other sites requires identifying the dates during which the data are valid. All sites were well behaved in terms of start and end date, except for Mt Somers, which required trimming.

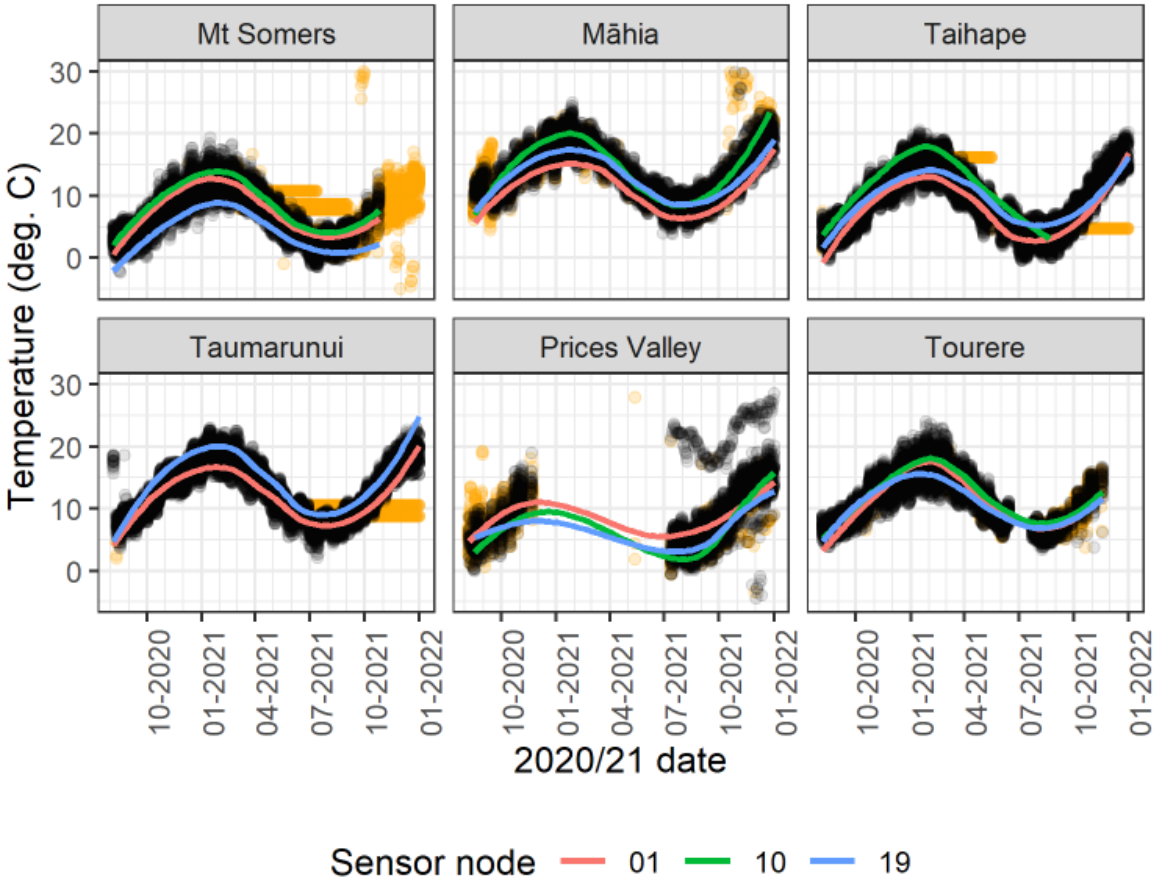


**Figure 22. Daily median soil temperature data for all sites after trimming of the start and end dates, removal of small and large temperatures, and periods of no change in soil temperature. Locally estimated scatterplot smoothing (LOESS) lines are drawn through data for sensor nodes 1, 10, and 19 for each site. Points that have been excised from the data are shown in orange.**

Figure 22 shows daily median soil temperature data for all sites after applying the processing steps, with locally estimated scatterplot smoothing (LOESS) lines (Cleveland 1979; Cleveland & Devlin 1988) drawn through the data for nodes 1, 10, and 19, and with points removed from the data set indicated in orange. The filtered data appear to be as expected and suitable for analysis. Most importantly, the points that have been removed appear to be true outliers.

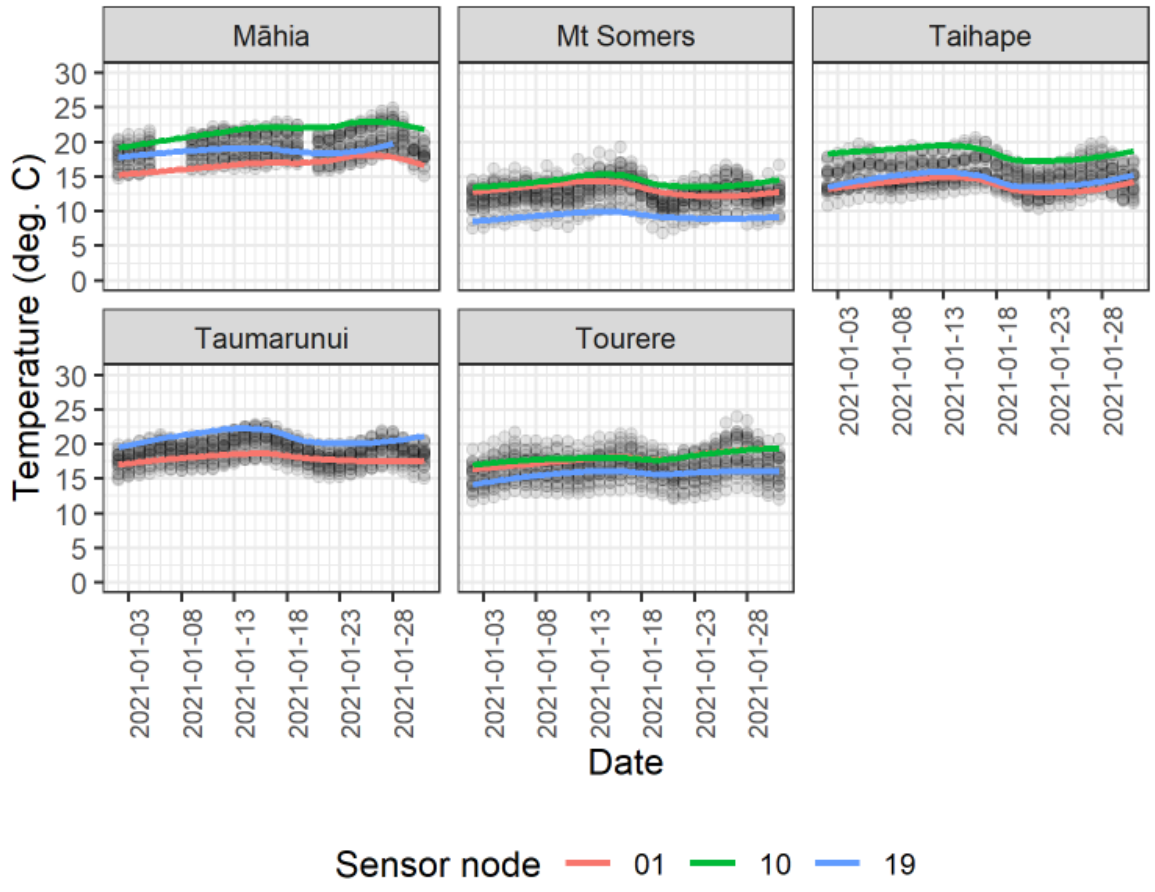


**Figure 23. Daily median soil temperature data for all sites for January 2021, to show fine temporal-scale behaviour. For a given day of January, each point corresponds to one sensor node. Prices Valley is not shown because there is no data from that site for January 2021.**

Figure 23 shows a plot like Figure 22, but only for the month of January 2021, to show the nature of fine temporal-scale behaviour (if any). There is some variation (the graphs suggested a period of about 10 days[6]), but it is minor. The fine temporal-scale behaviour is important in the construction of a model for soil temperature and moisture to properly characterise the uncertainty of predictions.

### 2.4.2 Soil moisture

Figure 24 shows a plot of soil moisture from Mt Somers after restricting the data to values in the range 0 to 100% (the possible range of values). A seasonal pattern is not very clear in this case and there are several artefacts, including:

- a short period at the start of the record where there are spurious moisture values
- some periods where the moisture does not change over time.

[6] A 10-day cycle is frequently seen in temperature and atmospheric data in New Zealand, although it is surprising to see it expressed in soil temperature data.

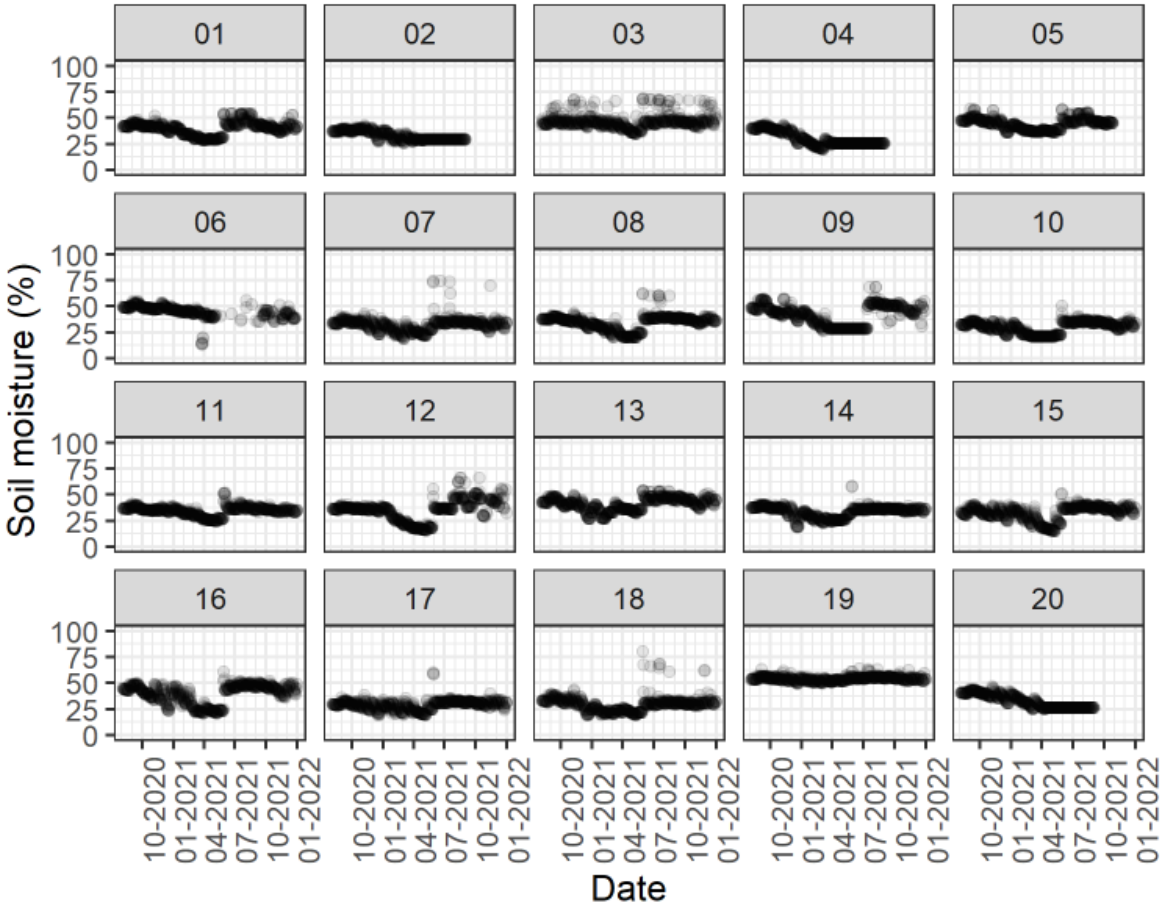


**Figure 24. Raw soil moisture data for the Mt Somers site. Panel labels indicate the respective sensor node.**

As we did for soil temperature, the following transformations were carried out (in order) on the soil moisture data to remove the artefacts.

1 Data were removed if they were outside the range 0 to 100%.

2 Data were restricted to a window date and time to avoid spurious soil moisture values.

3 Data were removed if the soil moisture difference between samplings was precisely zero.

4 Data were removed if the number of samples within a day was less than 15.

5 The maximum, minimum, median, and standard deviation of the soil moisture were calculated for each date.

Transformation 1 retains soil moisture data that are within the expected range for volumetric soil moisture. Transformation 2 removes data that were recorded after the gateway was commissioned but before sensor nodes were installed in the field. Transformation 3 accounts for malfunctioning sensor nodes. Transformation 4 allows for stable daily summary statistics of the soil moisture data.

Figure 25 shows a plot of median site soil moisture for each date from Mt Somers after processing the data in the above manner. Plots for the other sites are presented in the Appendix. The problematic regions of data are now missing, and the trends are somewhat clearer (although not necessarily as clear as for soil temperature). Figure 26 shows median soil moisture data for all sites after processing, as before, with LOESS lines drawn through data for sensor nodes 1, 10, and 20 for each site, and with points that were excised from the data set filled-in in orange.

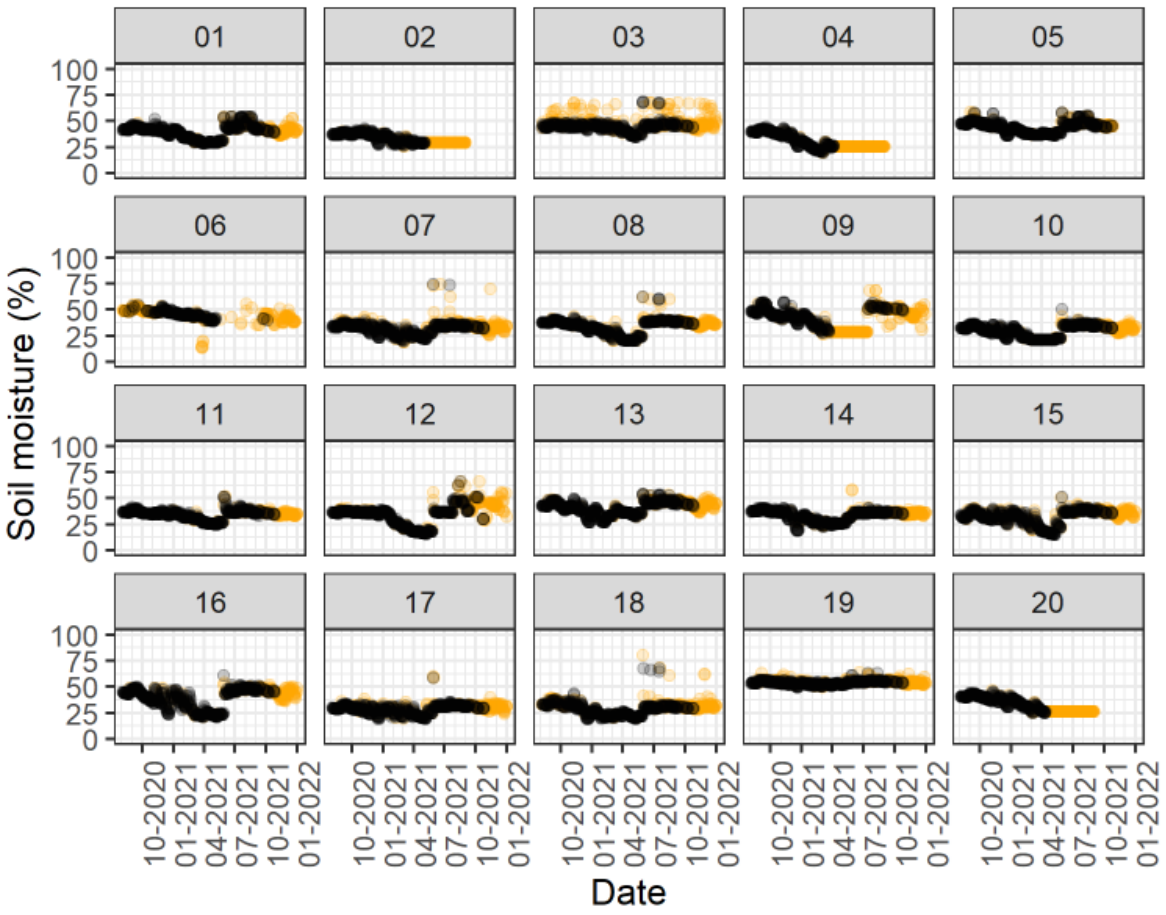


**Figure 25. Daily median soil moisture data for the Mt Somers site after trimming of the start and end dates, removal of low and high soil moisture values, and periods of no change in soil moisture. Panel labels indicate the respective sensor node. Points excised from the data are shown in orange.**

The filtered data appear to be reasonably well behaved and suitable for analysis. Most importantly, the points that have been excised appear to be true outliers. The trend is for a minimum soil moisture some time in February or March, and a maximum in July or August, much as expected.

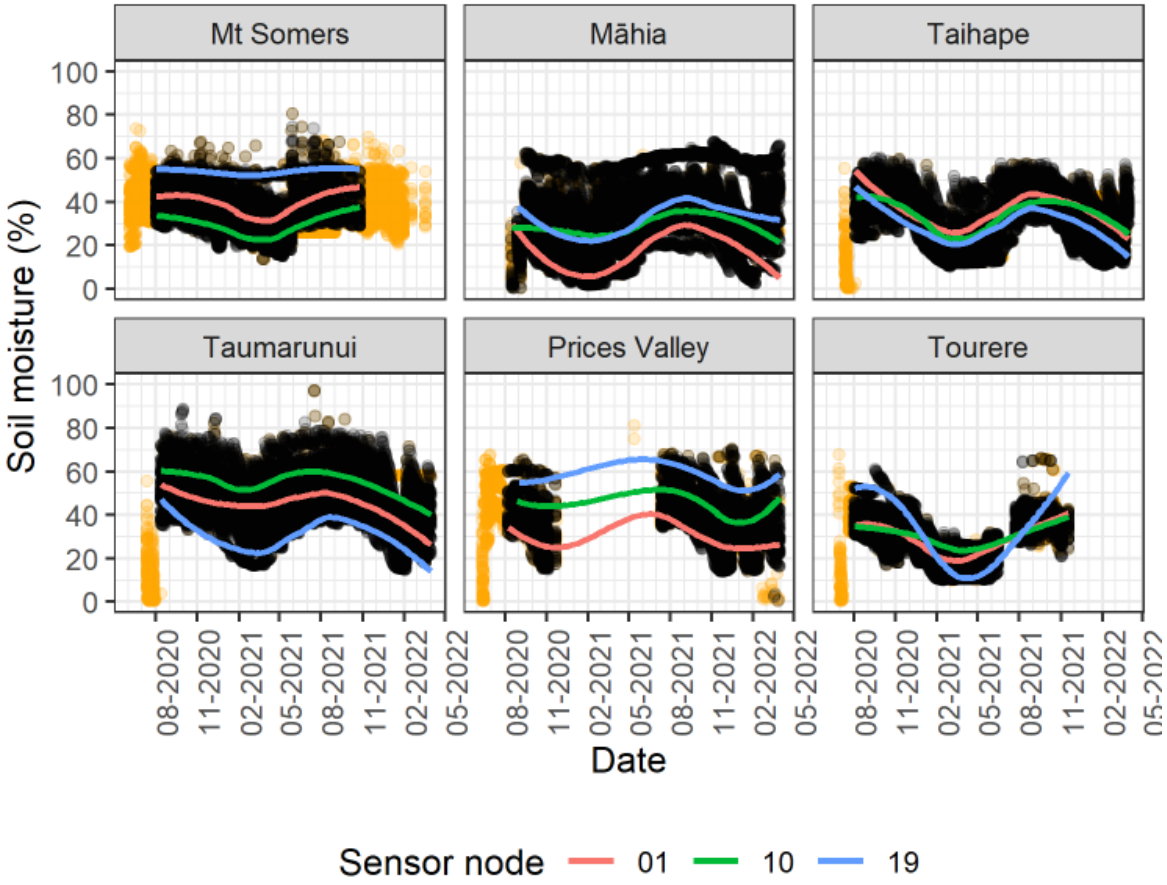


**Figure 26. Daily median soil moisture data for all sites after trimming of the start and end dates, removal of small and large soil moisture values, and periods of no change in soil moisture. Smoothed LOESS lines are drawn through data for sensor nodes 1, 10, and 19 for each site. Points that have been excised from the data are shown in orange.**

## 2.5 Modelling

### 2.5.1 Soil temperature and moisture

*General approach*

One could use many different approaches to establish a relationship between the scorpan covariates and the response variables of interest. Because the data are sampled over time, it appears that a time series model would be suitable because the data probably exhibit some degree of temporal auto-correlation. There are, however, several problems with the time series approach.

1 Gaps in temporal sampling are not always easily handled. The usual approach is imputation of the missing data using contextual data and covariates (e.g. Afrifa-Yamoah et al. 2020). Figure 27 shows plots of the distribution of the difference in days between sorted samples for each site and sensor node. Because the data have been aggregated daily, the interval of 1 day is strongly represented, but there are

occasional gaps where one or more samples are missing (the time between samples is greater than 1 day). Occasionally there are longer gaps where stations have lost valid data completely. The short gaps could probably be easily fixed using imputation, but longer gaps present a much more difficult problem.

2 The time series model would be of considerable complexity, because it would need to incorporate relationships between sensor nodes at a site, between sites within the whole data set, and between soil temperature and soil moisture. Some of these relationships could be ignored, such as the relationship between sites, but the final model would still be highly complex.


**Figure 27. Distribution of the difference in time between aggregated daily data, in days, for each site and sensor node. Points are coloured by sensor node.**

The alternative approach to the problem is to use some variation on linear regression, with possibly a multivariate response of soil temperature and soil moisture. This has the advantage that gaps in the data are not important, while the relationship between sensor nodes and sites can be handled by way of the scorpan covariates. The complexities involved in this approach are as follows.

1 Because the data cover just over a year in total, and since most sites do not provide data for even one full year, it would be difficult to estimate the variation in the soil temperature and soil moisture between years. For this reason, the soil temperature

and soil moisture should be constrained to be circular over the year; i.e. the estimated soil temperature at the start of the year should be the same as the estimated soil temperature at the end of the year. This constraint is needed so that this within-year variation can be added to fixed values for the soil temperature and soil moisture for each year, whether derived from data or presumed from other sources.

2 Because the data are probably auto-correlated to some degree, it is likely that the residuals from a standard linear model would also be auto-correlated, violating an invariable assumption of independent data. Correcting for this behaviour is certainly possible, and important for correct calculation of uncertainty in predictions, but is not always straightforward, depending on the type of model chosen.

On balance, the regression-based approach appears to be the one with the fewest potential difficulties, so it was selected as the general approach for this problem. Although there are many different regression methods that could be used, here we use the generalised additive model (GAM; Wood 2017), which can be written as:

$$\hat{y} = \beta_0 + f_1(x_1) + f_2(x_2) + \mathrm{I} + f_n(x_n)$$

where the response $\hat{y}$, representing soil temperature or moisture, is the sum of the overall mean $\beta_0$ and smooth functions $f_1(\quad), f_2 I \ldots, f_n(\quad)$ of covariates $x_1, I, \ldots, x_n$. The method is generalised in the sense that non-Gaussian responses can be accommodated; this is important in the present case with soil moisture, which is constrained to the range 0 to 1 (i.e. 0–100%). The fitting method uses the R package `mgcv` (mixed GAM computational vehicle), which is based on the reduced rank solution approach with automatic smoothing parameter selection (Wood 2017).

The principal advantage of the GAM approach is that it easily (and generally, automatically) handles non-linearities in the relationship, as well as interactions and random effects. The potential problem with GAMs is overfitting, especially if there is un-modelled residual auto-correlation or unmodelled overdispersion. Careful inspection of residuals usually enables detection of these potential problems.

One important step is to deal with quantities that are wrapped over an interval. Specifically, since most sites only have a little over a full year of data available, estimating the year-to-year variability is essentially impossible. Instead, we assume that the effects are estimated relative to calendar year 2020, and any year-to-year effect needs to be incorporated from additional information outside the model. This suggests that the response (soil temperature and soil moisture) should be wrapped over the 2020 boundary (i.e. the response at the start of 2020 should be the same as the end of 2020). This is clearly only an approximation, so the residuals for the model are likely to be biased at the start and/or the end of 2020.

To accommodate the wrapped response, the model is first parameterised so that for each year the interval day = [01-Jan, 31-Dec] maps to $\theta = [-\pi, \pi]$ and then $\sin(\theta)$ and $\cos(\theta)$ are used as explanatory variables. Similarly, because aspect is wrapped at the 0/360° degree boundary, $\sin\big((\pi/180) \cdot \text{aspect}\big)$ and $\cos\big((\pi/180) \cdot \text{aspect}\big)$ are used as explanatory variables.

The constraint that the start and end must match is a practical consequence of having data limited to about one year, otherwise the asymmetrical start/end of year becomes specific to one year and not generic. This way we can at least say that (typically) this is the predicted behaviour over a year, and you add an offset for the response in a different year. If we had several years of data we would probably introduce a yearly random effect. If we had *lots* of yearly data, we might model the yearly behaviour.

The topographic explanatory variables slope gradient and aspect were calculated from a 15 m resolution digital elevation model (DEM) generated by Manaaki Whenua – Landcare Research. One could argue that site-measured slope and aspect would be likely to give a better regression result, and this seems very likely given that the spatial resolution of field-estimated slope and aspect would more accurately represent the true slope and aspect compared with moderate resolution information from the DEM. However, since the model is to be used to predict soil temperature and soil moisture for new locations within each site, then the only practical choice is the 15 m DEM. Note that although the original values for slope, aspect, and elevation are in degrees and metres, the values are scaled to radians and thousands of metres.

### *Soil temperature*

We fitted several candidate models to select a final model from.

1 **Model 1.** A fixed effect is included for each site, and smooth terms are used for $\sin(\theta)$, $\cos(\theta)$, TWI, elevation, slope gradient, $\sin\big((\pi/180)\cdot\text{aspect}\big)$, and $\cos\big((\pi/180)\cdot\text{aspect}\big)$. Importantly, the smooth terms for $\sin(\theta)$ and $\cos(\theta)$ are site-specific.

2 **Model 2.** The terms for the model are the same as for model 1, but the smooth terms for $\sin(\theta)$ and $\cos(\theta)$ are independent of the site. Logic would suggest that this model would be inferior to model 1.

3 **Model 3.** The terms are the same as for model 2, but the smooth terms for aspect incorporate interactions with slope. Logic would suggest that this model would perform better than model 1.

4 **Model 4.** The model is simplified using linear (i.e. non-smooth) terms for TWI and elevation, and the interaction between smooth aspect terms and the slope gradient are removed, while the smooth term for the slope is retained. Logic would suggest that this model would give the worst performance, but would require the fewest degrees of freedom.

5 **Model 5.** Similar to model 4, but incorporating interactions between $\theta$, slope gradient, and slope aspect in the smooths. This last model is of the following form:

$$\hat{y} = \beta_0 + f_{1,i}\big(\text{slope},\text{aspect},\sin(\theta)\big) + f_{2,i}\big(\text{slope},\text{aspect},\cos(\theta)\big) + \alpha\text{TWI} + \beta\text{elevation} + \gamma_i$$

where the response $\hat{y}$ is the overall mean soil temperature, which includes an overall mean $\beta_0$, smooth functions $f_{1,i}(\quad)$ and $f_{2,i}(\quad)$ that are based on topographic slope and aspect for each site separately, as well as fixed effects of TWI, elevation, and an offset $\gamma_i$ for site $i$.

The assessment of the five models is not straightforward due to the complexity of the relationships involved, and uses a comparison by way of an ANOVA, comparison of coefficient effects, and the overall computational simplicity (i.e. number of degrees of freedom). The preferred model is based on a consideration of quantitative measures, but also depends on interpretability, which is somewhat difficult to capture.

For spatial prediction we coarsened the 15 m grid to 30 m for computational expediency. We then used the preferred model to spatially predict the daily soil temperature onto the 30 m grid that covered each WSN site for one full year.

#### *Soil moisture*

The modelling for soil moisture follows a similar procedure to that of soil temperature, using a GAM with the same scorpan covariates. Four separate models were fitted, to determine the 'best' model using a mix of quantitative and qualitative features. The four models use the same terms as soil temperature models 1 to 4. We do not include an equivalent model 5 here, as preliminary analysis suggested that it was not a useful model for soil moisture.

As for soil temperature, we used the preferred model to spatially predict the daily soil moisture content onto the 30 m grid at each WSN site for one full year.

### 2.5.2 Yield modelling

#### *Thermal time function*

In recent years there has been increased interest in increasing farm productivity on New Zealand hill country landscapes by introducing legumes such as lucerne (*Medicago sativa*; Mcgowan et al. 2003; Moot 2012; Tozer & Douglas 2016). Farm-scale modelling of forage yield has the potential to shed light on the potential productivity of species such as lucerne and how it might vary across the farm. Farm-scale mapping of micro-indicators may be able to be used as input into yield models.

We estimated the potential yield of a lucerne crop using a simple thermal time function developed by Moot et al. (2021). The function accumulates yield by multiplying the daily thermal time with a standardised growth rate (SGR) measured in units of kilograms of dry matter per hectare per degree-day (kg DM/ha/°Cd). The rate of dry matter production changes during the growing season, associated with a change in biomass partitioning to recharge root reserves after the summer solstice (21 December). For increasing photoperiods (days where day length is increasing; 1 July – 31 December), the SGR is at 9.68 ± 0.26 kg DM/ha/°Cd from 181 to 1,500°Cd, whereas in decreasing photoperiods (day length is shortening; 1 January – 30 June) the SGR is lower (5.40 ± 0.76 kg DM/ha/°Cd). The full function is:

$$y = \begin{cases} \sum_{i=D_{\text{start}}}^{i=31\ \text{Dec.}} r_1 \cdot \text{Tt}_i \\ \sum_{i=1\ \text{Jan.}}^{i=30\ \text{Jun.}} r_2 \cdot \text{Tt}_i \end{cases}$$

where the response $y$ is the accumulated lucerne yield (t/ha) through an agricultural year (1 July to 30 June), $r_1$ is the SGR for the increasing photoperiod (9.68 kg DM/ha/°Cd), $r_2$ is the SGR for the decreasing photoperiod (5.4 kg DM/ha/°Cd) and $\text{Tt}_i$ is the thermal time at Day $i$. $D_{\text{start}}$ is the date when the accumulated Tt reaches 180°Cd.

Computation of the daily thermal time is based on methods used by Jones et al. (1986), Moot et al. (2001) and Moot et al. (2021). However, instead of estimating the mean daily air temperature as the weighted average of eight 3-hourly periods, we use the daily air temperature as predicted from the modelled soil temperature, as described in the following section.

The daily thermal time at day $i$, $\text{Tt}_i$, is estimated from the predicted daily air temperature using a broken stick model (Figure 28). Breakpoints in the broken stick model at 1°C, 15°C, 30°C, and 40°C are cardinal temperatures that relate to important growth thresholds for lucerne (Moot et al. 2001, 2021). The first cardinal temperature (1°C) is the base temperature below which minimal plant growth occurs. The second cardinal temperature (15°C) relates to the initial rate of thermal time accumulation required for lucerne growth in temperate climates. The third cardinal temperature (30°C) is the optimal temperature for growth, and the fourth cardinal temperature (40°C) is the temperature beyond which no thermal time is accumulated.

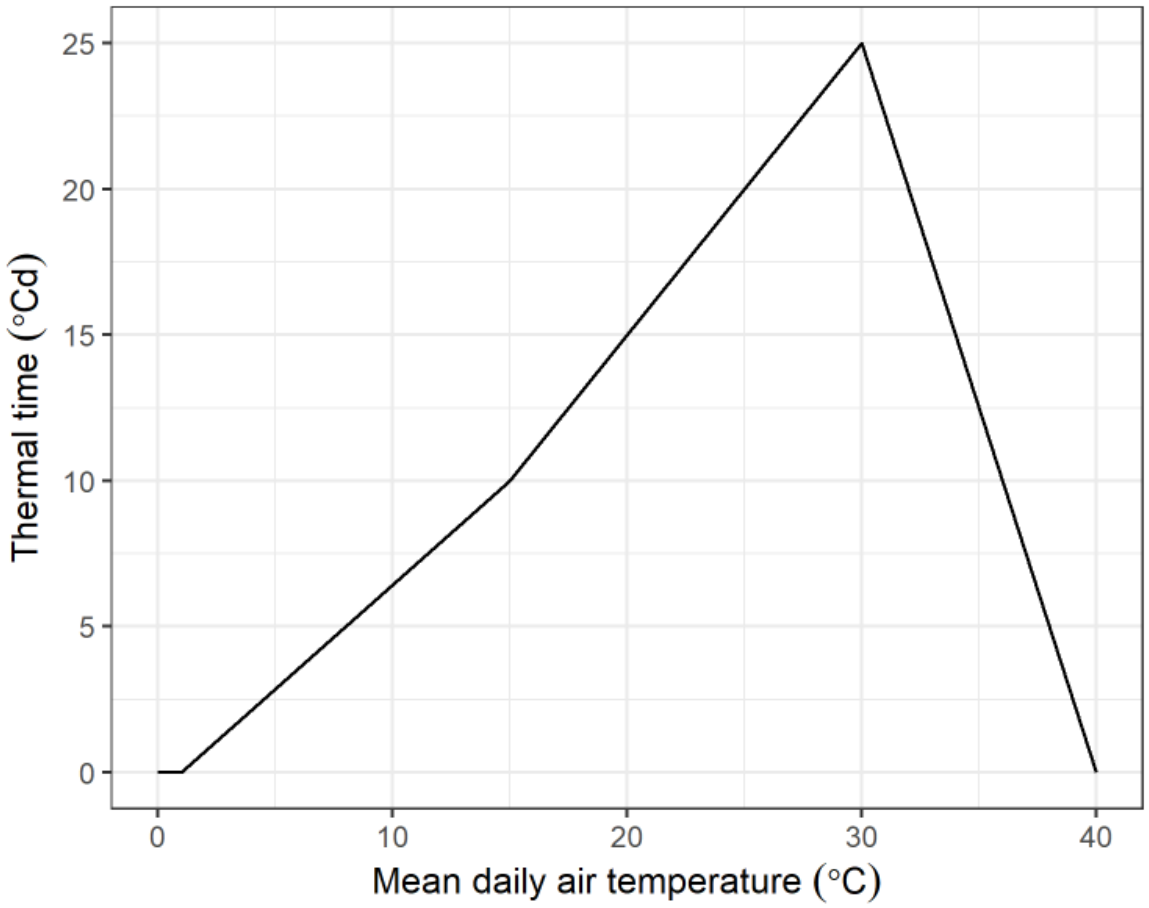


**Figure 28. Broken stick model, which relates mean daily air temperature to daily thermal time for lucerne.**

The yield model requires information about soil moisture expressed in millimetres of water, which is problematic because the sensor nodes measure volumetric soil moisture. One cannot convert from volumetric moisture to millimetres of water without knowing the thickness of the soil horizon or horizons across which the volumetric measurement applies. We did not collect that information at the sensor nodes, so for the yield model we assumed that soil moisture was not limiting.

### *Estimating air temperature from soil temperature*

The sensor nodes do not record air temperature, $T_{\text{air}}$, so we must predict it using soil temperature. This, too, is problematic, not least because of the lag effect caused by the thermal mass of the soil (Zheng et al. 1993). Here we made use of weather stations that report both air temperature and soil temperature to NIWA's National Climate Database.[7] We used weather stations located in the same regions as the WSNs: Canterbury, Hawke's Bay, and Wanganui.

[7] cliflo.niwa.co.nz

We retrieved 2 years of daily air and soil temperature from NIWA's National Climate Database for 82 weather stations across Canterbury, Hawke's Bay, and Wanganui that measured these variables. The data covered calendar years 2020 and 2021. All weather stations recorded air temperature, but not all recorded soil temperature, and not all recorded soil temperature at the same set of depths (Table 4).

**Table 4. Number of weather stations available with air temperature and soil temperature at specific depths**

| Variable | Number of weather stations | | |
|---|---|---|---|
| | Canterbury | Hawke's Bay | Wanganui |
| Air temperature, $T_{\text{air}}$ | 33 | 22 | 27 |
| Soil temperature at 5 cm, $T_{\text{soil},5}$ | 2 | 0 | 2 |
| Soil temperature at 10 cm, $T_{\text{soil},10}$ | 23 | 9 | 15 |
| Soil temperature at 20 cm, $T_{\text{soil},20}$ | 14 | 6 | 14 |
| Soil temperature at 30 cm, $T_{\text{soil},30}$ | 4 | 0 | 2 |
| Soil temperature at 50 cm, $T_{\text{soil},50}$ | 11 | 6 | 12 |
| Soil temperature at 100 cm, $T_{\text{soil},100}$ | 12 | 6 | 13 |

Few of the available weather stations, including none at all in Hawke's Bay, measure soil temperature at 30 cm, $T_{\text{soil},30}$, the same depth as our sensor nodes. There is clearly an insufficient number of weather stations to calibrate reliable relationships between air temperature and soil temperature at this depth. Instead, we fitted a relationship between the temperature variables at 20 cm depth, $T_{\text{soil},20}$ (the closest available depth above 30 cm), because more weather stations were available, and because we expect the soil–air temperature dynamics at 20 cm depth to be closer to those at 30 cm than those at 50 cm (the closest available depth below 30 cm).

For each region we used simple linear regression to model the response of $T_{\text{air}}$ to variation in $T_{\text{soil},20}$, but we found that this approach underestimated $T_{\text{air}}$. In the literature, studies that quantify relationships between soil and air temperature usually model the response of soil temperature to variation in air temperature, rather than treat air temperature as the response variable (Toy et al. 1978; Paul et al. 2004; Chudinova et al. 2006; Shati et al. 2018; Zhan et al. 2019). When we modified our approach to treat $T_{\text{soil},20}$ as the response variable the fitted relationships appeared to be more satisfactory.

The most pragmatic method of predicting $T_{\text{air}}$ from $T_{\text{soil},20}$ is to reverse the fitted equation for $T_{\text{soil},20}$ using basic arithmetic. In doing so we lose information about the errors but the approach should be sufficient for this proof of concept. We used the reversed air temperature models with the daily spatial predictions of soil temperature to spatially predict the daily air temperature across the WSN sites for one full year.

# 3 Results

## 3.1 Wireless sensor networks

### 3.1.1 Performance

It is useful to quantify the performance of the WSNs in terms of their resilience, which we define here as the ability of a WSN to consistently do what it was designed to do: make hourly measurements of soil temperature and soil moisture and report these data back to a cloud database via the WSN gateway. Two key components of the overall resilience are the resilience of the gateway and the resilience of the sensor nodes. We present results for each in turn.

#### *At the gateway*

The WSN gateways generally performed well. There have, however, been four notable outages.

- The Prices Valley WSN went offline in November 2020 and spontaneously came back online in July 2021.
- The Taihape and Tourere WSNs were offline for short periods (1 to 2 weeks) over winter 2021.
- The Tourere WSN was offline from November 2021 to April 2022.
- Transmission at Mt Somers began to degrade in late 2021 and the WSN has not transmitted regularly since February 2022.

We deduced that the Prices Valley outage may relate to characteristics of the cellular coverage in the area. We suspect the Taihape and Tourere WSN outages in winter 2021 were related to poor weather conditions and therefore insufficient insolation to keep the gateway batteries charged. The Tourere outage over summer 2021/22 appeared to be caused by grass growth around the photovoltaic panel causing insufficient insolation at the panel to keep the gateway battery charged.

We inspected the Mt Somers gateway in November 2021 and found that that the cellular antenna had been chewed off and removed. Replacement of the antenna did not resolve the transmission problems. After further investigation, we learned that the problem was due to interference caused by recently installed LoRa transmitters on nearby Spark cell towers, which overlap the LoRa radio channel and frequency that we use. In July 2022 we updated the software in the Mt Somers gateway to filter out the interference. This restored transmission of the sensor telemetry to the cloud database, but we were not able to restore communication with six sensor nodes.

In addition to these longer outages, regular intermittent outages have occurred at Māhia. These outages consist of regular 2- to 4-hour outages interspersed by long periods of normal hourly data transmission. We think these outages are due to cellular connectivity: the Māhia gateway is further from the nearest cell tower than the other WSN gateways.

**Table 5. Days since installation for each WSN and some metrics of performance**

| Site | Days since installation, at 15 March 2022 | Days with no hourly records (%) | Days with at least 1 hourly record (%) | Days with 24 hourly records (%) |
|---|---|---|---|---|
| Māhia | 543 | 2.2 | 97.8 | 59.3 |
| Mt Somers | 647 | 6.5 | 93.5 | 43.6 |
| Prices Valley | 560 | 49.5 | 50.5 | 22.3 |
| Taihape | 585 | 3.1 | 96.9 | 45.5 |
| Taumarunui | 578 | 0.0 | 100.0 | 38.4 |
| Tourere | 599 | 30.4 | 69.6 | 23.2 |

We quantified the resilience of the WSNs by analysing the number of gateway transmissions recorded by the cloud database. For each WSN we computed three variables:

1. the percentage of days since installation where precisely zero hourly records were received by the cloud database, which represents the worst-case situation (poorest resilience) and includes the protracted outages and any other day-long outages)
2. the percentage of days where at least one transmission was received – this metric is the complement of metric 1; metrics 1 and 2 sum to 100%
3. the percentage of days where all 24 expected transmissions were received by the cloud database, which represents the best case situation (perfect resilience).

The length of the period over which these percentages were computed varied according to the WSN. The start date of the assessment period was defined as the second day after completion of installation, which was different for each WSN, and the end date was 15 March 2022 (inclusive). The resilience statistics are reported in Table 5.

Table 5 indicates that the gateway resilience varied considerably between WSNs. The Taumarunui, Māhia, and Taihape WSNs had the smallest percentage of days with no hourly records received. The Mt Somers WSN also performed very well on this metric. The relatively poor scores for the Tourere and Prices Valley WSNs reflect the protracted outages there. The Taumarunui WSN is the only WSN that transmitted at least one hourly record for every day of operation.

Gateway resilience as measured by metric 3 was low to moderate, as no WSNs transmitted the expected 24 hourly records for every day of operation. This probably reflects daily variations in the quality and consistency of the sensor to gateway radio communications between sites, but the number also accounts for the protracted outages experienced at Prices Valley and Tourere. The Māhia WSN was the best performer, reporting a full set of records 59.3% of the time. Figure 29 and Figure 30 explore the number of daily transmissions in more detail. Most sites experienced a wide distribution in the number of daily transmissions, including more than the expected 24 hourly transmissions.

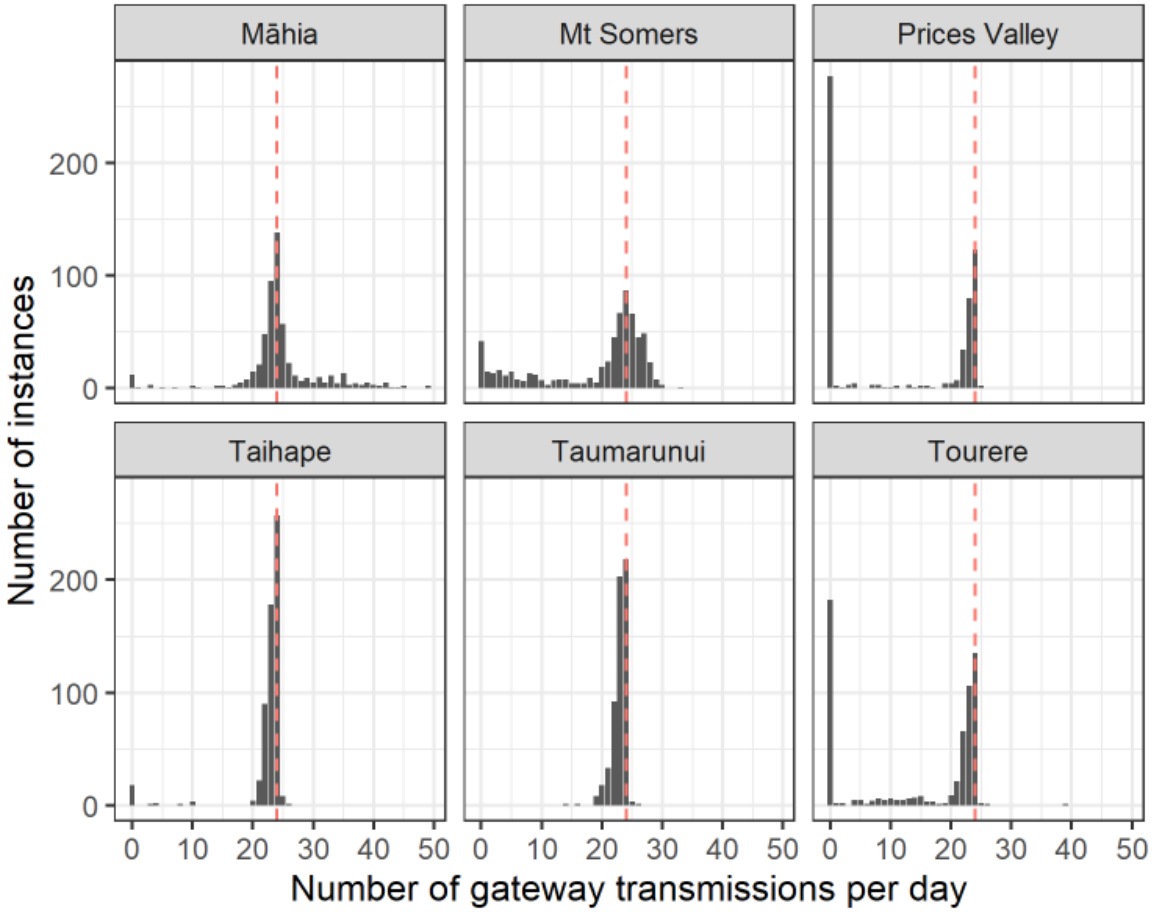


**Figure 29. Histograms of the number of WSN gateway transmissions per day. Dashed vertical line is the expected number of transmissions per day.**

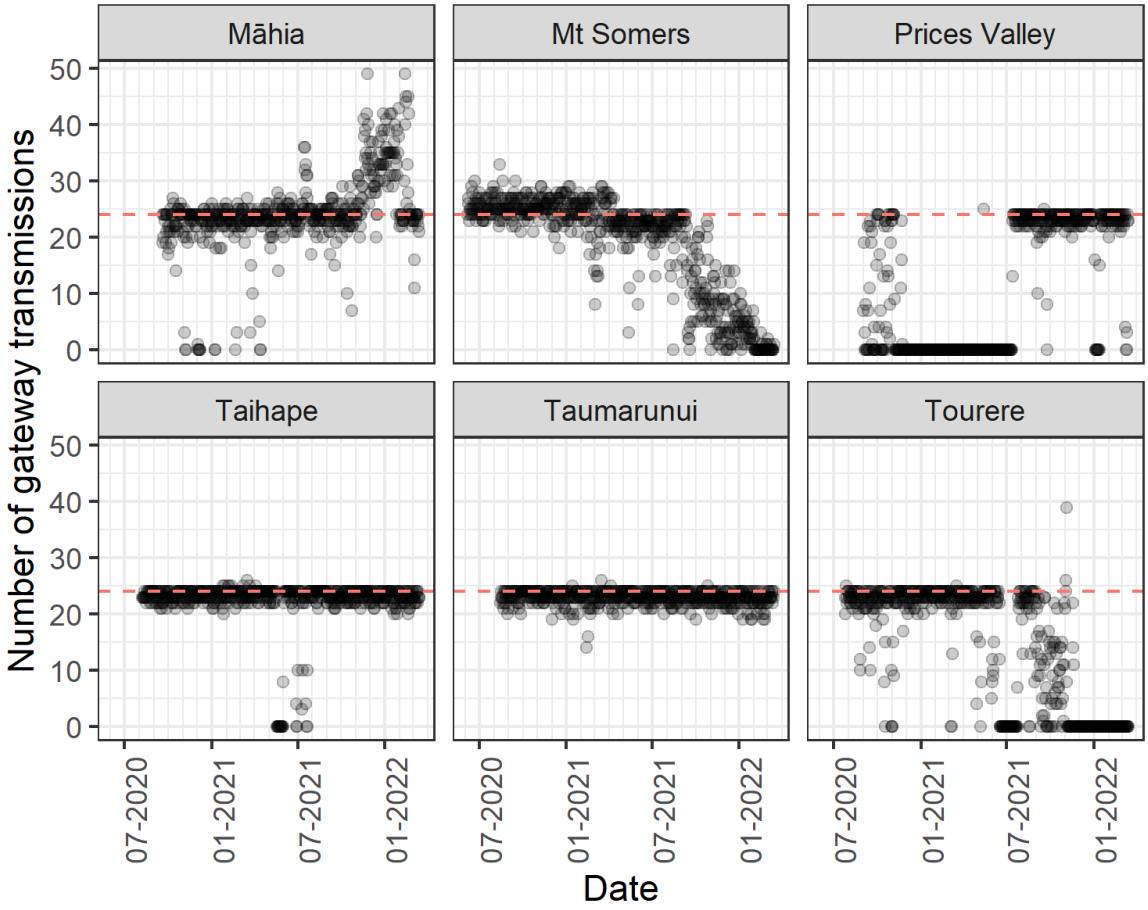


**Figure 30. Number of gateway transmissions per day over time. Dashed horizontal line is the expected number of transmissions per day.**

### *Of the sensor nodes*

Sensor nodes were resilient when they consistently reported hourly soil temperature and moisture measurements to the WSN gateway. Over time some nodes stopped reporting measurements of soil temperature or soil moisture, or both. We expected some level of attrition and were pleased that only a small proportion of sensor nodes were affected (Table 6).

**Table 6. Number of sensor node failures at each WSN, at 15 March 2022**

| Site | Node failures at 15 March 2022 |
|---|---|
| Māhia | 4 |
| Mt Somers | 5 |
| Prices Valley | 2 |
| Taihape | 4 |
| Taumarunui | 3 |
| Tourere | 1 |

Figure 31 explores the idea of sensor node resilience in more detail. For each WSN it shows the median number of sensors reporting soil temperature measurements per day, computed across all daily records received by the gateway. Sensor node resilience was greatest when all 20 sensor nodes consistently reported their measurements. Resilience degraded over time as sensors began to fail. In Figure 31, failures are indicated by downward steps over time, as exemplified in the Taihape panel, but at most other sites (especially Māhia and Mt Somers) noise relating to trouble with gateway transmissions is superimposed on the trend.

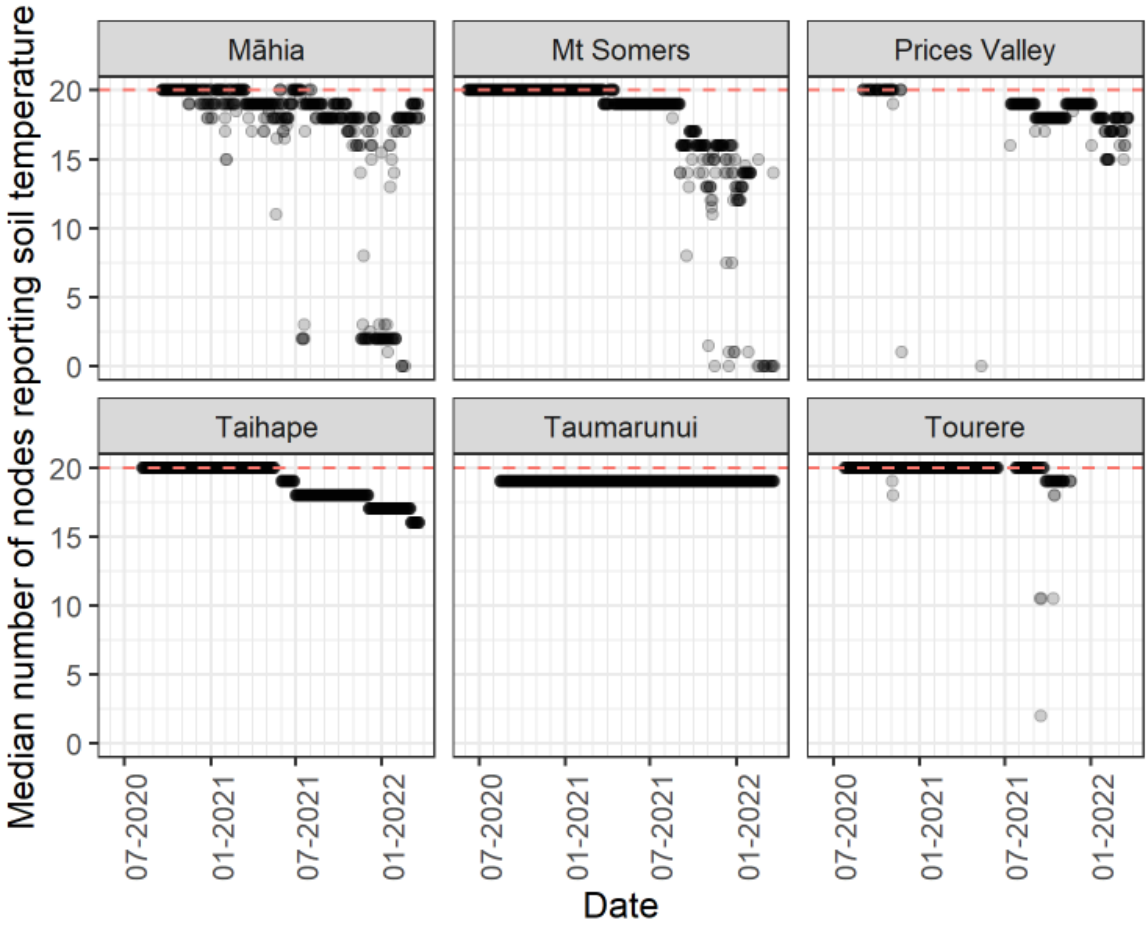


**Figure 31. Median number of sensor nodes reporting soil temperature per day. Dashed horizontal line is the expected number of sensor nodes reporting soil temperature per day.**

## 3.2 Modelling

### 3.2.1 Soil temperature

Table 7 provides the residual deviance, Akaike's information criterion (AIC), and the proportion of the total deviance explained ($R^2$) for all five soil temperature models. The best model has the smallest residual deviance and AIC, and the highest proportion of total deviance explained. A naive comparison between the models suggests that model 3 is the best since it has the lowest overall residual deviance. The key question is whether, despite differences in AIC and residual deviance between models, the 'best' model provides any relevant improvement over the other models, and whether choosing a more complicated model introduces additional problems.

**Table 7. Residual deviance, Akaike's information criterion, and proportion of the total deviance explained for each of the generalised additive models fitted for the soil temperature data**

| Model | Residual deviance | AIC | $R^2$ |
|---|---|---|---|
| 1 | 121,730 | 189,555 | 91.1 |
| 2 | 127,923 | 192,029 | 90.7 |
| 3 | 102,877 | 180,951 | 92.5 |
| 4 | 129,499 | 192,643 | 90.6 |
| 5 | 108,281 | 183,831 | 92.1 |

Marginal effects plot of model 3 (not shown) appear reasonable, but there were some worrying features:

- the marginal effect for slope was very large compared with the effect of date
- the marginal effects for the aspect/slope interaction smooth terms were also very large.

Both of the above observations were unexpected, and we concluded that the slope and aspect terms were large but cancelling each other (one positive, one negative). This is undesirable because it leads to excessive and unrealistic estimates of uncertainty. This is an example of over-fitting.

Figure 32 shows a marginal effects plot of the simplest model for soil temperature (model 4). In this model, the terms for TWI and elevation are not smoothed, so their interpretation is trivial. The size of the marginal effects for all variables is of the same order (the effect size for the date is the largest, as expected). The smooth term for slope is somewhat unusual (it is non-monotonic), but the overall effect of slope is relatively small compared with the other variables, so this is unlikely to be a problem.

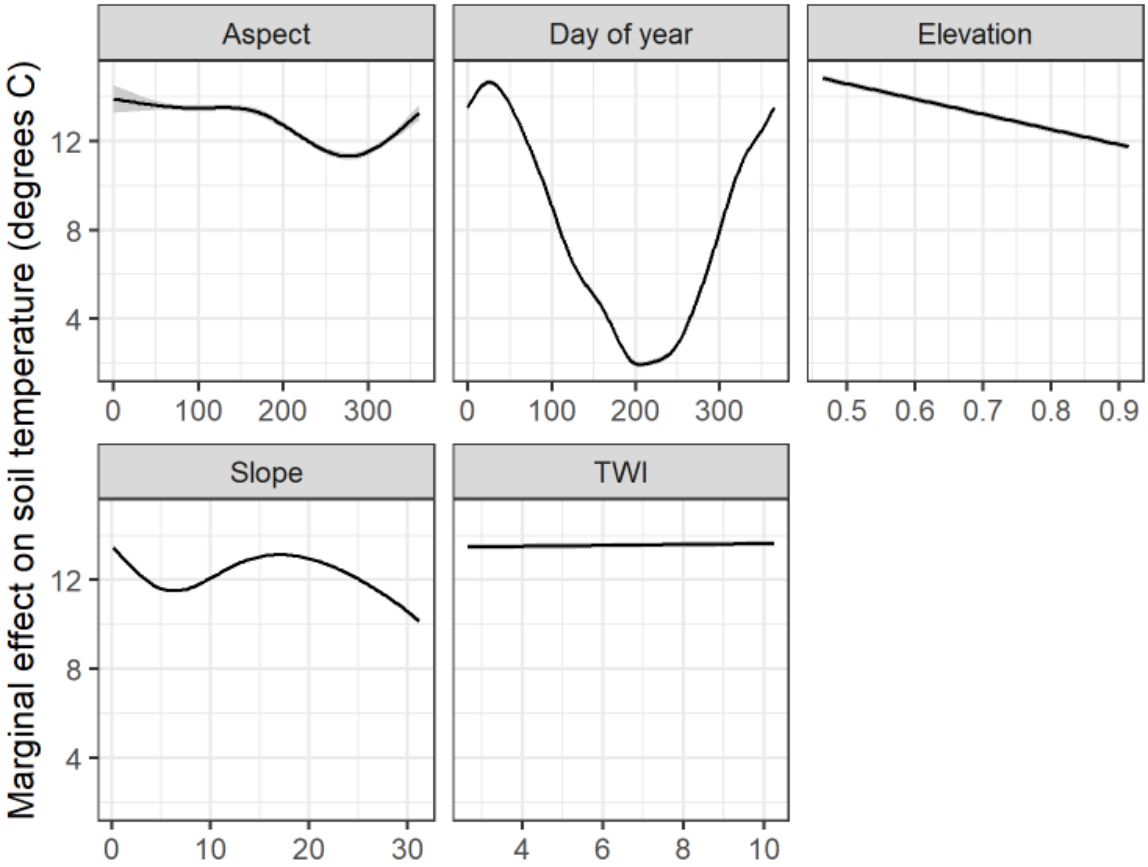


**Figure 32. Plot of the effect of the different explanatory variables for soil temperature, model 4. Explanatory variables are given in their natural units. For each panel, the explanatory variables that are not changing are held at a fixed value (generally the median or a sensible default). The limits of the vertical axis are the same for all panels. The solid line is the nominal estimate, while the shaded area (often not visible) is the 95% confidence interval of the mean estimate.**

A marginal effects plot for model 5, which has significantly better performance than model 4, is not straightforward because it incorporates a three-way interaction.

The final model choice is a balance between performance and interpretability. Although model 3 gives the best performance, the effect sizes for aspect and slope are not sensible. The simplest model is certainly the most easily interpreted, and the penalty for using it amounts to a few percentage points in total deviance explained. Therefore, on balance, we chose to use the simplest model augmented by interactions with slope and aspect (model 5) as the basis for soil temperature, and all the subsequent analysis uses this model.

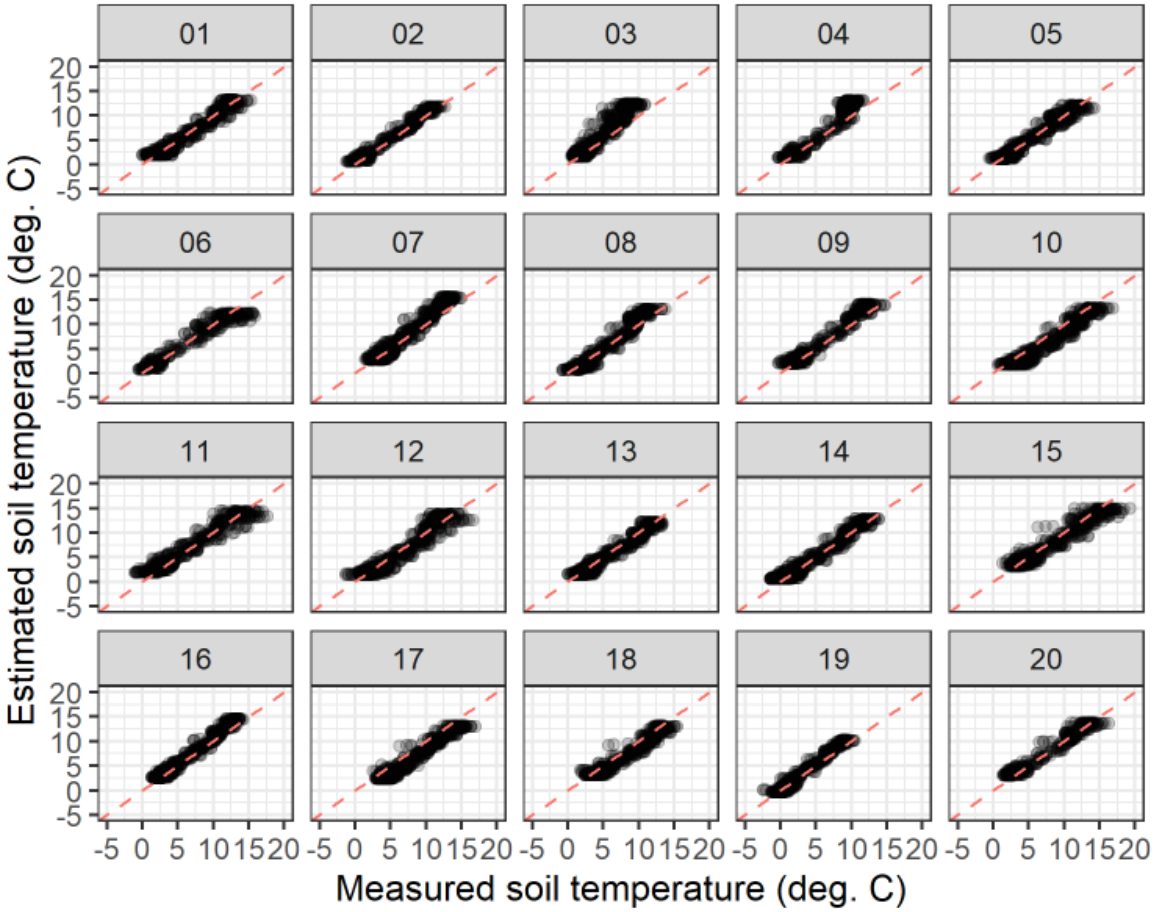


**Figure 33. Measured versus fitted soil temperature plot for the Mt Somers site using model 5. Panel labels indicate the respective sensor node. The dashed red line is the one-to-one line.**

Figure 33 shows a measured-versus-fitted plot of soil temperature for the Mt Somers site, by sensor node. Plots for the other sites are presented in the Appendix. The Mt Somers site was chosen because the sampling from that site covers the longest period of time. Most of the plots show close adherence to the 1:1 line, as expected, and as reflected in the value for Lin's concordance correlation coefficient (CCC, Lin 1989) in Table 8.

**Table 8. Statistics for the evaluation of the relationship between measured and predicted soil temperature for the chosen soil temperature, model 5**

| Site | RMSE (°C)[a] | R-sq | CCC[b] | Bias (°C) | SE (°C)[c] |
|---|---|---|---|---|---|
| Māhia | 1.48 | 0.88 | 0.94 | 0 | 1.48 |
| Mt Somers | 1.31 | 0.91 | 0.95 | 0 | 1.31 |
| Prices Valley | 1.60 | 0.89 | 0.94 | 0 | 1.60 |
| Taihape | 1.52 | 0.90 | 0.94 | 0 | 1.52 |
| Taumarunui | 1.38 | 0.91 | 0.95 | 0 | 1.38 |
| Tourere | 1.51 | 0.87 | 0.93 | 0 | 1.51 |
| **Overall** | **1.46** | **0.92** | **0.96** | **0** | **1.46** |

[a]Root mean squar'd error; [b]Lin's concordance correlation coefficient; [c]standard error

Figure 34 shows measured (points) and predicted (lines) values of soil temperature for the Mt Somers site using model 5. Plots for the other sites are presented in the Appendix. The predicted trend shows a maximum soil temperature in late December and a minimum in July at most sensor nodes, which is in line with our expectations.

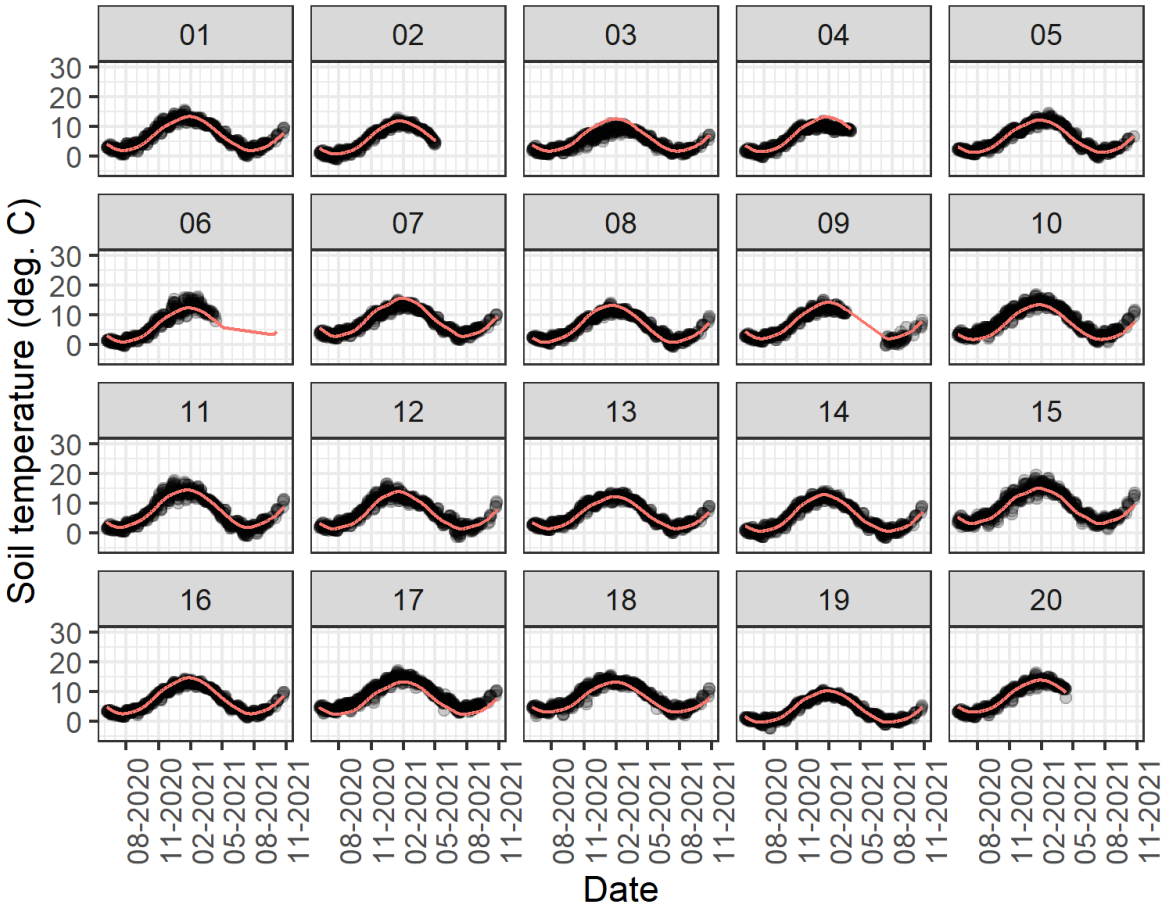


**Figure 34. Measured (points) and fitted (line) soil moisture for the Mt Somers site over time, using model 1. Panel labels indicate the respective sensor node.**

Figures 35 and 36 depict spatial predictions of soil temperature at the Mt Somers site when the soils are at their coolest (about 15 July) and warmest (15 January), respectively. Figure 37 shows how predictions vary across individual hillslopes on 15 July on the high-resolution prediction grid. There is little spatial variation in the maps of standard error because most of the values are so low. Maps for the other sites are presented in the Appendix. Soil temperatures are roughly 5 to 10°C warmer in summer than in winter (Figure 38).

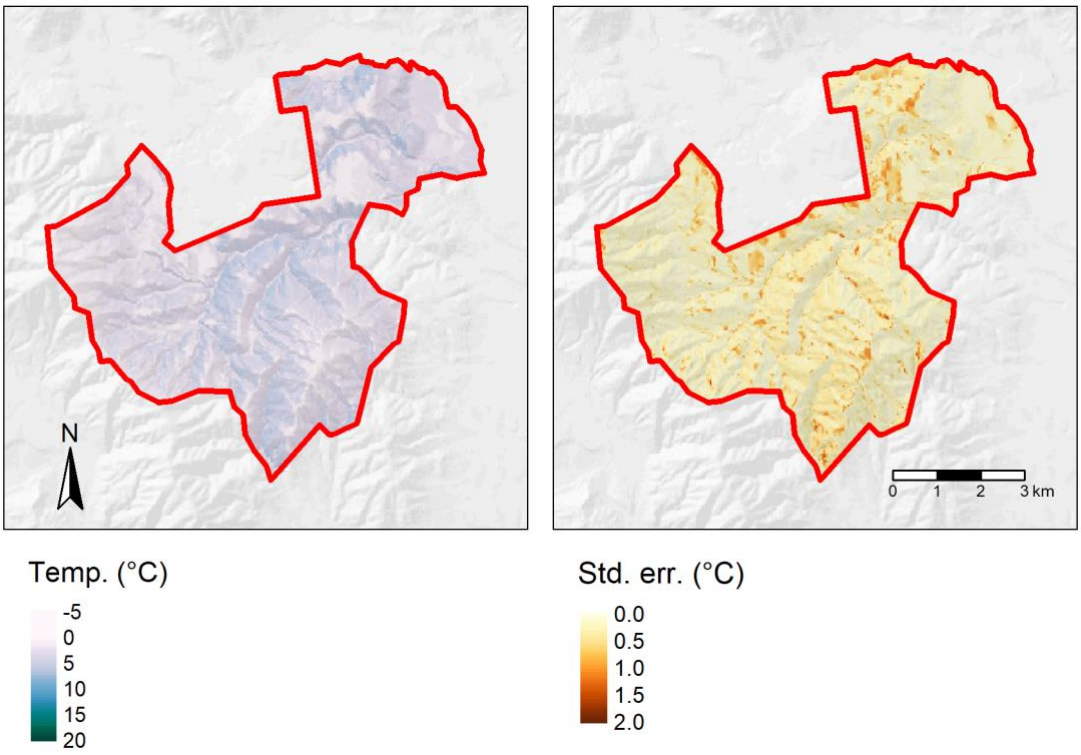


**Figure 35. Predicted soil temperature at Mt Somers on 15 July, when soils are near their coolest.**

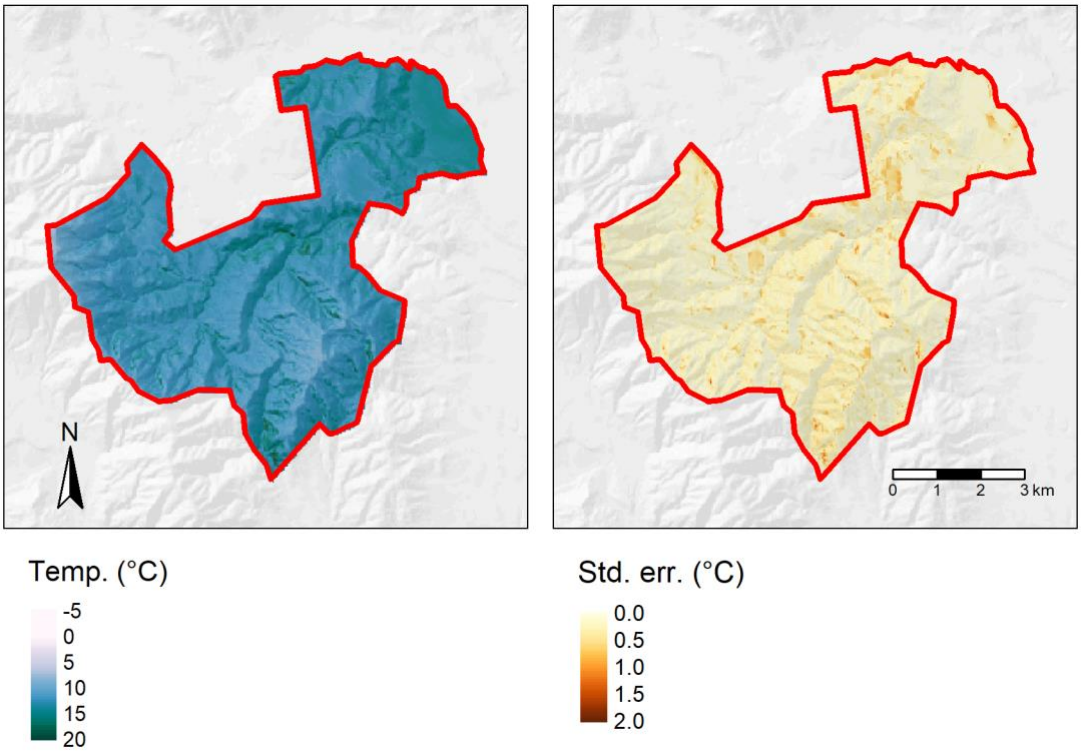


**Figure 36. Predicted soil temperature at Mt Somers on 15 January, when soils are near their warmest.**

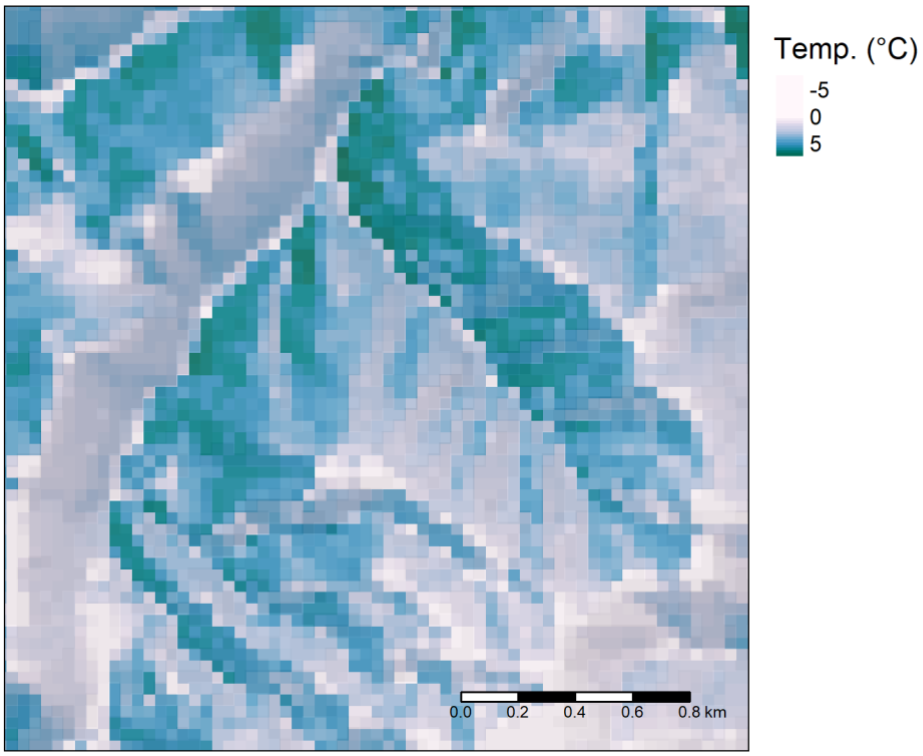


**Figure 37. Predicted soil temperature at Mt Somers on 15 July, showing variation in predicted temperature across individual hillslopes. Resolution of the prediction grid is 30 m.**

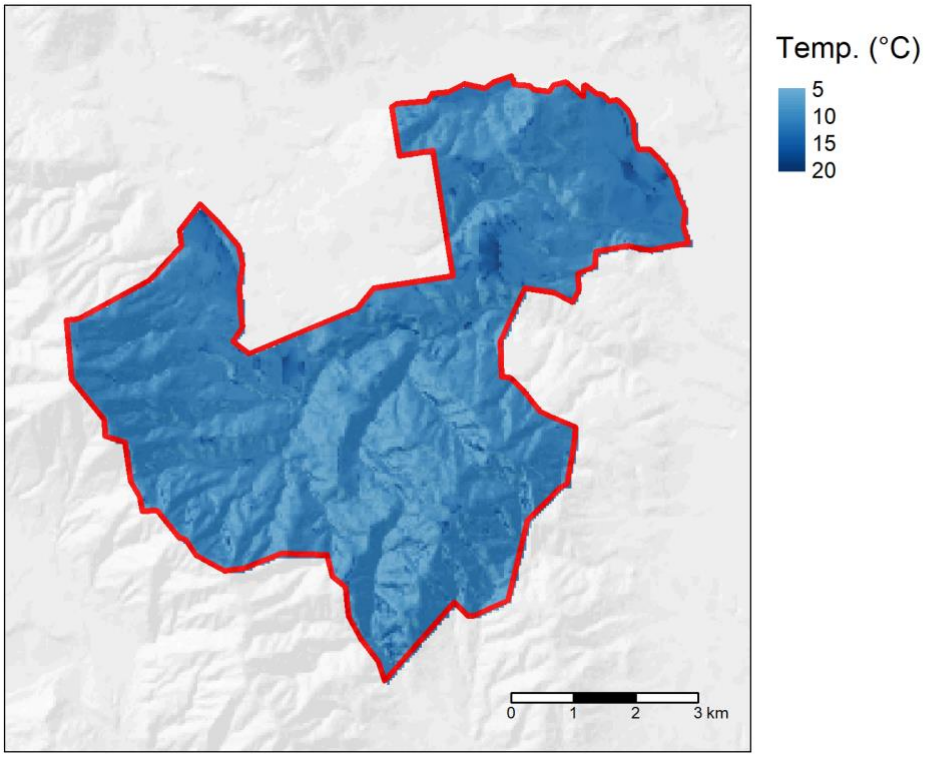


**Figure 38. Predicted difference in soil temperature between 15 December and 15 July.**

*Aspect-related differences in soil temperature*

With respect to plant growth and development, we are particularly interested in understanding potential differences in soil temperature between north- and south-facing slopes, including the timing and magnitude of minimum soil temperatures and how quickly the soil warms from the minimum in spring. This is because aspect-related differences may be meaningful for pasture management if they are large.

**Table 9. Summary of aspect-related differences in observed minimum soil temperature and days taken for soil temperature to reach 10°C and 15°C. Note: Because of gaps in the data, values are based on 2020 observations at some sites and 2021 observations at other sites.**

| Site | Aspect | Mean minimum temp. | Med. min. date | Med. date to reach 10°C | Med. days to reach 10°C | Med. date to reach 15°C | Med. days to reach 15°C | Year |
|---|---|---|---|---|---|---|---|---|
| Māhia | N | 7.6 | 2021-07-15 | 2021-08-28 | 19.0 | 2021-10-27 | 104.0 | 2021 |
| | S | 6.2 | 2021-07-15 | 2021-09-22 | 64.0 | 2021-11-19 | 120.0 | 2021 |
| Mt Somers | N | 1.1 | 2020-07-25 | 2020-11-04 | 102.0 | 2020-12-29 | 138.0 | 2020 |
| | S | -0.3 | 2020-07-25 | 2020-12-16 | 144.0 | | | 2020 |
| Prices Valley | N | 3.5 | 2021-08-09 | 2021-10-01 | 53.5 | 2021-11-08 | 91.0 | 2021 |
| | S | -0.2 | 2021-07-13 | 2021-11-09 | 118.0 | 2021-12-24 | 164.5 | 2021 |
| Taihape | N | 3.6 | 2021-07-27 | 2021-10-25 | 88.0 | 2021-11-30 | 125.5 | 2021 |
| | S | 0.7 | 2021-07-06 | 2021-10-27 | 111.0 | 2021-12-09 | 142.0 | 2021 |
| Taumarunui | N | 6.6 | 2021-07-13 | 2021-09-10 | 53.0 | 2021-11-01 | 105.5 | 2021 |
| | S | 4.5 | 2021-07-14 | 2021-10-05 | 83.0 | 2021-11-10 | 119.5 | 2021 |
| Tourere | N | 6.7 | 2020-07-27 | 2020-10-05 | 70.0 | 2020-10-25 | 90.0 | 2020 |
| | S | 5.2 | 2020-07-27 | 2020-09-26 | 61.0 | 2020-12-08 | 134.0 | 2020 |

The sensor data indicate that minimum values of the median daily soil temperatures do vary between north- and south-facing slopes and also by site (Table 9). Values were computed as the mean of the nodes on the respective aspects. On south-facing sites, the minimum daily soil temperature ranged from –0.3°C (Mt Somers) to 6.2°C (Māhia). On north-facing sites, the minimum daily soil temperature ranged from 1.1°C (Mt Somers) to 7.6°C (Māhia). Within sites, the difference in the mean of the minimum daily soil temperatures between north- and south-facing slopes ranged from 1.36°C (Mt Somers) to 3.7°C (Prices Valley).

Soils warmed at different rates depending on aspect, as quantified by the number of days taken to reach two arbitrary temperature thresholds (10°C and 15°C) from the minimum temperature (Table 9). As expected, north-facing slopes warmed faster than south-facing slopes at all sites, except to 10°C at Tourere. On north-facing slopes, the median number of days taken to reach 10°C ranged from 19 at Māhia (28 August) to 102 at Mt Somers (4 November). On south-facing slopes, the number of days to reach 10°C ranged from 61 at Tourere (26 September) to 144 at Mt Somers (16 December). Soils at the inland, higher-elevation sites generally took longer to warm than sites closer to the coast.

Table 10 summarises the difference in warming rates between north- and south-facing slopes at each site. For example at Taihape, soils on north-facing slopes reached a temperature of 10°C 23 days sooner than south-facing slopes. At the other extreme, north-facing soils at Prices Valley reached 10°C 64.5 days sooner than south-facing soils. We suspect the negative value for 10°C at Tourere, indicating south-facing soils warmed faster than north-facing soils, is an anomaly due to the small sample size on each aspect.

**Table 10. Difference in number of days for soil on north- and south-facing slopes to reach 10°C and 15°C. Positive values indicate north-facing soils reached the temperature threshold sooner.**

| Site | Diff. in time to reach 10°C (days) | Diff. in time to reach 15°C (days) |
|---|---|---|
| Māhia | 45.0 | 16.0 |
| Mt Somers | 42.0 | |
| Prices Valley | 64.5 | 73.5 |
| Taihape | 23.0 | 16.5 |
| Taumarunui | 30.0 | 14.0 |
| Tourere | -9.0 | 44.0 |

### 3.2.2 Soil moisture

The procedure for selecting a soil moisture model follows the approach we used for soil temperature. Table 11 provides the residual deviance, Akaike's information criterion (AIC), and the proportion of the total deviance explained ($R^2$) for all models. A naive comparison suggests that model 3 is the best because it has the best figures for all three model metrics.

**Table 11. Residual deviance, Akaike's information criterion, and proportion of the total deviance explained for each of the generalised additive models fitted for the soil moisture data**

| Model | Residual deviance | AIC | $R^2$ |
|---|---|---|---|
| 1 | 1,654 | 47,764 | 56.3 |
| 2 | 1,781 | 47,663 | 53.1 |
| 3 | 1,584 | 46,798 | 58.7 |
| 4 | 1,781 | 47,641 | 53.1 |

A marginal effect plot for model 3 (not shown) indicates regions where the aspect and slope interaction cannot be estimated. This would probably cause problems in prediction for the wider study area, because they would inevitably include combinations of slope and aspect not covered by the training data. Figure 41 shows the marginal effects of the somewhat simpler soil moisture model 1.

The final model choice is a balance between performance and interpretability. Although model 3 gives the best performance, the interaction between aspect and slope is poorly characterised in the training data. The simplest model is certainly the most easily interpreted, but there is a reasonably large difference in the percentage of deviance explained between this model and the optimal model. On balance, we chose to use model 1 as the basis for soil moisture because it gives almost the same percentage of deviance as the optimal model, although it is somewhat more complicated. All the subsequent analysis uses this model.

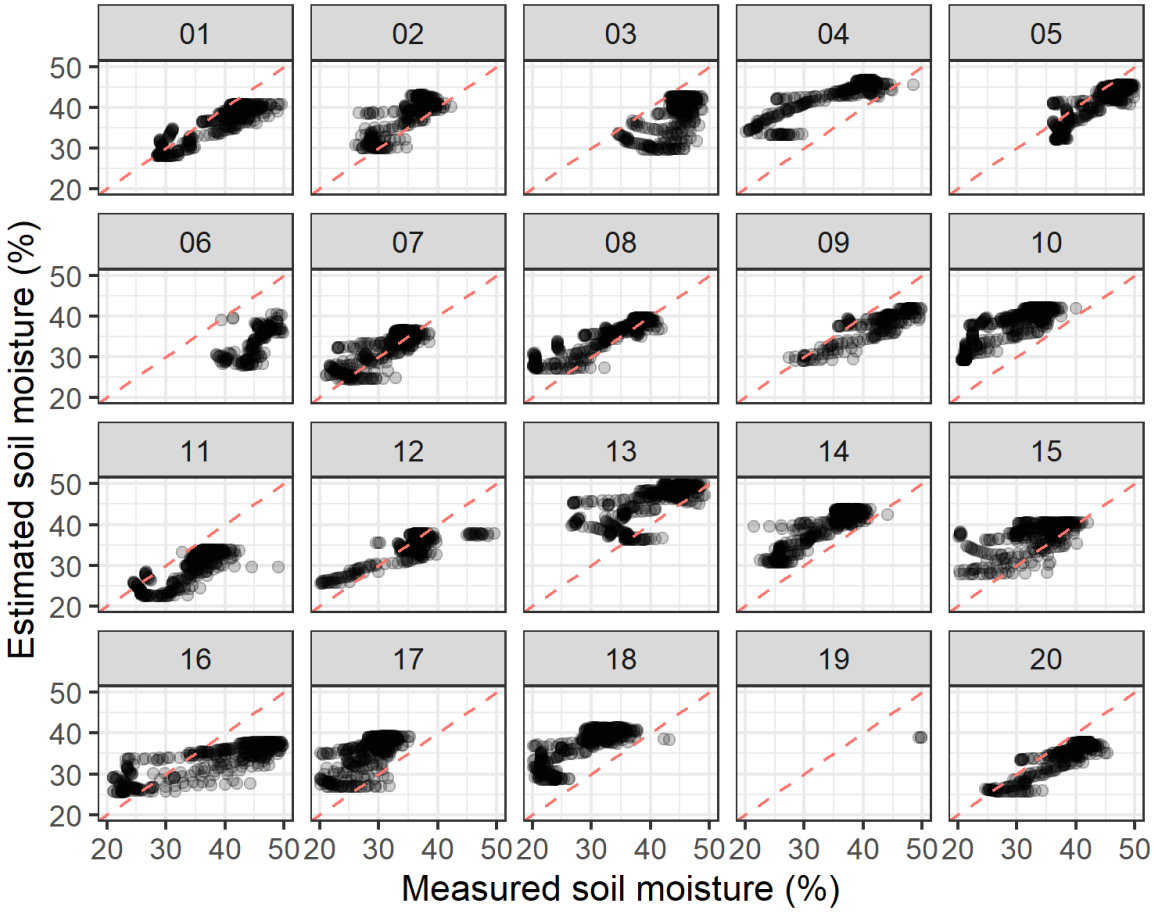


**Figure 39. Measured versus fitted soil moisture plot for the Mt Somers site using model 1. Panel labels indicate the respective sensor node. The dashed red line is the 1:1 line.**

Figure 39 shows a measured-versus-fitted plot of soil temperature for the Mt Somers site, by sensor node. Plots for the other sites are presented in the Appendix. The CCC indicates that the conformance to the 1:1 line is overall very poor (Table 12), especially when compared to soil temperature (Figure 33 and Table 8), but is still reasonable for certain sensor nodes (e.g. node 1). Measured-versus-fitted plots for the other sites are presented in the Appendix.

**Table 12. Statistics for the evaluation of the relationship between measured and predicted soil moisture for soil moisture model 1**

| Site | RMSE (%)[a] | R-sq | CCC[b] | Bias (%) | SE (%)[c] |
|---|---|---|---|---|---|
| Māhia | 37.08 | 0.33 | 0.00 | -34.50 | 37.08 |
| Mt Somers | 38.42 | 0.30 | 0.00 | -37.41 | 38.42 |
| Prices Valley | 39.95 | 0.31 | 0.00 | -38.33 | 39.96 |
| Taihape | 35.62 | 0.64 | 0.01 | -34.00 | 35.62 |
| Taumarunui | 48.92 | 0.47 | 0.00 | -47.51 | 48.92 |
| Tourere | 30.74 | 0.55 | 0.01 | -29.37 | 30.75 |
| Overall | 39.20 | 0.56 | 0.01 | -37.14 | 39.21 |

[a]Root mean squared error; [b]Lin's concordance correlation coefficient; [c]standard error

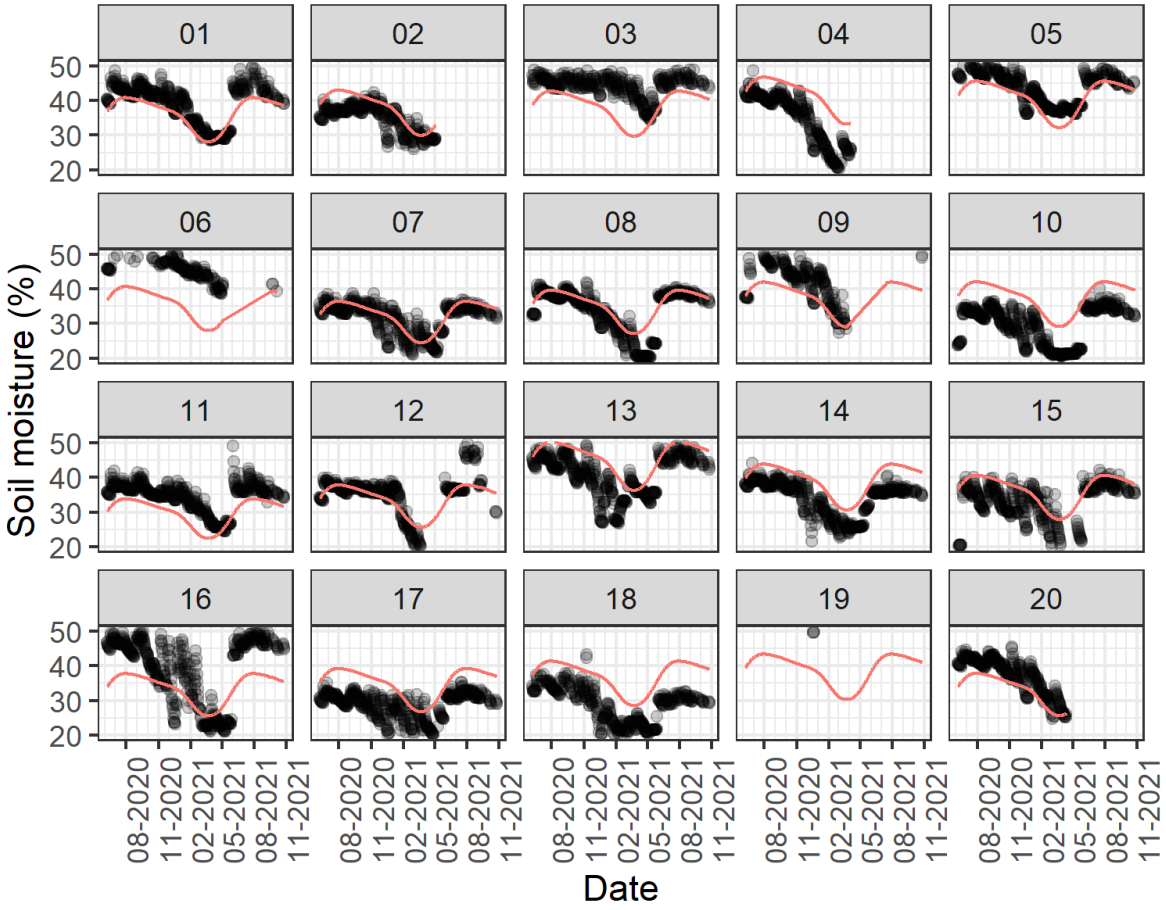


**Figure 40. Measured (points) versus fitted (line) soil moisture for the Mt Somers site over time, using model 1. Panel labels indicate the respective sensor node.**

Figure 40 shows measured (points) and predicted (lines) values of soil moisture for the Mt Somers site using model 1. Plots for the other sites are presented in the Appendix. Figure 40 shows one clear reason why the conformance between the data and the model are poor: the model is forced to wrap at the 1 January/31 December boundary, whereas the data obviously cannot enforce this behaviour. Nevertheless, the predicted trend shows the highest soil moisture towards the middle of the year and the lowest in late summer, as expected. Measured-versus-fitted plots for the other sites are presented in the Appendix.

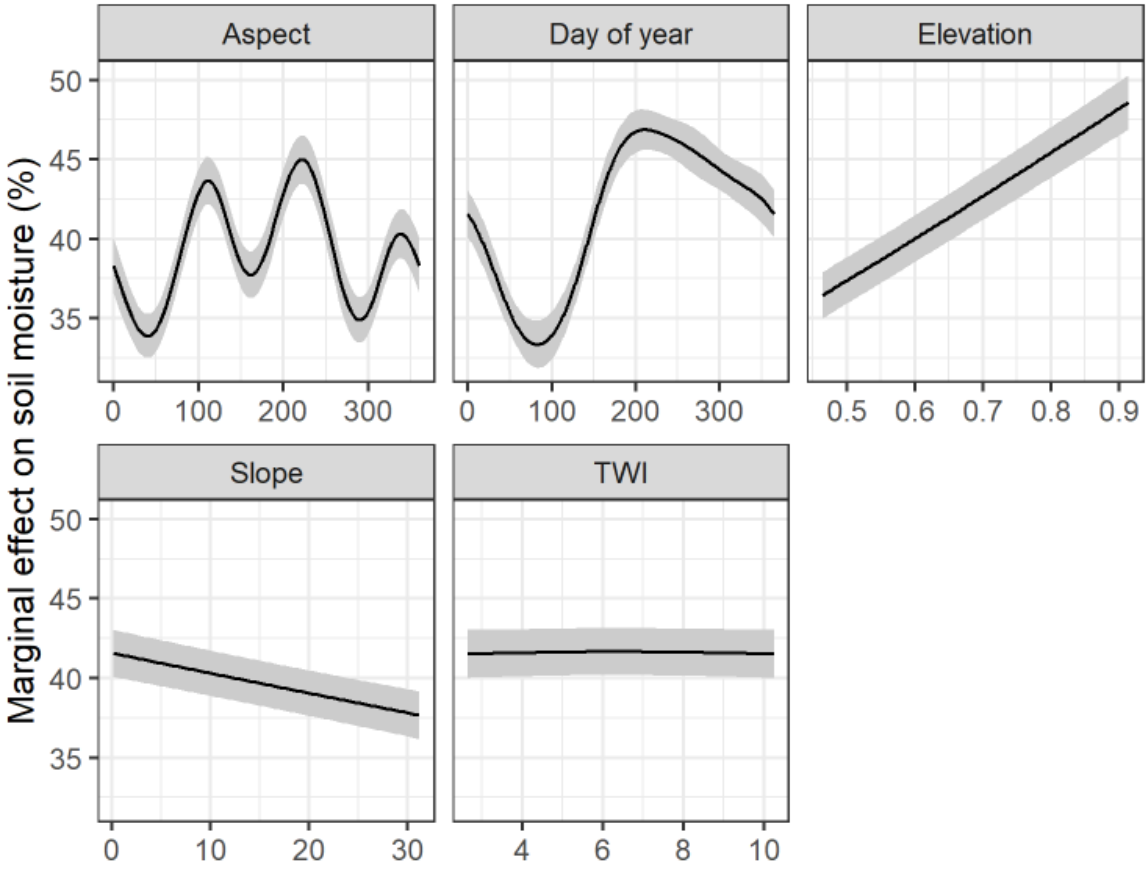


**Figure 41. Plot of the effect of the different explanatory variables for soil moisture model 1. Explanatory variables are given in their natural units. For each panel, the explanatory variables that are not changing are held at a fixed value (generally the median or a sensible default). The vertical axis is the same for all panels. The solid line represents the mean estimate, while the shaded area represents the 95% confidence interval of the mean estimate.**

Figure 42 and Figure 43 depict spatial predictions of soil moisture at the Mt Somers site when the soils are assumed to be close to wilting point (about 1 March, based on the modelled trend in Figure 40) and field capacity (25 June), respectively. Figure 44 shows how predictions vary across individual hillslopes on 25 June on the high-resolution prediction grid. Maps for the other sites are presented in the Appendix.

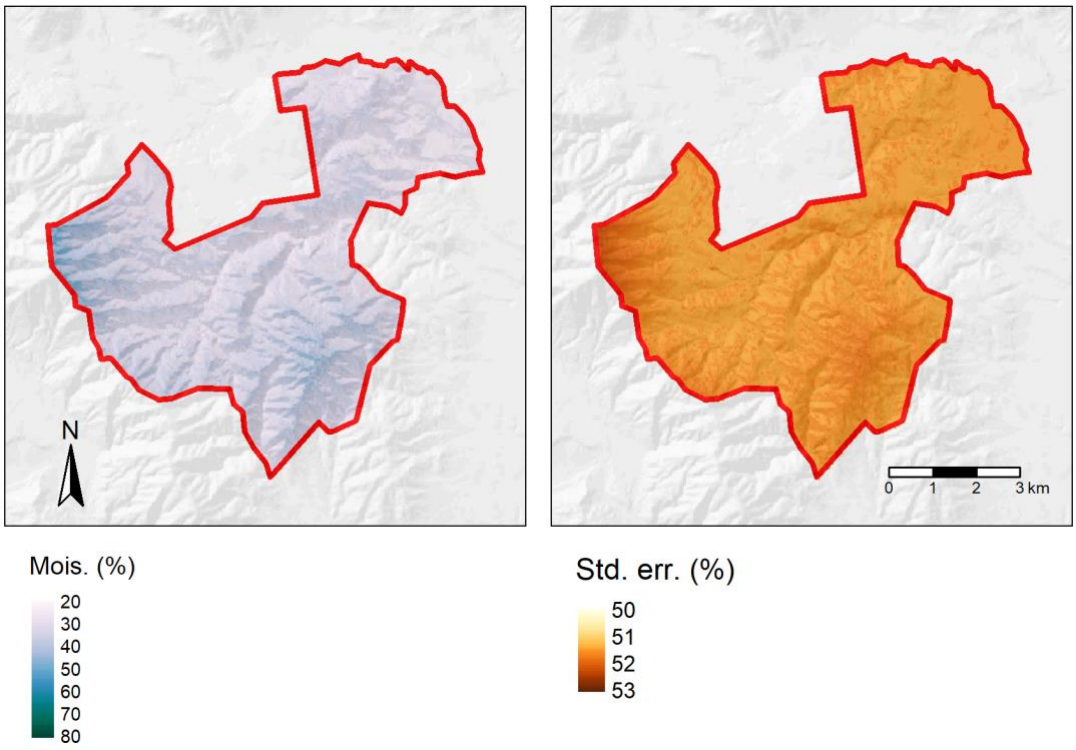


**Figure 42. Predicted soil moisture at Mt Somers on 1 March, when soils are near their driest.**

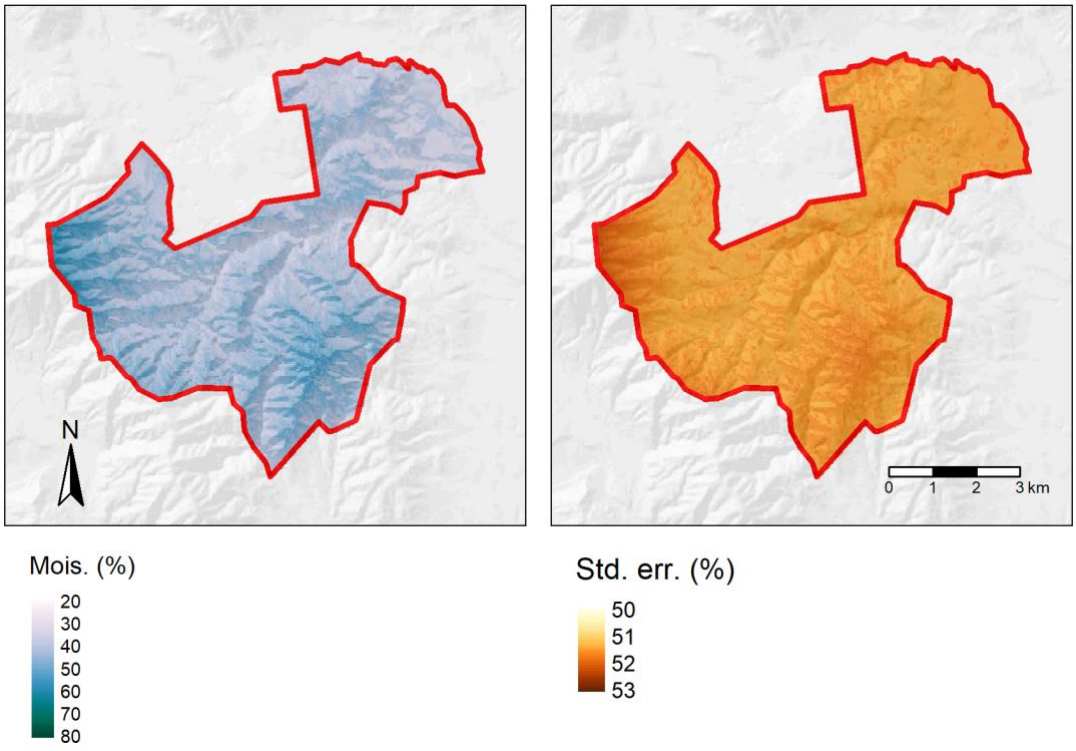


**Figure 43. Predicted soil moisture at Mt Somers on 25 June, when soils are near their wettest.**

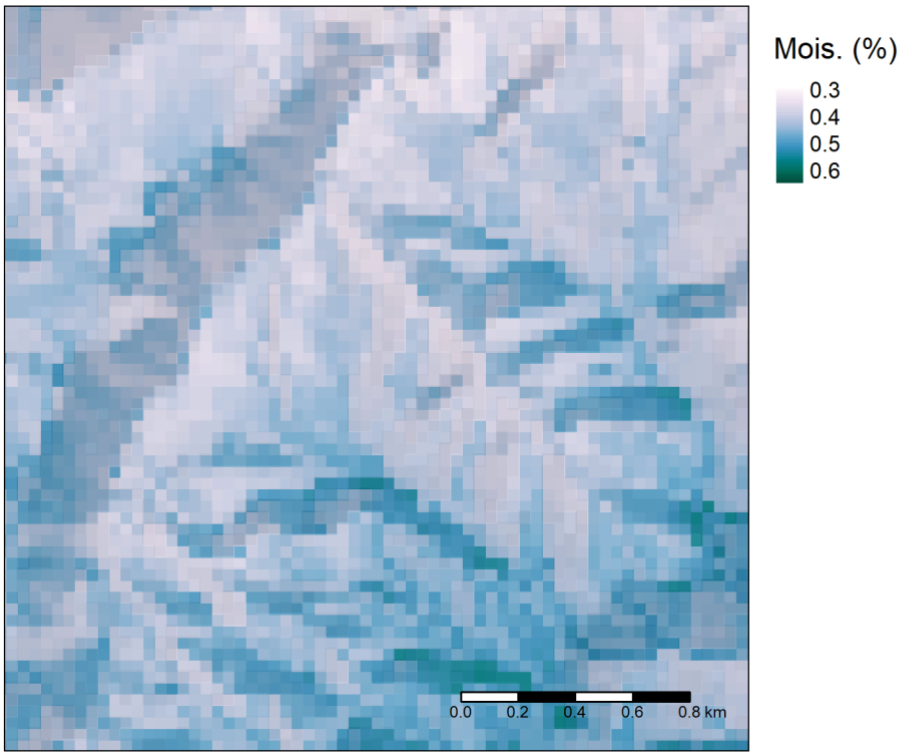


**Figure 44. Predicted soil moisture at Mt Somers on 15 July, showing variation in predicted moisture across individual hillslopes. Resolution of the prediction grid is 30 m.**

### 3.2.3 Yield modelling

*Air temperature calibration*

**Canterbury weather stations**

The fitted equation for prediction of $T_{\text{soil},20}$ from $T_{\text{air}}$ at Canterbury weather stations is

$$T_{\text{soil},20} = 0.846T_{\text{air}} + 1.8$$

The fitted relationship has an $R^2$ of 0.74 (Figure 45). The reversed equation for predicting $T_{\text{air}}$ from $T_{\text{soil},20}$ is

$$T_{\text{air}} = 1.182T_{\text{soil},20} - 2.128$$

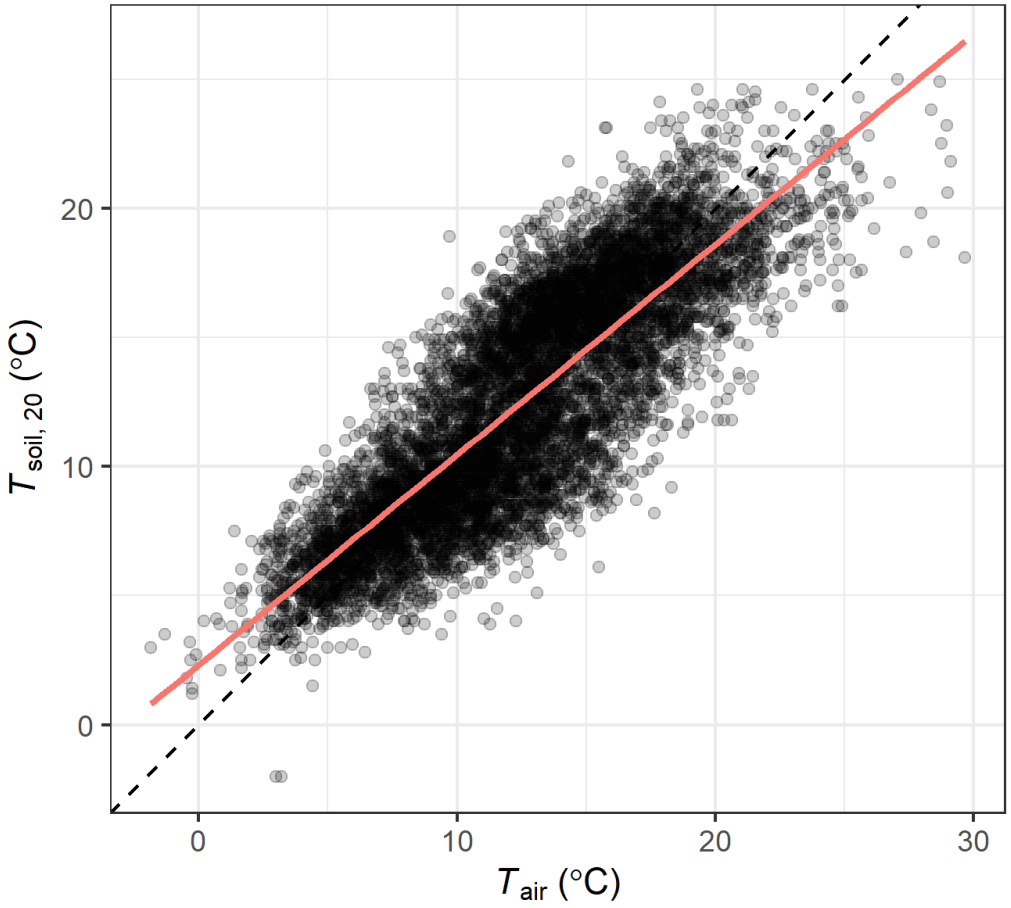


**Figure 45. Relationship between air temperature and 20 cm soil temperature measured at Canterbury weather stations. Dashed line is the 1:1 line and solid line is the line of best fit.**

### Hawke's Bay weather stations

The fitted equation for prediction of $T_{\text{soil},20}$ from $T_{\text{air}}$ at Hawke's Bay weather stations is

$$T_{\text{soil},20} = 0.911T_{\text{air}} + 1.847$$

The fitted relationship has an $R^2$ of 0.77 (Figure 46). The reversed equation for predicting $T_{\text{air}}$ from $T_{\text{soil},20}$ is

$$T_{\text{air}} = 1.098T_{\text{soil},20} - 2.027$$

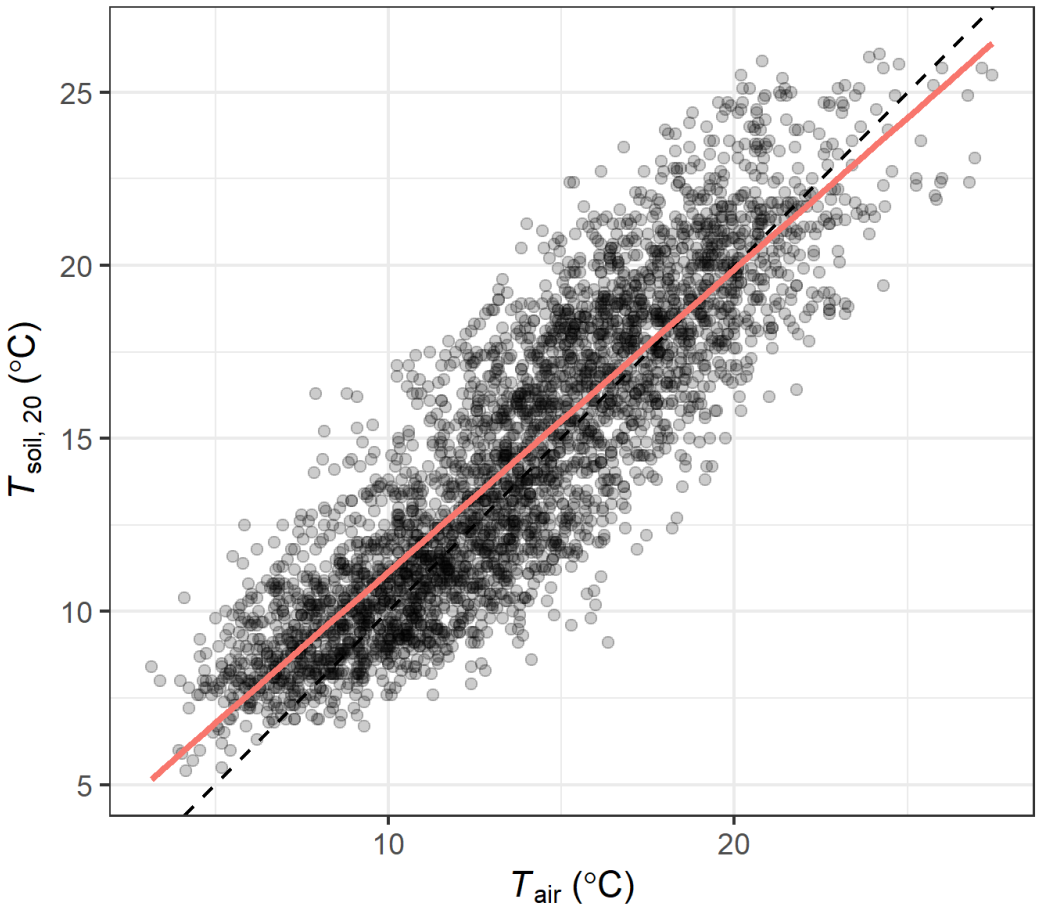


**Figure 46. Relationship between air temperature and 20 cm soil temperature measured at Hawke's Bay weather stations. Dashed line is the 1:1 line and solid line is the line of best fit.**

### Wanganui weather stations

The fitted equation for prediction of $T_{\text{soil},20}$ from $T_{\text{air}}$ at Wanganui weather stations is

$$T_{\text{soil},20} = 0.896T_{\text{air}} + 2.233$$

The fitted relationship has an $R^2$ of 0.80 (Figure 47). The reversed equation for predicting $T_{\text{air}}$ from $T_{\text{soil},20}$ is

$$T_{\text{air}} = 1.116T_{\text{soil},20} - 2.492$$

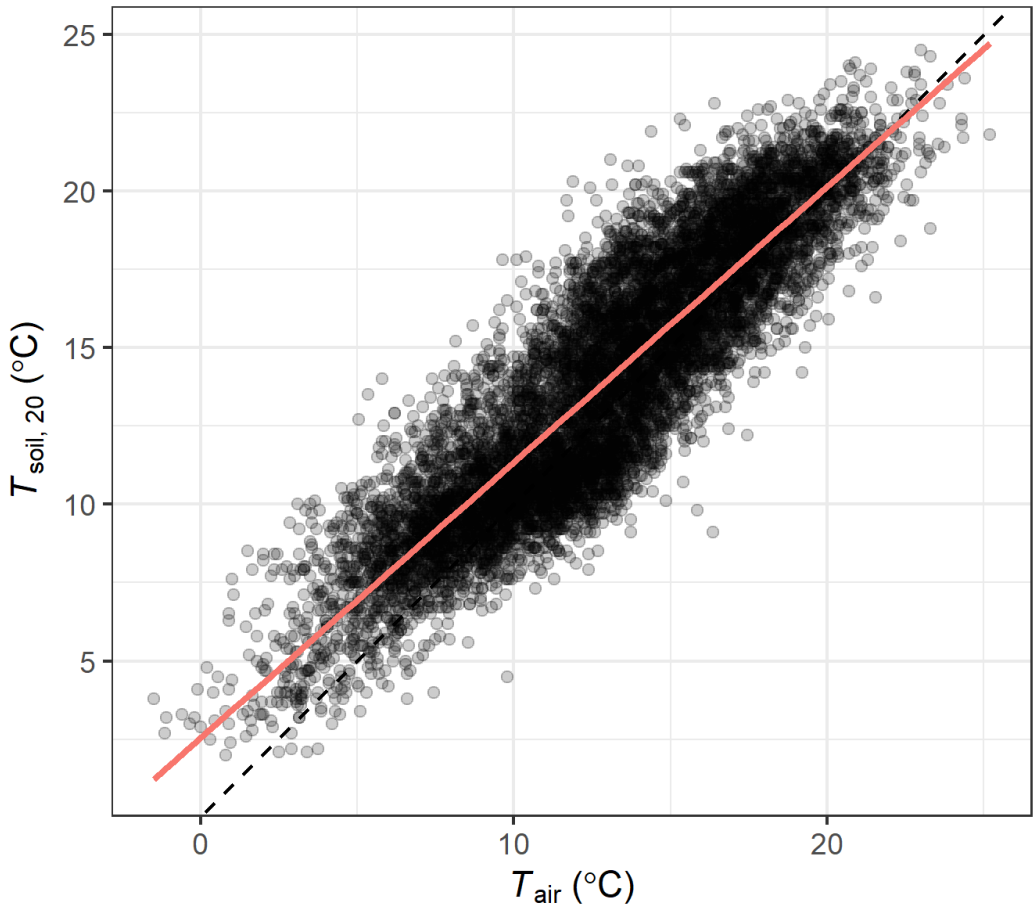


**Figure 47. Relationship between air temperature and 20 cm soil temperature measured at Wanganui weather stations. Dashed line is the 1:1 line and solid line is the line of best fit.**

*Yield prediction*

Figure 48 depicts the annual predicted lucerne yield at Mt Somers. Figure 49 shows how predictions vary across individual hillslopes on the high-resolution prediction grid. The yield decreases with elevation and tends to be greater on north- and west-facing slopes. Maps for the other sites are found in the Appendix.

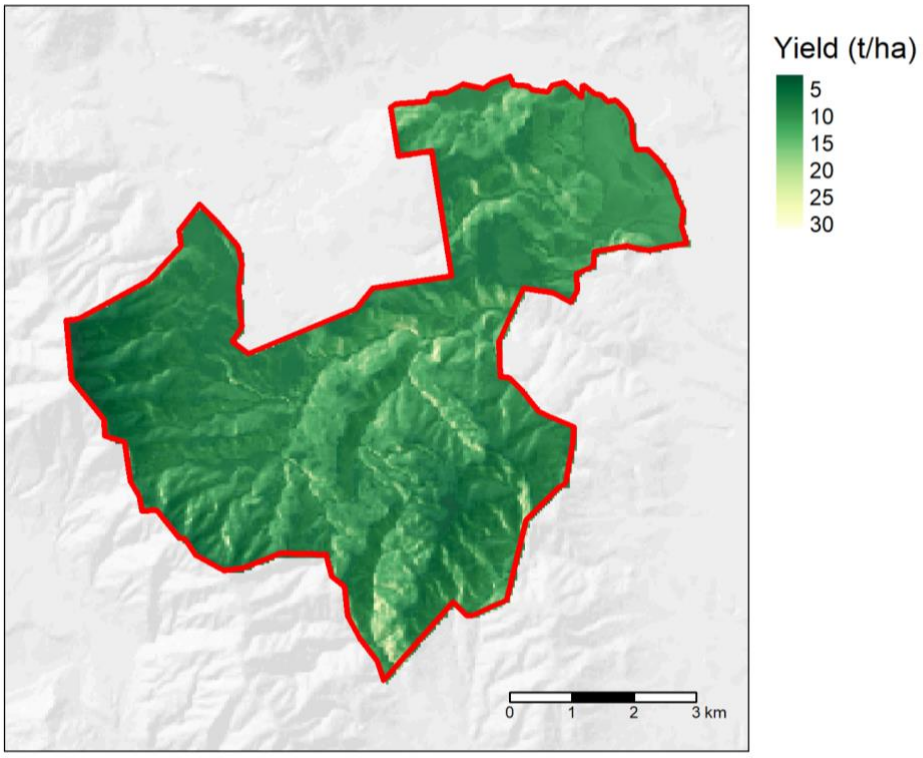


**Figure 48. Predicted annual lucerne yield at Mt Somers for 2020.**

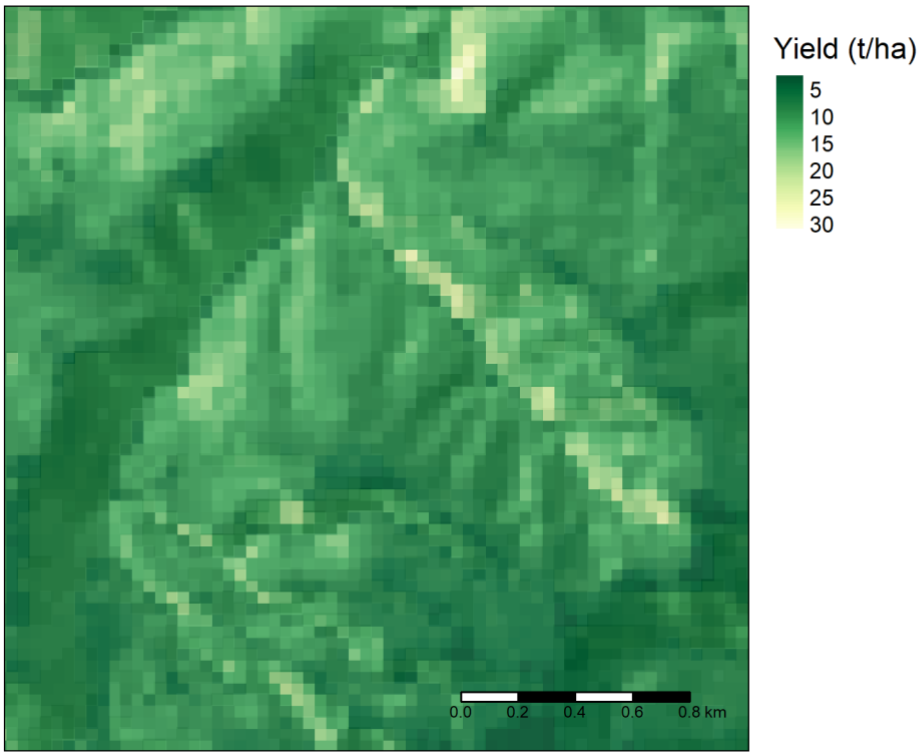


**Figure 49. Predicted annual lucerne yield for Mt Somers for 2020, showing variation in predicted yield across individual hillslopes. Resolution of the prediction grid is 30 m.**

# 4 Discussion

## 4.1 Wireless sensor networks

Overall the wireless sensor networks (WSNs) performed fairly well. We expected some level of attrition of sensor nodes, but fortunately never more than a quarter of nodes at a given site failed. The most frequent cause of failure was water vapour ingress into the above-ground enclosure that contains the electronics; when this happened, the accumulation of moisture over time was eventually sufficient to cause a short circuit and destroy the electronics. Water vapour was able to get into the enclosure through an imperfect seal in the lid of the enclosure, which we had not anticipated. We were able to get the water-damaged sensor nodes back up and running by replacing their electronics.

We noted that some WSN gateways occasionally transmitted more than the expected 24 hourly records per day (Figure 29 and Figure 30). The reason for this is as follows. After a sensor node sends data to the gateway it expects an acknowledgement message from the gateway. If the node does not receive the acknowledgement message it will try twice more to send the data. Sometimes the gateway receives the node's data and forwards it to the cloud database, but the node does not receive the acknowledgement message so it tries again. The node may not receive the acknowledgement message because radio communication from the gateway to the node is not always as good as communication from the node to the gateway (section 1.4).

Figure 29 indicates that duplicate records were transmitted by all WSNs, but especially by the Māhia and Mt Somers WSNs. The other WSNs transmitted fewer than 10 duplicate records each. Figure 30 indicates that the temporal distribution of duplicate records was not uniform. Low numbers of duplicate records were transmitted by the Māhia WSN until July 2021, after which time the number of duplicate records greatly increased. At Mt Somers low numbers of duplicate records were transmitted frequently, but only until May 2021.

At Māhia, duplicate records would often contain data for only one or two sensor nodes. The sensor nodes were often, but not always, nodes located further from the gateway or in relatively sheltered parts of the landscape, where one might expect radio communication with the gateway to be poorer quality. At Mt Somers, duplicate records usually contained data for all sensor nodes, which suggests a different root cause.

## 4.2 Soil temperature

The marginal effects plot for the soil temperature model (Figure 32) indicates that day of year has the largest effect on soil temperature at Mt Somers, as we might expect, followed by elevation and aspect. TWI did not appear to have an appreciable effect on soil temperature. As expected, soil temperature decreased as elevation increased. The effects of day of year, slope, and aspect are difficult to interpret individually due to the three-way interaction between them in model 5. Nevertheless the effects plot indicates that the lowest soil temperatures at Mt Somers occur around day of year 200 (18 July), and that the warmest temperatures should be found around day 20 (20 January), which is broadly

consistent with the sensor data. The effects plot also indicates that the coolest temperatures occur on broadly south-facing slopes, which is what we would expect (Gillingham & Bell 1977; Sheath & Boom 1985).

We are pleased with the performance of the soil temperature model. The percentage of deviance explained by the predictors is high (Table 7) and the relationship between the measured and fitted data (Figure 33) adheres closely to the 1:1 line (Table 8). The prediction uncertainty, as quantified by the standard error, is very low.

Direct comparison of our soil temperature model with others in the literature is difficult because of the diversity of approaches used and landscapes modelled. Despite this we are heartened that our soil temperature model performs about as well as other daily soil temperature models, as assessed by the usual metrics of performance (e.g. Zheng et al. 1993; Horton & Corkrey 2011; Tabari et al. 2011; Xing et al. 2018; Mehdizadeh et al. 2020).

Due to the interaction of day of year with slope gradient and slope aspect in the model, the difference in predicted soil temperature between the warmest and coolest parts of the year was allowed to vary spatially (Figure 38). This intra-annual difference was greatest on relatively flat slopes and smallest on west-facing slopes. The difference tended to be larger on east- and north-facing slopes than on south- and west-facing slopes and was up to 27°C on relatively flat slopes. The size of the predicted difference on flat slopes seems implausible and may represent extrapolation due to undersampling of flat landscapes in our data set. We note, though, that some of the National Climate Database weather stations in Canterbury occasionally report soil temperatures in the order of 22°C, so it may be possible to attain annual warm–cool differences in the order of 20°C, especially in extreme years.

The median date at which the minimum soil temperature was experienced did not differ between north- and south-facing aspects by more than 1 day at most sites (Table 9), with the exception of Taihape and Prices Valley, where north-facing slopes experienced minimum soil temperatures up to 27 days later than south-facing slopes. Between sites, we could not discern a latitudinal trend in the median date of the minimum soil temperature. The median date was generally in mid to late July, except for north-facing slopes at Prices Valley (early August).

It was also difficult to discern meaningful relationships between the differences in the rates of warming to 10°C and to 15°C (Table 10). Data from Māhia, Taihape, and Taumarunui suggest that between north- and south-facing slopes the difference in time taken to reach 15°C is smaller than the difference in time taken to reach 10°C, but the data from Prices Valley and Tourere are inconsistent with this behaviour. At Mt Somers, no south-facing slopes recorded a median daily soil temperature of 15°C.

There is scope for future work. In time, given additional data, we can begin to assess the inter-annual variability in soil temperature. With sufficient length of the soil temperature record it may be possible to avoid wrapping the model at year end and even explore forecasting soil temperature in the near term.

The primary objective of this study is to determine whether we can map micro-indicators such as soil temperature at the farm scale. In light of the performance of the model (Table

7), the plausibility of the modelled soil–landscape relationships found by the model (Figure 32), and the quality of the predictions as judged by the evaluation on the sensor node data (Table 8), we are confident that soil temperature can be mapped at the farm scale.

## 4.3 Soil moisture

Day of year, aspect, and elevation had the largest effect on the modelled soil moisture, followed by slope gradient (Figure 41). Once again TWI had a negligible effect. The other effects were generally as expected.

Predicted soil moisture was higher in the second half of the year than in the first half of the year, presumably due to recharge from autumn and winter rain. Soil moisture predictions tended to be higher on broadly south-facing slopes and lower on broadly north-facing slopes, although the effect of aspect did not vary smoothly from north to south. The smoothness of the curve could be improved by using a GAM with a smaller number of knots.

As elevation increases it apparently has a positive effect on soil moisture (Figure 41). This is interesting, but possibly unremarkable. There is uncertainty in the literature about the degree to which soil moisture gradients at the hillslope scale are controlled by topography versus soil characteristics. There is evidence to suggest that in some landscapes, the main driver could be either factor depending on season or drought status (e.g. Grayson et al. 2002; Western et al. 1999; Yeakley et al. 1998). As slope gradient increases it has a negative effect on soil moisture, possibly due to the greater propensity for surface runoff on steeper slopes.

The performance of the soil moisture model was mediocre (Table 11, Figure 39, and Table 12), and the uncertainty associated with the predictions is large and often exceeded the predicted soil moisture values themselves. Taken together, these problems cast doubt on the usefulness of the predicted soil moisture values as input for agronomic models.

Figure 40 shows one clear reason why the conformance between the data and the model are poor: the model is forced to wrap at the 1 January/31 December boundary, whereas the data obviously cannot enforce this behaviour. In hindsight it may be better to wrap the model at the 30 June/1 July boundary, because the inter-annual variability in soil moisture may be smaller in winter than in summer.

Despite these shortcomings, the predicted trend shows the highest soil moisture towards the middle of the year and the lowest in late summer, as expected. It is possible to detect when the soil is assumed to be near field capacity and when it is close to wilting point (Figure 50), which suggests the predicted trend could be used to monitor moisture stress.

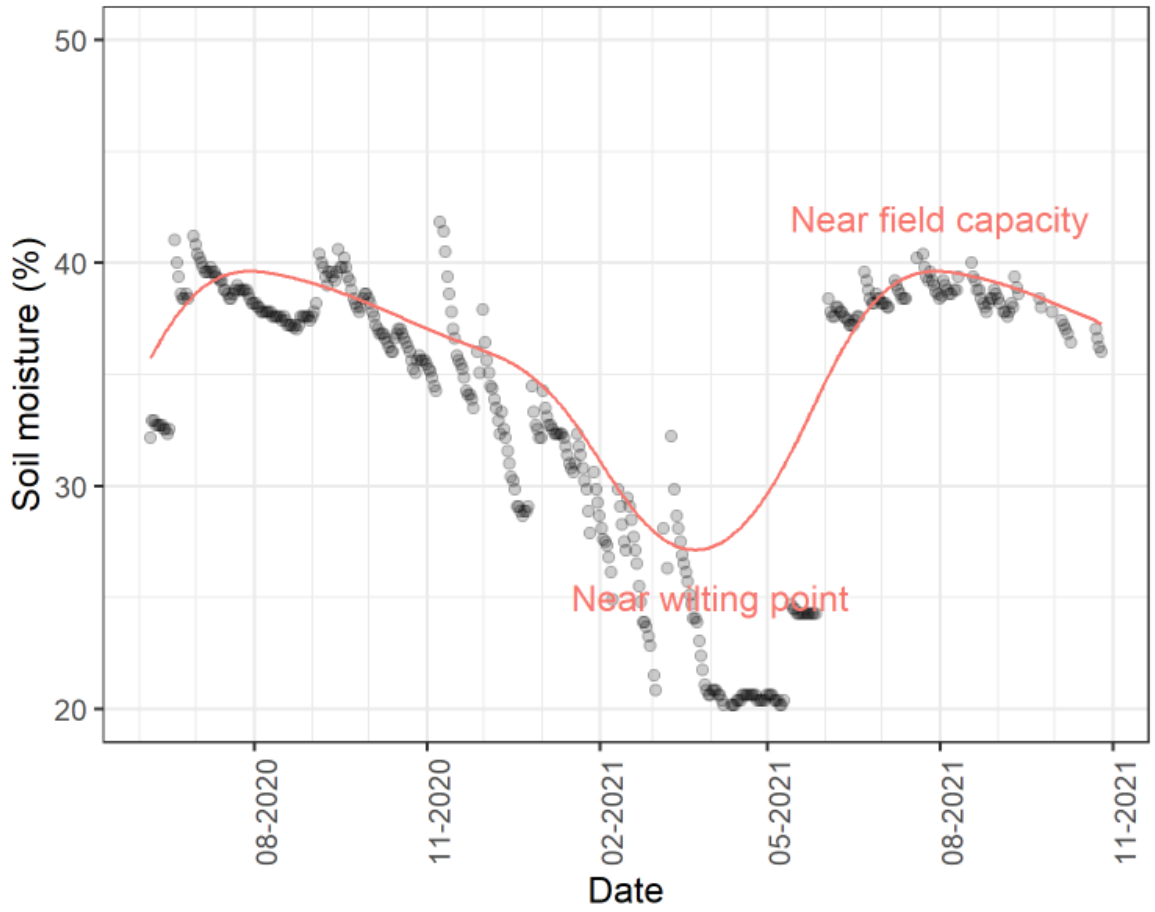


**Figure 50. Measured (points) and predicted (line) soil moisture for sensor 8 at Mt Somers. Annotations indicate where soil moisture is assumed to be near field capacity and wilting point.**

The expected pattern of wetter soils on south-facing slopes and drier soils on north-facing slopes is demonstrated in the sensor node data, except at Māhia, where north-facing soils were consistently wetter throughout the year, regardless of season (e.g. summer versus winter) or relative moisture conditions (e.g. wetter versus drier periods), as indicated in Table 13. We are not sure how to explain this, considering aspect-related differences in soil temperature at the nodes were as expected. We assume the reason is geographical, potentially because the site was located on the flatter part of the Māhia Peninsula, where the effect of aspect was not as strongly expressed, or perhaps due to its location on a marine peninsula with respect to prevailing weather.

**Table 13. Differences in observed moisture at north- and south-facing sensor nodes, expressed as the average of the daily median on the dates indicated of sensor nodes on the indicated aspects. Data were not available for two dates at Prices Valley.**

| Site | Aspect | 1 January 2021 moisture (%)[a] | 2 March 2021 moisture (%)[b] | 1 August 2021 moisture (%)[c] |
|---|---|---|---|---|
| Māhia | N | 35.2 | 27.7 | 42.9 |
| | S | 16.1 | 12.8 | 35.2 |
| Mt Somers | N | 33.0 | 24.7 | 38.8 |
| | S | 36.9 | 40.1 | 49.1 |
| Prices Valley | N | | | 41.8 |
| | S | | | 49.8 |
| Taihape | N | 27.3 | 15.4 | 34.8 |
| | S | 34.6 | 22.9 | 47.6 |
| Taumarunui | N | 40.7 | 27.4 | 42.3 |
| | S | 49.3 | 38.4 | 55.2 |
| Tourere | N | 18.5 | 16.1 | 30.4 |
| | S | 26.5 | 16.9 | 33.5 |

[a]Summer; [b]drier; [c]winter, wetter

The primary objective of this study is to determine whether we can map micro-indicators such as soil moisture at the farm scale. We can map soil moisture at the farm scale, but our work highlighted the difference in predictability between soil temperature and soil moisture. Soil moisture appears to be much less predictable than soil temperature, due in part to the erratic timing and magnitude of rainfall events. It probably also depends on the nature of the spatial variability of soil moisture at the farm scale, which we presume is driven by soil and topographic factors, and on the relative nature of the moisture measurements from our sensors. This is all reflected in the mediocre performance of the fitted soil moisture model. We think the performance of the model can be improved by collecting additional data (especially in the parts of the year where gaps in the record currently exist), adding additional sensors at strategic locations (e.g. on undersampled landscape positions), or by modifying the structure of the model (e.g. by formally handling temporal auto-correlation in soil moisture).

## 4.4 Yield modelling

To meet the data requirements of the yield model we had to make some pragmatic decisions about how to work with the limitations imposed by the characteristics of our farm-scale soil temperature and moisture data. The clear trade-off is that the yield modelling is not as robust as it would have been had the modelled soil data been more suitable. It is obvious, in hindsight, that the sensor nodes should have been equipped with air temperature sensors, which would have avoided the problematic conversion of soil temperature to air temperature.

Furthermore, notwithstanding the quality of the soil moisture model, it is clear now that we should have collected information about soil horizons when the sensor nodes were installed, which would allow us to convert volumetric moisture to millimetres of water for use in the yield model. This would have required the inclusion of a pedologist in the field parties, which at the time was judged more than project resources could accommodate.

It is likely that the model overestimates the lucerne yield. Contributing factors include the quality of the air temperature estimates, the assumption of unlimited water available to the crop, and the accuracy of the standardised growth rates used in the yield model. We think that the assumption of unlimited water is probably the most important, as we would usually expect periods of moisture stress throughout the year. This is reflected in the annual soil moisture trend (refer to Figure 40 and Figure 50). The issues associated with the air temperature estimation are also probably important.

In spite of the limitations described above, our proof of concept shows that we can use micro-indicators to map pasture yield at the farm scale. By implication, the micro-indicators should also be able to be used as input to other types of models that require soil information. We have learned a lot during this study and have identified several factors that, if remediated, we are confident would lead to much more robust estimates of pasture.

# 5 Summary and conclusions

Taking into account the limitations discussed in the report, we are confident that we have achieved the primary and secondary objectives, as set out in section 1.4. The farm-scale soil monitoring and mapping system we developed has shed light on the spatial variability of two key soil properties at the six sites at a resolution that is not possible using contemporary, widely available sources of data, such as from the VCSN and the SMAP and SMOS remote sensing missions. We also demonstrated that the farm-scale soil information can be built upon to produce other agronomically relevant layers of information.

The study has three key outputs:

1 a spatial database of measurements of soil temperature and soil moisture, updated in near real time, for the 120 sensor nodes

2 fitted soil–landscape models for soil temperature and soil moisture, and models for translating between soil temperature and air temperature

3 for each site, daily farm-scale maps of soil temperature, soil moisture, and lucerne yield for 1 year.

## 5.1 Recommendations

We recommend that the WSNs continue to operate. The availability of farm-scale information on micro-indicators in diverse hill country landscapes across New Zealand is critical to inform models that predict pasture production, especially in light of pressures

such as policy changes that affect land use, and global factors such as climate change (Mills et al. 2021).

More data, especially for the parts of the year where data are missing (e.g. over winter at Tourere, or over summer at Prices Valley), should improve the quality of our soil temperature and moisture models. With a greater length of record we should also be able to assess the potential inter-annual variability in soil temperature and moisture at the farm scale.

We recommend the sensor nodes be fitted with air temperature sensors according to meteorological standards, which would complement the existing sensor package, allow for greater understanding of soil–air temperature dynamics on sloping land, and provide a broader platform of farm-scale information to feed into agronomic models.

We recommend the collection of additional pedological information at the sensor nodes, especially the depths of soil horizon boundaries, which should enable us to convert volumetric soil moisture to soil moisture in millimetres, as required for the yield model.

## 5.2 Future work

There are a number of opportunities for future work, with respect to both the soil monitoring systems themselves and the bigger picture regarding how they might fit into hill-country farming systems.

### 5.2.1 Soil monitoring systems

It is worth further exploring how well the locations of the sensor nodes represent hill-country landscapes at the study sites. Evidence from the soil moisture modelling indicated that we may not have adequately sampled some combinations of slope and aspect. Also, because we prioritised accessibility (e.g. proximity to farm tracks) in the specification of the sampling domain at each site, it is possible that the sampling domains were biased away from certain types of landscape. For example, we suspect that at some sites, locations that have strong slopes, and therefore strong expression of aspect-related effects, may not be adequately represented. Further analysis is required to assess the extent to which this is true. It may be worth adding a small number of additional sensor nodes across the six sites at strategic, data-driven locations to assess the extent to which they improve the modelling (Carré et al. 2007b).

Adding additional sensing instruments to the sensor nodes would increase the breadth of soil properties that could be monitored. We have already presented a case for measuring air temperature. Soil pH is another candidate because of its importance as a regulator of nutrient availability and soil microbial composition (Wakelin et al. 2013). The measurement of other properties, especially with novel sensors, may also be relevant in certain landscapes. For example, redox sensors (Farrell et al. 1991) may be informative in wetter landscapes; nitrate sensors (Birrell & Hummel 2000; Ali et al. 2019) would give insight into nitrogen movement in the soil profile.

Future work could include adding additional sensors at a shallower depth in the soil profile, such as 20 cm, to be more consistent with NIWA's National Climate Database.

### 5.2.2 Hill country farming systems

We have not explored how soil monitoring systems like the one we developed can fit into hill-country farming systems. We do not presume that the farm-scale maps of soil properties in the format we present here are by themselves the most useful tool for farmers. Rather we think they are the essential building blocks of additional information layers, information systems, and decision-support tools that farmers can use to their fullest potential.

The provision of information layers is an example of digital soil assessment (Carré et al. 2007a; Kidd et al. 2015). In New Zealand hill country, we suspect that tools that help fine-tune the spatial and temporal qualities of decision-making on strongly contrasting hillslopes is a vein worth tapping. But ultimately the development of the systems themselves (e.g. what a useful tool looks like, which information layers are relevant) should involve, and be informed by, the lived experience of farmers and other agricultural professionals.

Ultimately we think the success of these systems depends on involving the farming community, and not just at the individual farm level. We can envisage soil monitoring systems rolled out in a cooperative fashion across groups of farms in a catchment or even wider regional scales, perhaps by employing a citizen science model where farmers receive support, tools, and other information products in exchange for deploying a handful of sensor nodes at strategic locations on their farm. Key issues that would need to be resolved include the number and placement of network gateways in order to minimise the cost of cellular service, and the number of sensor nodes per farm required to achieve modelling of adequate quality.

## 6 Acknowledgements

The authors would like to acknowledge members of the field team and others who provided invaluable technical support to the programme: Harley Betts, Ben Jolly, Kishor Kumar, Paul Peterson, Balin Robertson, and Anthony Ward.

We acknowledge the owners of the land on which our sensor networks are located. We are grateful for their support of the project, their willingness to allow us access, and their assistance in troubleshooting.

Funding for this project was provided by Beef + Lamb New Zealand, the Ministry of Business, Innovation and Employment, Seed Force New Zealand, and PGG Wrightson Seeds, as part of the Hill Country Futures research programme (BLNZT1701).

# 7 Intellectual property

**Table 14. New intellectual property created during this study.**

| Contributor | Intellectual property | Owner |
|---|---|---|
| MWLR | Soil temperature and moisture models and associated data | B+LNZ |
| MWLR | Soil–air temperature models | B+LNZ |
| MWLR | Yield model predictions | B+LNZ |
| MWLR | Embedded software in wireless sensor network components | B+LNZ |

# 8 References


Afrifa-Yamoah E, Mueller UA, Taylor SM, Fisher AJ 2020. Missing data imputation of high-resolution temporal climate time series data. Meteorological Applications 27(1): e1873. doi:10.1002/met.1873

Ali MA, Wang X, Chen Y, Jiao Y, Mahal NK, Moru S, et al. 2019. Continuous monitoring of soil nitrate using a miniature sensor with poly(3-octyl-thiophene) and molybdenum disulfide nanocomposite. ACS Applied Materials & Interfaces 11(32): 29195–29206. doi:10.1021/acsami.9b07120

Amundson RG, Chadwick OA, Sowers JM 1989. A comparison of soil climate and biological activity along an elevation gradient in the eastern Mojave Desert. Oecologia 80(3): 395–400. doi:10.1007/BF00379042

Barringer JRF 1997. Meso-scale mapping of soil temperatures in the Mackenzie Basin, New Zealand. In: Proceedings of GeoComputation '97 & SIRC '97. Dunedin, New Zealand. Pp. 15–18.

Barringer JRF, Lilburne LR 2000. Developing fundamental data layers to support environmental modelling in New Zealand: Progress and problems. In: Proceedings of the 4th International Conference on Integrating GIS and Environmental Modeling (GIS/EM4): Problems, Prospects and Research Needs. Banff, Alberta, Canada.

Beven K, Kirkby MJ 1979. A physically based, variable contributing area model of basin hydrology. Hydrological Sciences Bulletin 24: 43–69. doi:10.1080/02626667909491834

Birrell SJ, Hummel JW 2000. Membrane selection and ISFET configuration evaluation for soil nitrate sensing. Transactions of the American Society of Agricultural and Biological Engineers 43(2): 197–206. doi:10.13031/2013.2694

Brady NC, Weil RR 2017. The nature and properties of soils. 15th edn. Columbus, Ohio, Pearson.

Bui EN, Loughhead A, Corner R 1999. Extracting soil-landscape rules from previous soil surveys. Australian Journal of Soil Research 37: 495–508. doi:10.1071/S98047

Burt TP, Butcher DP 1985. Topographic controls of soil moisture distributions. Journal of Soil Science 36(3): 469–486. doi:10.1111/j.1365-2389.1985.tb00351.x

Carré F, McBratney AB, Mayr T, Montanarella L 2007a. Digital soil assessments: beyond DSM. Geoderma 142(1–2): 69–79. doi:10.1016/j.geoderma.2007.08.015

Carré F, McBratney AB, Minasny B 2007b. Estimation and potential improvement of the quality of legacy soil samples for digital soil mapping. Geoderma 141: 1–14. doi:10.1016/j.geoderma.2007.01.018

Chudinova SM, Frauenfeld OW, Barry RG, Zhang T, Sorokovikov VA 2006. Relationship between air and soil temperature trends and periodicities in the permafrost regions of Russia. Journal of Geophysical Research: Earth Surface 111. doi:10.1029/2005JF000342

Cleveland WS 1979. Robust locally weighted regression and smoothing scatterplots. Journal of the American Statistical Association 74(368): 829–836. doi:10.1080/01621459.1979.10481038

Cleveland WS, Devlin SJ 1988. Locally weighted regression: an approach to regression analysis by local fitting. Journal of the American Statistical Association 83(403): 596–610. doi:10.1080/01621459.1988.10478639

Dawson GB, Fisher RG 1964. Diurnal and seasonal ground temperature variations at Wairakei. New Zealand Journal of Geology and Geophysics 7(1): 144–154. doi:10.1080/00288306.1964.10420166

Drewry JJ, Hedley CB, Ekanayake J 2019. Maximising the value of irrigation through improved use of soil resources and sensor technology. Journal of New Zealand Grasslands 81: 223–230. doi:10.33584/jnzg.2019.81.376

Ekanayake J 2021. Gizmos, gadgets and wireless sensor networks: from garage door openers to satellites. Manaaki Whenua – Landcare Research contract report LC4030. Lincoln, Manaaki Whenua – Landcare Research.

Ekanayake JC, Hedley CB 2018. Advances in information provision from wireless sensor networks for irrigated crops. Wireless Sensor Network 10(4): 71–92. doi:10.4236/wsn.2018.104004

Farrell RE, Swerhone GDW, Kessel C van 1991. Construction and evaluation of a reference electrode assembly for use in monitoring in situ soil redox potentials. Communications in Soil Science and Plant Analysis 22(11-12): 1059–1068. doi:10.1080/00103629109368474

Gillingham AG, Bell LD 1977. Effect of aspect and cloudiness on grass and soil temperatures at a hill site in Raglan County. New Zealand Journal of Agricultural Research 20(1): 37–44. doi:10.1080/00288233.1977.10427299

Gillingham AG, Gray MH, Smith DR 1998. Pasture responses to phosphorus and nitrogen fertilisers on dry hill country. Proceedings of the New Zealand Grassland Association 60: 135–140. doi:10.33584/jnzg.1998.60.2319

Gloyne RW 1971. A note on the average annual mean of daily earth temperature in the United Kingdom. The Meteorological Magazine 100(1182): 1–6.

Grayson RB, Blöschl G, Western AW, McMahon TA 2002. Advances in the use of observed spatial patterns of catchment hydrological response. Advances in Water Resources 25(8): 1313–1334. doi:10.1016/S0309-1708(02)00060-X

Gruijter JJ de, Brus DJ, Bierkens MFP, Knotters M 2006. Sampling for natural resource monitoring. Berlin, Springer-Verlag.

Hedley CB, Roudier P, Yule IJ, Ekanayake J, Bradbury S 2013. Soil water status and water table depth modelling using electromagnetic surveys for precision irrigation scheduling. Geoderma 199: 22–29. doi:10.1016/j.geoderma.2012.07.018

Horton B, Corkrey R 2011. A weighted coefficient model for estimation of Australian daily soil temperature at depths of 5 cm to 100 cm based on air temperature and rainfall. Soil Research 49(4): 305–314. doi:10.1071/SR10151

IoT Technical Spectrum Working Group 2019. IoT spectrum in New Zealand: spectrum available in New Zealand for IoT systems. New Zealand IoT Alliance, Auckland.

Jones CA, Ritchie JT, Kiniry JR, Godwin DC 1986. Subroutine structure. In: Jones CA, Kiniry JR eds. CERES-Maize: a simulation model of maize growth and development. College Station, Texas, Texas A&M University Press. Pp. 49–111.

Kaspar TC, Bland WL 1992. Soil temperature and root growth. Soil Science 154(4): 290–299.

Kidd DB, Webb MA, Malone BP, Minasny B, McBratney AB 2015. Digital soil assessment of agricultural suitability, versatility and capital in Tasmania, Australia. Geoderma Regional 6: 7–21. doi:10.1016/j.geodrs.2015.08.005

Knotters M, Brus DJ, Voshaar JHO 1995. A comparison of kriging, co-kriging and kriging combined with regression for spatial interpolation of horizon depth with censored observations. Geoderma 67: 227–246. doi:10.1016/0016-7061(95)00011-C

Lagacherie P, Voltz M 2000. Predicting soil properties over a region using sample information from a mapped reference area and digital elevation data: a conditional probability approach. Geoderma 97(3–4): 187–208. doi:10.1016/S0016-7061(00)00038-0

Lilburne LR, Webb TH, Hewitt AE, Lynn IH 2012. S-map database manual version 1.3. Landcare Research Contract Report LC 478. Lincoln, New Zealand, Landcare Research.

Lin LI-K 1989. A concordance correlation coefficient to evaluate reproducibility. Biometrics 45: 255–268. doi:10.2307/2532051

LoRa Alliance Technical Marketing Workgroup 2015. LoRaWAN: what is it? A technical overview of LoRa and LoRaWAN. LoRa Alliance, Fremont, California.

McBratney AB, Mendonça SM de L, Minasny B 2003. On digital soil mapping. Geoderma 117: 3–52. doi:10.1016/S0016-7061(03)00223-4

Mcgowan AW, Sheath GW, Webby RW 2003. Lucerne for high quality summer feed in North Island hill country. New Zealand Grassland Association Research and Practice Series 11: 169–174. doi:10.33584/rps.11.2003.3016

McKenzie NJ, Ryan PJ 1999. Spatial prediction of soil properties using environmental correlation. Geoderma 89: 67–94. doi:10.1016/S0016-7061(98)00137-2

McMichael BL, Burke JJ 1998. Soil temperature and root growth. HortScience 33(6): 947–951. doi:10.21273/HORTSCI.33.6.947

Mehdizadeh S, Fathian F, Safari MJS, Khosravi A 2020. Developing novel hybrid models for estimation of daily soil temperature at various depths. Soil and Tillage Research 197: 104513. doi:10.1016/j.still.2019.104513

Mills A, Thomson B, Muir P, Smith N, Moot D 2021. Resident hill country pasture production in response to temperature and soil moisture over 20 years in Central Hawke's Bay. New Zealand Grassland Association Research and Practice Series 17: 253–262. doi:10.33584/rps.17.2021.3451

Moot DJ 2012. An overview of dryland legume research in New Zealand. Crop and Pasture Science 63(9): 726–733. doi:10.1071/CP12103

Moot DJ, Robertson MJ, Pollock KM 2001. Validation of the APSIM-Lucerne model for phenological development in a cool-temperate climate. In: Rowe B, Donaghy D, Mendham N eds. Science and technology: Delivering results for agriculture? Hobart, Tasmania, Australian Agronomy Society.

Moot DJ, Yang X, Ta HT, Brown HE, Teixeira EI, Sim RE, et al. 2021. Simplified methods for on-farm prediction of yield potential of grazed lucerne crops in New Zealand. New Zealand Journal of Agricultural Research 0(0): 1–19. doi:10.1080/00288233.2021.1909078

MWLR 2020. Science during lockdown. Lincoln, Manaaki Whenua – Landcare Research.

Odeh IOA, McBratney AB, Chittleborough DJ 1994. Spatial prediction of soil properties from landform attributes derived from a digital elevation model. Geoderma 63: 197–214. doi:10.1016/0016-7061(94)90063-9

Odeh IOA, McBratney AB, Chittleborough DJ 1995. Further results on prediction of soil properties from terrain attributes: heterotopic cokriging and regression-kriging. Geoderma 67: 215–226. doi:10.1016/0016-7061(95)00007-B

Paul KI, Polglase PJ, Smethurst PJ, O'Connell AM, Carlyle CJ, Khanna PK 2004. Soil temperature under forests: a simple model for predicting soil temperature under a range of forest types. Agricultural and Forest Meteorology 121(3): 167–182. doi:10.1016/j.agrformet.2003.08.030

Piikki K, Söderström M 2019. Digital soil mapping of arable land in Sweden – validation of performance at multiple scales. Geoderma 352: 342–350. doi:10.1016/j.geoderma.2017.10.049

Pregitzer KS, King JS 2005. Effects of soil temperature on nutrient uptake. In: BassiriRad H ed. Nutrient acquisition by plants: an ecological perspective. Ecological Studies 181. Berlin, Heidelberg, Springer. Pp. 277–310. doi:10.1007/3-540-27675-0_10

Radcliffe JE 1982. Effects of aspect and topography on pasture production in hill country. New Zealand Journal of Agricultural Research 25(4): 485–496. doi:10.1080/00288233.1982.10425211

Radcliffe JE, Lefever KR 1981. Aspect influences on pasture microclimate at Coopers Creek, North Canterbury. New Zealand Journal of Agricultural Research 24(1): 55–66. doi:10.1080/00288233.1981.10420871

Robertson BL, Brown JA, McDonald T, Jaksons P 2013. BAS: balanced acceptance sampling of natural resources. Biometrics 69(3): 776–784. doi:10.1111/biom.12059

Schmidlin TW, Peterson FF, Gifford RO 1983. Soil temperature regimes in Nevada. Soil Science Society of America Journal 47(5): 977–982. doi:10.2136/sssaj1983.03615995004700050027x

Shati F, Prakash S, Norouzi H, Blake R 2018. Assessment of differences between near-surface air and soil temperatures for reliable detection of high-latitude freeze and thaw states. Cold Regions Science and Technology 145: 86–92. doi:10.1016/j.coldregions.2017.10.007

Sheath GW, Boom RC 1985. Effects of November–April grazing pressure on hill country pastures 3. Interrelationship with soil and pasture variation. New Zealand Journal of Experimental Agriculture 13(4): 341–349. doi:10.1080/03015521.1985.10426102

Shreve F 1924. Soil temperature as influenced by altitude and slope exposure. Ecology 5(2): 128–136. doi:10.2307/1929010

Tabari H, Sabziparvar A-A, Ahmadi M 2011. Comparison of artificial neural network and multivariate linear regression methods for estimation of daily soil temperature in an arid region. Meteorology and Atmospheric Physics 110(3): 135–142. doi:10.1007/s00703-010-0110-z

Toy TJ, Kuhaida Jr. AJ, Munson BE 1978. The prediction of mean monthly soil temperature from mean monthly air temperature. Soil Science 126(3): 181–189.

Tozer KN, Douglas GB 2016. Pasture establishment on non-cultivable hill country: a review of the New Zealand literature. New Zealand Grassland Association Research and Practice Series 16: 213–224. doi:10.33584/rps.16.2016.3233

Wakelin S, Koten C van, O'Callaghan M, Brown M 2013. Physicochemical properties of 50 New Zealand pasture soils: a starting point for assessing and managing soil microbial resources. New Zealand Journal of Agricultural Research 56(4): 248–260. doi:10.1080/00288233.2013.822003

Western A, Blöschl G 1999. On the spatial scaling of soil moisture. Journal of Hydrology 217: 203–224. doi:10.1016/S0022-1694(98)00232-7

Western A, Grayson RB, Blöschl G, Willgoose G, McMahon TA 1999. Observed spatial organization of soil moisture and its relation to terrain indices. Water Resources Research 35: 797–810. doi: 10.1029/1998WR900065

Will GM 1959. Soil-moisture and soil-temperature studies under radiata pine, Whakarewarewa Forest, 1954–55. New Zealand Journal of Agricultural Research 2(1): 184–193. doi:10.1080/00288233.1959.10427137

Wood SN 2017. Generalized additive models: an introduction with R. 2nd ed. Texts in statistical science. New York, Chapman Hall/CRC. doi:10.1201/9781315370279

Xing L, Li L, Gong J, Ren C, Liu J, Chen H 2018. Daily soil temperatures predictions for various climates in United States using data-driven model. Energy 160: 430–440. doi:10.1016/j.energy.2018.07.004

Yeakley JA, Swank WT, Swift LW, Hornberger GM, Shugart HH 1998. Soil moisture gradients and controls on a southern Appalachian hillslope from drought through

recharge. Hydrology and Earth System Sciences 2(1): 41–49. doi:10.5194/hess-2-41-1998

Young D 2020. Five scientific achievements that happened during coronavirus lockdown. Washington (DC): Smithsonian Institute; accessed 2022 May 16. https://www.smithsonianmag.com/innovation/five-scientific-achievements-happened-during-coronavirus-lockdown-180975271/.

Zhan M, Xia L, Zhan L, Wang Y 2019. Recognition of changes in air and soil temperatures at a station typical of China's subtropical monsoon region (1961–2018). Advances in Meteorology 2019: e6927045. doi:10.1155/2019/6927045

Zheng D, Hunt ER, Running SW 1993. A daily soil temperature model based on air temperature and precipitation for continental applications. Climate Research 2(3): 183–191.

# Appendix – maps and charts for Māhia, Prices Valley, Taihape, Taumarunui and Tourere

## Māhia

*Sampling*

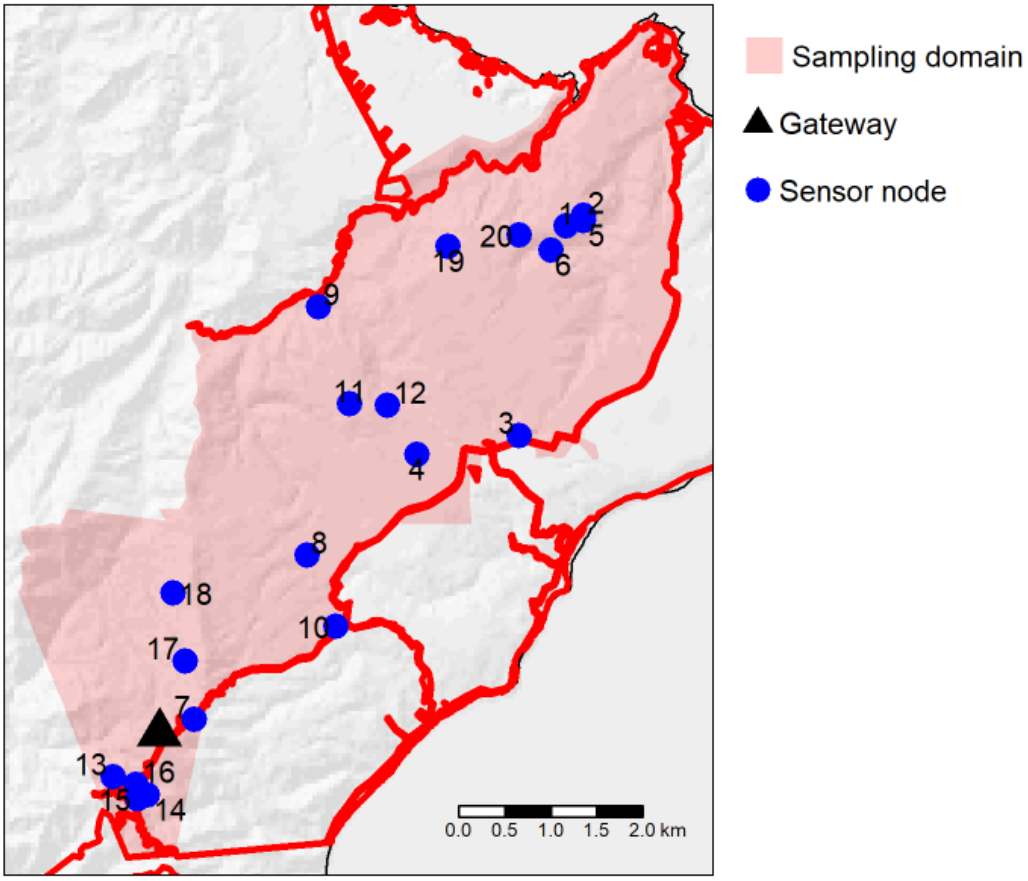


**Figure A1. Location of sampling domain, WSN gateway, and sensor nodes at Māhia.**

*Scorpan covariates*

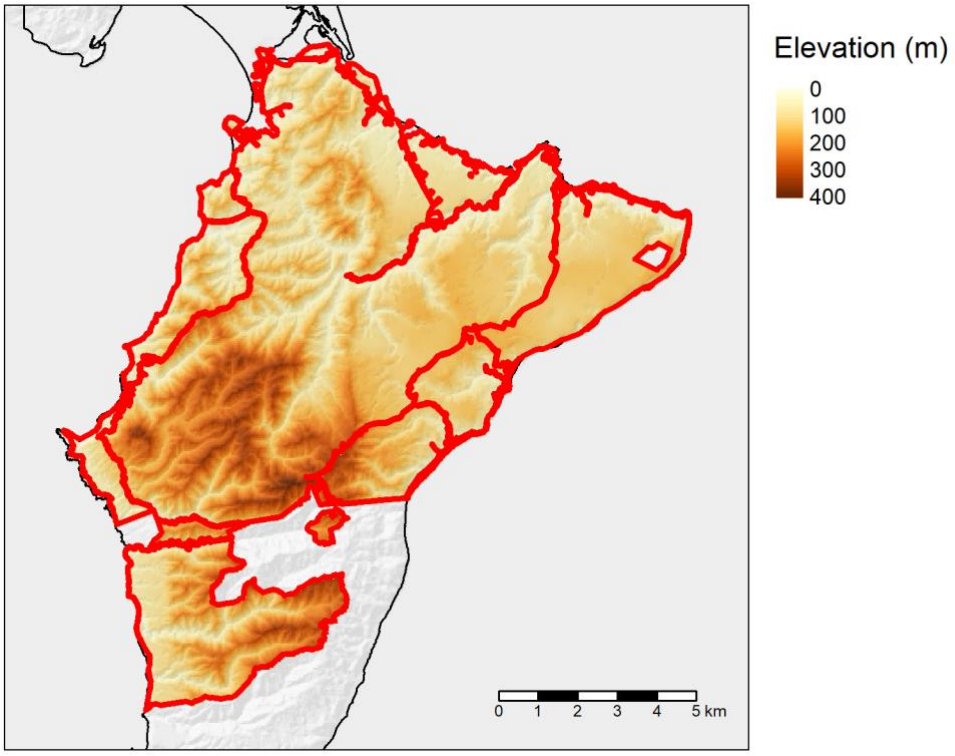


**Figure A2. Elevation at Māhia.**

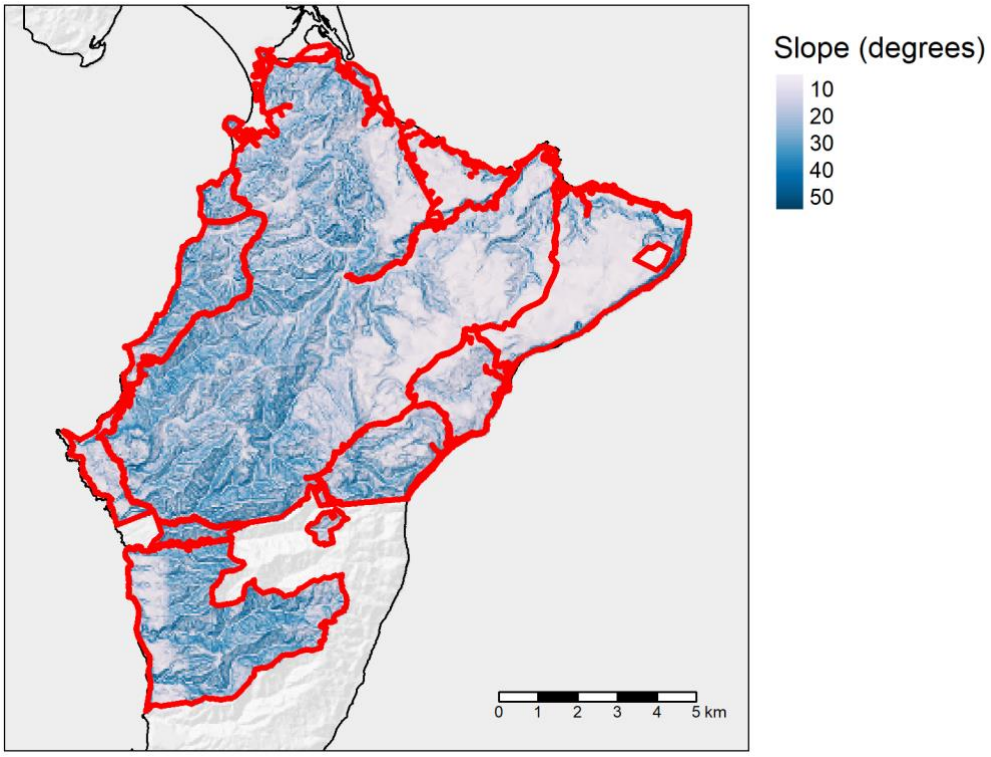


**Figure A3. Slope at Māhia.**

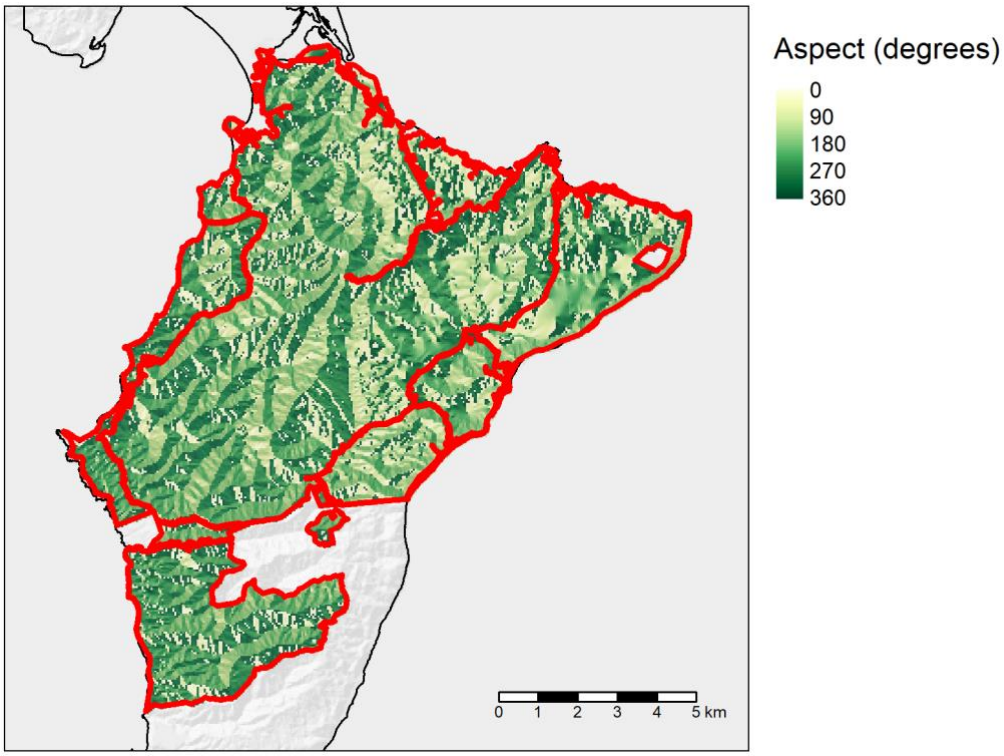


**Figure A4. Aspect at Māhia.**

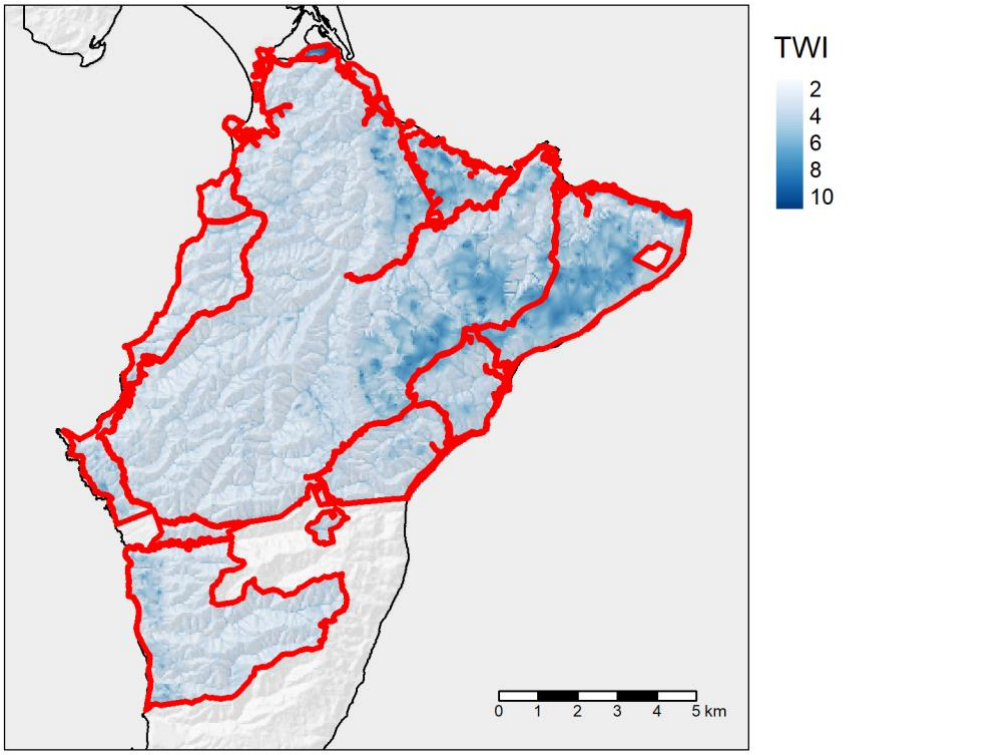


**Figure A5. Topographic wetness index at Māhia.**

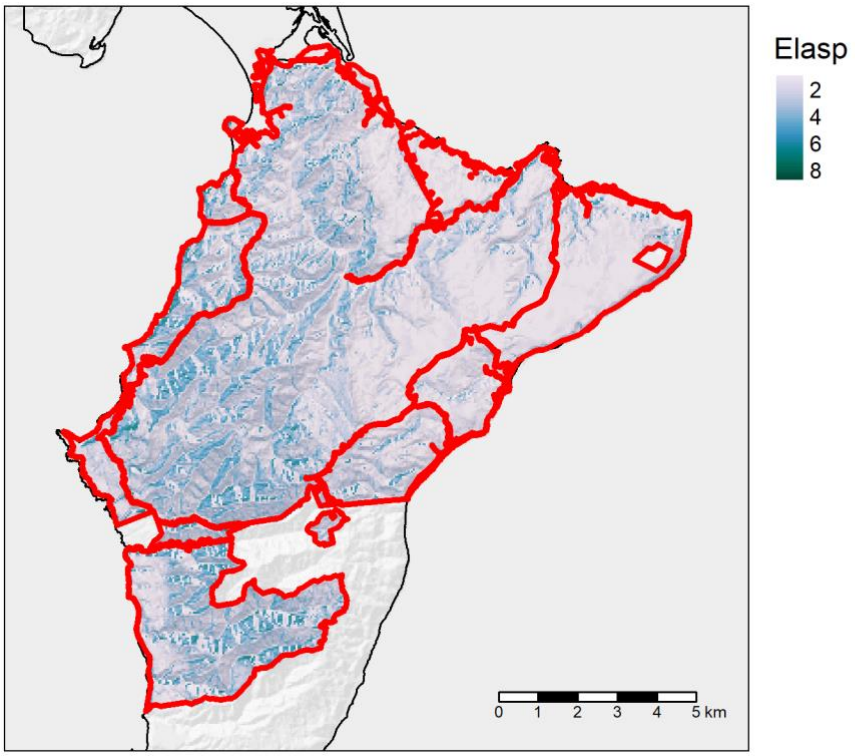


**Figure A6. Elasp at Māhia.**

*Soil temperature*

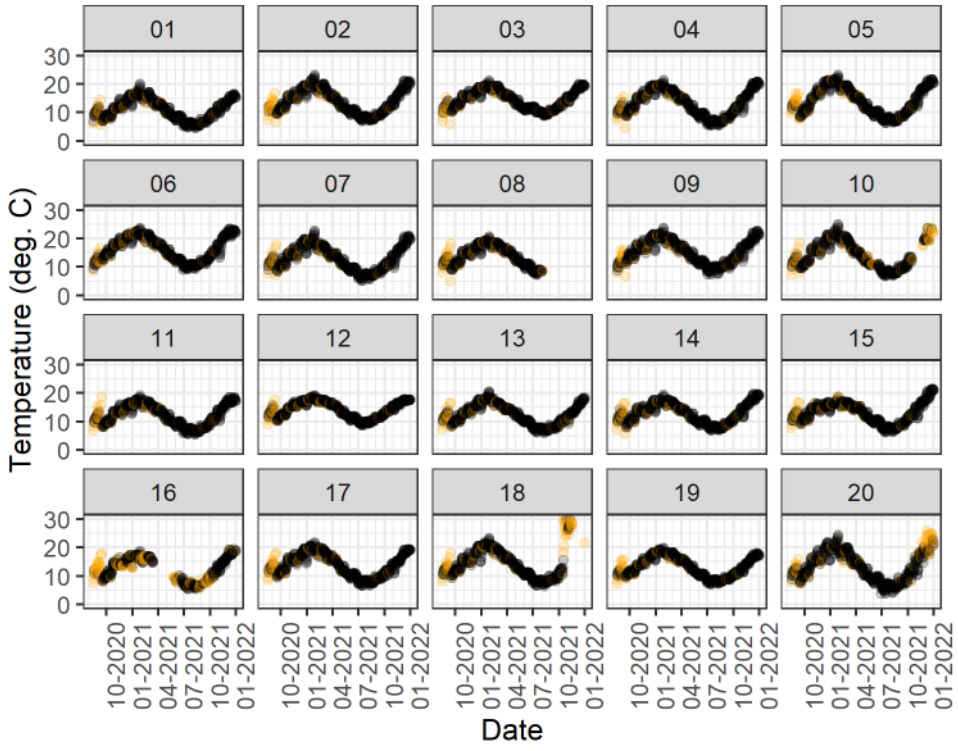


**Figure A7. Daily median soil temperature data for the Māhia WSN after trimming of the start and end dates, and removal of low and high temperatures, and periods of no change in soil temperature. Panel labels indicate the respective sensor node. Points that were removed as a result of the data trimming are shown in orange, while presumed valid points are in black.**

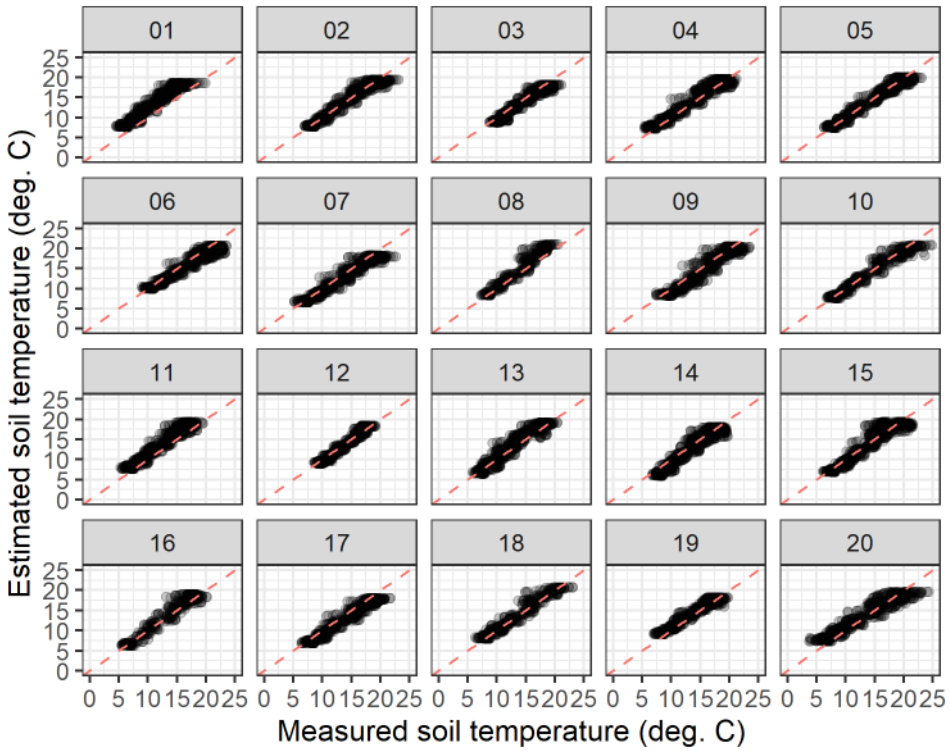


**Figure A8. Measured versus fitted soil temperature plot for the Māhia site using model 5. Panel labels indicate the respective sensor node.**

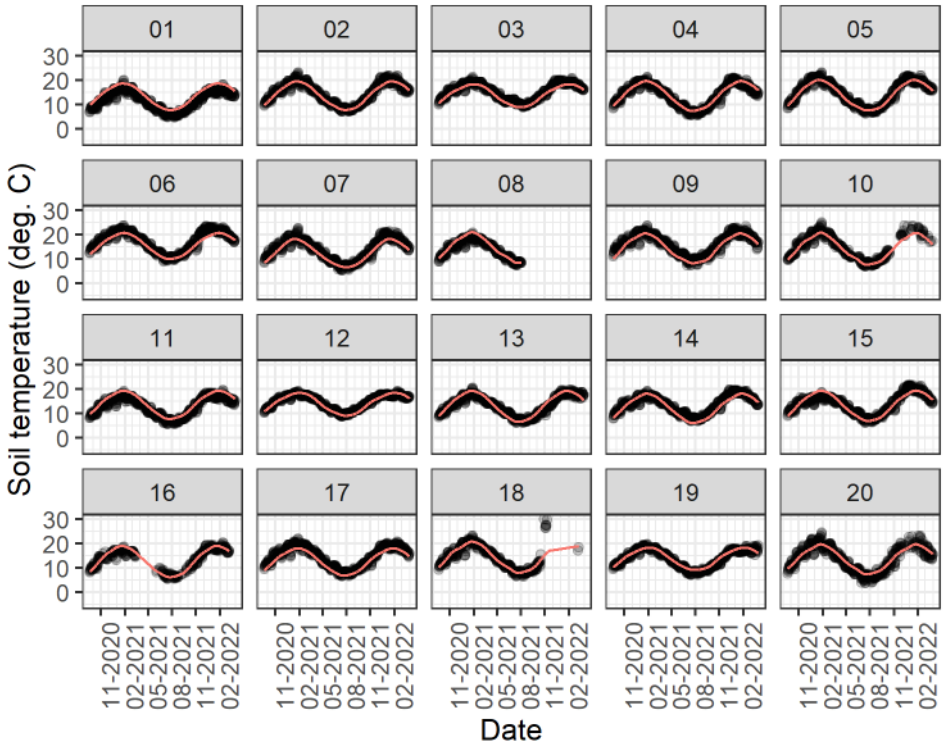


**Figure A9. Measured (points) versus fitted (line) soil temperature for the Māhia site over time, using model 5. Panel labels indicate the respective sensor node.**

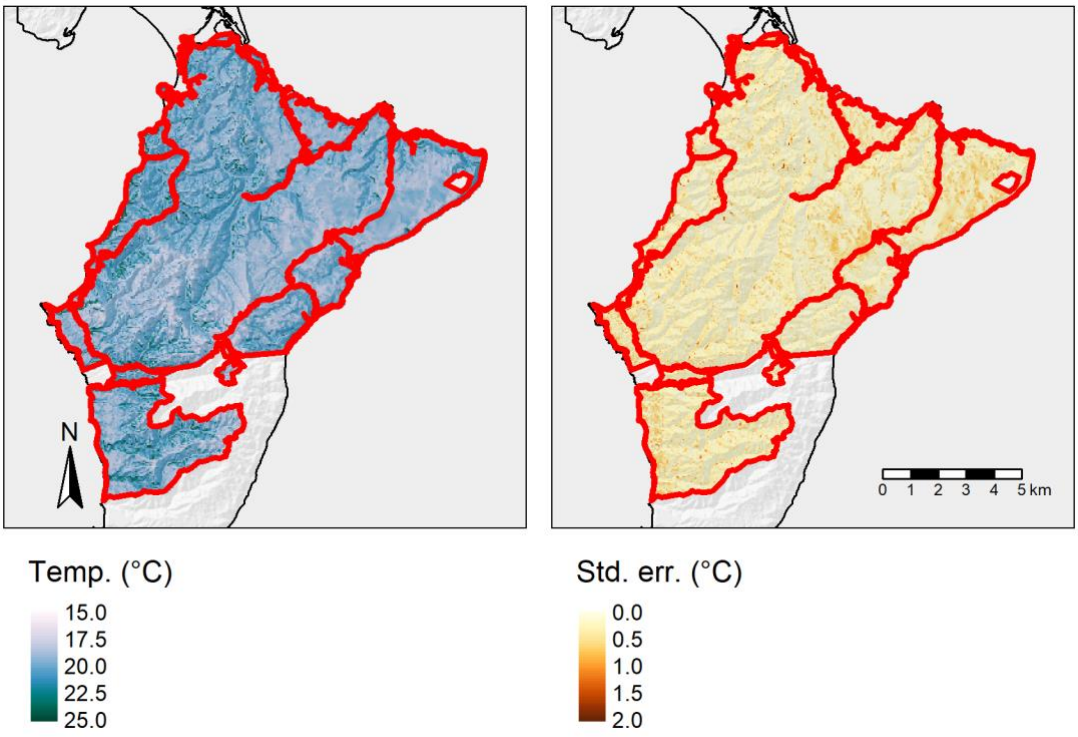


**Figure A10. Predicted soil temperature at Māhia on 15 January, when soils are near their warmest.**

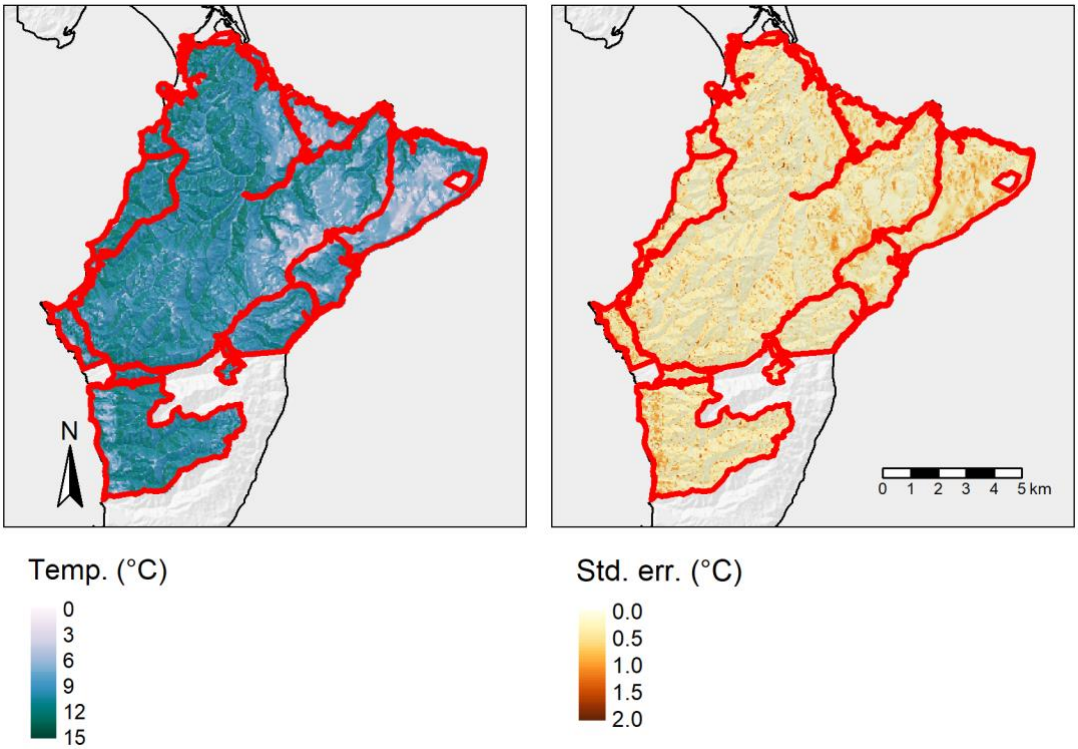


**Figure A11. Predicted soil temperature at Māhia on 15 July, when soils are near their coolest.**

*Soil moisture*

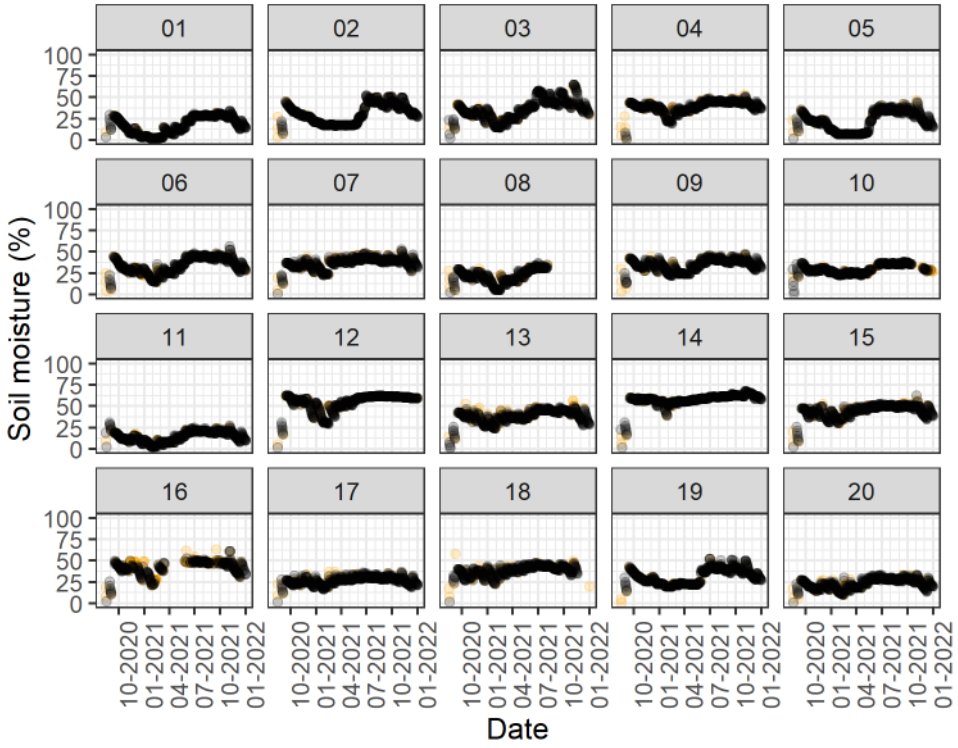


**Figure A12. Daily median soil moisture data for the Māhia site after trimming of the start and end dates, and removal of low and high soil moisture values, and periods of no change in soil moisture. Panel labels indicate the respective sensor node. Points excised from the data have been coloured orange.**

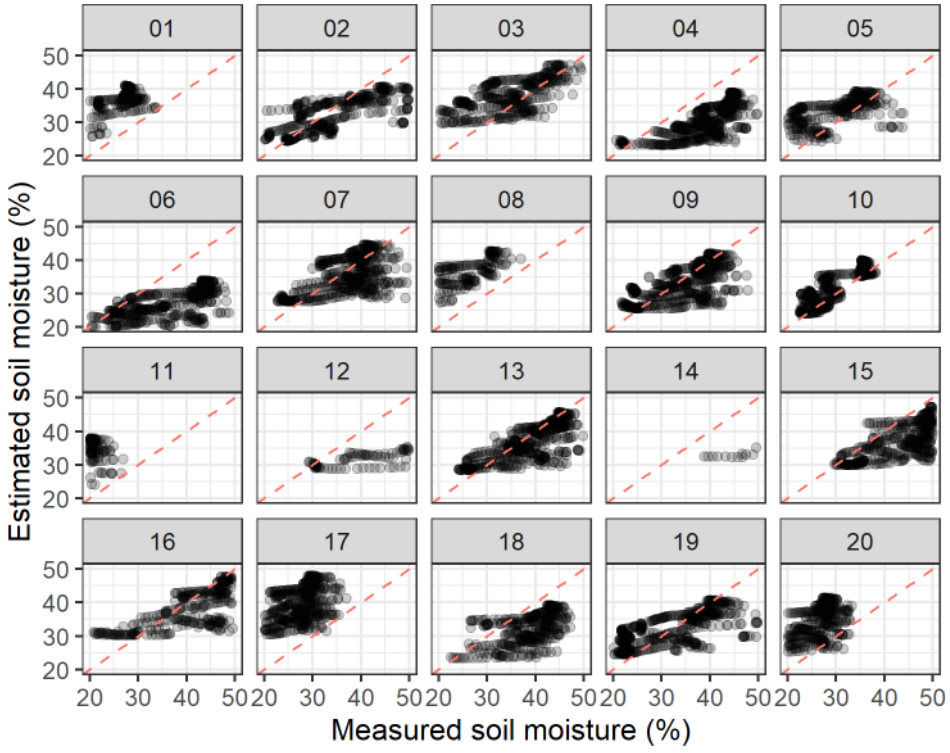


**Figure A13. Measured versus fitted soil moisture plot for the Māhia site using model 1. Panel labels indicate the respective sensor node.**

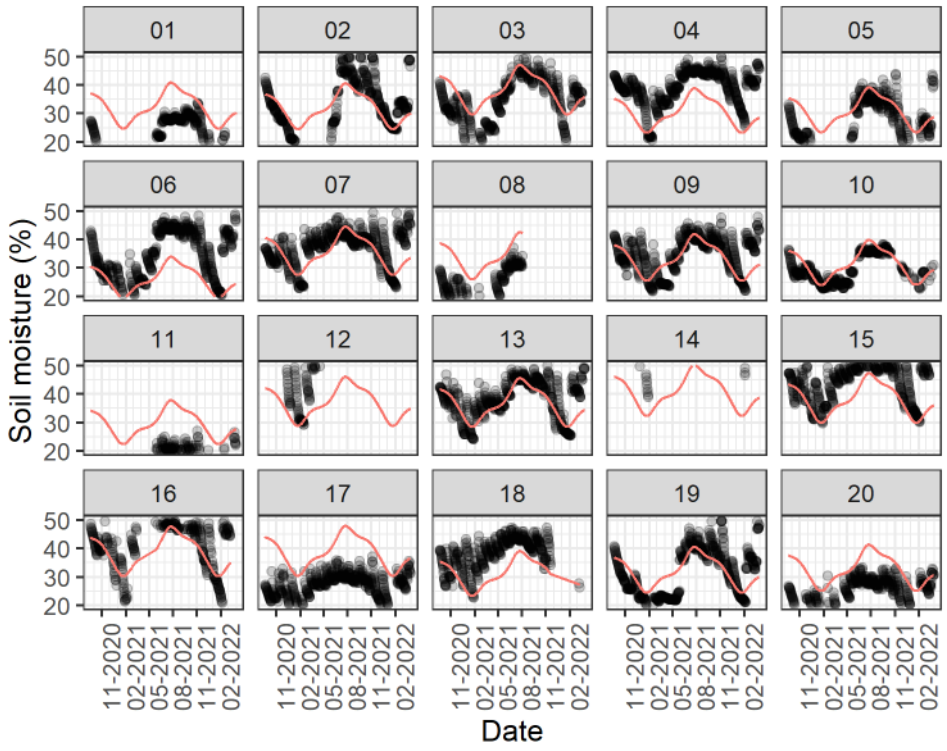


**Figure A14. Measured (points) versus fitted (line) soil moisture for the Māhia site over time, using model 1. Panel labels indicate the respective sensor node.**

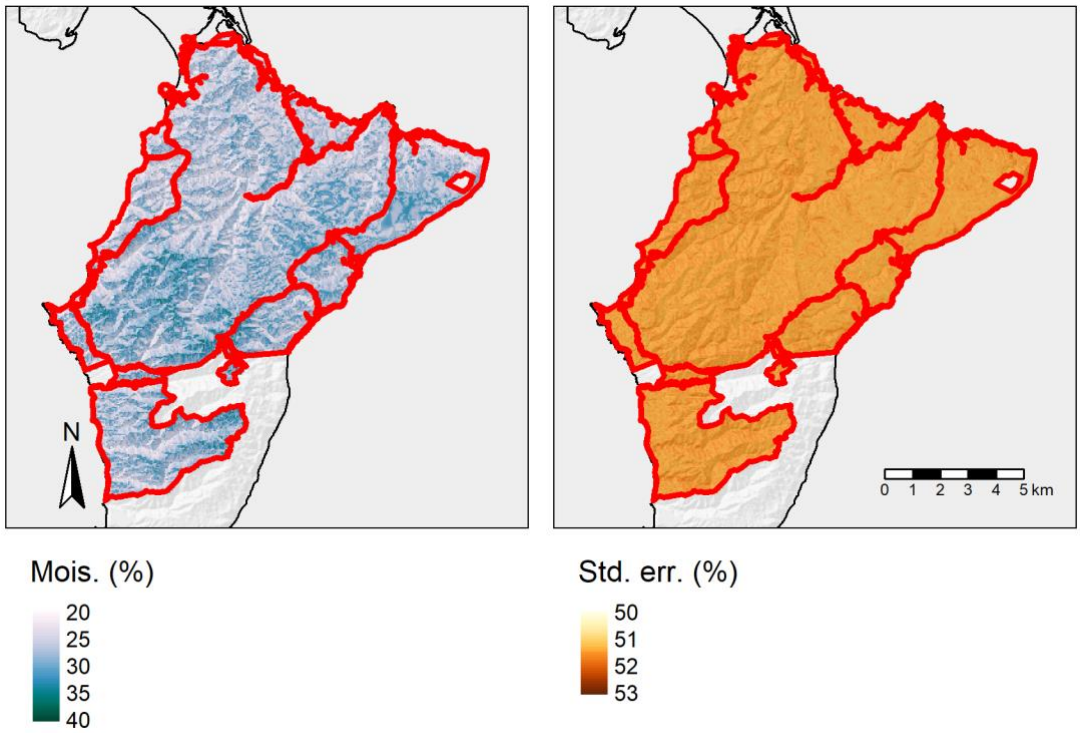


**Figure A15. Predicted soil moisture at Māhia on 1 March, when soils are near their driest.**

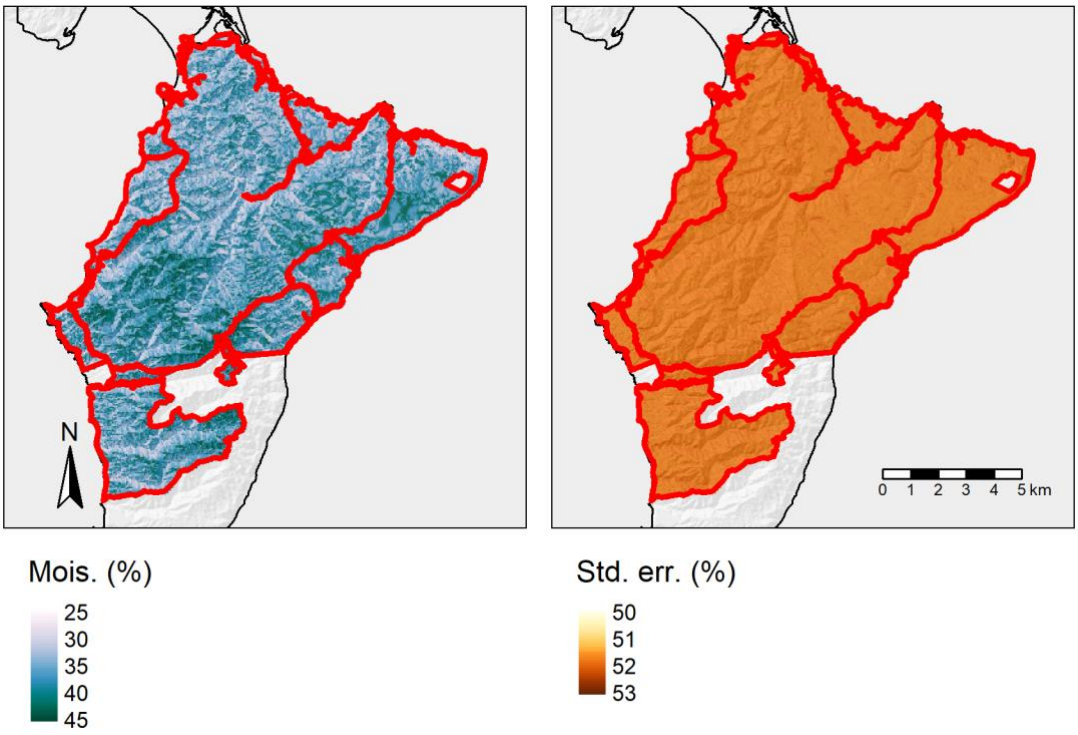


**Figure A16. Predicted soil moisture at Māhia on 25 June, when soils are near their wettest.**

*Yield*

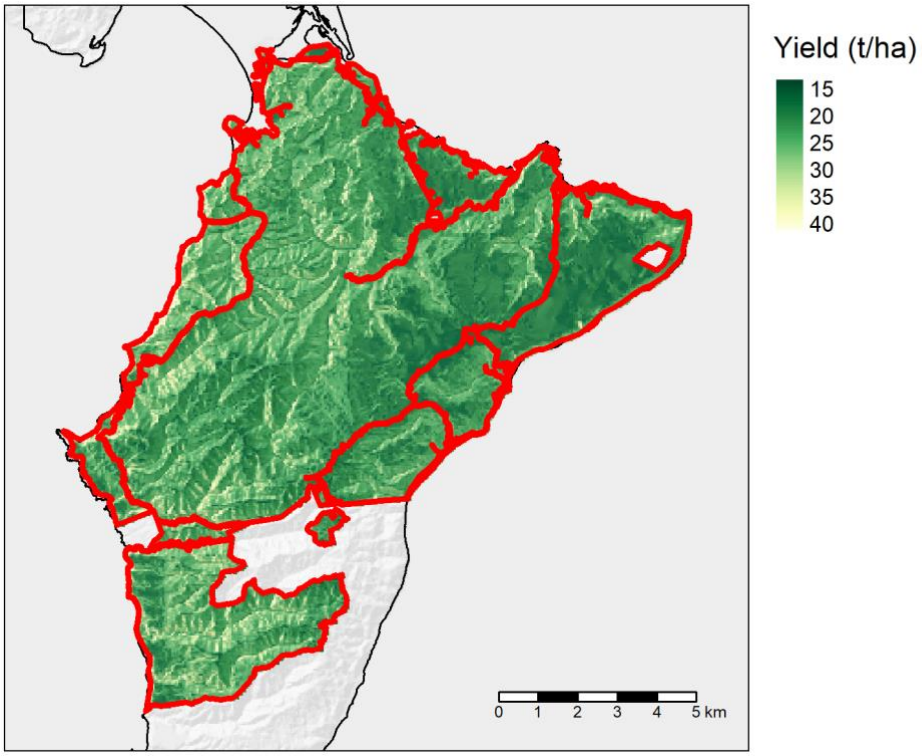


**Figure A17. Predicted annual lucerne yield at Māhia for 2020.**

## Prices Valley

*Sampling*

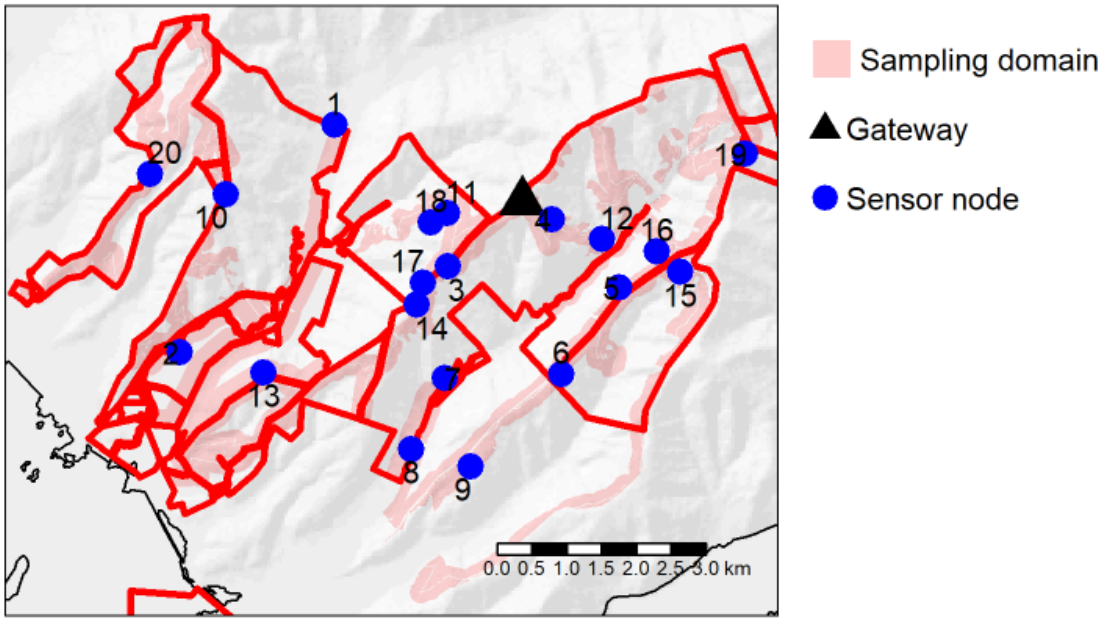


**Figure A18. Location of sampling domain, WSN gateway, and sensor nodes at Prices Valley.**

*Scorpan covariates*

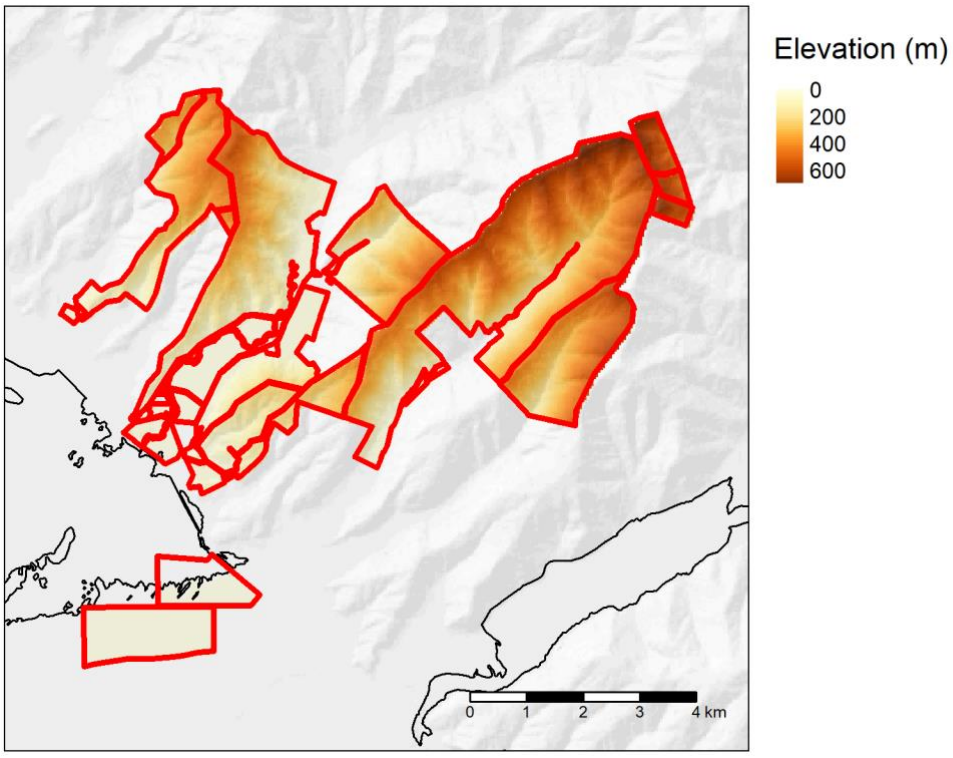


**Figure A19. Elevation at Prices Valley.**

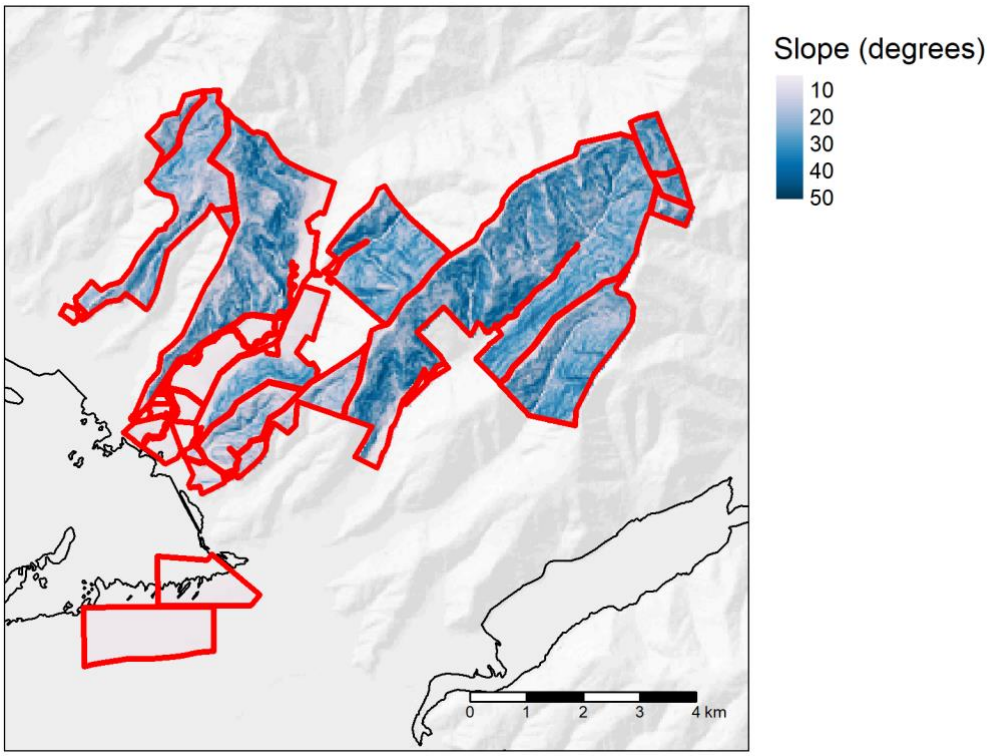


**Figure A20. Slope at Prices Valley.**

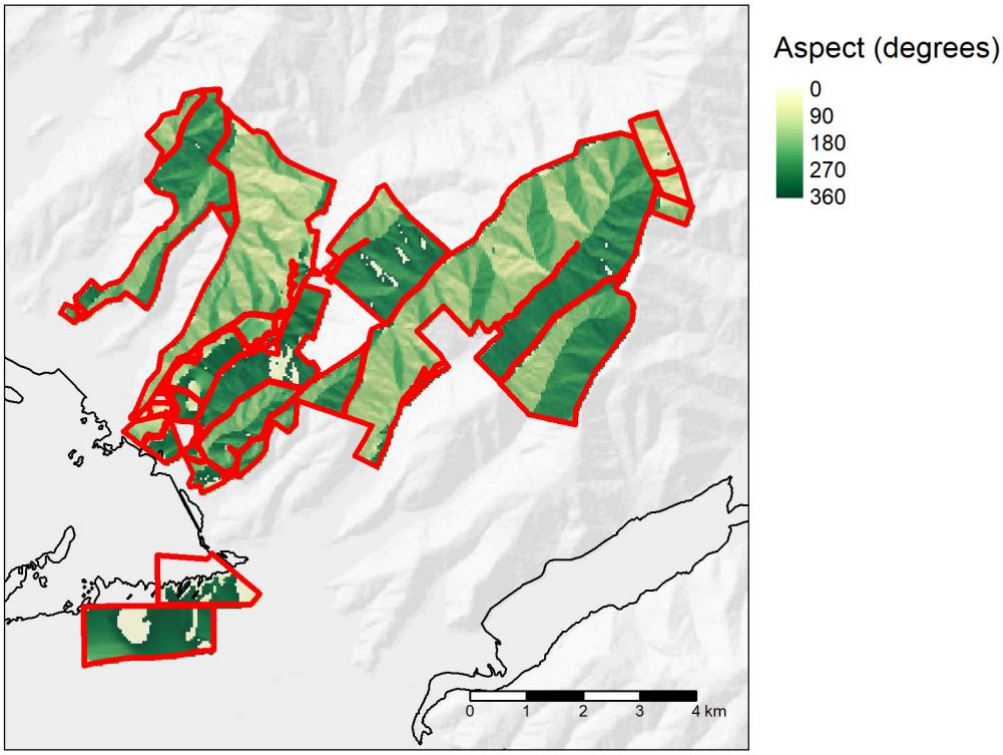


**Figure A21. Aspect at Prices Valley.**

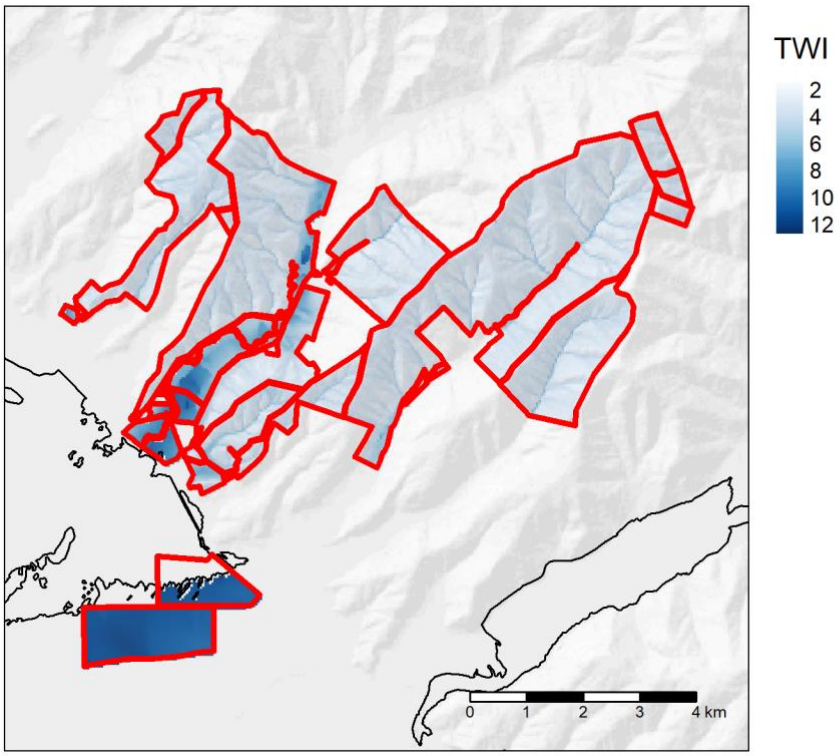


**Figure A22. Topographic wetness index at Prices Valley.**

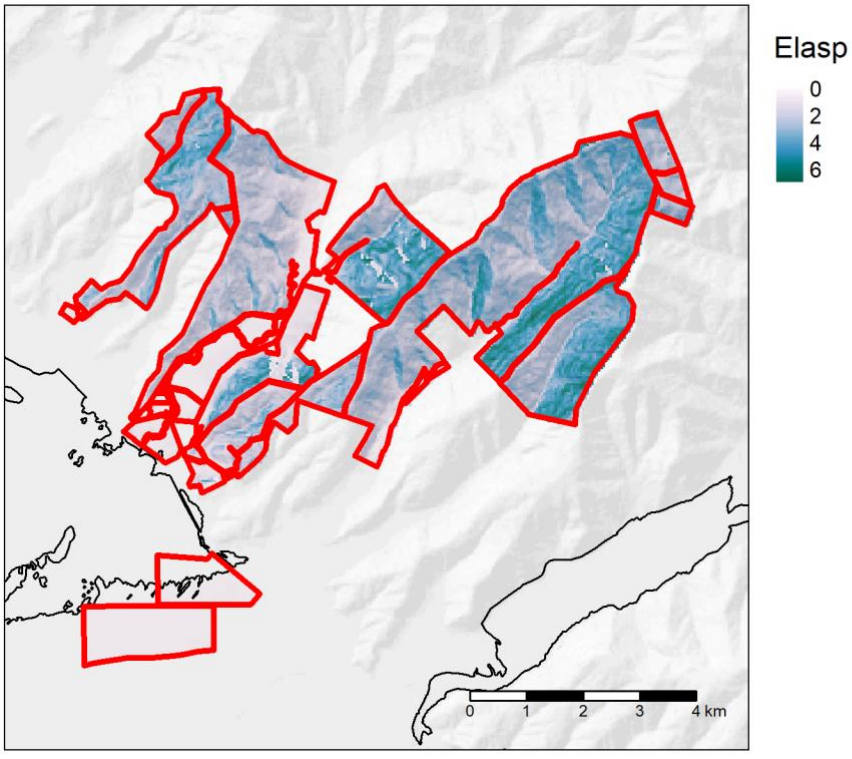


**Figure A23. Elasp at Prices Valley.**

*Soil temperature*

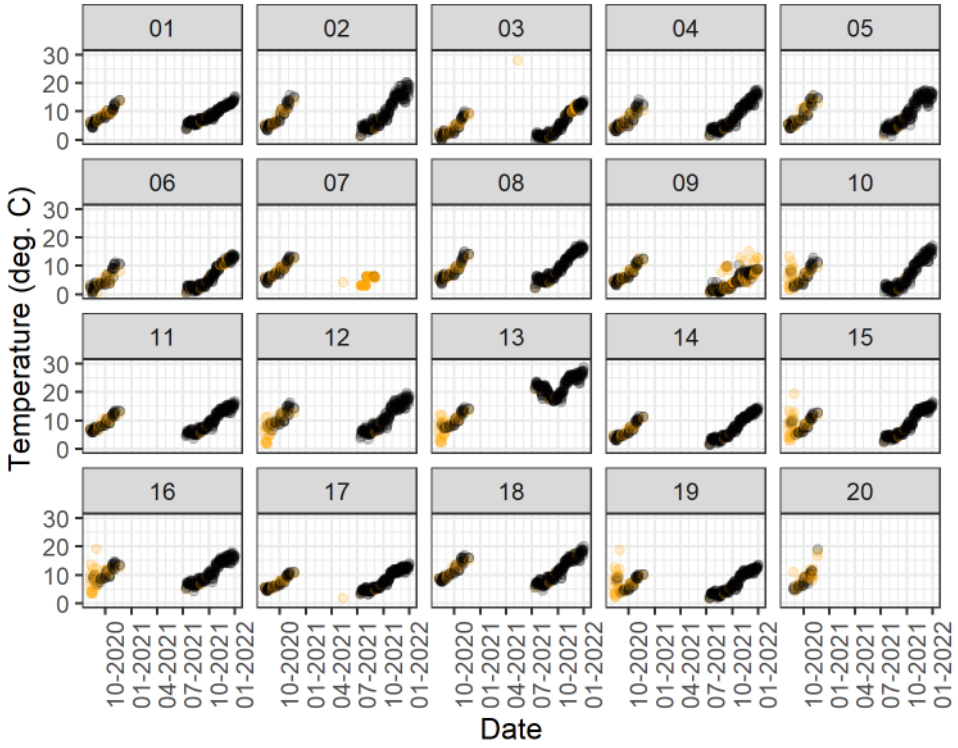


**Figure A24. Daily median soil temperature data for the Prices Valley WSN after trimming of the start and end dates, and removal of low and high temperatures, and periods of no change in soil temperature. Panel labels indicate the respective sensor node. Points that were removed as a result of the data trimming are shown in orange, while presumed valid points are in black.**

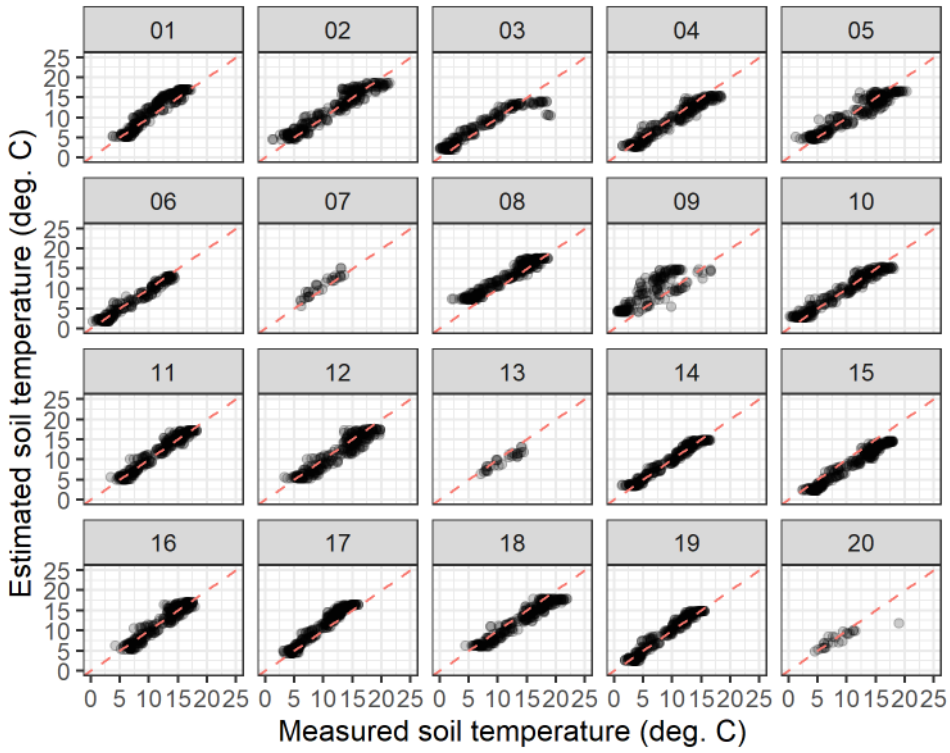


**Figure A25. Measured versus fitted soil temperature plot for the Prices Valley site using model 5. Panel labels indicate the respective sensor node.**

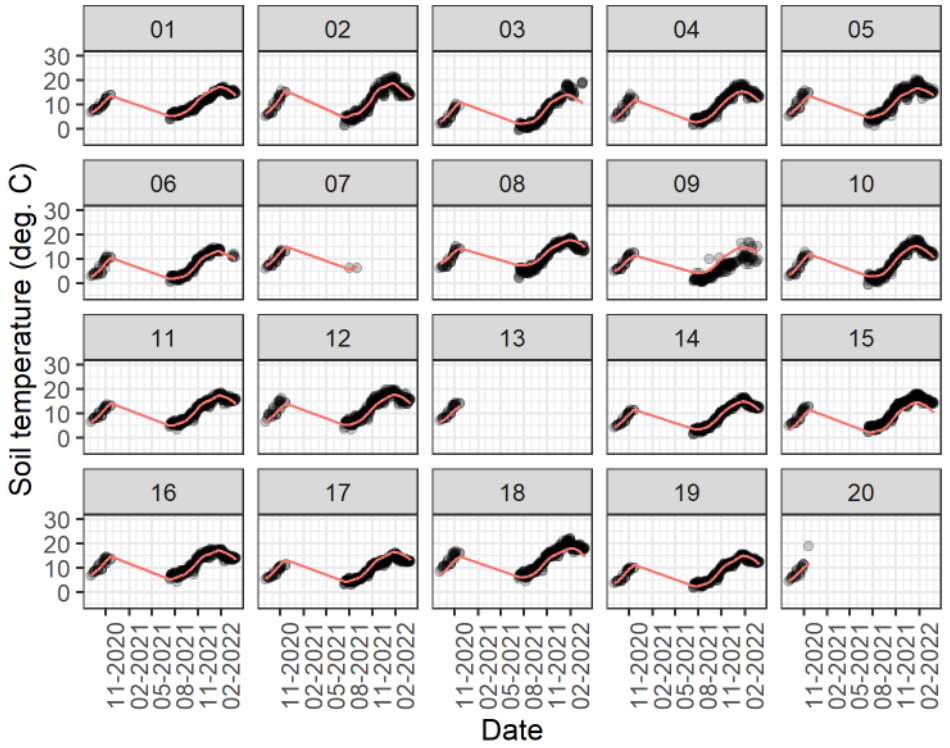


**Figure A26. Measured (points) versus fitted (line) soil temperature for the Prices Valley site over time, using model 5. Panel labels indicate the respective sensor node.**

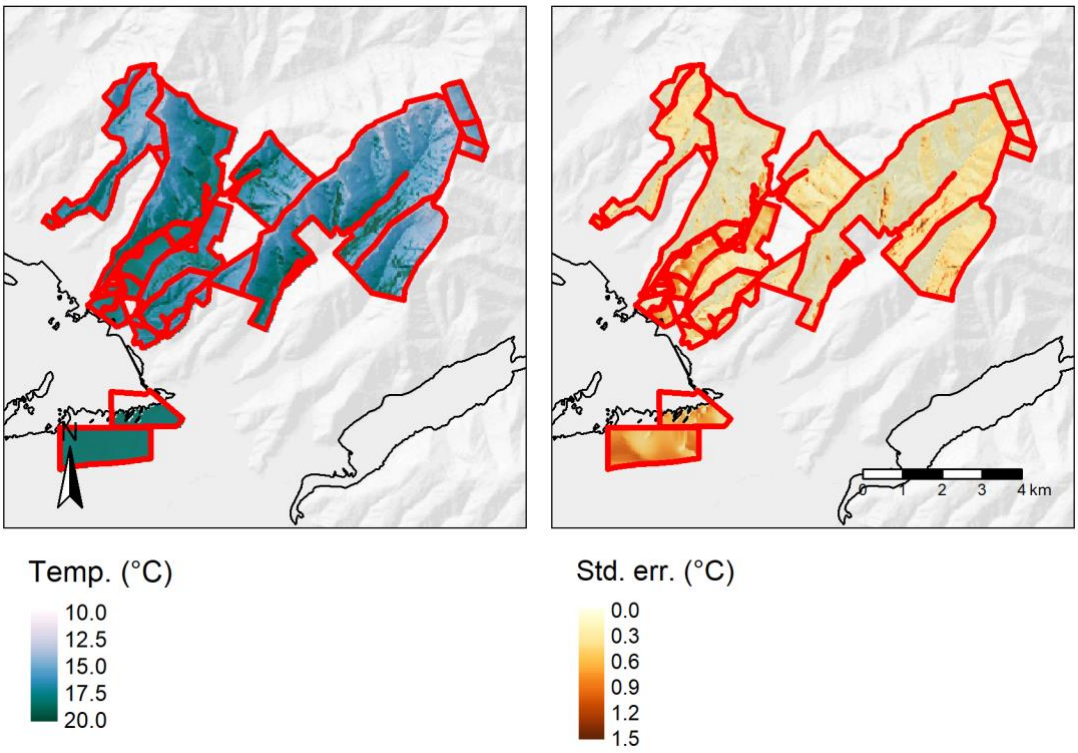


**Figure A27. Predicted soil temperature at Prices Valley on 15 January, when soils are near their warmest.**

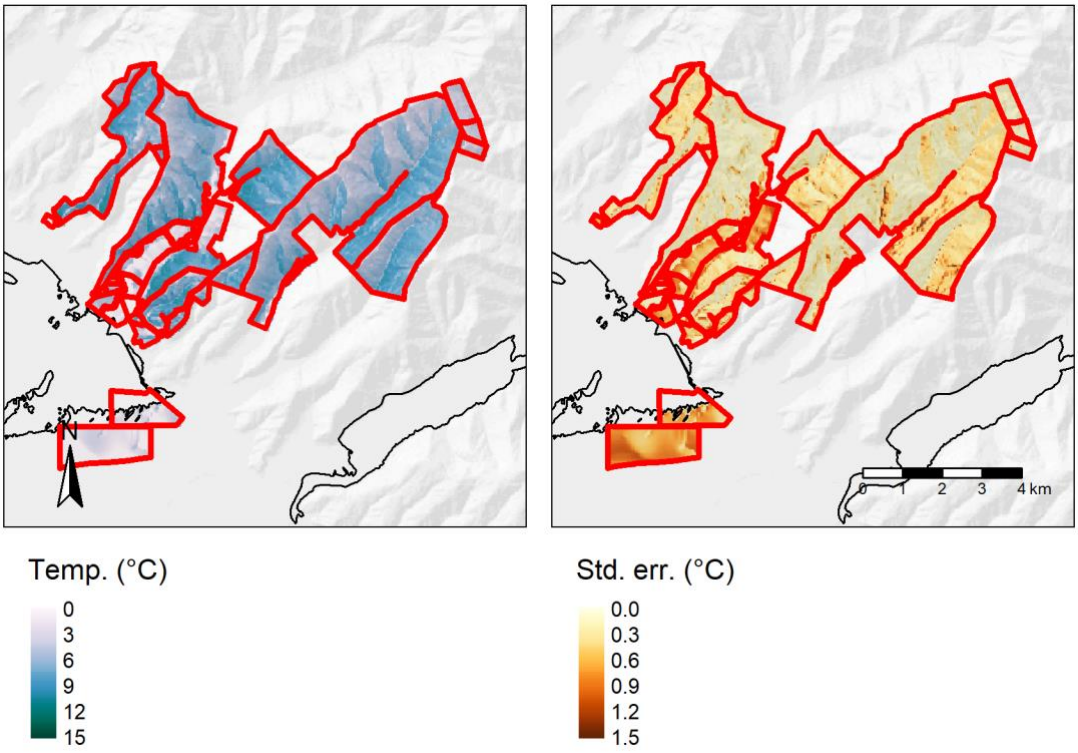


**Figure A28. Predicted soil temperature at Prices Valley on 15 July, when soils are near their coolest.**

*Soil moisture*

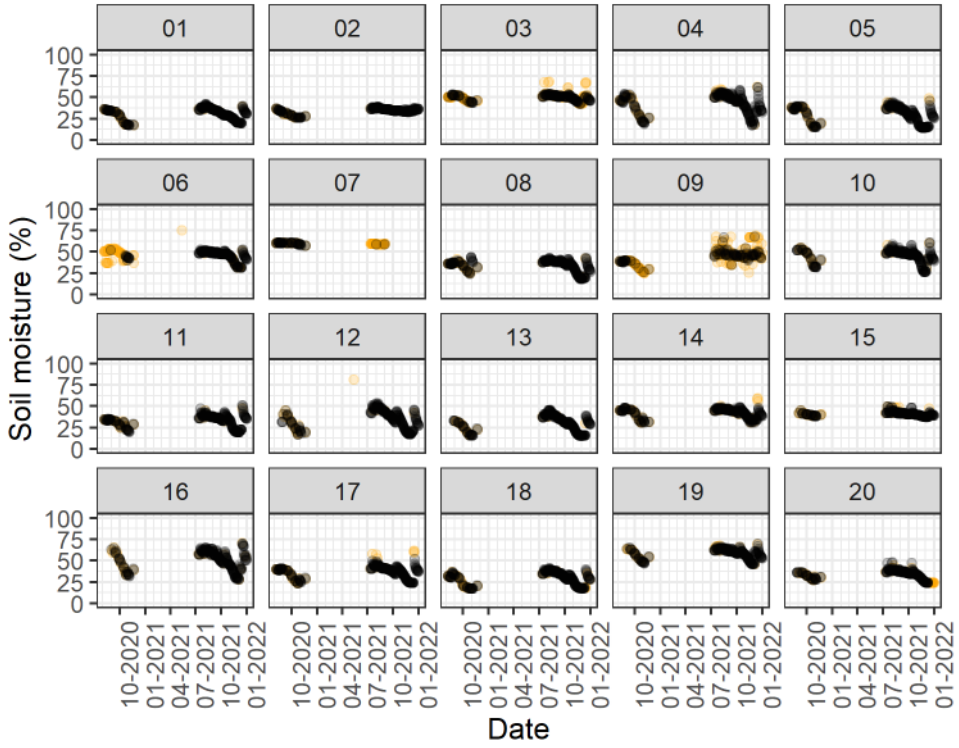


**Figure A29. Daily median soil moisture data for the Prices Valley site after trimming of the start and end dates, and removal of low and high soil moisture values, and periods of no change in soil moisture. Panel labels indicate the respective sensor node. Points excised from the data have been coloured orange.**

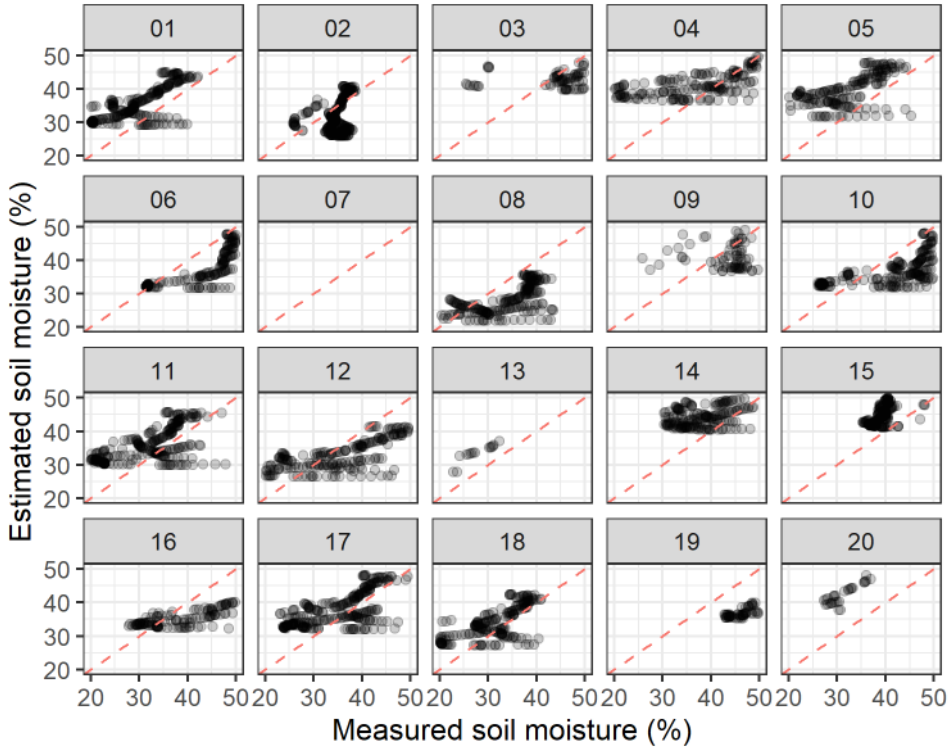


**Figure A30. Measured versus fitted soil moisture plot for the Prices Valley site using model 1. Panel labels indicate the respective sensor node.**

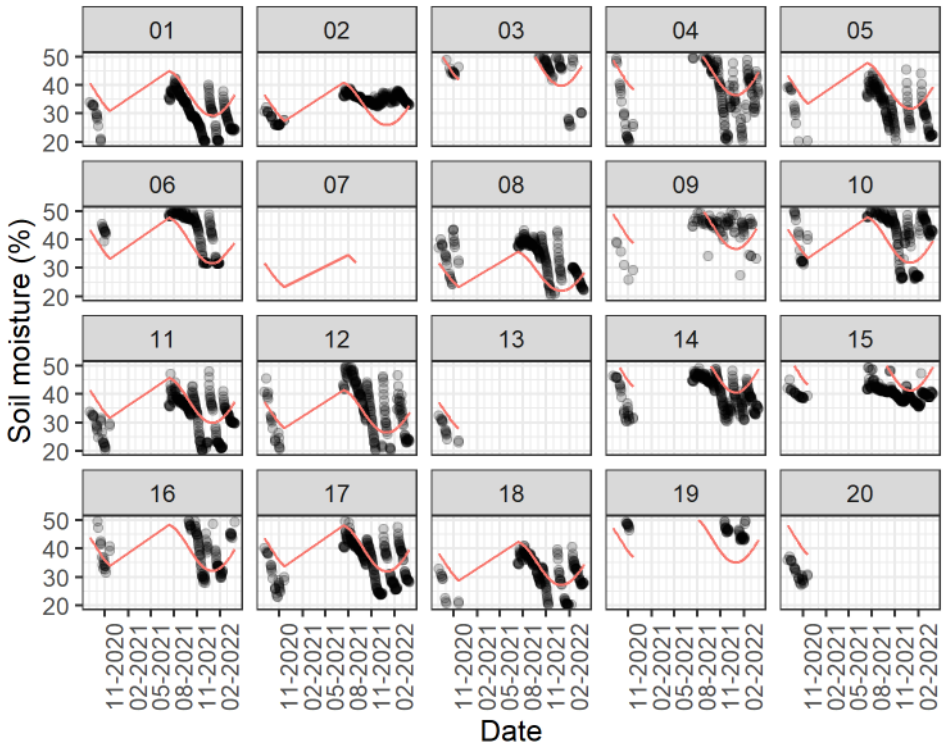


**Figure A31. Measured (points) versus fitted (line) soil moisture for the Prices Valley site over time, using model 1. Panel labels indicate the respective sensor node.**

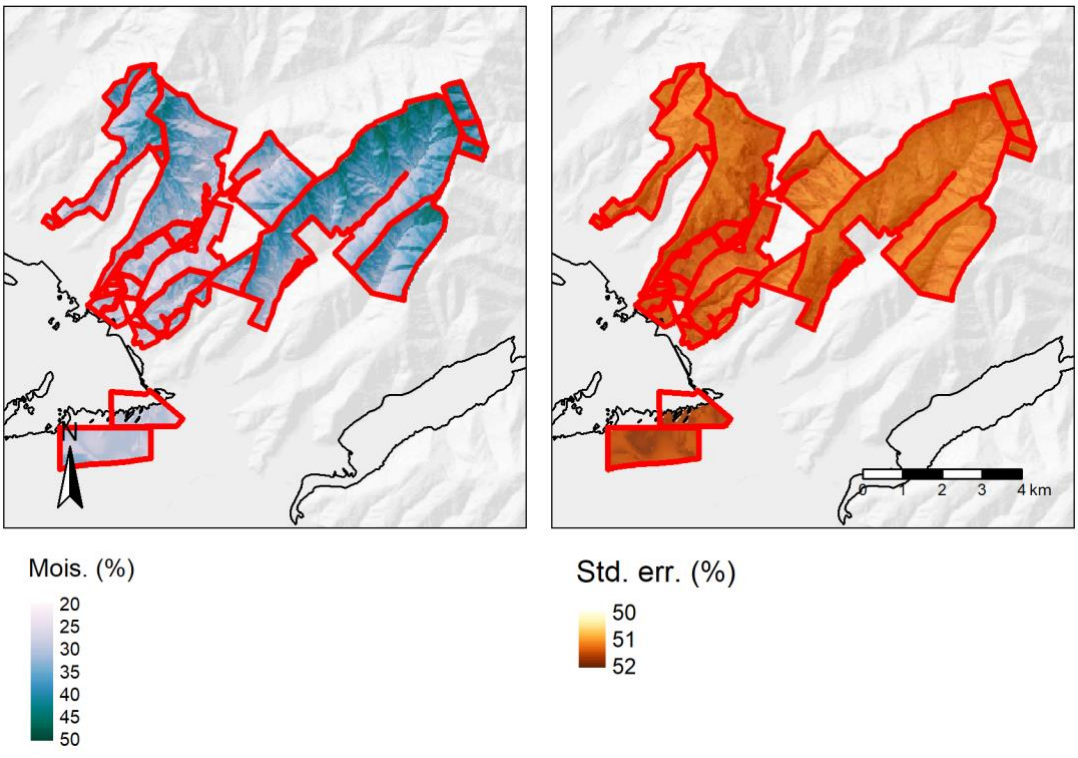


**Figure A32. Predicted soil moisture at Prices Valley on 1 March, when soils are near their driest.**

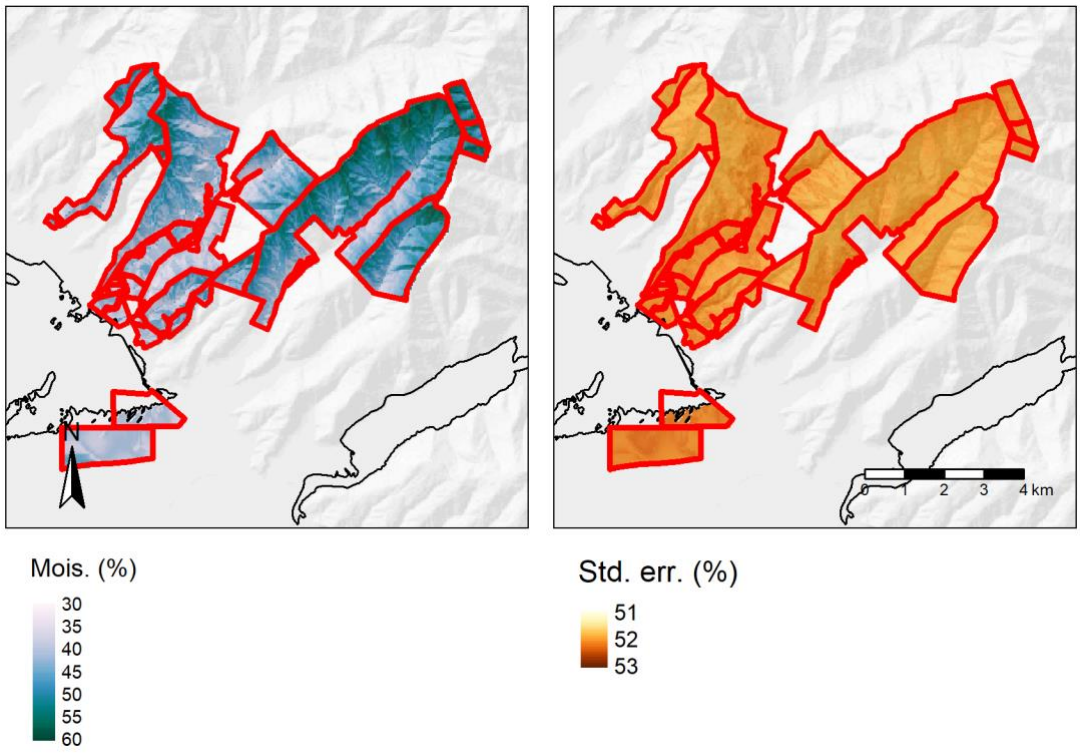


**Figure A33. Predicted soil moisture at Prices Valley on 25 June, when soils are near their wettest.**

*Yield*

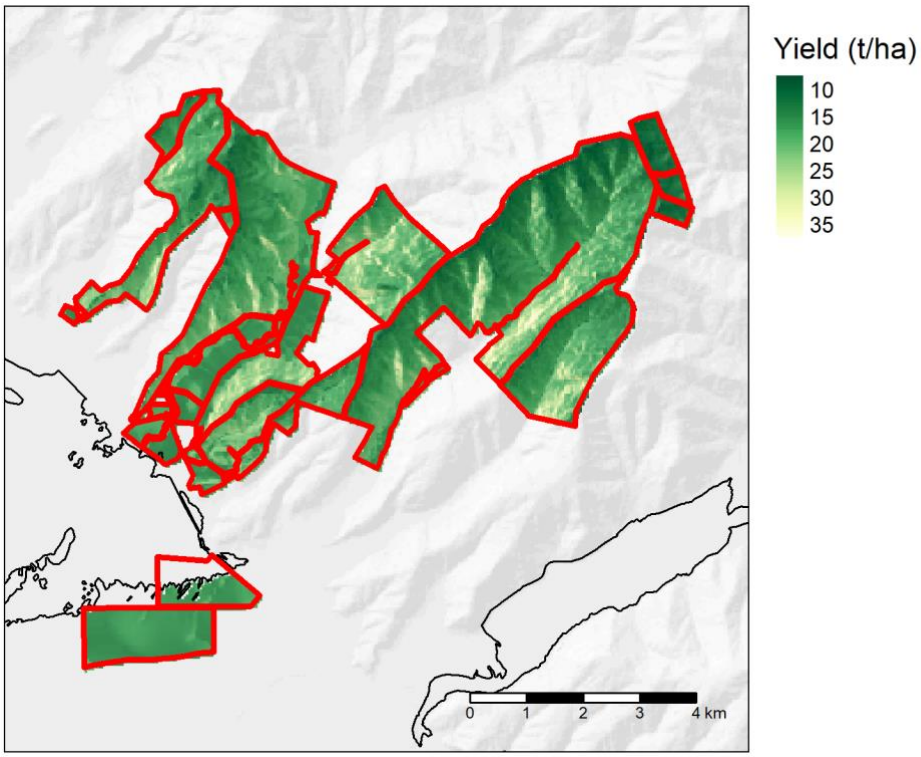


**Figure A34. Predicted annual lucerne yield at Prices Valley for 2020.**

## Taihape

*Sampling*

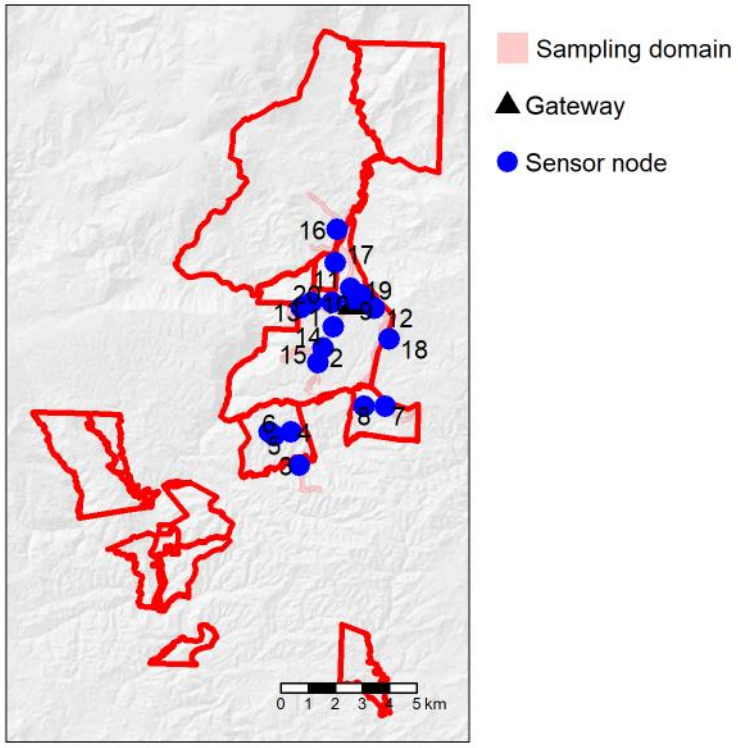


**Figure A35. Location of sampling domain, WSN gateway, and sensor nodes at Taihape.**

*Scorpan covariates*

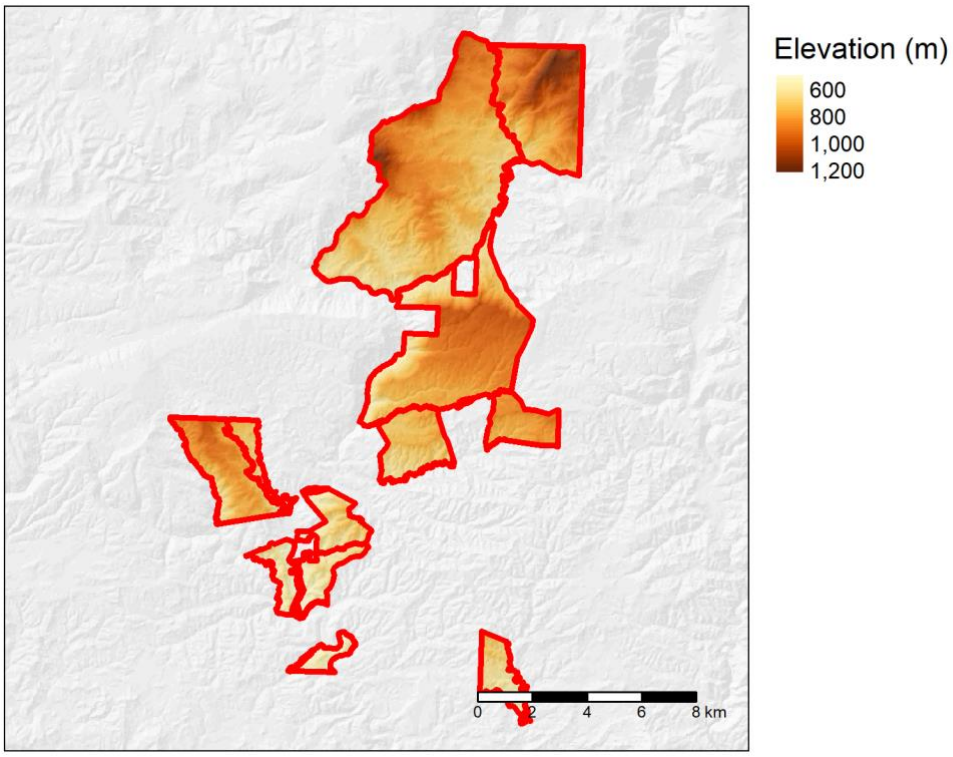


**Figure A36. Elevation at Taihape.**

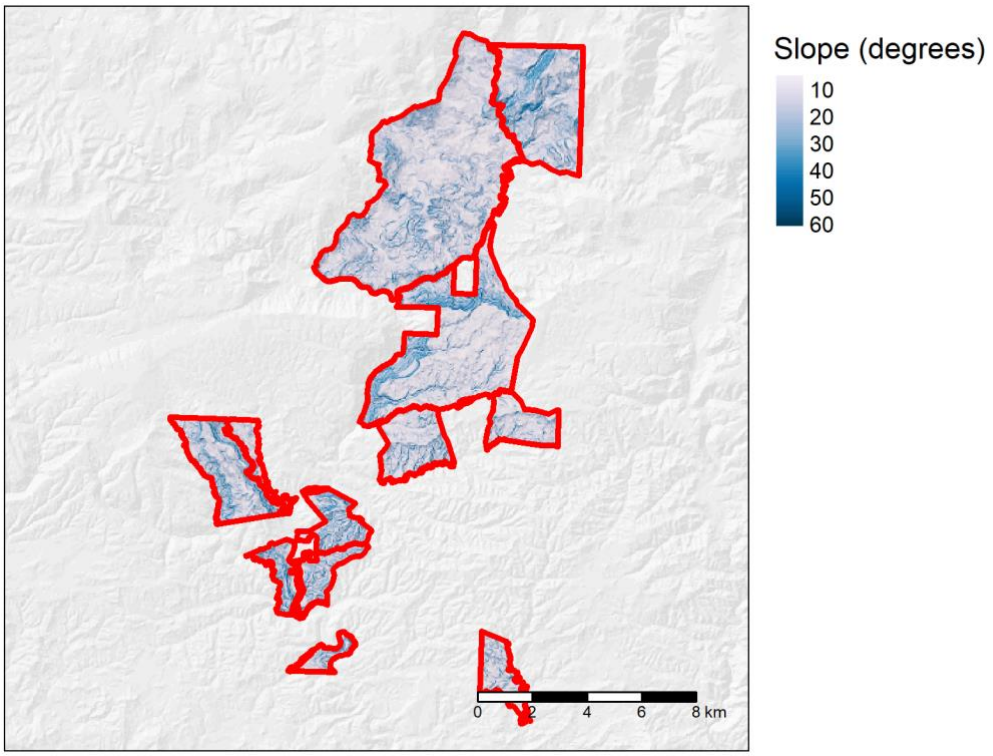


**Figure A37. Slope at Taihape.**

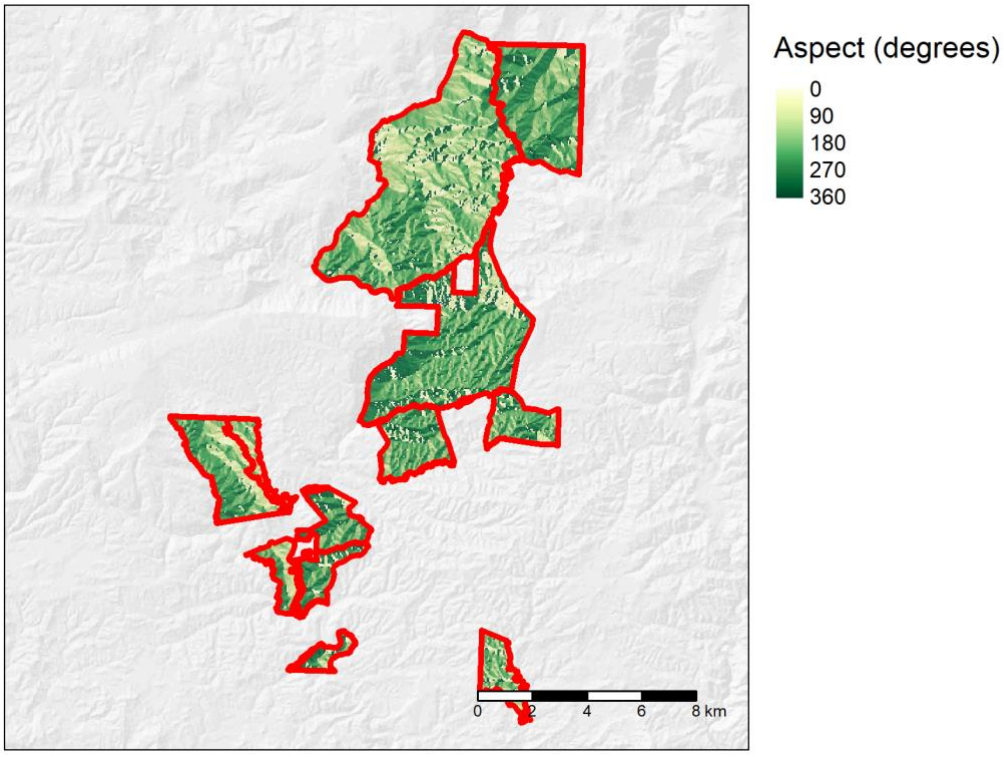


**Figure A38. Aspect at Taihape.**

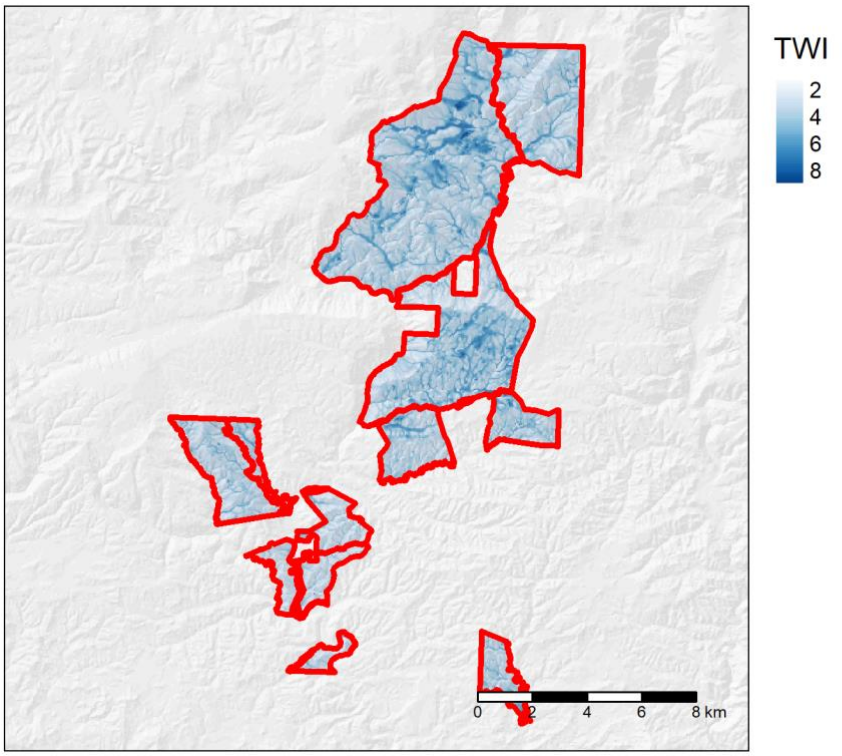


**Figure A39. Topographic wetness index at Taihape.**

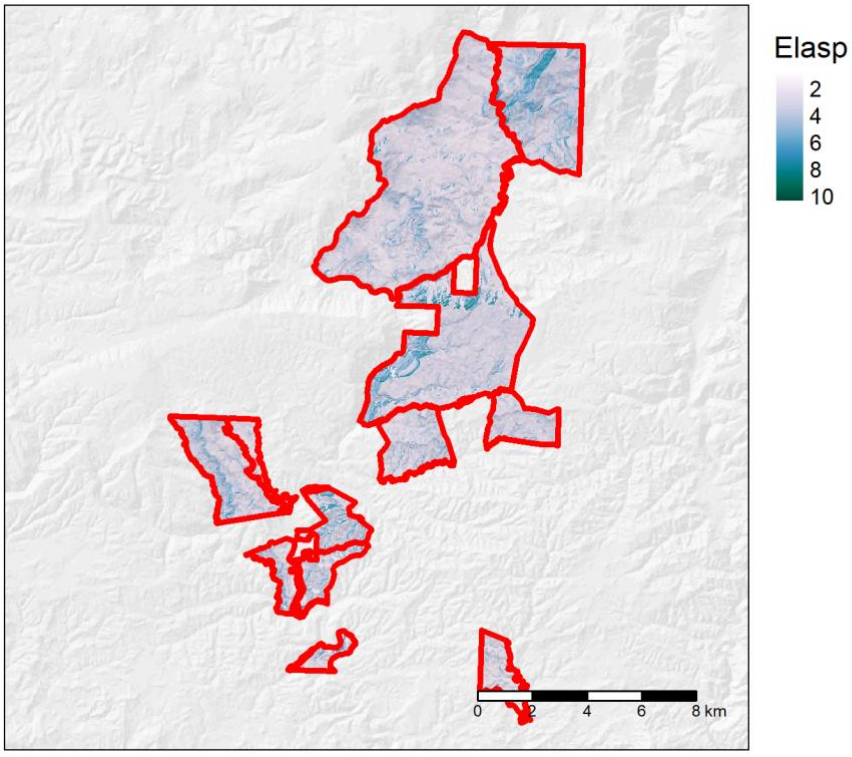


**Figure A40. Elasp at Taihape.**

*Soil temperature*

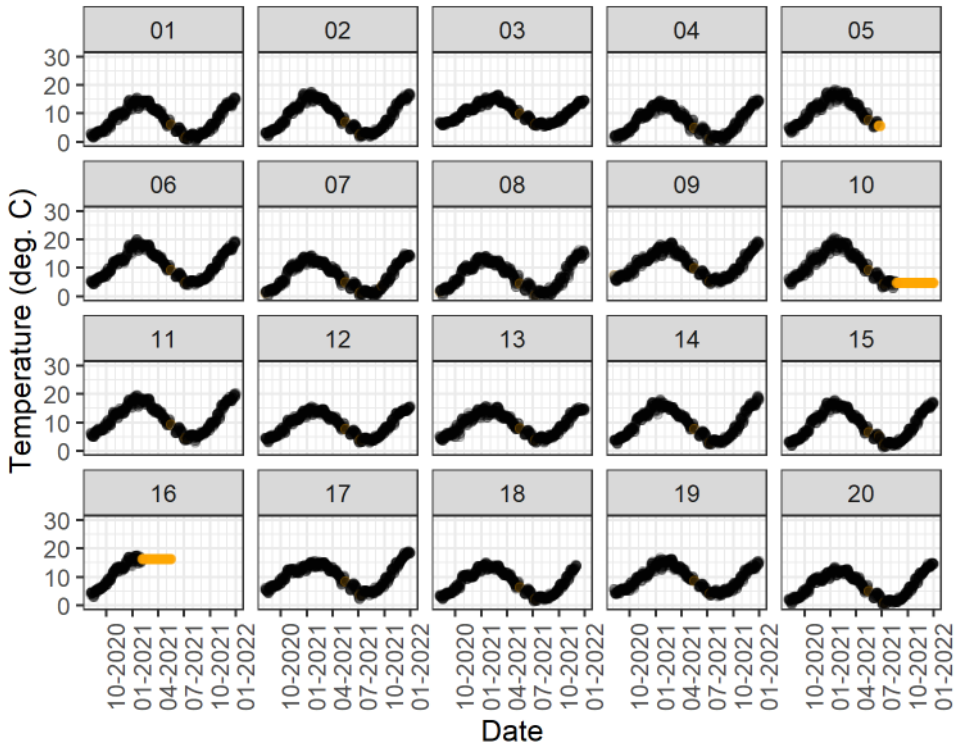


**Figure A41. Daily median soil temperature data for the Taihape WSN after trimming of the start and end dates, and removal of low and high temperatures, and periods of no change in soil temperature. Panel labels indicate the respective sensor node. Points that were removed as a result of the data trimming are shown in orange, while presumed valid points are in black.**

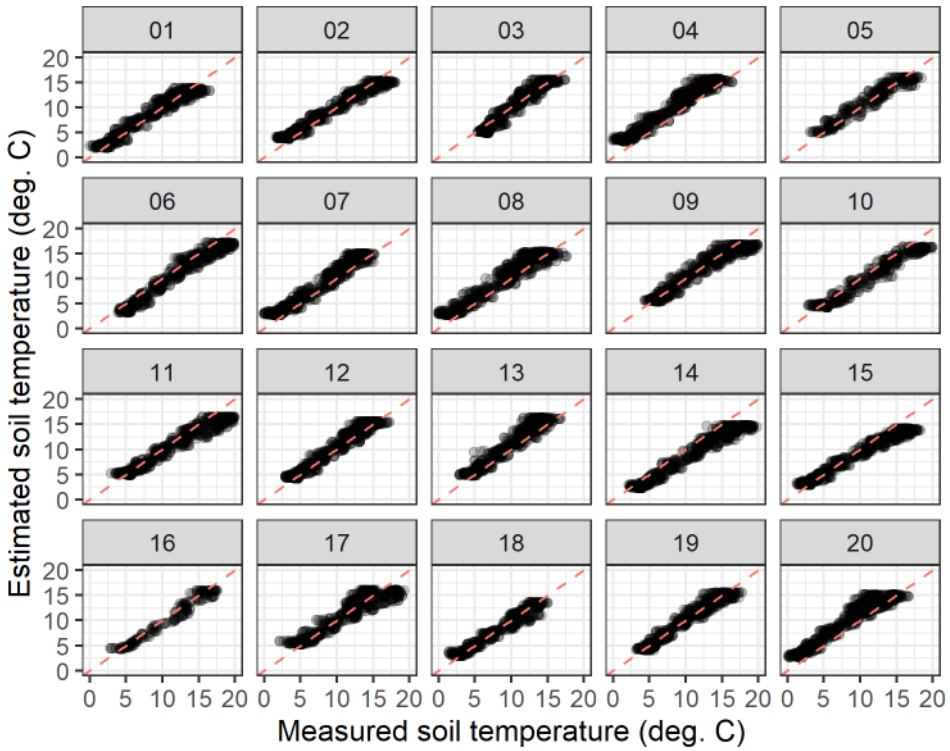


**Figure A42. Measured versus fitted soil temperature plot for the Taihape site using model 5. Panel labels indicate the respective sensor node.**

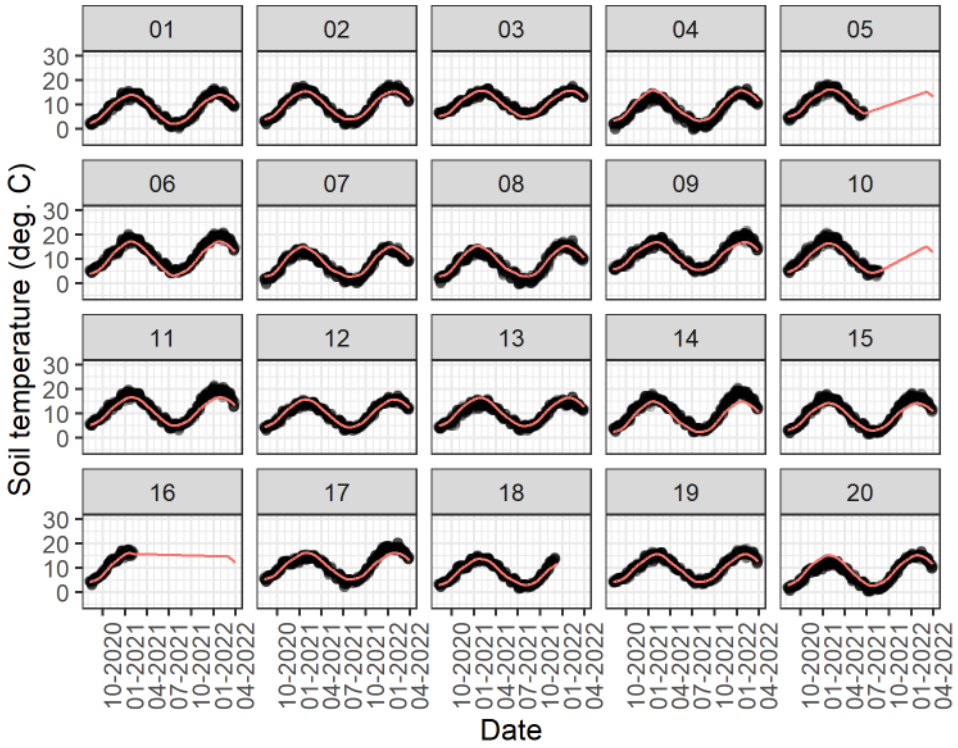


**Figure A43. Measured (points) versus fitted (line) soil temperature for the Taihape site over time, using model 5. Panel labels indicate the respective sensor node.**

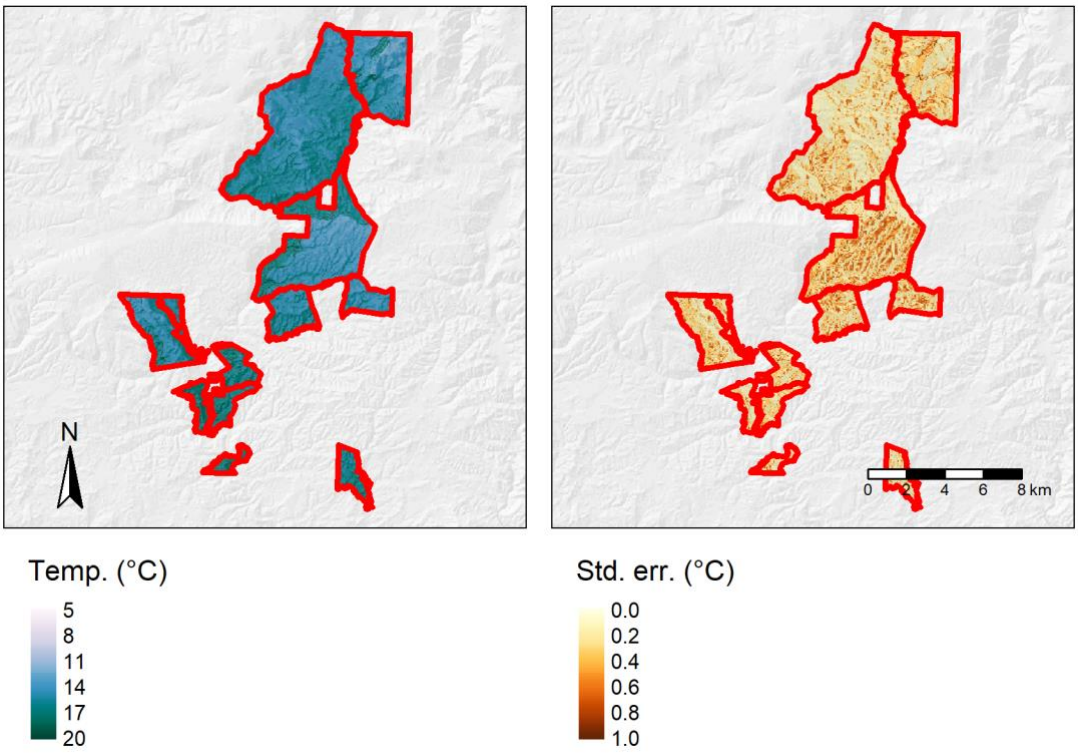


**Figure A44. Predicted soil temperature at Taihape on 15 January, when soils are near their warmest.**

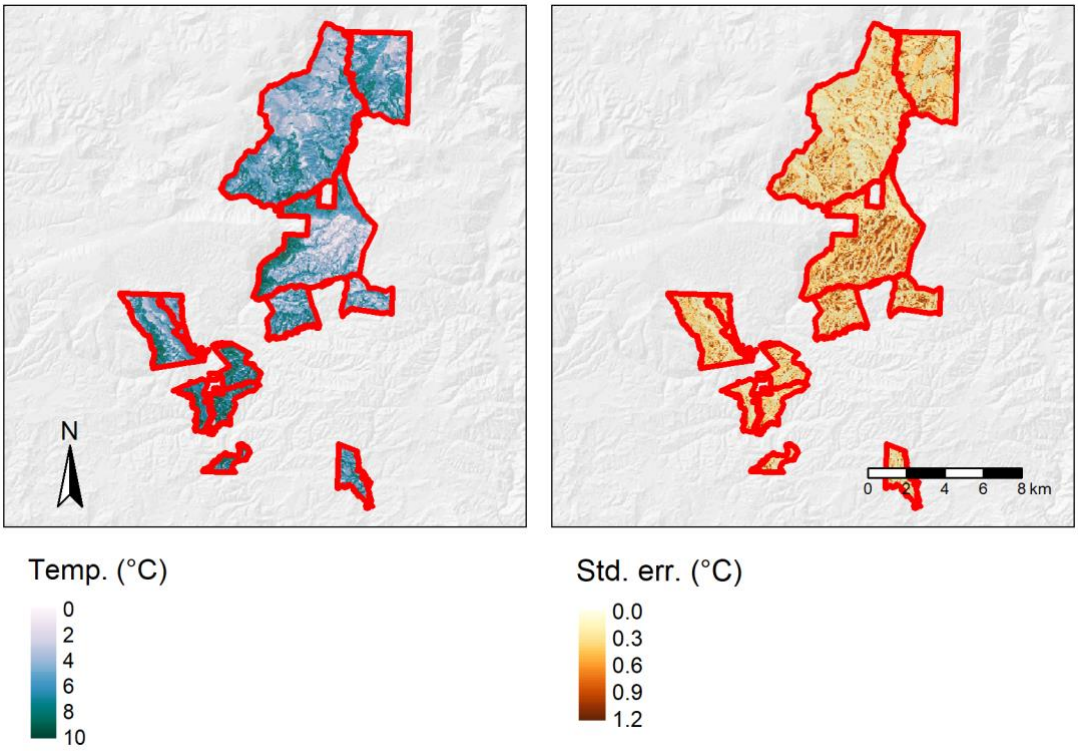


**Figure A45. Predicted soil temperature at Taihape on 15 July, when soils are near their coolest.**

*Soil moisture*

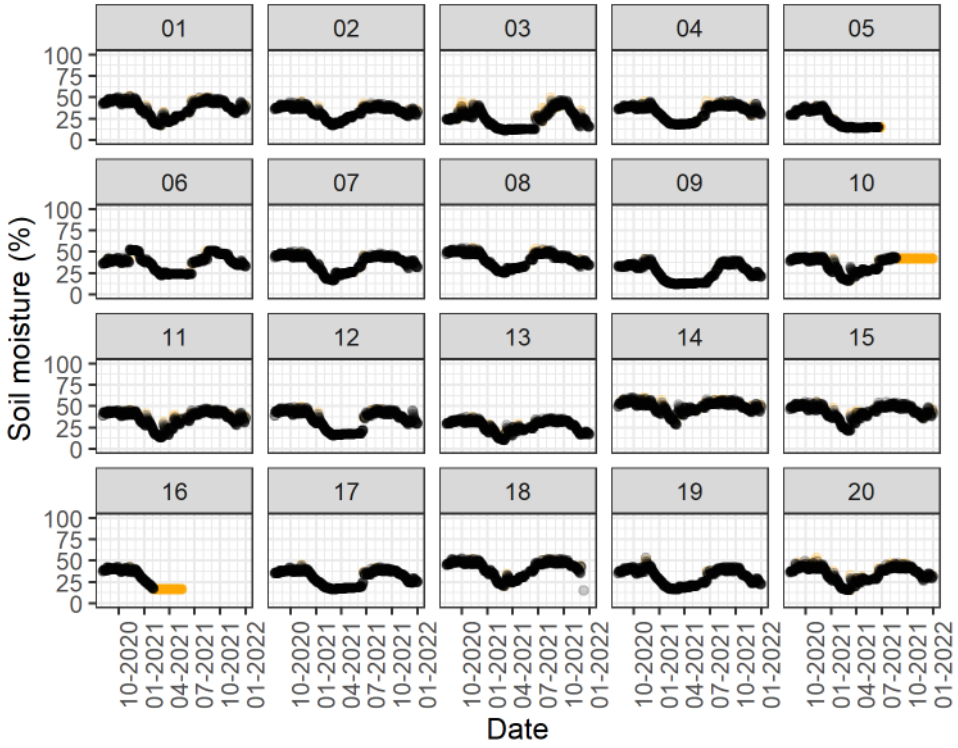


**Figure A46. Daily median soil moisture data for the Taihape site after trimming of the start and end dates, and removal of low and high soil moisture values, and periods of no change in soil moisture. Panel labels indicate the respective sensor node. Points excised from the data have been coloured orange.**

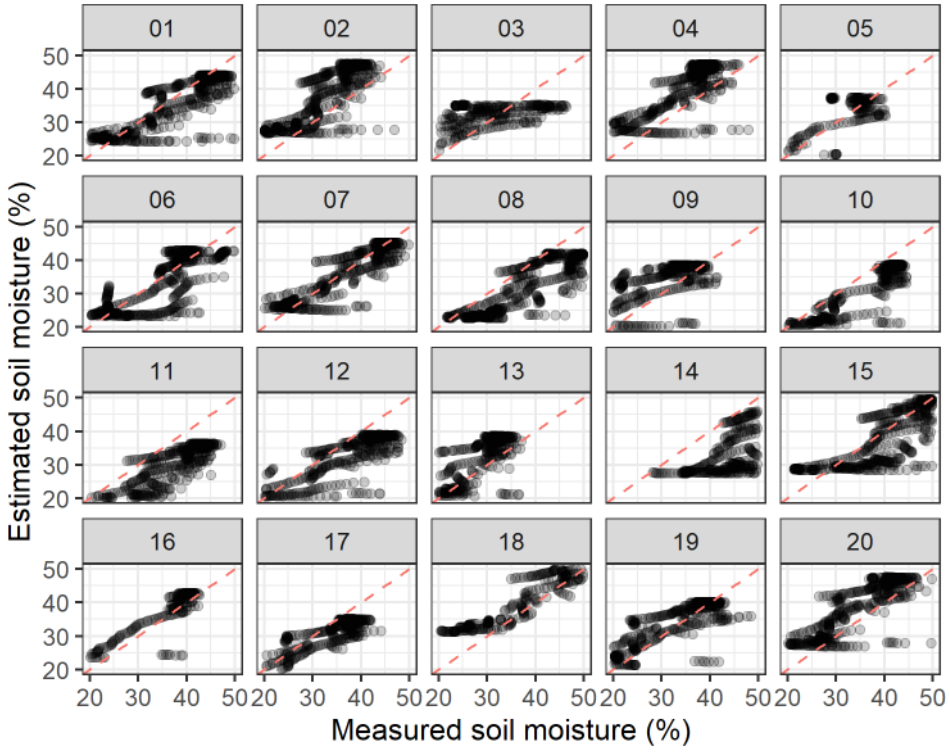


**Figure A47. Measured versus fitted soil moisture plot for the Taihape site using model 1. Panel labels indicate the respective sensor node.**

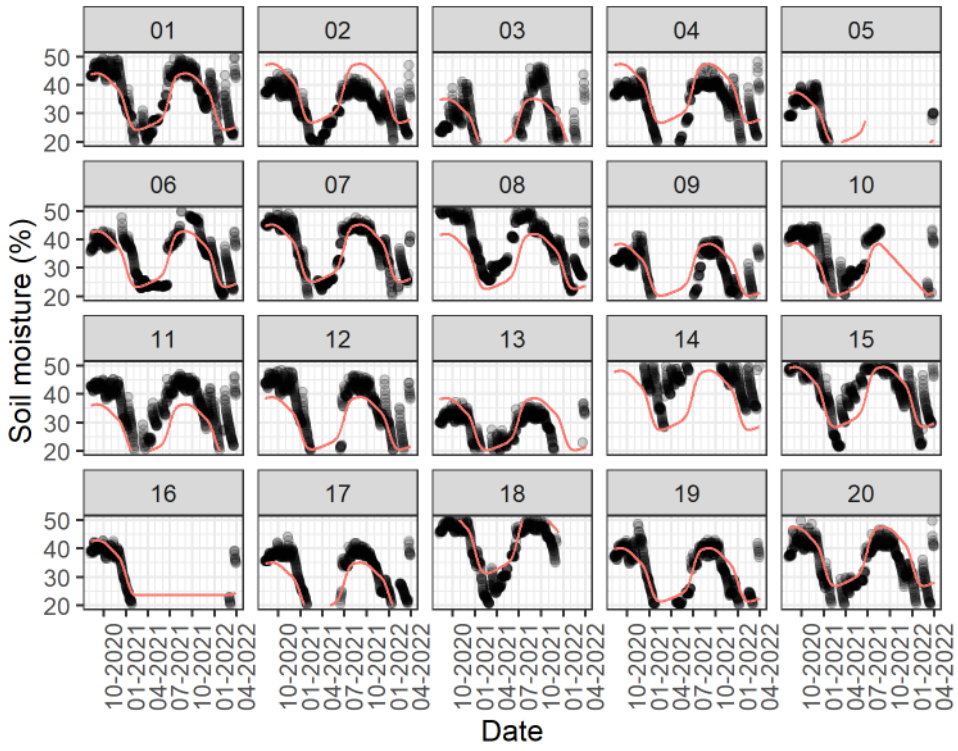


**Figure A48. Measured (points) versus fitted (line) soil moisture for the Taihape site over time, using model 1. Panel labels indicate the respective sensor node.**

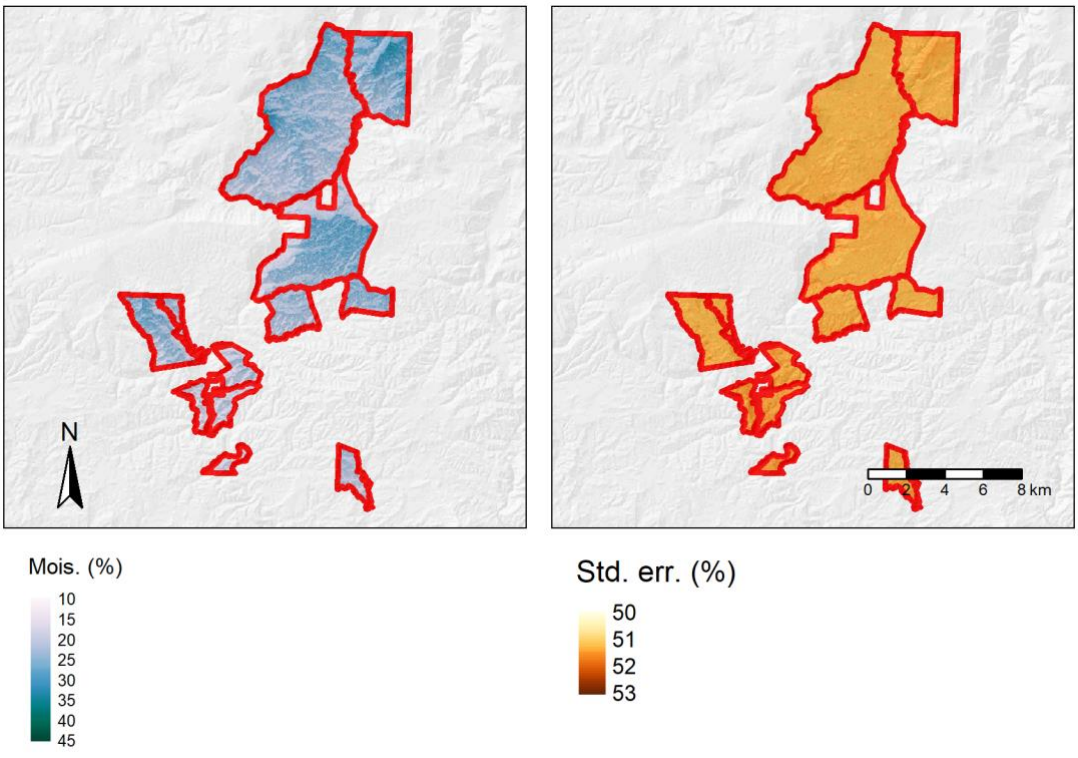


**Figure A49. Predicted soil moisture at Taihape on 1 March, when soils are near their driest.**

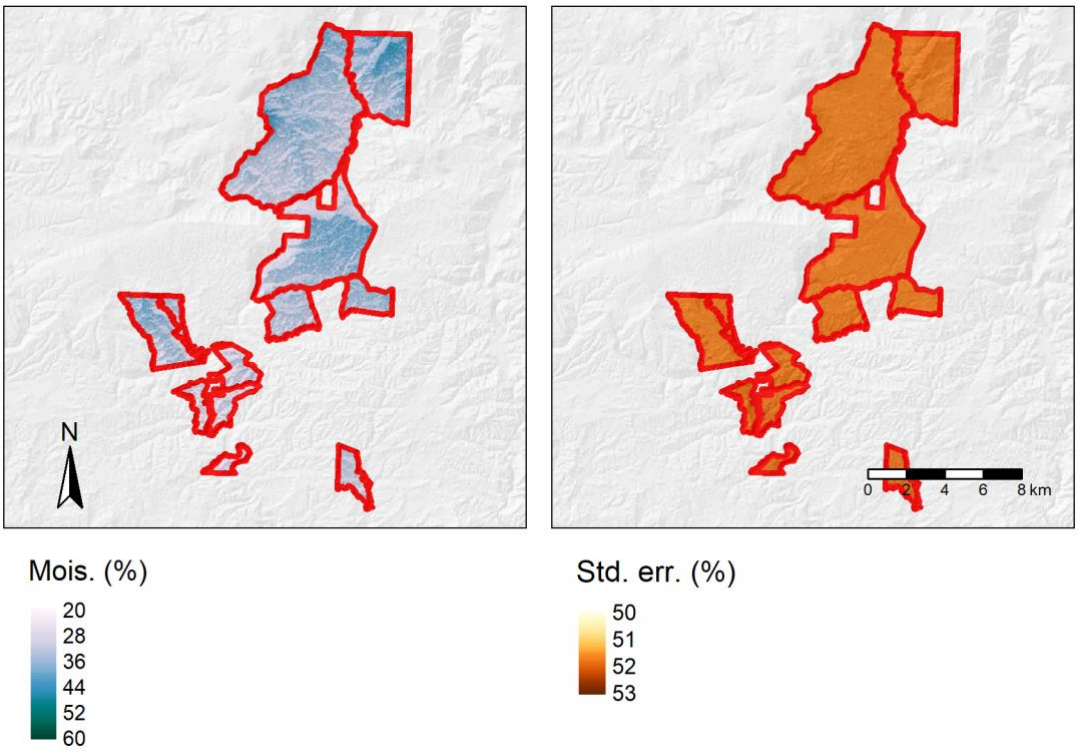


**Figure A50. Predicted soil moisture at Taihape on 25 June, when soils are near their wettest.**

*Yield*

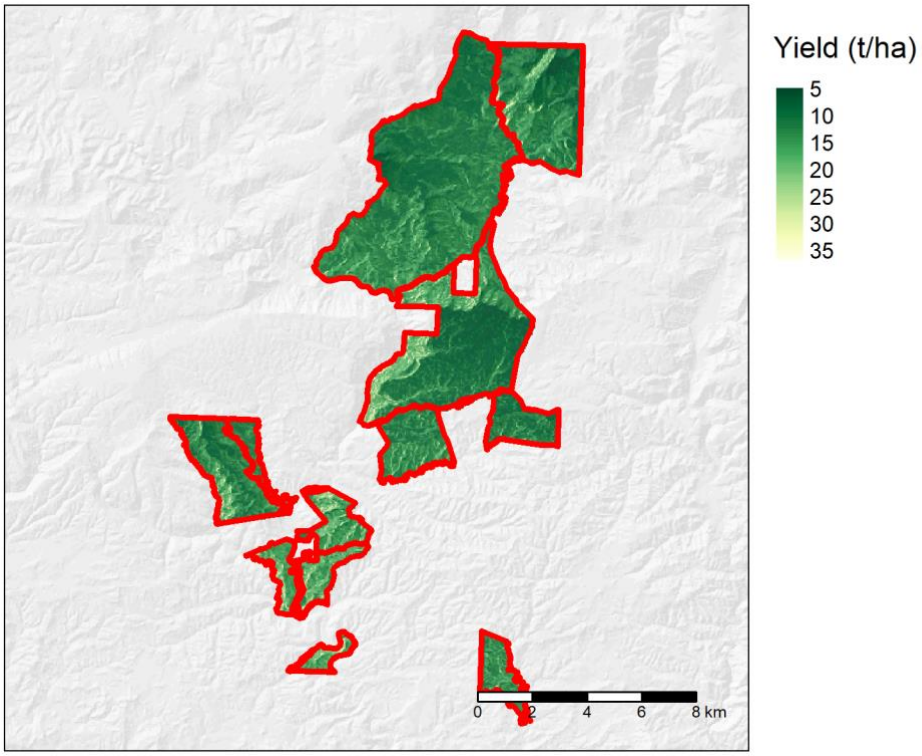


**Figure A51. Predicted annual lucerne yield at Taihape for 2020.**

## Taumarunui

*Sampling*

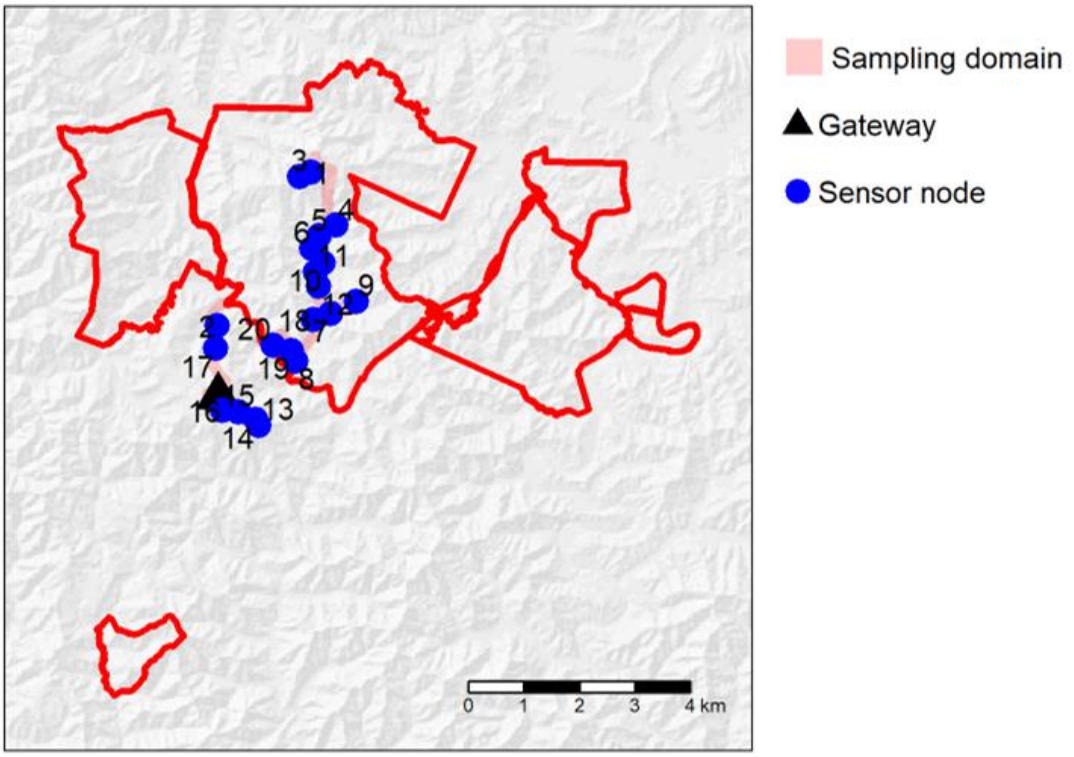


**Figure A52. Location of sampling domain, WSN gateway, and sensor nodes at Taumarunui.**

*Scorpan covariates*

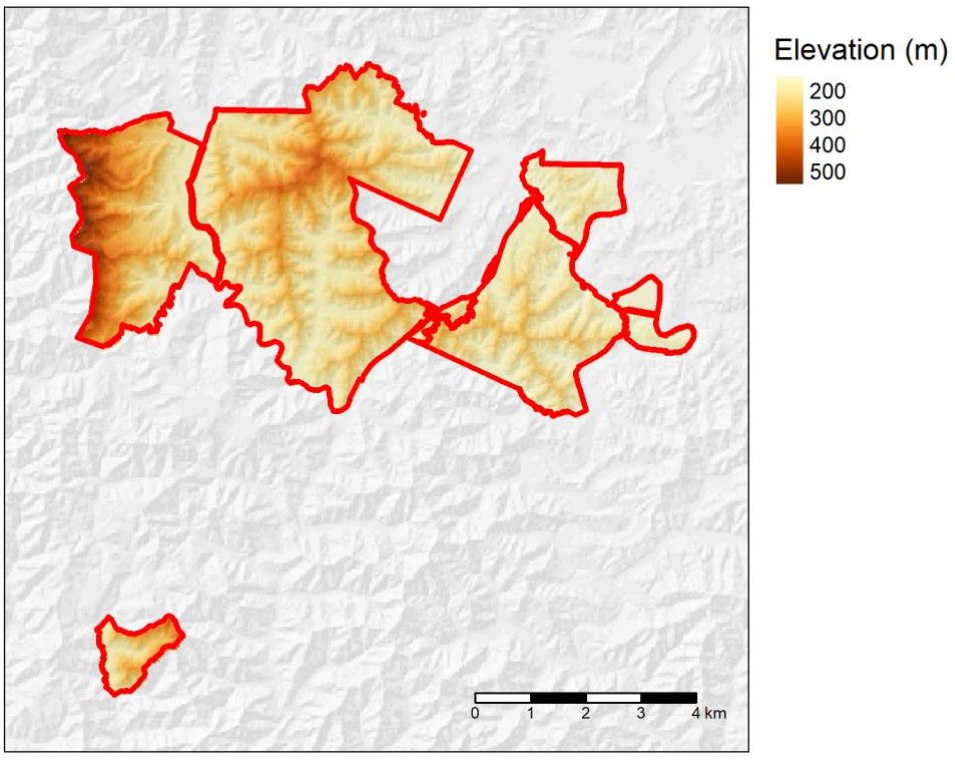


**Figure A53. Elevation at Taumarunui.**

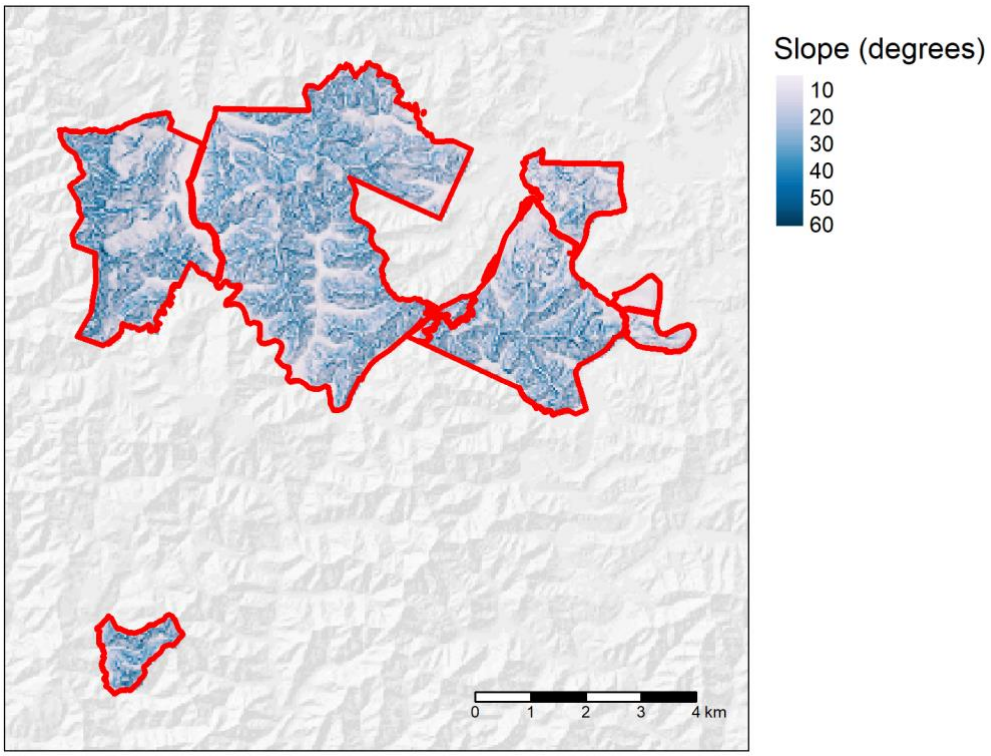


**Figure A54. Slope at Taumarunui.**

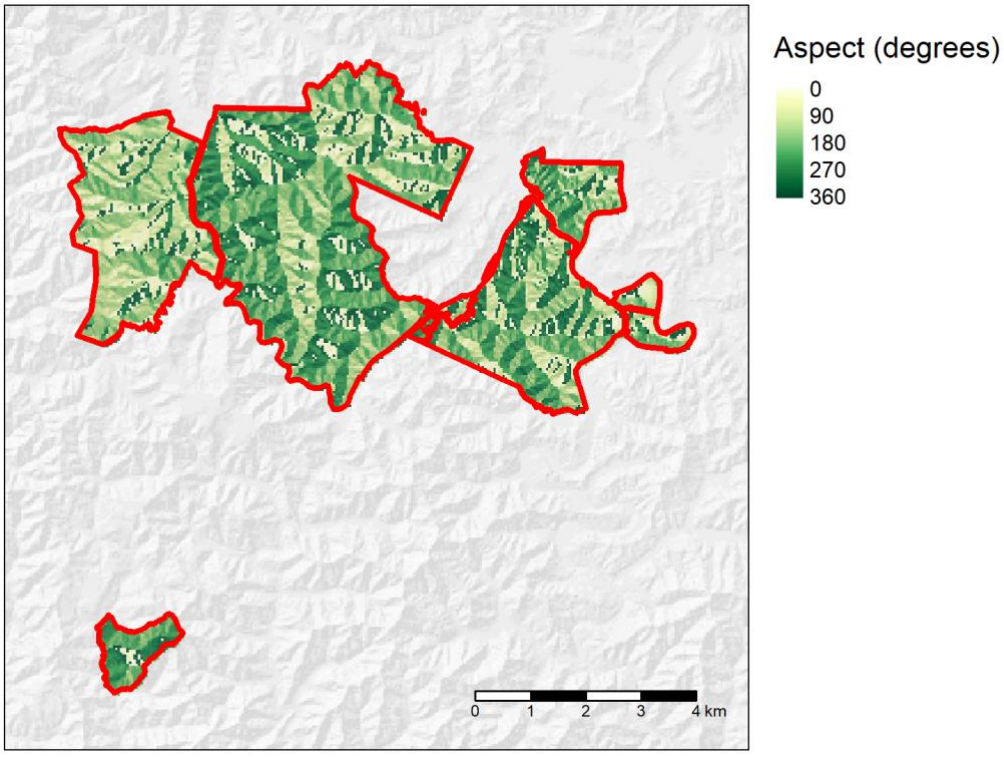


**Figure A55. Aspect at Taumarunui.**

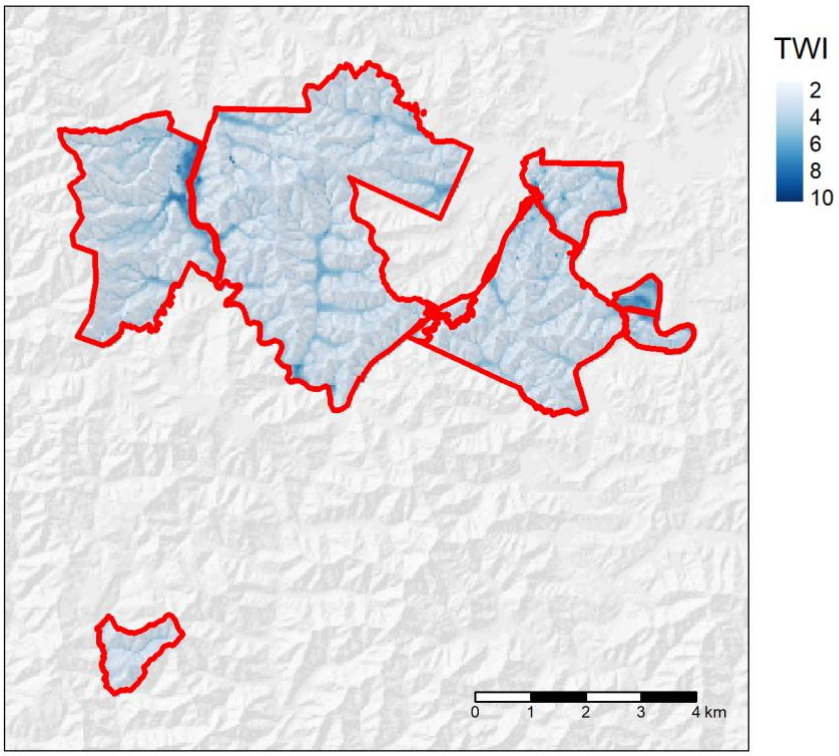


**Figure A56. Topographic wetness index at Taumarunui.**

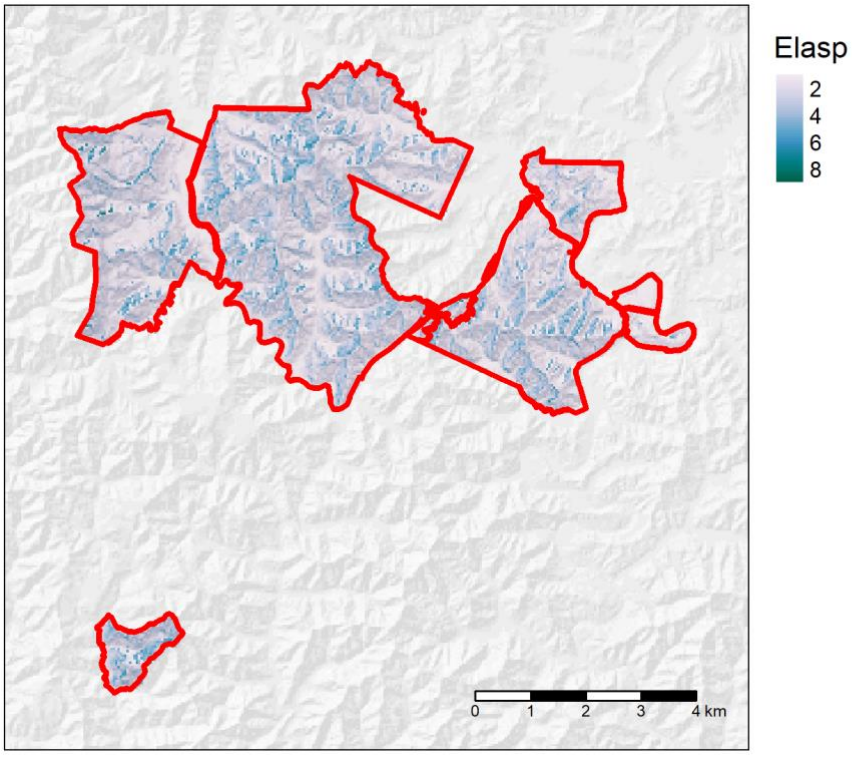


**Figure A57. Elasp at Taumarunui.**

*Soil temperature*

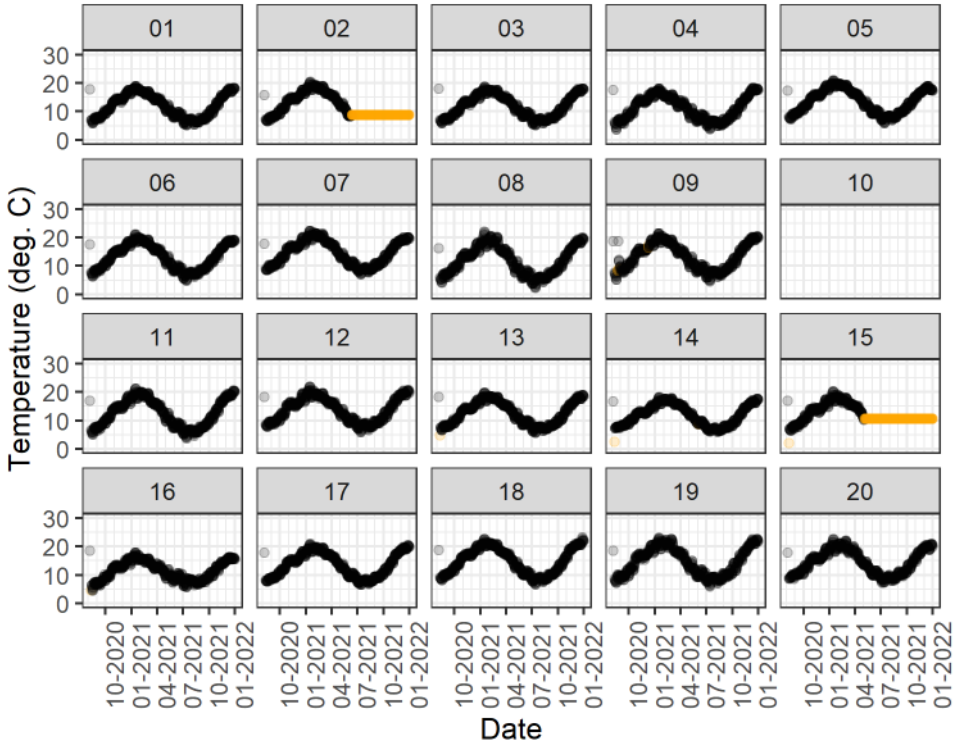


**Figure A58. Daily median soil temperature data for the Taumarunui WSN after trimming of the start and end dates, and removal of low and high temperatures, and periods of no change in soil temperature. Panel labels indicate the respective sensor node. Points that were removed as a result of the data trimming are shown in orange, while presumed valid points are in black.**

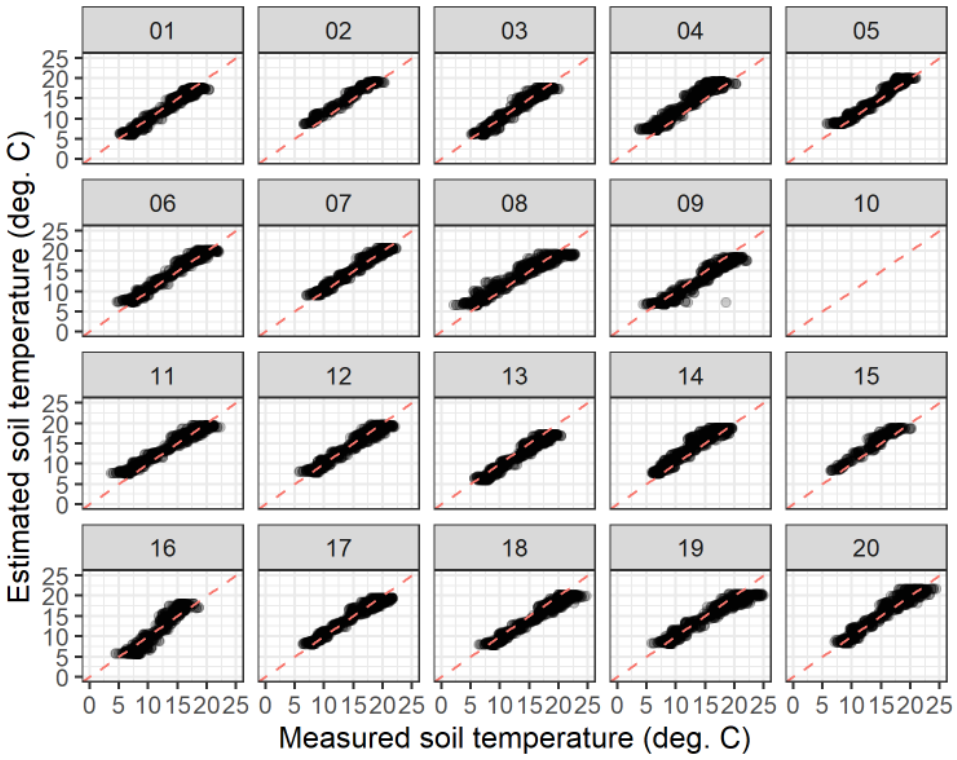


**Figure A59. Measured versus fitted soil temperature plot for the Taumarunui site using model 5. Panel labels indicate the respective sensor node.**

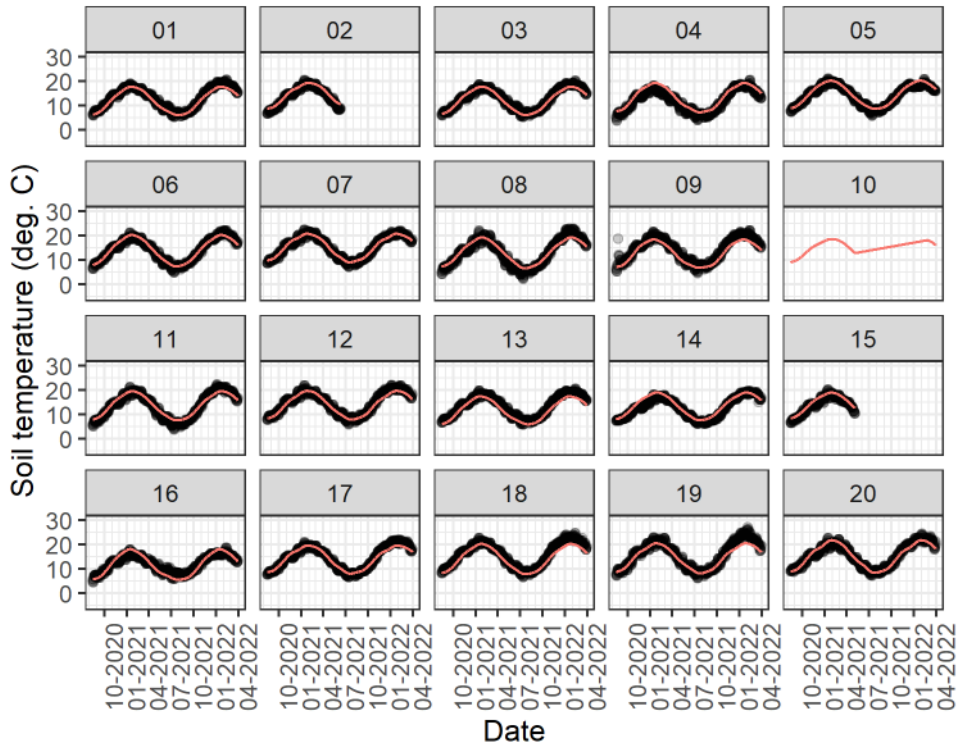


**Figure A60. Measured (points) versus fitted (line) soil temperature for the Taumarunui site over time, using model 5. Panel labels indicate the respective sensor node.**

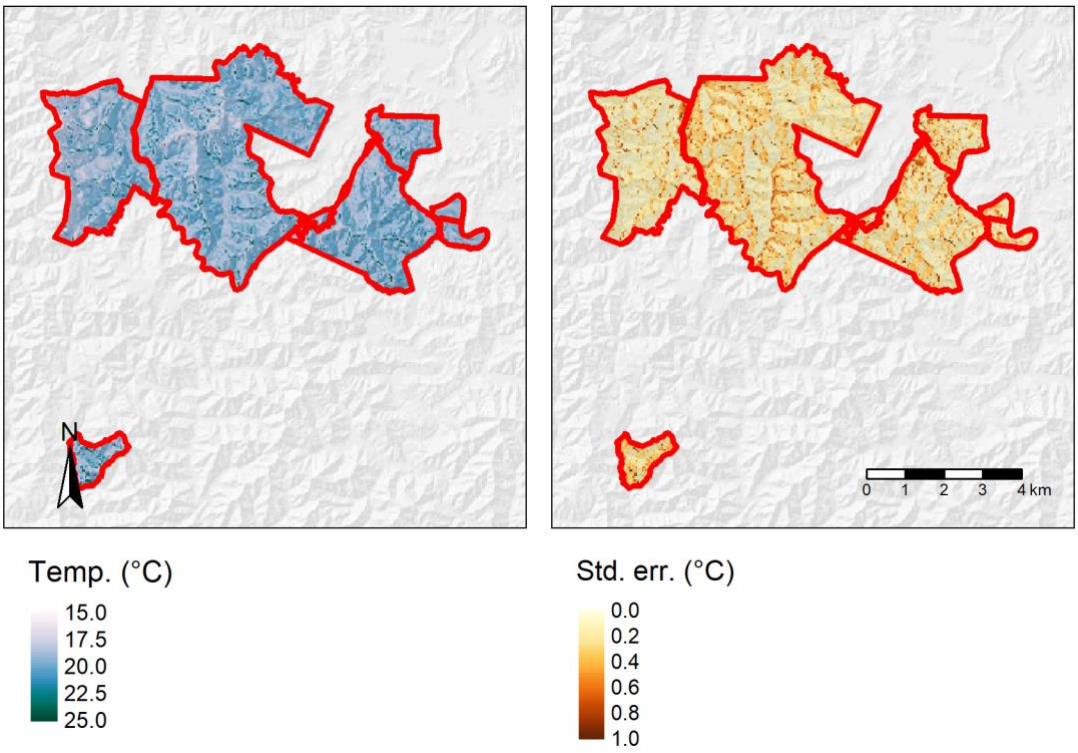


**Figure A61. Predicted soil temperature at Taumarunui on 15 January, when soils are near their warmest.**

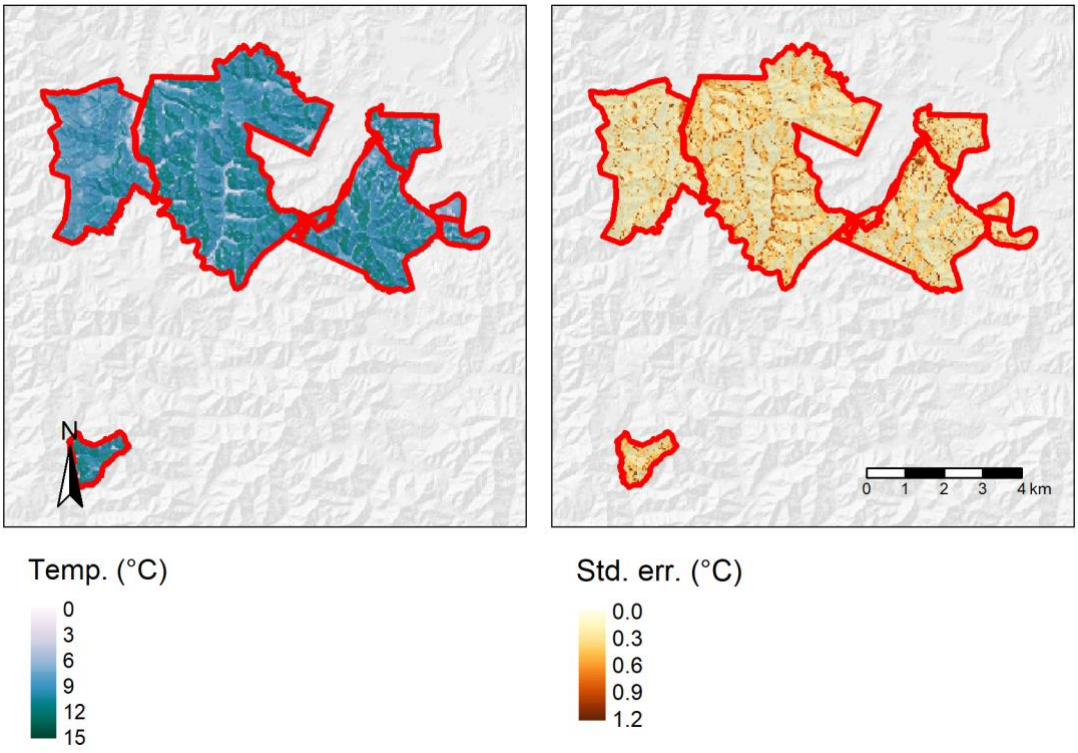


**Figure A62. Predicted soil temperature at Taumarunui on 15 July, when soils are near their coolest.**

*Soil moisture*

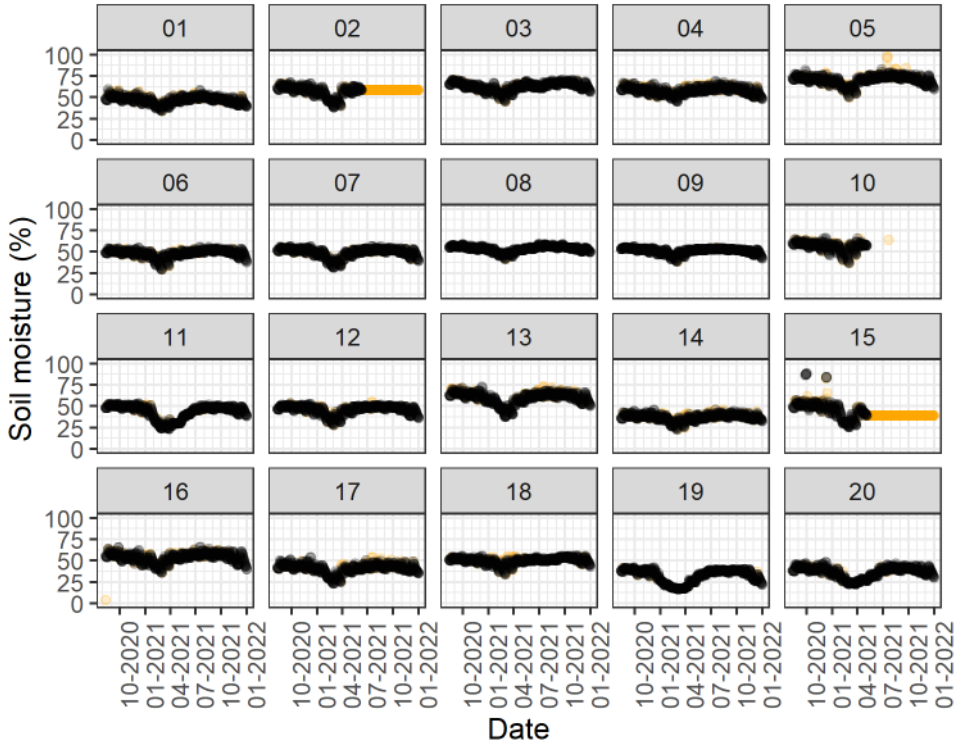


**Figure A63. Daily median soil moisture data for the Taumarunui site after trimming of the start and end dates, and removal of low and high soil moisture values, and periods of no change in soil moisture. Panel labels indicate the respective sensor node. Points excised from the data have been coloured orange.**

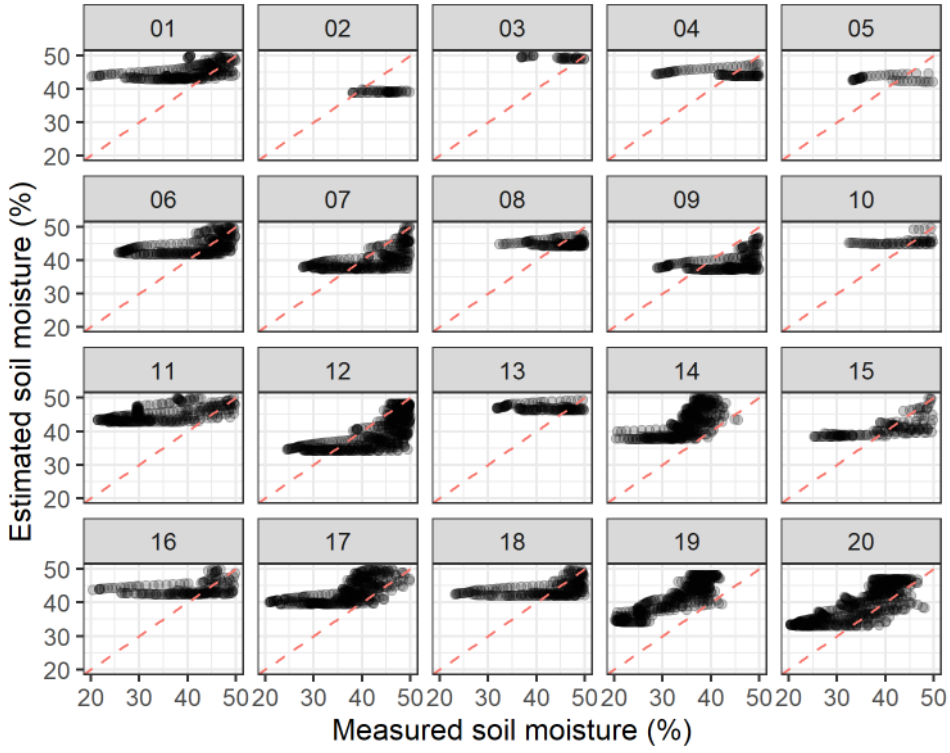


**Figure A64. Measured versus fitted soil moisture plot for the Taumarunui site using model 1. Panel labels indicate the respective sensor node.**

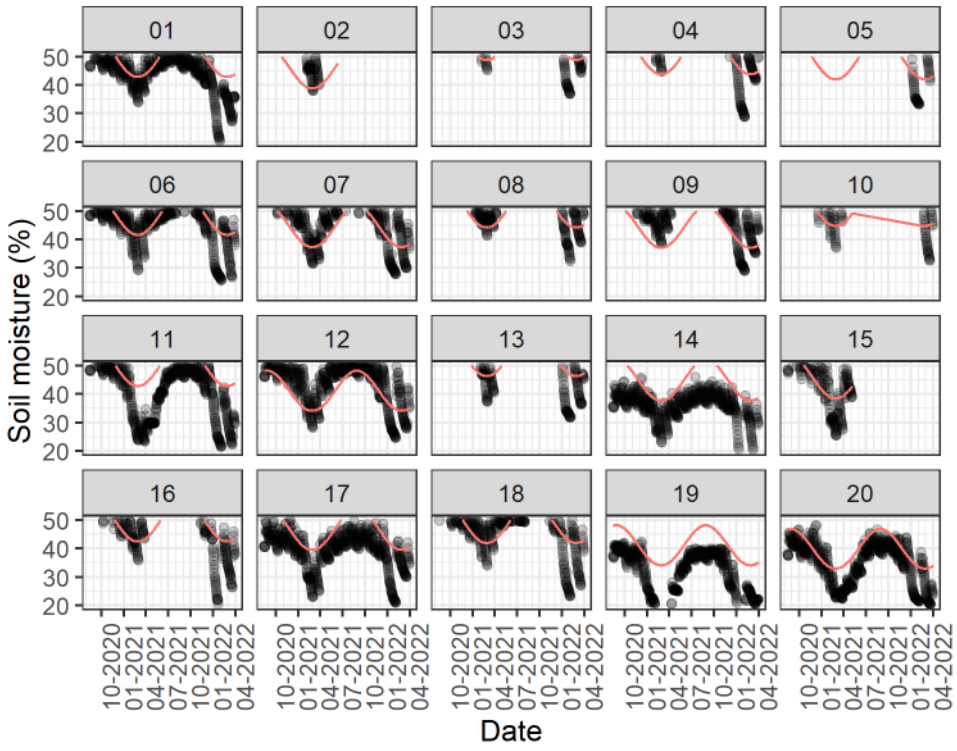


**Figure A65. Measured (points) versus fitted (line) soil moisture for the Taumarunui site over time, using model 1. Panel labels indicate the respective sensor node.**

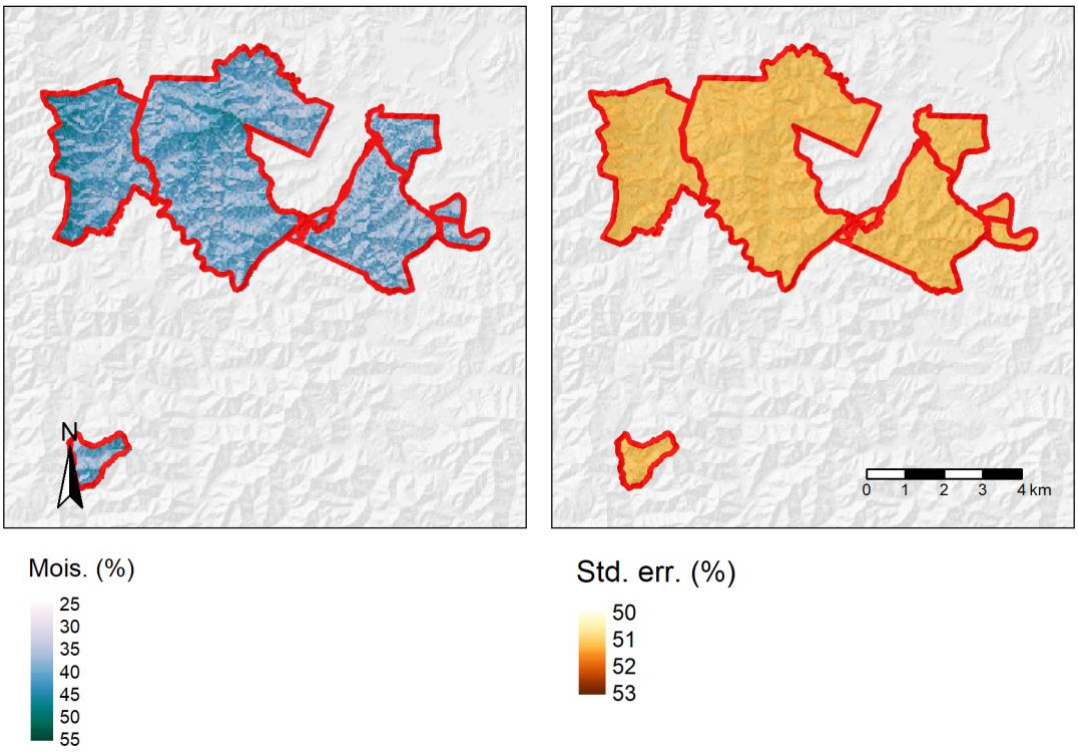


**Figure A66. Predicted soil moisture at Taumarunui on 1 March, when soils are near their driest.**

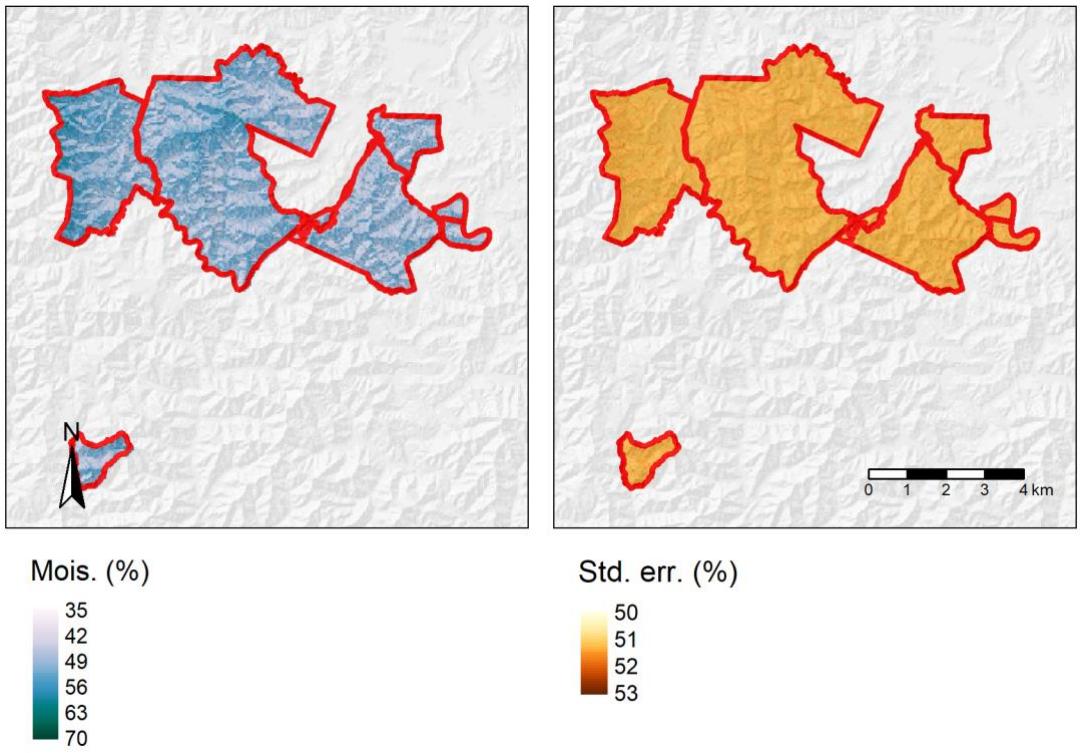


**Figure A67. Predicted soil moisture at Taumarunui on 25 June, when soils are near their wettest.**

*Yield*

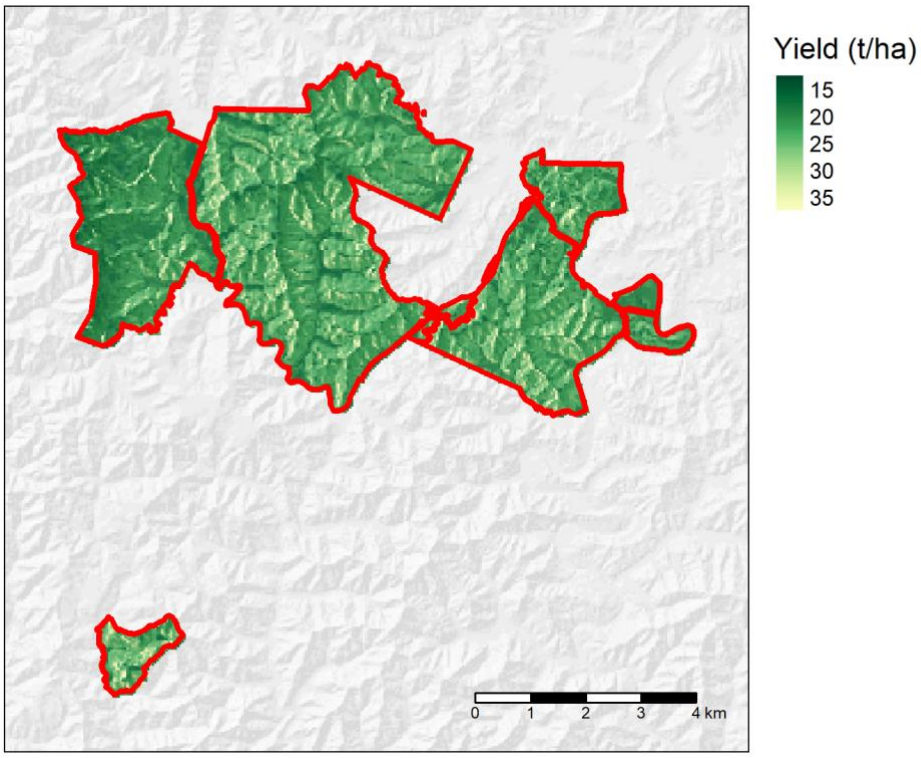


**Figure A68. Predicted annual lucerne yield at Taumarunui for 2020.**

## Tourere

*Sampling*

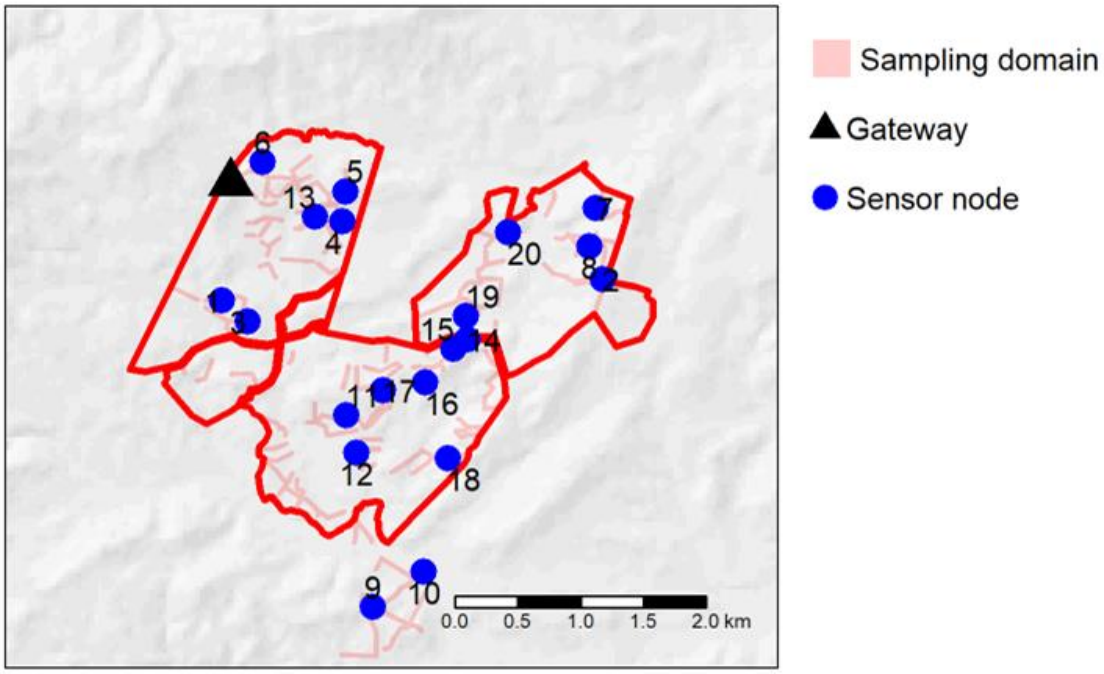


**Figure A69. Location of sampling domain, WSN gateway, and sensor nodes at Tourere.**

*Scorpan covariates*

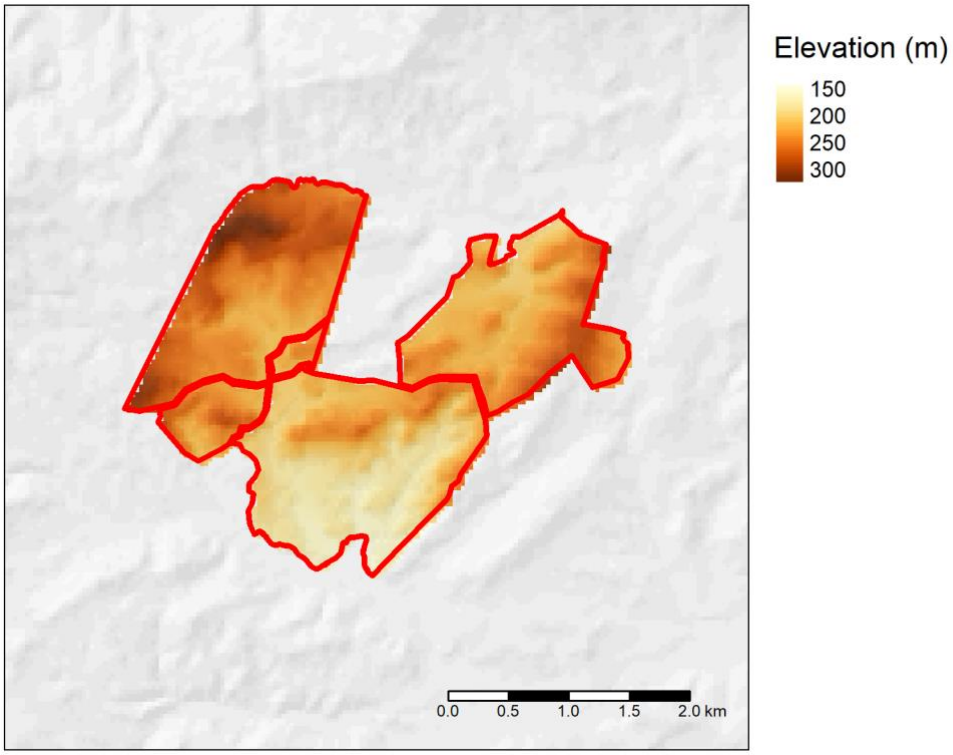


**Figure A70. Elevation at Tourere.**

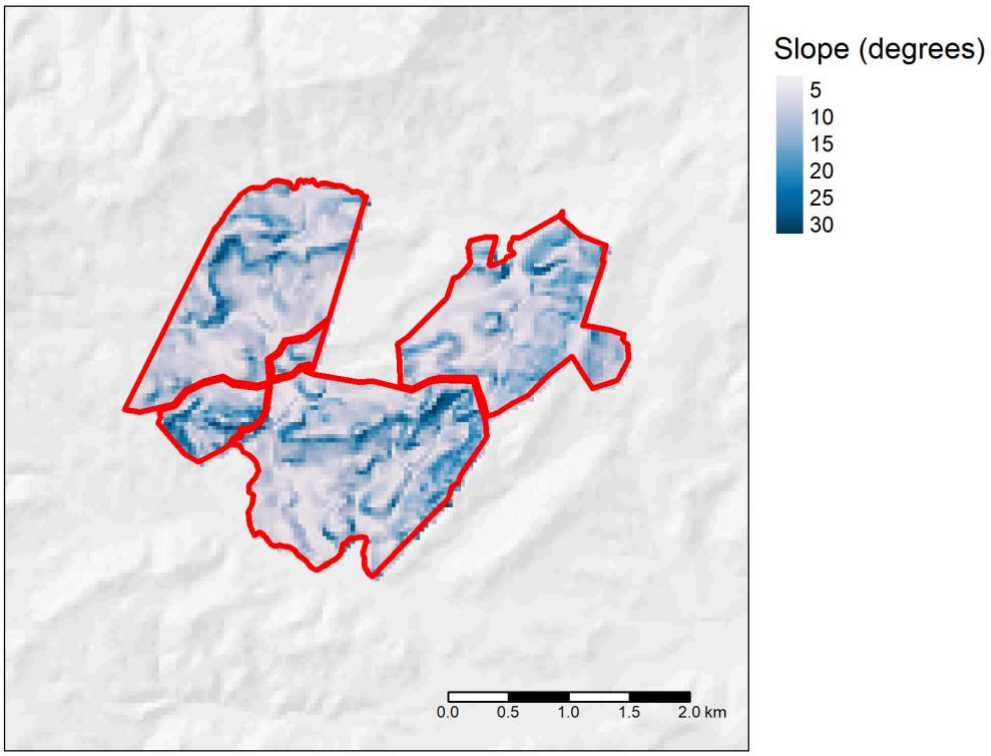


**Figure A71. Slope at Tourere.**

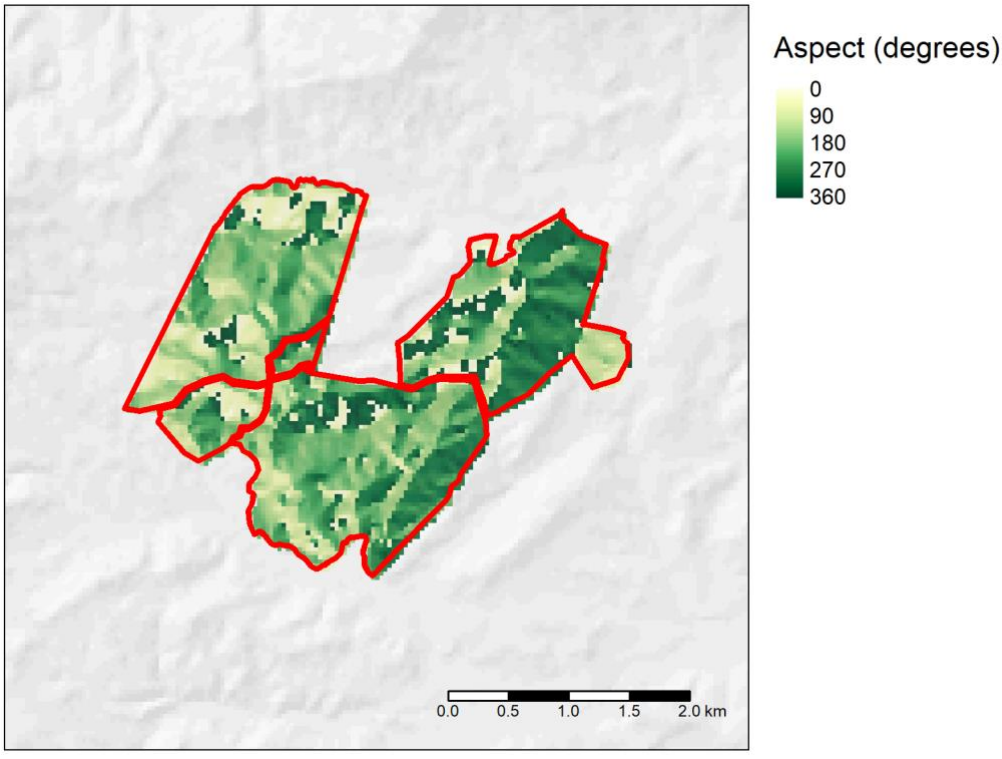


**Figure A72. Aspect at Tourere.**

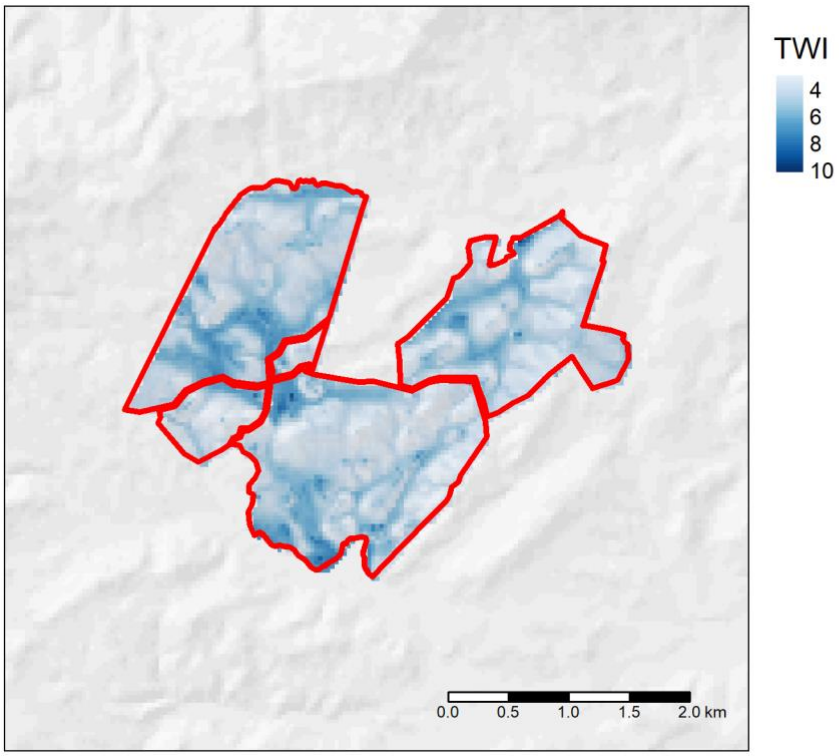


**Figure A73. Topographic wetness index at Tourere.**

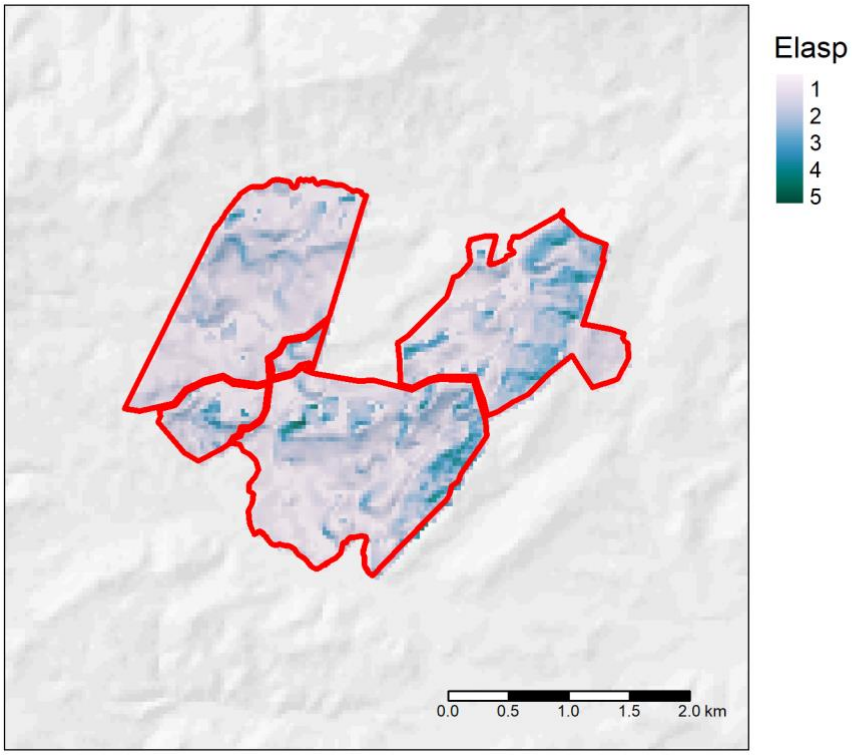


**Figure A74. Elasp at Tourere.**

*Soil temperature*

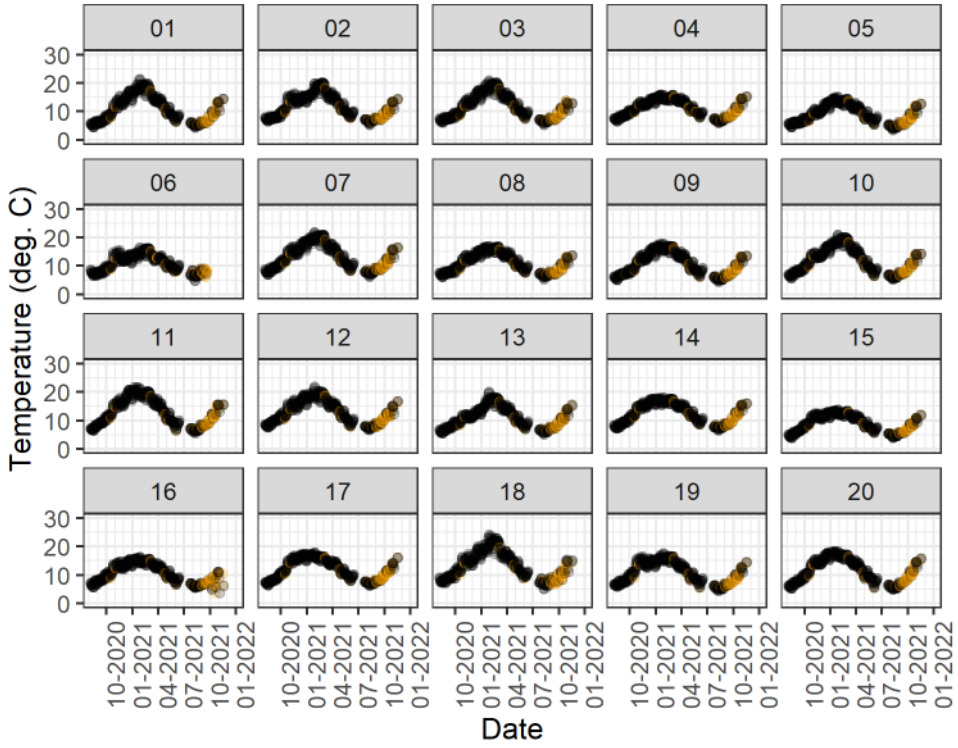


**Figure A75. Daily median soil temperature data for the Tourere WSN after trimming of the start and end dates, and removal of low and high temperatures, and periods of no change in soil temperature. Panel labels indicate the respective sensor node. Points that were removed as a result of the data trimming are shown in orange, while presumed valid points are in black.**

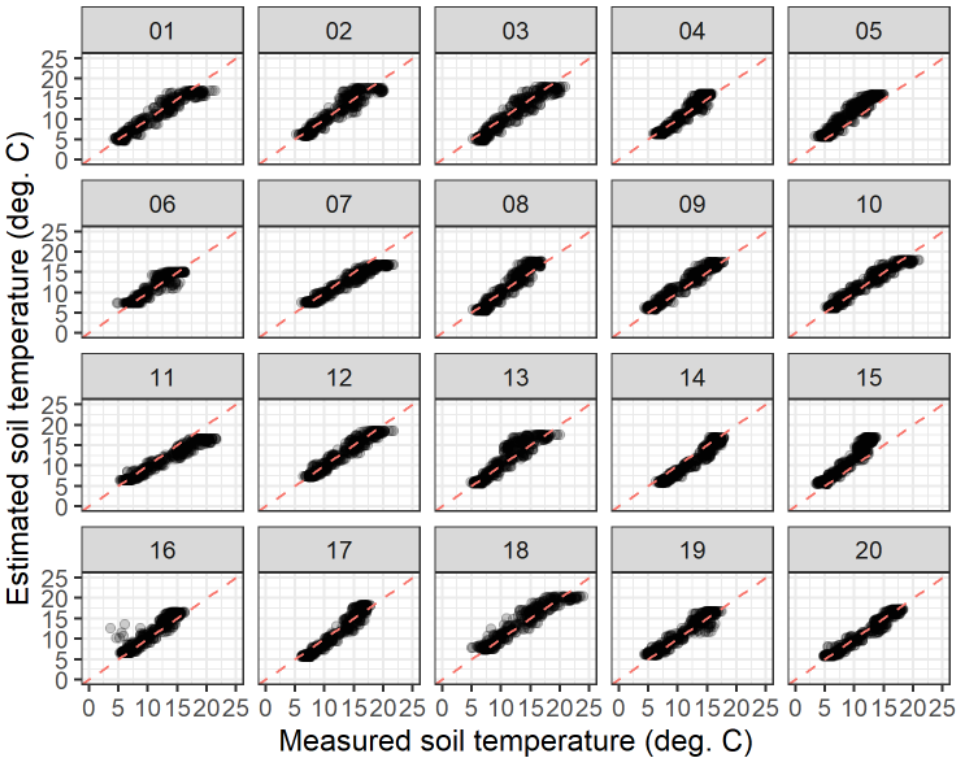


**Figure A76. Measured versus fitted soil temperature plot for the Tourere site using model 5. Panel labels indicate the respective sensor node.**

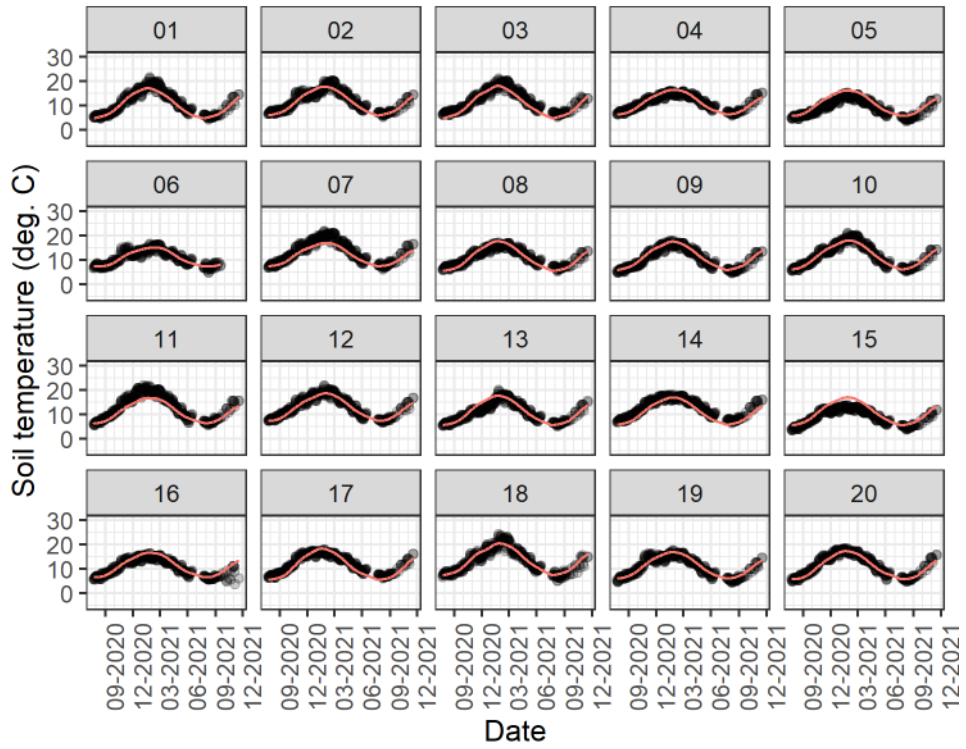


**Figure A77. Measured (points) versus fitted (line) soil temperature for the Tourere site over time, using model 5. Panel labels indicate the respective sensor node.**

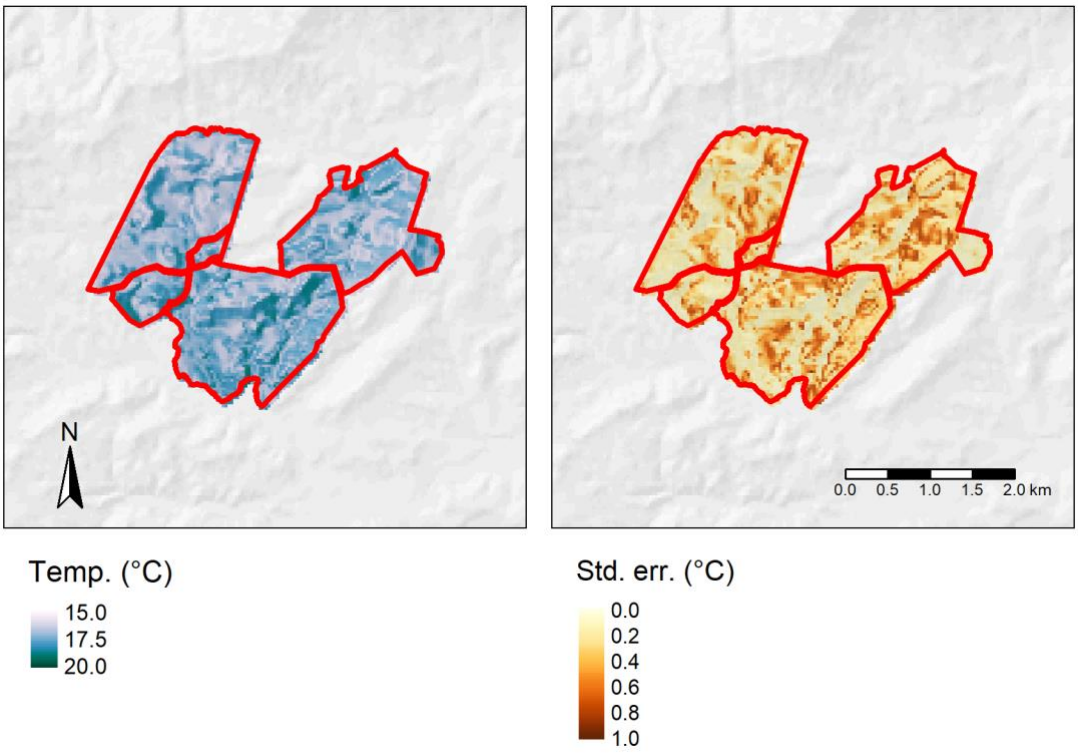


**Figure A78. Predicted soil temperature at Tourere on 15 January, when soils are near their warmest.**

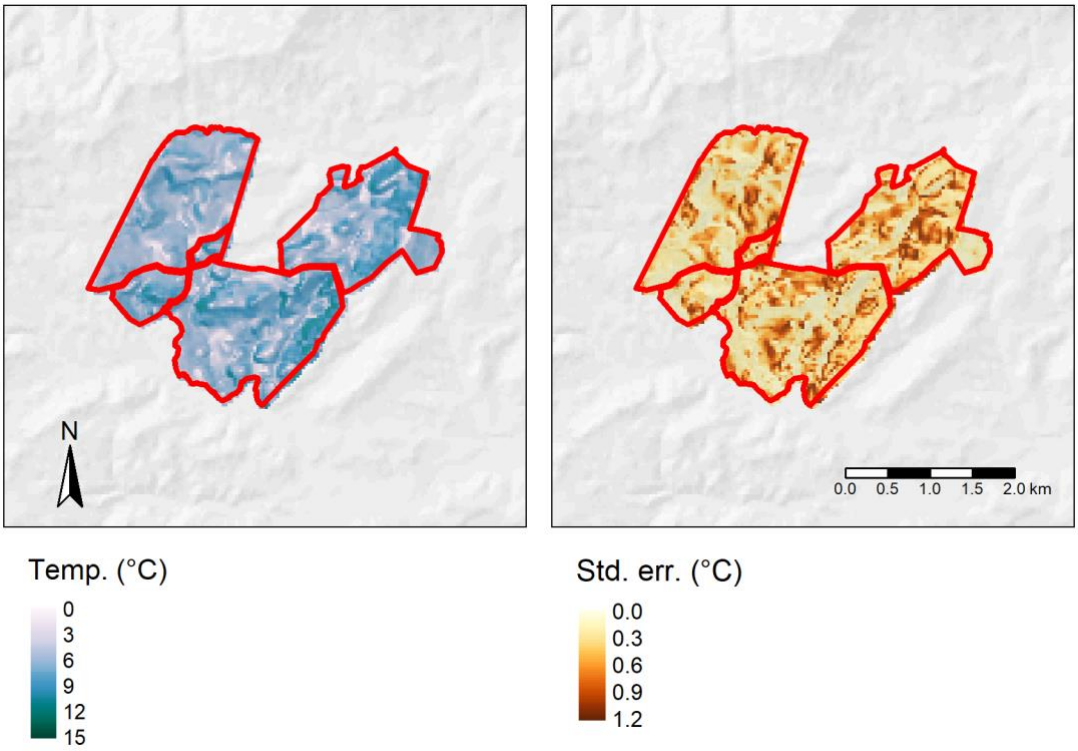


**Figure A79. Predicted soil temperature at Tourere on 15 July, when soils are near their coolest.**

*Soil moisture*

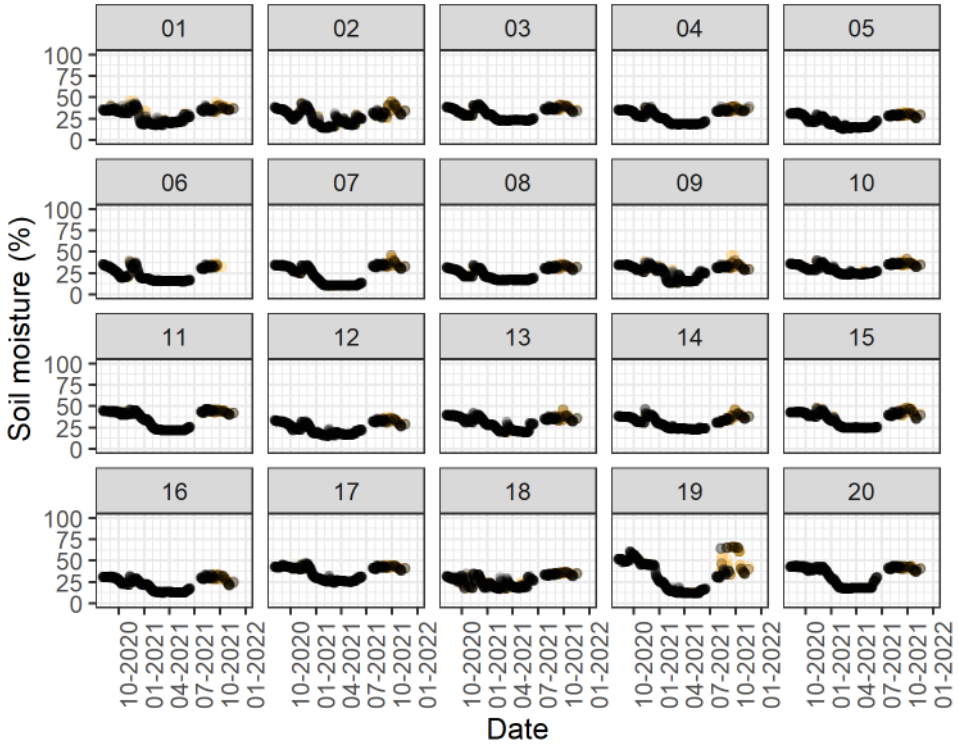


**Figure A80. Daily median soil moisture data for the Tourere site after trimming of the start and end dates, and removal of low and high soil moisture values, and periods of no change in soil moisture. Panel labels indicate the respective sensor node. Points excised from the data have been coloured orange.**

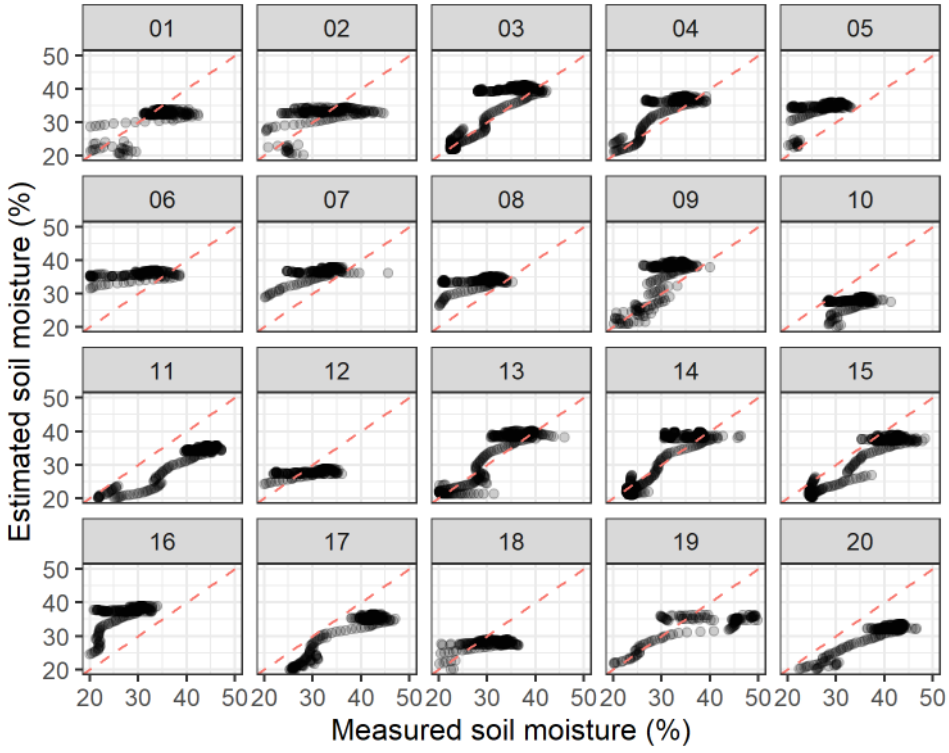


**Figure A81. Measured versus fitted soil moisture plot for the Tourere site using model 1. Panel labels indicate the respective sensor node.**

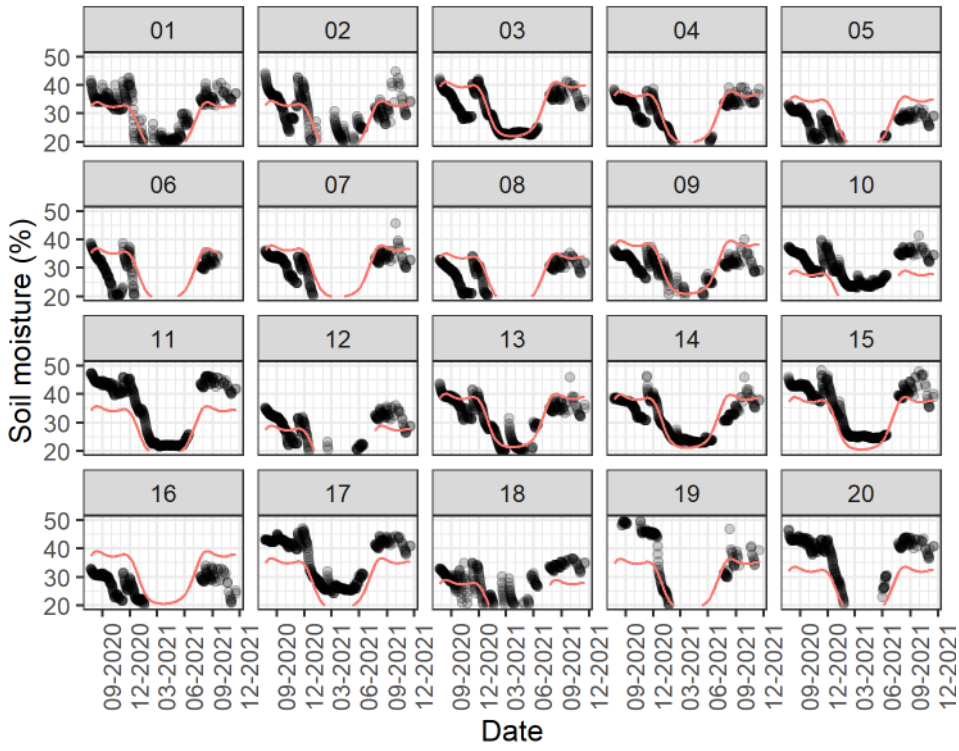


**Figure A82. Measured (points) versus fitted (line) soil moisture for the Tourere site over time, using model 1. Panel labels indicate the respective sensor node.**

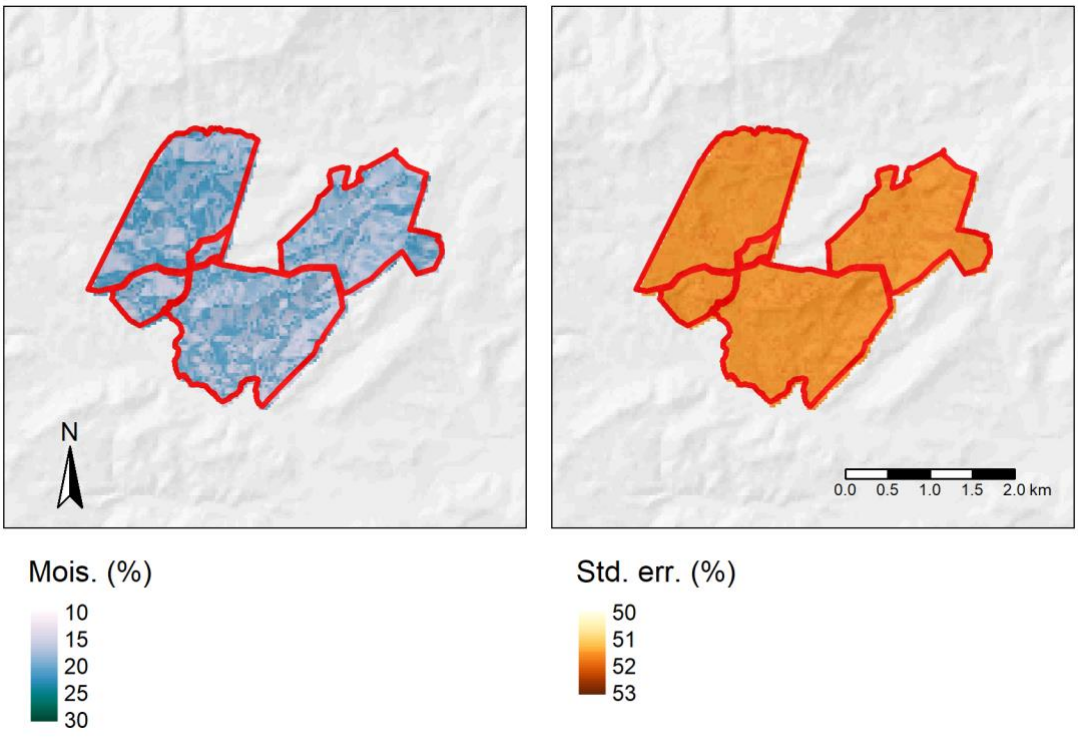


**Figure A83. Predicted soil moisture at Tourere on 1 March, when soils are near their driest.**

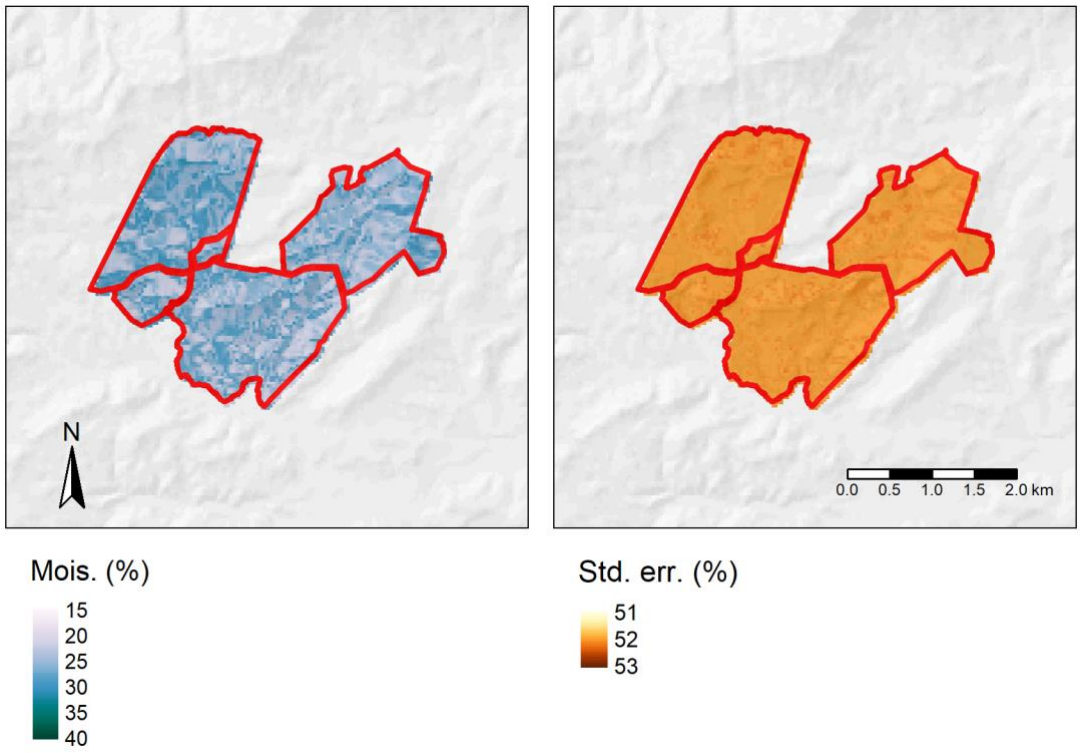


**Figure A84. Predicted soil moisture at Tourere on 25 June, when soils are near their wettest.**

*Yield*

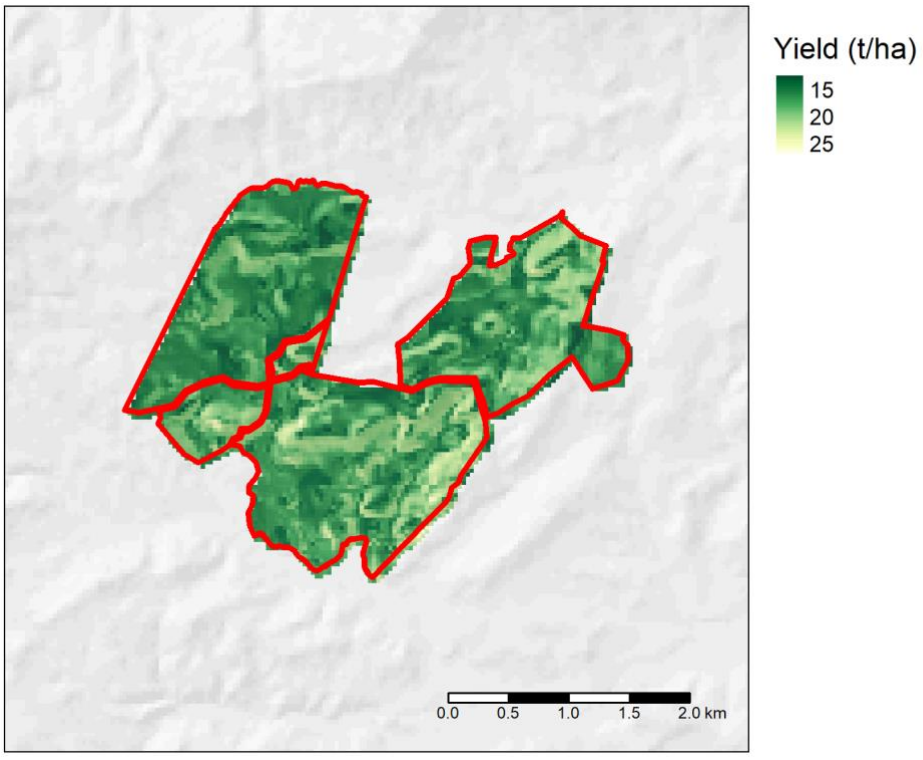


**Figure A85. Predicted annual lucerne yield at Tourere for 2020.**